Development of Bottom-up and Iterative Methods for Non-Markovian Coarse-Grained Modeling of Molecular Dynamics

Zur Erlangung des Grades eines Doktors der Naturwissenschaften (Dr. rer. nat.)
Genehmigte Dissertation von Viktor Klippenstein aus Schortandy
Tag der Einreichung: 15. März 2023, Tag der Prüfung: 8. Mai 2023

1. Gutachter: Prof. Dr. Ir. Nico F. A. van der Vegt
2. Gutachterin: Prof. Dr. Friederike Schmid
Darmstadt, Technische Universität Darmstadt

TECHNISCHE UNIVERSITÄT DARMSTADT

Chemistry Department
Eduard-Zintl-Institut für Anorganische und Physikalische Chemie
Computational Physical Chemistry

Development of Bottom-up and Iterative Methods for Non-Markovian Coarse-Grained Modeling of Molecular Dynamics

Accepted doctoral thesis by Viktor Klippenstein

Date of submission: 2023-03-15
Date of thesis defense: 2023-05-08

Darmstadt, Technische Universität Darmstadt

Erklärungen laut Promotionsordnung

§ 8 Abs. 1 lit. c PromO

Ich versichere hiermit, dass die elektronische Version meiner Dissertation mit der schriftlichen Version übereinstimmt.

§ 8 Abs. 1 lit. d PromO

Ich versichere hiermit, dass zu einem vorherigen Zeitpunkt noch keine Promotion versucht wurde. In diesem Fall sind nähere Angaben über Zeitpunkt, Hochschule, Dissertationsthema und Ergebnis dieses Versuchs mitzuteilen.

§ 9 Abs. 1 PromO

Ich versichere hiermit, dass die vorliegende Dissertation selbstständig und nur unter Verwendung der angegebenen Quellen verfasst wurde.

§ 9 Abs. 2 PromO

Die Arbeit hat bisher noch nicht zu Prüfungszwecken gedient.

Darmstadt, 15. März 2023

Viktor Klippenstein

Erklärung zum Eigenanteil an den Veröffentlichungen der kumulativen Dissertation

Die vorliegende Dissertation wurde der unter Leitung von Herrn Prof. Dr. Nico F. A. van der Vegt in der Zeit vom 1. Juli 2018 bis zum 31. Dezember 2022 im Fachbereich Chemie der Technischen Universität Darmstadt durchgeführt. Teile dieser Arbeit sind bereits veröffentlicht.

Im Folgenden ist aufgelistet, mit welchem Anteil ich an der Veröffentlichung beteiligt war.

Mein Anteil an der folgenden Veröffentlichung beträgt 25 %
[1] V. Klippenstein, M. Tripathy, G. Jung, F. Schmid, N. F. A. van der Vegt, „Introducing Memory in Coarse-Grained Molecular Simulations“, *The Journal of Physical Chemistry B* **2021**, *125*, 4931–4954

Mein Anteil an der folgenden Veröffentlichung beträgt 100 %
[2] V. Klippenstein, N. F. A. van der Vegt, „Cross-Correlation Corrected Friction in (Generalized) Langevin Models“, *The Journal of Chemical Physics* **2021**, *154*, 191102

Mein Anteil an der folgenden Veröffentlichung beträgt 100 %
[3] V. Klippenstein, N. F. A. van der Vegt, „Cross-Correlation Corrected Friction in Generalized Langevin Models: Application to the Continuous Asakura–Oosawa Model“, *The Journal of Chemical Physics* **2022**, *157*, 044103

Mein Anteil an der folgenden Veröffentlichung beträgt 100 %
[4] V. Klippenstein, N. F. A. van der Vegt, „Bottom-Up Informed and Iteratively Optimized Coarse-Grained Non-Markovian Water Models with Accurate Dynamics“, *Journal of Chemical Theory and Computation* **2023**, *19*, 1099–1110

_____
Datum

_____
Viktor Klippenstein

Die Veröffentlichungen [1], [2], [3] und [4] sind in der Version des akzeptierten Manuskripts in diese Dissertation eingebunden. Zu den Veröffentlichungen [2], [3] und [4] wurden zusätzlich die *Supporting Information* (oder Teile dieser) eingebunden. Die Kapitel 2, 4, 5 und 6 entsprechen den Veröffentlichungen [1-4] in der selben Reihenfolge.

Erklärung zur Begutachtung der Veröffentlichungen

Weder Referent Prof. Dr. Nico F. A. van der Vegt noch Co-Referentin Prof. Dr. Friederike Schmid der vorliegenden kumulativen Doktorarbeit waren an der Begutachtung nachstehender Veröffentlichungen beteiligt.

[1] V. Klippenstein, M. Tripathy, G. Jung, F. Schmid, N. F. A. van der Vegt, "Introducing Memory in Coarse-Grained Molecular Simulations", *The Journal of Physical Chemistry B* **2021**, *125*, 4931–4954

[2] V. Klippenstein, N. F. A. van der Vegt, "Cross-Correlation Corrected Friction in (Generalized) Langevin Models", *The Journal of Chemical Physics* **2021**, *154*, 191102

[3] V. Klippenstein, N. F. A. van der Vegt, "Cross-Correlation Corrected Friction in Generalized Langevin Models: Application to the Continuous Asakura–Oosawa Model", *The Journal of Chemical Physics* **2022**, *157*, 044103

[4] V. Klippenstein, N. F. A. van der Vegt, "Bottom-Up Informed and Iteratively Optimized Coarse-Grained Non-Markovian Water Models with Accurate Dynamics", *Journal of Chemical Theory and Computation* **2023**, *19*, 1099–1110

_____

Datum

_____	_____
Referent Prof. Dr. Nico F. A. van der Vegt	Co-Referentin Prof. Dr. Friederike Schmid

Acknowledgments

With every major milestone throughout my academic life, I never could have anticipated actually succeeding. In particular, the pursuit of a Ph.D. felt like such an enormous task, whose finalization always felt like an unrealistic vision for the future. Now that it is finally done, it is obvious that I could not come that far alone and I am indebted to so many people who made this possible for me.

First of all, I want to thank my supervisor Nico van der Vegt, for the opportunity to pursue my Ph.D. in his group. I am grateful that he gave me the opportunity to work on a topic that kept me interested and engaged over the years. He was patient and gave me the time to explore the field and to find my path driven by my own interests and curiosity while also always being available to discuss new ideas. Also, his open nature directly translates into a great working environment which I enjoyed a lot. Thank you Prof. Friederike Schmid for examining this thesis. Thank you and Gerhard Jung for the collaboration on our review paper and several insightful discussions which inspired parts of this thesis. I also want to thank Prof. Florian Müller-Plathe and Prof. Rolf Schäfer for taking part in the evaluation committee.

Staying motivated over the years would not have been possible without my great colleagues in the CPC group. I am grateful that I could spend my daily life surrounded by so many competent, helpful, kind, and also just fun people. Thank you, Marvin, it has been a pleasure to share an office with you. I am grateful for the enumerable times you helped me out with technical and scientific problems and, maybe even more importantly, I am grateful that I always could just talk to you when in need of a distraction from work. Thanks to you, I really had a great time. Thank you Madhu for the collaboration on our joint projects, for many scientific discussions along the way, for proofreading parts of this work, and also for your warm and caring character. Thank you, Swami, Vishal, and Angelina. The three of you have imprinted your fun and likable characters onto the group and I really enjoyed our social events outside of work. I am especially thankful to Swami just for being Swami. Meeting such an unique and inspiring person meant a lot to me and I will try to preserve some of your spirit within myself. Thank you, Moritz. It has been a pleasure to have you in the group as a master's student and I am happy that you decided to join the group to pursue your Ph.D.. Thank you for taking over many duties such as managing the clusters, organizing the rest of our hardware, and many more. I also want to thank Abhishek, Varun, Bin, Gregor, David, Ellen B., Cahit, Ellen P., Imke, Alexandra, and all the others. I am also grateful for the opportunity to supervise very talented students from whom I learned a lot. Again thank you to Moritz and also Frederick and Niklas. I am also thankful to the group Prof. Florian Müller-Plathe for the regular joint seminars which have always been a great opportunity to learn about science outside of my immediate research topic.

My Ph.D. has been made possible by the TRR146, funded by the Deutsche Forschungsgemeinschaft. I am grateful for the funding and also for the opportunity of meeting other Ph.D. students for interesting scientific exchanges.

I also want to thank all my friends inside and outside of the university, for being part of my journey. Thank you, Tobias, Jasmin, Marius, Inga, Tim, Lucia, and many more. A very special thanks goes to Dominik and Jurek, for all the time we spent preparing for exams and writing lab reports. My motivation would not have lasted if I would have been on my own.

I am deeply thankful to my parents who gave me the freedom to pursue a university degree, even if it was elusive what exactly I was spending all this time on. A big thank you goes to my brother Dmitrij for being so caring. I know that you always would be there when I am in need. Thank you to Karl-Heinz, Anja, and Max, for taking me in as part of your family.

And finally, thank you, Sina. Thank you for being understanding when I was a total mess, thank you for being encouraging when I was down, and thank you for always making sure that I do not forget the social aspects of life. It was because of you that I could have never given up even when I have been at my lowest. Thank you! And of course, thank you to my furry friend Sam.

Abstract

While computational power has been steadily increasing throughout the recent decades, computational modeling in terms of atomistic molecular dynamics simulations is still limited in scope with respect to length and time scales. Thus, there is a need for the development of coarser models which allow to study molecular systems for which relevant length and time scales are not accessible with typical atomistic models with a reasonable expenditure of computational resources. In the quite well established field of systematic bottom-up coarse-graining many methods have been developed for the derivation of effective coarse-grained interactions from fine-grained reference models. On the one hand, these models, used in conjunction with standard molecular dynamics simulations, allow to study structural and thermodynamic properties of the underlying reference more efficiently. On the other hand, the correct representation of dynamic properties with coarse-grained models poses additional distinct challenges. The reduction of complexity due to the reduced number of modeled degrees of freedom inevitably leads to a loss of friction in the coarse-grained representation. Subsequently, this leads to a speed-up of dynamics and thus to a misrepresentation of time scales. In particular, whenever the chosen level of coarsening is kept moderate the speed-up can affect different processes to different degrees. This is due to the fact that whenever the time scales of the dynamics of fine-grained and coarse-grained degrees of freedom are not sufficiently separated, friction due to the fine-grained degrees of freedom, acting on the coarse-grained degrees of freedom, becomes time (frequency) dependent and thus non-Markovian. To correct for these effects in coarse-grained models, modified equations of motion, which explicitly incorporate friction or, if required, time dependent friction have to be utilized in coarse-grained simulations. A common class of such equations of motion are generalized Langevin equations, which are non-Markovian stochastic integro-differential equations explicitly incorporating time dependent friction via, the so called, memory kernels. While the field of structural coarse-graining is quite well established, methodological development for deriving dynamically consistent coarse-grained models falls behind in comparison.

The focus of the work reported within this thesis is the furthering of methods for parametrizing optimal memory kernels for generalized Langevin equations to achieve dynamic consistency in coarse-grained simulations. Simultaneously this endeavor allows to further the understanding of the role of memory effects in coarse-grained modeling.

This thesis is structured as follows. Chapter 1 gives a short introduction on and motivation of non-Markovian models in coarse-graining. In chapter 2, a peer-reviewed review article is presented, which provides a detailed overview on Markovian and non-Markovian coarse-grained modeling and numerical evaluation of memory kernels. Chapter 3 summarizes the key theoretical background, relevant for the understanding of the following chapters.

Chapters 4-6 contain the main results of this thesis, based on 3 peer-reviewed research articles. In all three chapters, coarse-grained models are developed to yield consistent dynamic properties. In chapter 4, a novel route for *a-priori* bottom-up estimation of memory kernels is presented. In this study it is shown that by splitting the memory kernel of an exactly solvable single-particle interpretation of a coarse-grained degree of freedom into different contributions stemming from conservative coarse-grained interactions and residual fluctuating interactions, a good choice for the memory kernel in many-body coarse-grained generalized Langevin simulations can be estimated. In particular, it is found that the contributions from

coarse-grained conservative and fluctuating interactions are strongly correlated. These cross-correlations have a strong impact on the overall dynamics and thus have to be considered in the parametrization of coarse-grained models. This method is developed and tested on a prominent test case for coarse-grained methods: a generic star-polymer melt. While this approach has shown to be quite accurate, small deviations between fine-grained and coarse-grained dynamics persist. The data presented in this chapter indicates that these residual deviations might mainly stem from modeling errors in the coarse-grained conservative interactions.

To improve the understanding of the role of the accuracy of coarse-grained conservative interactions, the work presented in chapter 5 aims at illuminating the origin of the remaining discrepancies by deliberately choosing a test case, the well known Asakura-Oosawa model, for which it is *a-priori* known that very accurate coarse-grained conservative interactions can be derived. By doing so, one generally hard to control error source is removed and the previously proposed methodology is examined under idealized circumstances. The data presented in this chapter validate the general soundness of the proposed approach and confirms that inaccuracies in conservative interactions are likely to be the main error source in non-idealized applications. At the same time, subtle but relevant limitations of using a simple isotropic thermostat in many-body simulations are discussed. The chosen equation of motion includes hydrodynamic interactions only in an averaged sense. This can can yield to errors in the hydrodynamic scaling of e.g. velocity autocorrelation functions, in particular, in systems with low viscosity. Thus, a key insight from this study is that bottom-up informed approaches for the derivation of memory kernels are useful for a better interpretation of the origin of memory effects. At the same time, for the practical development of coarse-grained models, even subtle error sources due to both modeling errors in coarse-grained potentials and general limitations of the chosen coarse-grained equation of motion can not always be safely ignored. As a way to circumvent these limitations, three novel, simple, iterative optimization procedures are presented for optimizing the generalized Langevin thermostat parametrization to match the references velocity autocorrelation function exactly.

In chapter 6, the newly developed methods are applied for coarse-graining a realistic molecular system, namely water. The complex local structuring and strong electrostatic interactions in water poses additional hurdles in developing consistent coarse-grained models. Despite that, it is demonstrated that bottom-up informed memory kernels can correct dynamic properties quite well. To get an exact match between fine-grained and coarse-grained velocity autocorrelation functions, the most promising of the newly developed iterative methods (in this chapter referred to as iterative optimization of memory kernels (IOMK)) is successfully employed. Also, it is demonstrated that the IOMK method is roughly ten times more efficient than the best alternative previously proposed optimization scheme in literature. By studying dynamic properties beyond single-particle time correlation functions, the distinct Van Hove function as a measure of the relaxation of pair structure, it is found that the IOMK method yields very accurate results and, in particular, that Markovian models are not sufficient to achieve comparably good results. By furthermore comparing different coarse-grained conservative interactions, the role of multi-body interactions on structural relaxations is discussed.

A few preliminary and unpublished results and ideas, which can serve as motivation for further research, are discussed in chapter 7. In section 7.1, the challenges in a naive application of the IOMK method to systems which include bonds are discussed. Such mapping schemes give rise to high frequency modes in mapped trajectories. A smoothing approach is proposed, to access the most relevant features and thus to obtain memory kernels which yield comparably good results as in single-bead mapping schemes. In section 7.2 an implementation of the IOMK method as a Gauss-Newton method is proposed, which allows to directly optimize a few parameters which serve as input of the auxiliary variable generalized Langevin thermostat. Such an approach would further simplify the procedure of the IOMK method and thus improve its applicability as a out of box tool for dynamically consistent coarse-graining.

A summary and an outlook into future research is provided in the final chapter.

Zusammenfassung

Während die Rechenleistung in den letzten Jahrzehnten stetig zugenommen hat, ist die Modellierung mit Hilfe von atomistischen Molekulardynamiksimulationen in Bezug auf Längen- und Zeitskalen immer noch begrenzt. Daher besteht ein Bedarf an der Entwicklung gröberer Modelle, die es ermöglichen, molekulare Systeme zu untersuchen, für die relevante Längen- und Zeitskalen mit typischen atomistischen Modellen nicht mit vertretbarem Rechenaufwand zugänglich sind. Auf dem recht gut etablierten Gebiet der systematischen Bottom-up-Vergröberung sind viele Methoden zur Herleitung effektiver vergröberter Wechselwirkungen aus hochaufgelösten Referenzmodellen entwickelt worden. Einerseits ermöglichen diese Modelle in Verbindung mit Standard-Molekulardynamiksimulationen eine effizientere Untersuchung der strukturellen und thermodynamischen Eigenschaften der zugrunde liegenden Referenz. Andererseits stellt die korrekte Darstellung der dynamischen Eigenschaften mit vergröberten Modellen eine zusätzliche Herausforderung dar. Die Verringerung der Komplexität aufgrund der reduzierten Anzahl von modellierten Freiheitsgraden führt unweigerlich zu einem Reibungsverlust in der vergröberten Darstellung. In der Folge führt dies zu einer Beschleunigung der Dynamik und damit zu einer falschen Darstellung von Zeitskalen. Insbesondere dann, wenn der gewählte Vergröberungsgrad moderat gehalten wird, kann die Beschleunigung verschiedene Prozesse in unterschiedlichem Maße betreffen. Dies ist darauf zurückzuführen, dass, wenn die Zeitskalen der Dynamik von hochaufgelösten und vergröberten Freiheitsgraden nicht ausreichend voneinander getrennt sind, die Reibung durch die hochaufgelösten Freiheitsgrade, die auf die vergröberten Freiheitsgrade einwirkt, zeit-(bzw. frequenz-)abhängig und somit nicht Markov wird. Um diese Effekte in vergröberten Modellen zu korrigieren, müssen in vergröberten Simulationen modifizierte Bewegungsgleichungen verwendet werden, die die Reibung oder, falls erforderlich, die zeitabhängige Reibung explizit einbeziehen. Eine gängige Klasse solcher Bewegungsgleichungen sind verallgemeinerte Langevin-Gleichungen, bei denen es sich um nicht Markov'sche stochastische Integro-Differentialgleichungen handelt, die explizit die zeitabhängige Reibung über Gedächtnisfunkionen (engl. *memory kernel*) einbeziehen. Während das Gebiet der strukturellen Vergröberungsmethoden recht gut etabliert ist, sind Methoden zur Entwicklung dynamisch konsistenter vergröberter Modelle weniger gut untersucht.

Der Schwerpunkt dieser Arbeit liegt auf der Weiterentwicklung von Methoden zur Parametrisierung optimaler Gedächntisfunktionen für verallgemeinerte Langevin-Gleichungen, um dynamische Konsistenz in vergröberten Simulationen zu erreichen. Gleichzeitig soll mit dieser Arbeit das Verständnis der Rolle von "Gedächtniseffektenïn der vergröberten Modellierung verbessert werden.

Diese Arbeit ist wie folgt gegliedert. Kapitel 1 gibt eine kurze Einführung in und Motivation für die Verwendung von nicht-Markov'schen Modellen vergröberten Molekulardynamiksimulation. In Kapitel 2 wird ein begutachteter Übersichtsartikel vorgestellt, der einen detaillierten Überblick über die Markov'sche und nicht-Markov'sche vergröberte Modellierung und die numerische Auswertung von Gedächtnisfunktionen gibt. Kapitel 3 fasst die wichtigsten theoretischen Hintergründe zusammen, die für das Verständnis der folgenden Kapitel relevant sind.

Die Kapitel 4-6 enthalten die wichtigsten Ergebnisse dieser Arbeit, die auf 3 von Experten begutachteten Forschungsartikeln basieren. In allen drei Kapiteln werden vergröberte Modelle entwickelt, um konsistente dynamische Eigenschaften zu erhalten. In Kapitel 4 wird eine neue Methode zur Bottom-up-Abschätzung von Gedächtnisfunktionen vorgestellt. In dieser Studie wird gezeigt, dass durch Aufteilung

der Gedächtnisfunktion einer exakt lösbaren Ein-Teilchen-Interpretation eines vergröberten Freiheitsgrades in verschiedene Beiträge, die aus konservativen vergröberten Wechselwirkungen und fluktuierenden Restwechselwirkungen stammen, eine gute Wahl für die Gedächtnisfunktion in vergröberten verallgemeinerten Langevin-Simulationen mit vielen Teilchen abgeschätzt werden kann. Insbesondere wird festgestellt, dass die Beiträge von vergröberten konservativen und fluktuierenden Wechselwirkungen stark korreliert sind. Diese Kreuzkorrelationen haben einen starken Einfluss auf die Gesamtdynamik und müssen daher bei der Parametrisierung von vergröberten Modellen berücksichtigt werden. Diese Methode wird an einem prominenten Testfall für vergröberte Methoden, einer generischen Sternpolymerschmelze, entwickelt und getestet. Obwohl sich dieser Ansatz als recht genau erwiesen hat, bleiben kleine Abweichungen zwischen hochaufgelöster und vergröberter Dynamik bestehen. Die in diesem Kapitel vorgestellten Daten deuten darauf hin, dass diese Restabweichungen hauptsächlich auf Modellierungsfehler bei den vergröberten konservativen Wechselwirkungen zurückzuführen sein könnten.

Um das Verständnis der Rolle der Genauigkeit der konservativen Wechselwirkungen zu verbessern, zielt die in Kapitel 5 vorgestellte Arbeit darauf ab, den Ursprung der verbleibenden Diskrepanzen besser zu verstehen, indem bewusst ein Testfall, das bekannte Asakura-Oosawa-Modell, gewählt wird, für das bereits bekannt ist, dass sehr genaue konservative Wechselwirkungen abgeleitet werden können. Auf diese Weise wird eine im Allgemeinen schwer zu kontrollierende Fehlerquelle beseitigt und die zuvor vorgeschlagene Methodik unter idealisierten Bedingungen untersucht. Die in diesem Kapitel vorgestellten Daten validieren die allgemeine Validität des vorgeschlagenen Ansatzes und bestätigen, dass Ungenauigkeiten in konservativen Wechselwirkungen eine der Hauptfehlerquellen in nicht-idealisierten Anwendungen sind. Gleichzeitig werden subtile, aber relevante Einschränkungen der Verwendung eines einfachen isotropen Thermostaten in Vielteilchensimulationen diskutiert. Die gewählte Bewegungsgleichung beinhaltet hydrodynamische Wechselwirkungen nur in einem gemittelten Sinn. Dies kann zu Fehlern in der hydrodynamischen Skalierung von z.B. Geschwindigkeits-Autokorrelationsfunktionen führen, insbesondere in Systemen mit niedriger Viskosität. Eine wichtige Erkenntnis aus dieser Studie ist daher, dass Bottom-up-Ansätze für die Ableitung von Gedächtnisfunktionen für eine bessere Interpretation des Ursprungs von Gedächtniseffekten nützlich sind. Gleichzeitig können bei der praktischen Entwicklung von vergröberten Modellen selbst subtile Fehlerquellen aufgrund von Modellierungsfehlern in vergröberten Wechselwirkungen und allgemeinen Einschränkungen der gewählten vergröberten Bewegungsgleichung nicht immer sicher ignoriert werden. Um diese Einschränkungen zu umgehen, werden drei neuartige, einfache, iterative Optimierungsverfahren vorgestellt, mit denen die verallgemeinerte Langevin-Thermostat-Parametrisierung so optimiert werden kann, dass sie eine genaue Reproduktion der Geschwindigkeitsautokorrelationsfunktion der Referenz ermöglicht.

In Kapitel 6 werden die neu entwickelten Methoden zur Vergröberung eines realistischen molekularen Systems, nämlich Wasser, angewandt. Die komplexe lokale Strukturierung und die starken elektrostatischen Wechselwirkungen in Wasser stellen zusätzliche Hürden bei der Entwicklung konsistenter vergröberter Modelle dar. Dennoch kann gezeigt werden, dass Bottom-up informierte Gedächtnisfunktionen dynamische Eigenschaften recht gut korrigieren können. Um eine exakte Übereinstimmung zwischen hochaufgelösten und vergröberten Geschwindigkeitsautokorrelationsfunktionen zu erreichen, wird die vielversprechendste der neu entwickelten iterativen Methoden (in diesem Kapitel als *iterative optimization of memory kernels* (IOMK) bezeichnet) erfolgreich eingesetzt. Außerdem wird gezeigt, dass die IOMK-Methode etwa zehnmal effizienter ist als das beste alternative, zuvor in der Literatur vorgeschlagene, Optimierungsverfahren. Durch die Untersuchung dynamischer Eigenschaften jenseits von Einzelteilchenzeitkorrelationsfunktionen, der Van-Hove-Funktion als Maß für zeitabhängige Korrelationen der Teilchendichte, wird festgestellt, dass die IOMK-Methode sehr genaue Ergebnisse liefert und insbesondere, dass Markov'sche Modelle nicht ausreichen, um vergleichbar gute Ergebnisse zu erzielen. Durch den Vergleich verschiedener vergröberter konservativer Wechselwirkungen wird außerdem die Rolle von Mehrteilchenwechselwirkungen auf die

strukturelle Relaxation von Wasser diskutiert.

Einige vorläufige und bisher unveröffentlichte Ergebnisse und Ideen, die als Motivation für weitere Forschung dienen können, werden in Kapitel 7 diskutiert. In Abschnitt 7.1 werden die Herausforderungen bei einer naiven Anwendung der IOMK-Methode auf Systeme, die Bindungen auf der vergröberten Skala enthalten, diskutiert. Solche Abbildungsschemata führen zu hochfrequenten Moden in den vergröberten Skala. Es wird ein Glättungsansatz vorgeschlagen, um auf die relevantesten Merkmale zuzugreifen und so Gedächtnisfunktionen zu erhalten, die vergleichbar gute Ergebnisse wie bei Einteilchenabbildungsschemata liefern. In Abschnitt 7.2 wird eine Implementierung der IOMK-Methode als Gauß-Newton-Methode vorgeschlagen, die es ermöglicht, einige wenige Parameter direkt zu optimieren, die direkt als Eingabeparameter für den genutzten Thermostaten genutzt werden können. Ein solcher Ansatz würde das Verfahren der IOMK-Methode weiter vereinfachen und damit seine Anwendbarkeit als standardisiertes Werkzeug für dynamisch konsistente vergröberte Modelierung verbessern.

Das letzte Kapitel enthält eine Zusammenfassung und einen Ausblick auf zukünftige Forschung.

Contents

1 Introduction

As humans, our experience of every day life is based on the perception of objects on a macroscopic scale. At the latest with the confirmation of the atomic theory of matter it is well accepted that any observation or measurement on length and time scales of human perception can only yield a *coarse* description of reality, neglecting many details at a higher resolution. Within the modern sciences many different sub-fields emerged, wherein nature is studied on all perceivable length and time scales, ranging from the very small subatomic constituents of matter to motion of galaxies and the evolution of the whole universe. Arguably, the holy grail of theoretical physics is to develop a "theory of everything"; this is to find a description of nature based on simple and irreducible fundamental principles from which every other effective theory can be deduced, at least in principle. While this reductionist perspective has been very successful in the recent centuries in furthering our understanding of nature, in practice it often is of little use to describe physical systems beyond a few molecules in terms of the evolution of the systems wave-function following Schrödinger's equation. Different problems on different scales can be successfully described and understood based on different effective theories, using different mathematical and experimental tools. While it can be reasonably assumed that every observation which is beyond the reach of a quantum mechanical description can be understood as emerging from more fundamental descriptions, it is often useful to rely on effective theories which allow to directly incorporate emergent phenomena as essential constituents of the coarse-grained (CG) theory.

The concept of coarse-graining is ubiquitous in physics, even if the term is not always employed explicitly. One of the oldest and maybe most prominent examples in modern physics is the description of planets as point masses following Newtons laws. A hierarchy of theories and associated computational methods allows to describe condensed matter systems on different length and time scales. Starting from quantum dynamics for the description of the evolution of electronic degrees of freedom, to molecular dynamics with classical atomistic force-fields, for the description of the motion of nuclei, to stochastic mesoscopic models as Brownian dynamics, for the description of micron sized constituents, to for example fluid dynamics for the description of macroscopic systems.[1] The mentioned examples (which is an incomplete list of relevant theories and methodologies) follow very distinct rules and at every step of coarsening the description, certain assumptions and approximations have to be made which neglect details from the more fine-grained (FG) descriptions. Being confronted with this hierarchy, one can take two distinct approaches to model a given system of interest. One can start from the top-down, and ask the question of how one can model a given system at a length and time scale of interest with the appropriate theory. Alternatively, one can start from the bottom-up and ask the question of how do CG properties emerge from the underlying FG constituents.

In the field of molecular dynamics (MD) simulations, CG modeling refers to the reduction of complexity in the representation of the system by reducing the number of explicitly modeled interaction sites. These interaction sites are often referred to as beads and are typically used to represent a collection of atoms.[2–7] The strategies of modeling the interactions between such CG beads in CG models can also be roughly categorized into *top-down* and *bottom-up* methods. Herein, a top-down approach is comparable to the common approach of deriving all-atom molecular dynamics models, that is, one chooses a set of experimentally accessible properties of the system one wishes to reproduce and optimizes the parameters of

the model accordingly. The same can be done for top-down CG models. A prominent example for top-down derived CG models is the Martini force field in which the non-bonded interactions are modeled to reproduce experimental partitioning of free energies between polar and apolar phases.[8] Bottom-up CG models are derived directly from FG, often all-atom (AA), models. Here the parameterization of the CG model is informed by reference FG MD simulations. Herein, different strategies can be employed. In structural coarse-graining iterative optimization methods are used which systematically adjust CG pair-potentials until the pair structure in terms of the radial distribution function (RDF) of the mapped reference system is reproduced. Prominent methods following this strategy are the iterative Boltzmann inversion (IBI) method,[9] the inverse Monte Carlo (IMC) method[10] or the hypernetted-chain (Gauss-) Newton method (HNC(G)N).[11, 12]

CG potentials, if appropriately constructed, when used in conjunction with standard molecular simulation methods as MD, can capture certain features of the underlying reference system. But whenever a physical system is described on a CG scale, one has to ask the question: what emergent phenomena occur on the CG scale which are not explicitly part of the underlying FG theory and how should an effective theory on the CG scale look like, to appropriately capture these emergent features?

In the context of MD simulations of e.g. molecular liquids, the thermal motion of molecules leads to a perpetual exchange of energy between different molecules which, on a CG scale, occur as friction and random fluctuations. In the underlying theory, Hamiltonian mechanics, there is no notion of friction and randomness. These features only emerge on the CG scale. Thus, naively using the same equation of motion (EoM) from Hamiltonian mechanics to describe the dynamics on a CG scale is bound to fail.

Consequently, it is well known[13–15] that CG-MD simulations fail to capture dynamic properties. Due to the neglect of friction and random fluctuations, standard CG-MD models always yield a mismatch of timescales compared to the FG reference due to accelerated dynamics. This can be utilized as a positive feature, as it allows for more rapid equilibration, more efficient sampling and thus, adding to the reduction of DoFs, further decreases computation time and thus costs. Also, there are attempts to improve the understanding of speed-up in CG-MD simulations with the aim to predict the correct speed-up factors in CG models such that the predictive power for dynamical properties can be preserved through rescaling of timescales. [16–21]

An alternative to the rescaling of time-scales, is to explicitly adjust the EoMs governing the dynamics of CG molecular systems by explicitly introduce friction and noise. The derivation of such effective CG EoMs has been formalized in terms of the Mori-Zwanzig theory (often referred to as projector operator formalism) [22–25]

The Mori-Zwanzig theory is a general and exact formalism, which allows to derive an effective EoM for an arbitrary set of CG variables of interest from the Hamiltonian dynamics of the FG DoFs. It is the exactness of the Mori-Zwanzig theory which makes its application for CG modeling quite challenging, as it effectively encompasses all details and thus complexity of the underlying FG Hamiltonian description. Thus, in practice approximations have to be employed to ensure tractability. Nonetheless, the Mori-Zwanzig theory allows to understand the emergent features of CG EoMs and thus can inform the process for accurate CG modeling. When applied in the context of molecular coarse-graining, the Mori-Zwanzig theory yields integro-differential equations, which can be interpreted as variants of generalized Langevin equations (GLEs), a non-Markovian generalization of the well known Langevin equation.

While different forms of GLEs are applied in different contexts, the current work focuses of the application of GLEs of the form

$$\boldsymbol{F}_I(t) = \boldsymbol{F}_I^C(t) - \int_0^t ds \tilde{K}(t-s)\boldsymbol{P}_I(s) + \tilde{\boldsymbol{F}}_I^R(t), \tag{1.1}$$

whereby $\boldsymbol{F}_I(t)$ is the force acting on a CG bead I, $\boldsymbol{F}_I^C(t)$ is a conservative force contribution (typically from

a CG potential approximating the multi-body potential of mean force (MB-PMF)), $\boldsymbol{P}_I(t)$ is the momentum of CG bead I and $\tilde{\boldsymbol{F}}_I^R(t)$ is a random force, at time t.

The GLE includes an explicit dependency on the history in the second term and thus for the time propagation of the system knowledge about the current state is not sufficient, in contrast to Markovian equations. This dependency on the past is encoded in the *memory kernel* $\tilde{K}(t)$. Additionally, the stochastic term ($\tilde{\boldsymbol{F}}_I^R(t)$) in GLEs is modeled in terms of colored noise; this means random terms which have finite correlations in time.

Non-Markovian behavior (memory/memory effects) arise due to the change of resolution, because the response in the dynamics of FG DoFs upon the dynamics of CG DoFs has a finite lifetime. When "aggressive" coarse-graining is applied, i.e. the change of scales between FG and CG resolution is large, the relevant time scales of the CG DoFs might be well separated from the time scales of FG relaxation processes and thus Markovian behavior can be assumed. Whenever the timescales of FG and CG dynamics have a significant overlap, memory effects have a significant impact upon CG dynamics and thus cannot safely be ignored in CG modeling without introducing significant errors.

In recent years, substantial progress has been made towards deriving systematic approaches for deriving Markovian and non-Markovian dissipative models for reproducing dynamic properties of FG reference models in CG molecular simulations.[15] To a larger extent, the focus has been on Markovian approaches with the aim to correctly model long time diffusion processes. The literature on non-Markovian CG modeling of molecular systems is comparably sparse but in recent years the interest on this topic seems to be on the rise.[15, 24, 25] For example, Karniadakis *et al.*[26–28] and Voth et al.[29] developed methodology to parameterize and simulate non-Markovian dissipative particle dynamics (NM-DPD) models and Jung *et al.*[30] worked on developing non-Markovian CG implicit-solvent models of colloids with an explicit consideration of non-Markovian hydrodynamic interactions. These approaches encode the effects of FG DoFs on CG dynamics to a very high detail through configuration dependent memory terms and the introduction of cross-correlations between CG DoFs. While fundamentally very promising, the derivation of such CG models is quite sophisticated and CG simulations are quite costly. Eq. 1.1 however, due to its relative simplicity, can be integrated very efficiently while preserving the capability of explicitly modeling memory effects. Models utilizing Eq. 1.1 were also explored by different groups.[31, 32] For the parameterization of the memory kernel, Han *et al.*[31] used a bottom-up approach based on the inversion of Volterra Equations (see chapter 3 for more details) while Wang *et al.*[32] used a data-driven optimization process. The bottom-up approach, while yielding good results for the test case studied by the authors, tends to underestimate diffusion coefficients [33] and introduces errors in the detailed dynamics on shorter time scales.[34] The approach proposed by Wang *et al.*,[32] by construction, allows to reproduce the single-particle velocity autocorrelation function (VACF) and thus also the diffusion coefficient very accurately, but its parameterization relies on up to thousands of CG test simulations for the optimization process and is thus quite expensive.

Also, while it is understood that Eq. 1.1 can only be approximate[35] the range of applicability and limitations of Eq. 1.1 for dynamic CG modeling is not well explored. The work described in this thesis attempts to advance methodological developments while also improving the understanding of potential short-comings of the chosen approaches to guide future research. Thus, the current work attempts to illuminate the following questions:

1. How can a CG GLE model of the form of Eq. 1.1 be parameterized in a purely bottom-up approach to accurately represent dynamic properties of the FG reference model?

2. How can we understand and improve upon shortcomings of previously proposed bottom-up methods?

3. Similar to iterative methods in structural coarse-graining, can we derive an efficient and stable iterative

procedure to optimize GLE-thermostat parameterization to match target dynamic properties?

4. How does the introduction of memory effects in CG models affect dynamic properties?
5. What is the role of the CG conservative potential in the representation of dynamic properties and on the reliability of parameterization strategies of the GLE-thermostat?
   a) What are the effects of errors in the CG potential on dynamic properties in CG models?
   b) What are the limitations due to inherent approximations of the chosen approach?
6. To what extent does the agreement between targeted properties (the VACF in the context of the current work) translate to agreement between other dynamical quantities that were not explicitly targeted in the model?

This thesis is based on four peer-reviewed articles, which constitute the main chapters. Thereby one article, reproduced in chapter 2 is a review, which provides a broad overview on the literature of Markovian and non-Markovian modeling in dynamic CG molecular dynamics. The other three articles, reproduced in chapters 4-6 constitute original research addressing the aforementioned questions, and constitute the main part of this thesis.

In chapter 4, a novel purely bottom-up approach for the parameterization of GLE-thermostats for CG modeling is presented. This work was motivated by the Work of Lei *et al.*,[36] who derived CG Markovian Langevin models by explicitly neglecting the cross-correlations in the friction. The authors found that their approach leads to a significant underestimation of diffusivities, hinting to the fact that some effectively accelerating contribution to the friction were not considered. The aim of chapter 4 is to better understand the effect of the neglected contributions to the overall friction and to find a way to estimate the missing contributions in a bottom-up approach. Using the test case of a generic star polymer melt in chapter 4, a method is proposed to identify these missing contributions. With that, questions 1. and 2. are addressed. Alongside these key findings, question 4. is addressed by discussing the difference in long-time diffusivity in non-Markovian models compared to otherwise equivalent Markovian models. A key hypothesis, based on the results of chapter 4, is that modeling errors in the conservative potential are the main contributors of remaining errors in dynamic properties, namely the single-particle VACF, in the developed CG models.

To test this hypothesis, a test system is needed in which the quality of the conservative potential can be well controlled. To that end, in chapter 5 the newly developed approach is applied to coarse-grain (continuous) the Asakura-Oosawa model, where the MB-PMF can be exactly derived (within numerical accuracy).[37, 38] In these models, modeling errors in the conservative potentials are negligible and thus a better understanding of the bottom-up parameterization methodology and potential limitations of the chosen EoM can be achieved. With that, questions 5. a) and b) are addressed, in addition to serving as a validation of the results of chapter 4. Additionally, three novel iterative optimization schemes for memory kernels in many-body simulations are developed, which allow to target and achieve an exact match of the single-particle VACF in many-body CG simulations.

While in chapters 4 and 5 idealized, generic systems are considered, coarse-graining realistic molecular systems poses additional challenges. In chapter 6, the application of of the prior developed methods is explored for coarse-graining an atomistic water model. Attractive interactions, electrostatics, and strong multi-body correlations increase the difficulty in deriving accurate CG models. In particular in water, in which the dynamics is governed through quite stable transient hydrogen bond networks, it is not *a-priori* clear how well the proposed methods perform in this context. As the bottom-up informed models rely on accurate CG potentials modeling errors have to be expected. Different potentials for CG water models are explored to further the understanding of the influence the choice of the CG potential has upon dynamic properties, when used in non-Markovian GLE simulations. The most promising of the iterative optimization

schemes, introduced in chapter 5 (IOMK method), is compared to iterative methods for memory kernel optimization proposed by Jung *et al.*.[30, 39] Finally, structural relaxation in terms of the distinct Van Hove function is studied to evaluate how well dynamic properties which are not explicitly considered in the parametrization process can be reproduced with models following Eq. 1.1, thus tackling question 6.

2 Introducing Memory in Coarse-grained Molecular Simulations.

Abstract

Preserving the correct dynamics at the coarse-grained (CG) level is a pressing problem in the development of systematic CG models in soft matter simulation. Starting from the seminal idea of simple time scale mapping, there have been many efforts over the years towards establishing a meticulous connection between the CG and fine-grained (FG) dynamics based on fundamental statistical mechanics approaches. One of the most successful attempts in this context has been the development of CG models based on the Mori-Zwanzig (MZ) theory, where the resulting equation of motion has the form of a generalized Langevin equation (GLE) and closely preserves the underlying FG dynamics. In this review, we describe some of the recent studies in this regard. We focus on the construction and simulation of dynamically consistent systematic CG models based on the GLE, both in the simple Markovian limit and the non-Markovian case. Some recent studies of physical effects of memory are also discussed. The review is aimed at summarizing recent developments in the field while highlighting the major challenges and possible future directions.

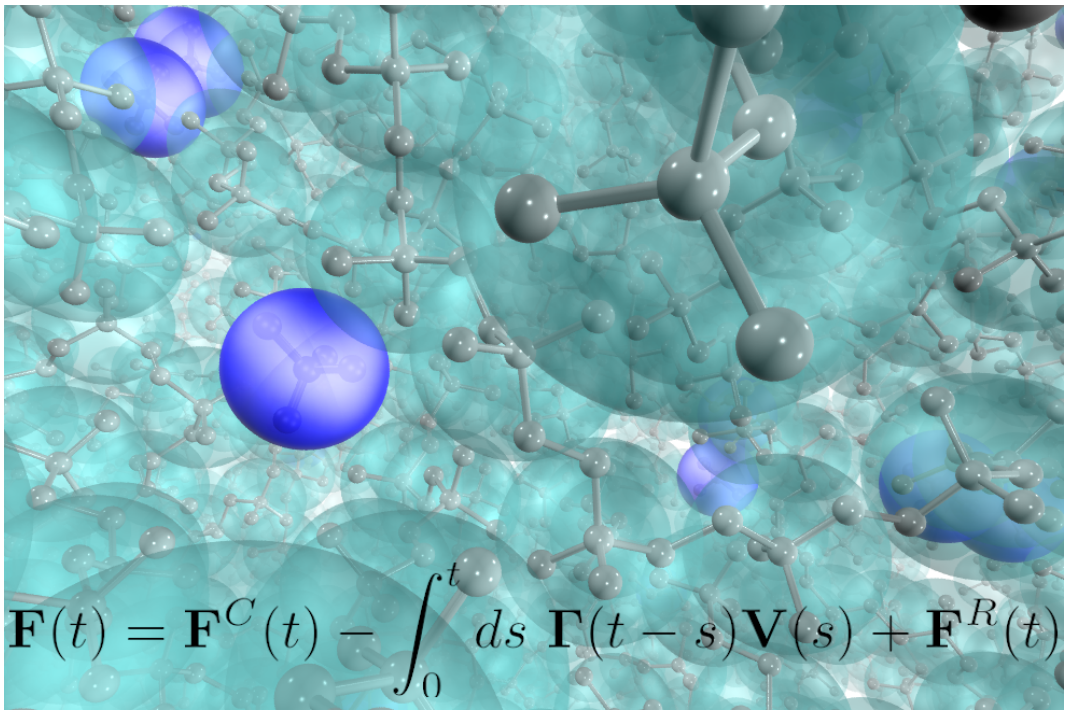

2.1 Introduction

The development of methods for dynamically consistent systematic coarse-grained simulations is a relatively new and promising research area in the field of soft matter simulations. In this review, we discuss the current state of affairs of introducing memory effects in coarse-grained molecular simulations. We particularly focus on recent methodological advances, highlighting the underlying challenges and capabilities. For alternative approaches in the field of dynamic coarse-graining and systematic coarse-graining methods based on structural and thermodynamic properties, we refer the reader to other recent reviews.[4, 15, 40–42]

The 1998 twin papers by Tschöp *et al.*[13, 14] have been seminal in the field of systematic coarse-graining of soft matter systems. They paved a new route for linking chemistry and properties of polymers based on ideas to map between a fine-grained (FG: high resolution) and a coarse-grained (CG: low resolution) configuration space in, both, forward and backward directions. Regarding the dynamics of the CG system, they made two important observations. First, they showed that structural quantities equilibrate faster and more efficiently in CG models, which is a good news from a sampling point of view. Second, in order to recover quantitatively reliable information on the dynamics of the system as well, they introduced the novel concept of time scale mapping: They proposed to identify the (reduced) time scale in the asymptotic long time regime of the CG molecular dynamics (MD) simulation with the corresponding experimental time scale by comparing the predicted melt viscosity (within the Rouse model) with its experimental counterpart.[13, 16] In later approaches, monomer mean-square displacements of the FG and CG models were used to define a so-called time-mapping (or speed-up) factor, effectively accounting for the lost friction of the fast atomistic degrees of freedom (DoF) in the CG model.[16, 43–45]

Applying this *a posteriori* time mapping procedure to CG MD simulation trajectories led to several successful quantitative predictions of dynamical properties on time and length scales, which went far beyond those that could be addressed with detailed atomistic simulations. These include dynamic chain scattering functions, [43] self-diffusion coefficients and viscoelastic properties of unentangled and entangled, high molecular weight, polymer melts.[46] Furthermore, the diffusive dynamics of small penetrant molecules in a polymer matrix (ethylbenzene in polystyrene) could be described with CG models and time mapping procedures in quantitative agreement with experiments, achieving transferability over a wide range of temperatures.[47, 48] This, heuristic, time mapping technique was the first to successfully link chemistry and dynamic properties of polymers used in daily life. However, the applicability of the approach was mostly limited to homogeneous single component systems. In the case of small penetrant diffusion in a polymer matrix, even though the temperature dependence of penetrant diffusion coefficient was in agreement with experiments, the scaling factor differed for the two components (polymer and penetrant) within the same system and depended on the composition of the binary system.[19]

The scale (or speed-up) factors, in general, depend on the simulation state point and system properties such as polymer tacticity, solvent volume fraction, *etc.* Several studies have attempted to predict this speed-up factor in simulations based on relative entropy, interactions, and mechanical considerations. [20, 49, 50] While this speed-up factor allows to quantify the dynamics at the CG level in agreement with the FG counterpart, its choice is rather empirical. Moreover, it relies on the existence of a single CG time scale corresponding to the long time diffusive limit. However, in multi-component systems where the overall dynamics of a system is governed by relaxation mechanisms on distinct time scales, coarse-graining affects the various energy barriers differently, thereby accelerating the dynamics of the various component to different extents. In realistic chemical systems with moderate degree of coarse-graining, such effects are expected to be more pronounced and therefore, the use of a simple time scale mapping approach is severely limited.

One way of preserving the real FG dynamics in a CG system is to apply the fundamental statistical

approach based on the generalized Langevin equation (GLE), where the friction resulting from the lost DoF upon coarse-graining is explicitly taken into account. Over the past two decades, such an approach has been formalized based on the Mori-Zwanzig (MZ) theory, [22, 23, 51, 52] which can, in fact, be viewed as one of the first rigorous theories of systematic coarse-graining. Starting from an underlying microscopic system with Hamiltonian dynamics, the MZ formalism uses projection operators to derive an exact equation of motion (EoM) for a reduced set of relevant variables at the CG level. The resulting EoM has the form of a GLE, with frictional and random forces coupled through the fluctuation-dissipation theorem (FDT). The GLE is non-Markovian as the instantaneous force depends on the entire dynamical history of the system, unlike the Hamiltonian EoM. However, depending on the nature of the system of interest this 'memory' can sometimes be short lived, in which case it can be replaced by an instantaneous friction term. The GLE can then be approximated by a simpler stochastic equation: the Langevin equation (LE). While analyzing the non-Markovian GLE in simulation is nontrivial and computationally demanding, several studies have attempted to employ this approach to investigate the dynamical properties of various chemical systems. In this review, we will highlight some of the recent works along this line.

The aim of this review is to summarize the recent methodological developments in the field of dynamically consistent systematic coarse-graining. We particularly focus on studies which employ GLEs to analyze and/or simulate physico-chemical systems based on the underlying FG dynamics. A concise, but not exhaustive, list of studies are briefly discussed to motivate the fundamental background and methodological progress. For a more general discussion on consistency of dynamics in CG simulations, readers are referred to another recent review. [15]

The present review is organized as follows. The GLE as derived from the MZ formalism is briefly discussed in Section 2.2. Section 2.3 describes selected studies that employ a Markovian approximation to the GLE. While highlighting the usefulness of the Markovian assumption, these studies also demonstrate the need to explicitly include memory effects depending on the nature of the underlying FG system. Section 2.4 discusses various possible ways to extract the memory kernel from FG trajectories with special focus on single diffusing particles. Strategies to go beyond single-particle systems and use GLE-based modeling in coarse-graining and multiscale modeling are reviewed in Section 2.5. A crucial issue in such simulations is the availability of efficient GLE integrators. Different approaches have been proposed, some based on straightforward integration and some based on techniques that introduce auxiliary variables to map the GLE on a system of coupled Markovian Langevin equations in an extended space. These are discussed in Section 2.6. Section 2.7 highlights selected recent studies of systems where memory effects have a qualitative impact on the dynamical behavior. We conclude in Section 2.8 with a discussion on open questions and possible future directions.

2.2 Mori-Zwanzig Formalism

The Langevin equation (LE), introduced by Paul Langevin in 1908,[53] is a prototypical example of a CG EoM. It is used to model the dynamics of a heavy Brownian particle dispersed in a fluid and describes it solely via a dynamical equation for the momentum of the Brownian particle itself, while its interactions with the fluid particles are modeled implicitly by frictional dissipation and impacts. For a given viscosity of the fluid and size of the Brownian particle, dynamical properties can be derived from the LE. The formal connection between the atomistic description of Brownian dynamics based on the Hamiltonian equation with all DoFs and a CG description of the form of a LE was established by Mori[22] and Zwanzig[51] based on a projection operator formalism. [23] In this section, we briefly summarize the main ideas behind the Mori-Zwanzig (MZ) theory as discussed in Ref. [23] and recent extensions in the context of dynamic coarse-graining.

The projection operator formalism is based on the idea that any dynamical variable for a given

Hamiltonian system can be described as a vector in a Hilbert space, consisting of a vector space spanned by a set of orthonormal basis functions and an inner product. The choice of the inner product is crucial for a consistent coarse-graining procedure. In equilibrium the most common choice is the phase space integral

$$(A, B) = \int dX f_{eq}(X) A(X) B^*(X) = \langle AB^* \rangle_{eq}\,, \tag{2.1}$$

for two arbitrary observables $A(X)$ and $B(X)$, phase space points X, and equilibrium probability distribution f_{eq}. The inner product, $(A, 1)$, thus corresponds to the usual phase space average.

In general, not all dynamical variables are of interest. For example, in coarse-graining, the central idea is to average over the fast microscopic processes and just keep a small number of slow effective variables that can represent a system on larger length and time scales. Having defined an inner product in the microscopic system now allows us to formally select some variables to be relevant (i.e., slow representatives) and others to be irrelevant via the introduction of a projection operator. Based on Eq. (2.1), a projection operator, $\mathcal{P}$, can be defined, which projects any dynamical variable B onto the subspace of relevant variables $\{A_j\}$, as

$$\mathcal{P}B = \sum_j \sum_k (B, A_j) \left[(A, A)^{-1}\right]_{jk} A_k. \tag{2.2}$$

Here, (A, A) denotes the $n \times n$ matrix of inner products (A_i, A_j), where n is the dimensionality of the relevant subspace. In the following, we will restrict ourselves to the one-dimensional case, which can easily be generalized to n dimensions.

$$\mathcal{P}B = (B, A)(A, A)^{-1} A. \tag{2.3}$$

With these definitions and starting from the Liouville equation

$$\frac{\partial}{\partial t} A(t) = \mathcal{L} A(t), \tag{2.4}$$

after some mathematically exact reordering which is described in detail in Ref. [23], a CG EoM for $A(t)$ can be derived as

$$\frac{\partial}{\partial t} A(t) = \mathrm{i}\Omega A(t) - \int_0^t \mathrm{d}s K(s) A(t - s) + F^R(t), \tag{2.5}$$

which has the form of a generalized Langevin equation (GLE). Here we have introduced the frequency matrix,

$$\mathrm{i}\Omega = (\mathcal{L}A, A)(A, A)^{-1}, \tag{2.6}$$

and the "noise",

$$F^R(t) = e^{t\mathcal{Q}\mathcal{L}} \mathcal{Q}\mathcal{L}A, \tag{2.7}$$

where $\mathcal{Q} = 1 - \mathcal{P}$ is the projector on the irrelevant dynamical variables. The extended time-evolution operator, $e^{t\mathcal{Q}\mathcal{L}}$, is often referred to as "orthogonal", "projected" or Q-dynamics. Finally, the memory kernel is formally given by,

$$K(t) = -(\mathcal{L}F^R(t), A)(A, A)^{-1}. \tag{2.8}$$

Eq. (2.5) is an exact reformulation of the original Liouville equation. Being in the form of a GLE, the interpretation of $F^R(t)$ as a random process allows to model the irrelevant variables of the original problem by a stochastic process with equivalent statistical properties. To illustrate the meaning of the separate terms in Eq. (2.5), we can assume the simplest case, in which the relevant variable is given by the momentum of a single particle $A(t) = p(t)$. We can then write the frequency matrix Ω as

$$\mathrm{i}\Omega = (\mathcal{L}p, p)(p, p)^{-1} = \frac{\langle Fp \rangle}{m k_B T} = 0, \tag{2.9}$$

where $F = \frac{\mathrm{d}}{\mathrm{d}t}p = \mathcal{L}p$ is the total force on the tagged particle. Here, Ω vanishes due to the fact that the dynamics are time-translationally invariant and the Liouville operator is anti-Hermitian[1]. The scalar memory function, in this case, is given as

$$K(t) = -(\mathcal{L}F^R(t), p)(p,p)^{-1} = (F^R(t), \mathcal{L}p)(p,p)^{-1} = \frac{\langle F^R(t)F^R(0)\rangle}{mk_BT}, \tag{2.10}$$

where we have exploited $\mathcal{P}F^R(t) = 0$ and $F^R(0) = (1-\mathcal{P})\mathcal{L}p$. Eq. (2.10) relates the random force $F^R(t)$ with the memory kernel $K(t)$ and is usually referred to as the second fluctuation-dissipation theorem (FDT). It should be noted that the derivation of the FDT only requires the assumption of an anti-Hermitian Liouville operator $\mathcal{L}$ and the definition of an inner product. The second FDT should thus be seen as a mathematical identity, which is valid independent of the specific choice of the inner product and which can even be extended to non-stationary systems [54]. Having identified the different contributions to the GLE, we can rewrite the full EoM for the single Brownian particle as

$$\frac{\mathrm{d}\,p(t)}{\mathrm{d}t} = F(t) = -\int_0^t \mathrm{d}s\ \Gamma(s)\, v(t-s) + F^R(t). \tag{2.11}$$

with $\Gamma(t) = mK(t)$.

If $A(t)$ stands for a set of momenta of different particles rather than the momentum of a single tagged particle in one dimension, the vector $\Omega A(t)$ in Eq. (2.5) represents linearized interaction forces between the particles. Importantly, since the MZ formalism is a purely linear theory, any non-linear contributions to the associated potential of mean force (PMF) or any non-linear friction terms will be absorbed in the distribution of the random forces and a renormalized memory kernel.

This structure is difficult to reconcile with standard philosophies of coarse-graining, where a clear distinction is typically made between external driving forces, conservative interactions that determine the stationary distribution of the variables at thermodynamic equilibrium (the Boltzmann distribution), and dissipative forces that determine the dynamics and the entropy production in non-equilibrium. [55, 56] Making such distinctions helps to devise coarse-grained models that are thermodynamically consistent by construction, and are thus clearly desirable.

To overcome these shortcomings of the MZ formalism, modified projection operator formalisms have therefore been proposed [57, 58], which allow to separate conservative and dissipative forces. Kinjo and Hyodo derived the equation of motion (EoM) for CG clusters of microscopic particles. A monoatomic fluid served as the microscopic system, while clusters of several atoms formed the CG particles, with centers at the respective center of masses (CoMs). The resulting CG EoM has the form of a GLE,

$$\frac{\mathrm{d}\boldsymbol{P}_I(t)}{\mathrm{d}t} = \boldsymbol{F}_I^C([\boldsymbol{X}(t)]) - \sum_{J=1}^{N}\int_0^t \mathrm{d}s\ \boldsymbol{\Gamma}_{IJ}(t-s)\boldsymbol{V}_J(s) + \boldsymbol{F}_I^R(t), \tag{2.12}$$

where $[\boldsymbol{X}, \boldsymbol{P}]$ defines the $6N$-dimensional phase space of CG particles. The first term on the *r*.h.s. represents the conservative force on the CG particle I, which now, indeed, corresponds to the gradient of the PMF. The second term represents the friction force (dissipation) due to the removed DoFs and involves the integral of the product of the memory kernel matrix, $\boldsymbol{\Gamma}_{IJ}$, with the velocities $\boldsymbol{V}_J(t) = M_J^{-1}\boldsymbol{P}_J(t)$ of all other particles. In general, $\boldsymbol{\Gamma}_{IJ}$ may be different for all pairs I, J and depend on their state (i.e. on the relative distance between particles I and J). The third term represents the random force, which is related to the friction term via the FDT

$$\left\langle \boldsymbol{F}_I^R(0)\boldsymbol{F}_J^R(t)\right\rangle = k_\mathrm{B}T\ \boldsymbol{\Gamma}_{IJ}(t). \tag{2.13}$$

[1] If the microscopic dynamics is diffusive and not Hamiltonian, a similar formalism can be applied. In this case, the frequency matrix Ω might not vanish.

In structural coarse-graining, multibody contributions to the PMF are often neglected and the conservative forces are pairwise decomposed, $\boldsymbol{F}_I^C \approx \sum_{J\neq I} \boldsymbol{F}_{IJ}^C$. If one additionally neglects many-body correlations in the friction forces, Eq. (2.12) can be reformulated as [27]

$$\frac{\mathrm{d}\boldsymbol{P}_I(t)}{\mathrm{d}t} = \sum_{J\neq I}\left[\boldsymbol{F}_{IJ}^C(\boldsymbol{X}_{IJ}(t)) - \int_0^t \mathrm{d}s\, \boldsymbol{\Gamma}_{IJ}^{\mathrm{DPD}}(t-s)\boldsymbol{V}_{IJ}(s) + \boldsymbol{F}_{IJ}^R(t)\right], \tag{2.14}$$

with relative positions $\boldsymbol{X}_{IJ}(t) = \boldsymbol{X}_I(t) - \boldsymbol{X}_J(t)$ and velocities $\boldsymbol{V}_{IJ}(t) = \boldsymbol{V}_I(t) - \boldsymbol{V}_J(t)$ of particles I and J. This pairwise GLE corresponds to a non-Markovian formulation of the EoM of dissipative particle dynamics (DPD).[59]

All generalized Langevin equations presented in this section are clearly non-Markovian, but they can be reduced to Markovian variants under specific assumptions (see Section 2.3 for details). In the case of a freely diffusing Brownian particle, the Markovian variant of the GLE (2.11) is the standard LE,

$$\frac{\mathrm{d}\,p(t)}{\mathrm{d}t} = -\gamma v(t) + F^R(t), \tag{2.15}$$

where $\gamma = \int_0^\infty \mathrm{d}t\, \Gamma(t)$ is the friction coefficient. The random force, F^R now describes uncorrelated white noise and is related to the friction coefficient via the usual FDT,

$$\left\langle F^R(0)F^R(t)\right\rangle = 2k_{\mathrm{B}}T\gamma\delta(t). \tag{2.16}$$

In a similar way, the Markovian version of the pairwise GLE as derived in Eq. (2.14) can be reduced to the DPD EoM,

$$\frac{\mathrm{d}\boldsymbol{P}_I(t)}{\mathrm{d}t} = \sum_{J\neq I}\left(\boldsymbol{F}_{IJ}^C(\boldsymbol{X}_{IJ}(t)) - \gamma_{IJ}\boldsymbol{V}_{IJ}(t) + \boldsymbol{F}_{IJ}^R(t)\right). \tag{2.17}$$

Since they are based on an underlying systematic coarse-graining procedure, these EoMs are thus suitable starting points for the parameterization of molecular CG models in simulations. Examples will be discussed in the following section.

2.3 The Markovian Assumption

While the evaluation of the memory kernel is a central step when constructing dynamically consistent coarse-grained models based on the GLE Eq. (2.12), its implementation in CG simulations is technically nontrivial and computationally expensive. Therefore, Markovian approximations to the GLE have been widely used in simulations.[36, 57, 60–65] The approach assumes the fluctuating forces to be delta-correlated in time, and not temporally correlated as in the non-Markovian case (which similarly holds for the memory kernel). The resulting EoM has the structure of a DPD equation, as defined in Eq. (2.17) and can be implemented in a relatively straightforward manner. This assumption, however, is valid only in the case where the time scales of the fast and slow variables in the system are completely separated: The time scale of the random force fluctuation must be sufficiently fast compared to the time scale of the CG bead motion. Intuitively, such an approximation should hold for high degrees of coarse-graining or systems at low density, where the atomic collisions happen on a much smaller time scale than the change in momentum of the CG beads. Whether or not this is the case can be inferred in simulations from the decay of the force and velocity autocorrelation functions (FACF and VACF): The time scales are well-separated if the former decays much faster than the latter. In contrast, in chemically specific molecular CG models with low to medium degrees of coarse-graining, the time scales of the slow and fast dynamics (the P- and

Q-DoF) are not fully separated and thus, the Markovian assumption breaks down. [63–65] Nonetheless, the Markovian DPD has been extensively used in molecular CG models. Some examples are briefly discussed in this section.

The GLE, as derived following the MZ formalism, takes into account the projected dynamics of the underlying FG system, which is different from the real FG dynamics that one observes in a molecular dynamics (MD) simulation. In such a case, one workaround is the so-called Q-approximation, where the projected (or Q-) dynamics is approximated by the real dynamics, i.e., one assumes for the orthogonal time-evolution operator $e^{t\mathcal{QL}} \approx e^{t\mathcal{L}}$ [36, 58, 65]. This implies $\int_0^\infty \mathrm{d}t \left\langle F^R(t)F^R(0)\right\rangle \approx \int_0^\tau \mathrm{d}t \left\langle F(t)F(0)\right\rangle$ on intermediate time scales τ. While this approach allows for an easier implementation of the CG EoM, it also leads to the well known 'plateau problem', where the friction for finite mass CG particles, as determined from Green-Kubo integrals of the FACF, vanishes on long time scales rather than converging to a finite plateau. [66–68] The existence of a plateau is guaranteed in the infinite mass limit, where the correlation function of the random forces in a GLE equals the correlation function of the total forces.[69] In this limit, the large inertia of the heavy particle ensures a good separation of the time scales of the slow and fast DoFs. In this line, Sanghi *et al.* used the GLE to characterize memory effects in fullerene nanoparticle dynamics and investigated the scaling of the memory kernel with the nanoparticle mass, shape and size. They observed that the FACF and the random force ACF are indeed comparable in the large nanoparticle mass limit. [70] Nonetheless, for finite mass CG models, an intermediate plateau can be found in several cases, and the plateau values can then be taken to determine the friction coefficient.[64, 65]

To circumvent the issue of time scale separation, Hijón *et al.* [60] proposed a scheme in which, by appropriately constraining the MD trajectory of the FG system, the CG dynamics was made exactly Markovian and the resulting Green-Kubo integrals were shown not to suffer from the plateau problem. The theoretical background was developed following the MZ formalism and a star polymer melt was considered as a specific example. The modified dynamics was obtained by constraining the relevant variable, i.e., the CoM of the polymers to their respective positions in a set of configurations and carrying out short independent MD runs from each configuration. The resulting time averaged FACF and its integral (friction), calculated using the constrained MD trajectories, were found to exhibit well-defined plateaus as opposed to those calculated using unconstrained trajectories. Also, the radial distribution function (RDF) and VACF, calculated in the CG simulation, were found to be comparable to their FG counterparts.[60]

Trément *et al.* [62] used the Markovian DPD approach to coarse-grain *n*-pentane and *n*-decane molecules as single DPD beads with degree of coarse-graining (number of carbon atoms per CG bead) $\lambda = 5$ and 10, respectively. The conservative force was calculated in constrained MD simulations as the PMF, and the normal and transverse pair frictions were calculated following Hijón *et al.*[60] The random forces were calculated from the FDT as linear combination of Wiener processes. [71] As expected, the conservative interaction was found to be softer, while the decay of friction became slower with increasing λ. The ratio of the transverse to radial friction also increased, highlighting the role of molecular anisotropy. The models could well reproduce the RDF, the diffusion coefficient, and the viscosity of underlying MD systems of *n*-pentane at 293 K and *n*-decane at 393 K. However, the results of the low temperature *n*-decane DPD simulation were less convincing, owing to the anisotropic shape of the molecules and the fact that the time scales were not well separated. To check the possible transferability of the DPD force field, the authors modeled *n*-decane as a dimer of two *n*-pentane blobs, and interestingly, it could reproduce the low temperature MD results quite well.

Lei, Karniadakis and co-workers [36] employed the GLE EoM as derived by Kinjo and Hyodo [58] to study the behavior of mesoscopic clusters of Lennard-Jones (LJ) particles, constrained within a constant radius of gyration (R_g). Under the Markovian assumption, they investigated the performance of three distinct CG models: 1) using only conservative forces, 2) using a Langevin thermostat and 3) using a MZ DPD thermostat. The first model could only capture the FG structural properties such as the RDF and the

pressure, but not the dynamical properties such as the diffusion coefficient and the viscosity. Furthermore, the resulting dynamical quantities could not even be matched with the corresponding FG results by simple time scale mapping approaches.[19, 46] In the Langevin dynamics, the friction coefficient was calculated using the autocorrelation function (ACF) of the fluctuating forces, and the random force on CG particles were assumed to be independent. The resulting diffusion coefficient was found to be four times smaller than that of the underlying FG system, which was attributed to the missing contribution of the configuration dependence of the frictional and random forces. In the MZ DPD model, the random force was considered to be pairwise additive. For each pair, the memory kernel and the random force were decomposed into the radial and perpendicular contributions. The resulting EoM had the form of a DPD equation, with a transverse friction[72] term in addition to the standard DPD friction term. This CG model could well capture the mean-square displacement (MSD), the diffusion coefficient, and the VACF of the FG system, except in the case of high R_g and high density where many-body correlations are important. In these cases, the Markovian assumption was also found to be inaccurate due to the lack of a clear time scale separation.

In their following work, Li, Karniadakis and co-workers [61] studied melts of star polymers with CG centers at the corresponding CoM. Based on unconstrained MD simulation, they derived various DPD models with increasing degree of complexity: from the standard parameterized DPD model to DPD with radial and transverse forces and frictions and finally DPD with interactions in all three spatial directions that include explicit rotational motion of the CG particles. According to their findings, the absence of transverse interaction at the CG level leads to an underestimation of friction, whereas including it leads to an overestimation in the absence of rotational motion. When the rotation of the CG particles was accounted for in the presence of spatially resolved interactions, the DPD model could reproduce both the short and long time dynamics of the system. As one might expect, all DPD models except for the standard one were able to reproduce the static structure of the FG system in terms of the RDF. Yet again, the results were most satisfactory in cases where the many-body correlations could be neglected and the Markovian assumption is valid, i.e., star polymers with short arms at low density.

With an aim to extend the conditional reversible work (CRW) model [73, 74] to retain dynamical properties, Deichmann *et al.*[63] used a Markovian DPD approach to coarse-grain a set of model molecular liquids, where the dissipative interactions were obtained using constrained simulations [36, 60, 62]: Neopentane, tetrachloromethane, and cyclohexane were coarse-grained into a single interaction site each, with centers at their respective CoMs, and a two site mapping was chosen for *n*-hexane. Based on the integral of FACF, they showed that the Markovian assumption was most inaccurate in the case of *n*-hexane, where the orientation of the CG *n*-hexane was a slow DoF explicitly present at the CG level. For this system, the radial and transverse frictions were found to be comparable, similar to Trément *et al.*, [62] whereas in the other three cases the latter was insignificant. The resulting dynamics in the CRW-DPD simulations showed varying accuracy in comparison to the FG results. The diffusion coefficient of all molecules, except neopentane, were found to be smaller than their FG counterpart when both the radial and transverse frictions were used, mainly due to the overestimation of the friction as previously observed by Lei *et al.*[36] In case of neopentane, however, the agreement with the FG result was very good. As we will discuss later, one possible reason for the varying performance could be the imposed constraints, [75] which affect the dynamics of these molecules to different extents. Nonetheless, the work of Deichmann *et al.* highlighted the issues of long-time tails in the FACF and the lack of time scale separation in molecular models that involve small to medium degree of coarse-graining and multiple CG sites. These factors are relevant in chemical specific coarse-graining of polymers, where the time scales of the FG and CG systems may not be well separated.

Lemarchand *et al.*[64] employed the framework of Hijón *et al.*[60] to coarse-grain *c*is- and *t*rans-1,4-polybutadiene and investigated the validity of the underlying Markovian and the pairwise interaction assumptions. They systematically studied the effect of the degree of coarse-graining (λ) on the ability of

the CG simulation to reproduce the correct dynamical and structural properties of the FG system. They observed that the dynamical properties improved with λ, owing to the better separation of the CG and FG time scales, and thereby, the accuracy of the Markovian assumption. However, the structural properties were found to deviate from those of the FG system with increasing λ due to the presence of many-body effects. Their study also highlighted the effect of constraints on the CG dynamics, where the slow rotation of the CG beads lead to a slower decay of the FACF, an artifact that is not present in unconstrained FG trajectories and had also been observed in previous studies. [63]

In their following work, Deichmann and Van der Vegt [65] performed MZ-DPD simulations of liquids, polymer solutions, and melts, comprising single- and multiple-site CG models of monomers, dimers, and 24mers based on 2,2-dimethylpropane repeat units. They used the effective-force coarse-graining (EF-CG) method[76] to extract the conservative interactions, which also included bonded potentials in the case of the dimer and 24mer. The Q-approximation[36, 58] was employed to calculate the frictional forces from the FACF. [60] They observed long-time tails in the FACFs, which were noticeable in the dimer case and most significant for the 24mer case. These were attributed to the slow rotation of the CG beads which led to a non-zero average fluctuating force on short time scales. The study, thus, highlighted one of the major challenges in multiple-bead representations of small molecules and polymers: Constraining the slow DoF by means of introducing bond connectivity in CG models also slows down the relaxation of intra-molecular DoF of the chemical repeat unit removed upon coarse-graining. The long tails were *a* posteriori fitted to linear functions and subsequently subtracted from the original FACFs, resulting in converging integrals. However, as shown in Fig. 2.1, the authors reported noticeable differences between the FG-MD and MZ-DPD VACF for all the systems under study. At short times, the particle motion is ballistic in FG-MD and dissipative in MZ-DPD, leading to faster decay of the VACF in the latter. On the other hand, elastic collisions of particles lead to a faster decay of the VACF in FG-MD at longer times. The resulting diffusion coefficients were however in good agreement with those calculated from the atomistic MD simulation of the pure liquids of monomers (see the inset of Fig. 2.1a) and dimers. The MZ-DPD model was also found to describe polymer diffusion in polymer solutions (mixtures of dimers and 24mers), especially at low polymer density, in good agreement with FG-MD, as shown in the inset of Fig. 2.1b. Finally, the authors investigated the dynamics of penetrants (monomers and dimers) in networks of long poly(2,2-dimethylpropane) chains in MZ-DPD. As shown in Fig. 2.1c, the resulting long time dynamics in this case was found it to be inconsistent with the FG-MD results. The authors concluded that in case of molecular liquids or polymer solutions, where particle collisions govern their dynamics, the Markovian MZ-DPD approach satisfactorily reproduces the dynamics of the FG system on long time scales, in spite of the deviations at short time scales (as apparent in the VACF). However, when many-body contributions are important (the case of polymer solutions at high polymer concentration) or the dynamics is governed by activated barrier crossing [75, 77, 78] (the case of penetrant diffusion in polymer matrix), the explicit inclusion of memory effects becomes necessary.

These studies, while exploring the viability of the Markovian assumption in molecular coarse-graining, also highlight its limitations. In spite of the relative simplicity, its application has so far been mostly limited to model systems with high degrees of coarse-graining, such as LJ clusters and star polymers at low density, where the Markovian approximation remains relatively accurate. However, this approximation breaks down in cases where chemically specific CG models are used with small to medium levels of coarse-graining. The results of Trément *et al.*,[62] Deichmann *et al.*, [63] and Lemarchand *et al.*[64] have emphasized this point. The work of Deichmann and Van der Vegt [65] has been a step forward towards the use of Markovian DPD in molecular coarse-graining of systems where time scale separation is incomplete. Contrary to standard DPD with soft conservative interactions, their work illustrated that MZ-DPD can be used to serve as a bottom-up-informed thermostat that fixes the long-time diffusive dynamics in the coarse-grained simulations of molecular liquids in which hard-core repulsions are retained. Their work additionally emphasized on the need to incorporate memory effects in the CG model when the dynamics is

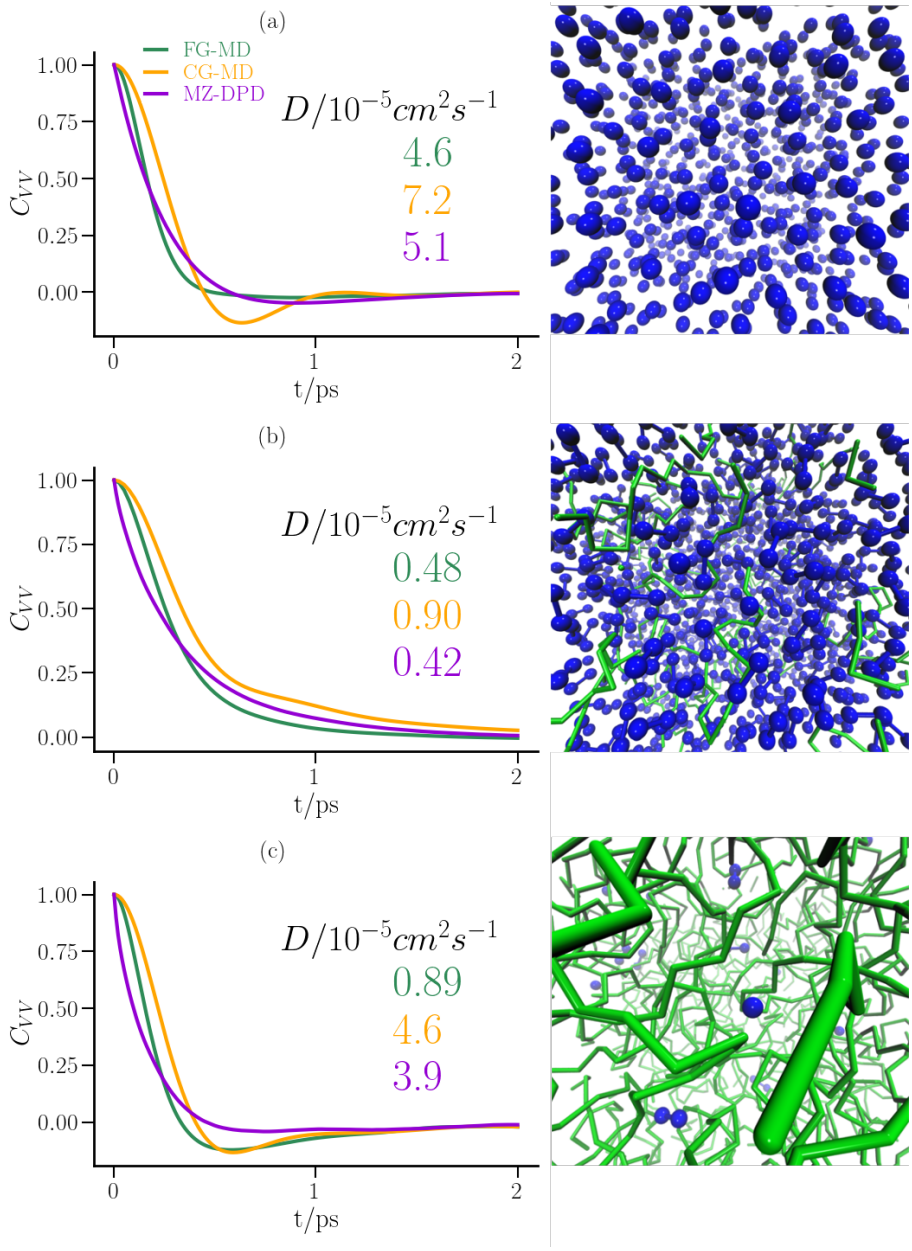

Figure 2.1: VACFs calculated using FG-MD, CG-MD, and MZ-DPD for various poly(2,2-dimethylpropane) systems: VACFs of the CoM of (a) monomers in single component system, (b) 24mers in 25% 24mer - 75% dimer solution, (c) monomers in a network of long poly(2,2-dimethylpropane) chains. The insets compare the corresponding diffusion constants. The right panel shows a representative configuration from each system where monomers are shown as blue beads and 24mers are shown as green chains. In spite of the apparent differences in the VACFs at shorter times, the long time diffusion constants are better reproduced with MZ-DPD than CG-DPD in the first two cases. The CG-MD and MZ-DPD models fail to reproduce the FG-MD monomer diffusion coefficient in the polymer network. Adapted from *J. Chem. Phys.* **2018**, *149*, 244114, with the permission of AIP Publishing.

governed by activated barrier crossing as opposed to particle collisions as in molecular liquids.

2.4 Reconstruction of Memory Kernels

While the original MZ theory was developed already in the early 60's,[22, 51] recently it has regained a lot of attention in the context of dynamic molecular coarse-graining, where the memory kernels are extracted from FG trajectories. As discussed in the previous section, the Q-approximation has been extensively used to parameterize CG DPD models of chemical systems with varying success [60, 62, 65] and the limitations have also been discussed. Recently, attempts are also being made to find solutions for the plateau problem. [79] Nonetheless, the most straightforward way to calculate friction coefficients is to formulate an appropriate GLE for the system under consideration, from which methods for the extraction of the memory kernel can be developed. This not only allows a more accurate determination of friction coefficients, but also enables the study of time- or frequency-dependent phenomena based on the memory kernel. In the case of low-dimensional GLEs, e.g., GLEs for single diffusing particles, it is possible to exactly reconstruct memory kernels (within numerical and statistical errors) from FG simulation trajectories. Several methods have been developed, some of which are reviewed in this section.

We begin with some general remarks. A typical problem in memory reconstruction is to determine memory kernels from a given autocorrelation function $C_{AA}(t) = \langle A(0)A(t)\rangle$ of a target CG observable A that is taken to evolve according to a GLE, Eq. (2.5). Multiplying (2.5) with $A(0)$ and taking the thermal average, one derives an equation for $C_{AA}(t)$

$$\partial_t C_{AA}(t) = \mathrm{i}\Omega C_{AA}(t) - \int_0^t \mathrm{d}s\, K_A(s)\, C_{AA}(t-s). \tag{2.18}$$

In the case $\Omega = 0$, Eq. (2.18) has the form of a Volterra equation of the first kind. It can be inverted numerically, e.g., by Laplace transform. However, from a point of view of numerical stability, it is often more convenient to first take the time derivative, thus converting Eq. (2.18) into a Volterra equation of the second kind [80]

$$\partial_{tt} C_{AA}(t) = \mathrm{i}\Omega \partial_t C_{AA}(t) - K_A(t)\,\langle A^2\rangle - \int_0^t \mathrm{d}s\, K_A(s)\, \partial_t C_{AA}(t-s) \tag{2.19}$$

for which more stable algorithms exist. We note that the time derivatives $\partial_t C_{AA}(t) = C_{\dot{A}A}(t)$ and $\partial_{tt} C_{AA}(t) = -C_{\dot{A}\dot{A}}(t)$ can often be determined directly from simulations, so that it is not necessary to numerically calculate the derivatives of $C_{AA}(t)$.

Alternatively, one can also integrate Eq. (2.18), [81–83] which yields an equation for the running integral over the memory kernel, $G_A(t) := \int_0^t \mathrm{d}s\, K_A(s)$,

$$C_{AA}(t) = \langle A^2\rangle + \int_0^t \mathrm{d}s\, C_{AA}(s)\,\big(\mathrm{i}\Omega - G_A(t-s)\big). \tag{2.20}$$

Replacing the origin of time $t = 0$ by $t = t_0$ throughout and taking the derivative with respect to t_0 for $t_0 \to 0$, one can derive an implicit equation [82] for the quantity $J_A(t) = \mathrm{i}\Omega - G_A(t)$:

$$J_A(t) = j_0(t) - \int_0^t \mathrm{d}s\, j_0(s)\, J_A(t-s) \tag{2.21}$$

with $j_0(t) = \frac{1}{\langle A^2\rangle}\partial_t C_{AA}(t)$. It can either be solved directly by matrix inversion after discretization in time[83] or iteratively[82] by successive application of Eq. (2.21),

$$J_A^{(n)}(t) = j_0(t) - \int_0^t \mathrm{d}s\, j_0(s)\, J_A^{(n-1)}(t-s) \quad \text{with } J_A^{(0)}(t) = j_0(t). \tag{2.22}$$

This method can also be used to determine memory kernels $K(t, t_0)$ in non-stationary non-equilibrium situations.[82] In that case, the Eq. (2.21) for $J_A(t, t_0) = \mathrm{i}\Omega(t) - \int_{t_0}^{t} \mathrm{d}s\, K_A(s, t_0)$ reads

$$J_A(t, t_0) = j_0(t, t_0) + \int_{t_0}^{t} \mathrm{d}s\, \mathcal{S}_0(s_0, s)\, J_A(s, t) \tag{2.23}$$

with $j_0(t, t_0) = \frac{1}{C_{AA}(t_0,t_0)} \partial_{t_0}(C_{AA}(t_0, t_0) - C_{AA}(t_0, t))$ and $\mathcal{S}_0(t_0, t) = \frac{1}{C_{AA}(t_0,t_0)} \partial_{t_0} C_{AA}(t_0, t)$.

The methods described above have been developed for linear GLEs and cannot easily be extended to GLEs that contain anharmonic conservative force terms (as may occur in Eq. (2.12)). In that case, numerical reconstruction methods can be applied that rely on an iterative refinement of $K_A(t)$ based on successive GLE simulations, [30, 39] similar to the iterative Boltzmann inversion (IBI) method in structural coarse-graining.[9]

In the next sections, we will now present specific examples of memory reconstruction methods for low-dimensional GLEs. In multi-dimensional systems, e.g., multi-particle systems, further approximations are necessary, which are mainly discussed in Section 2.5.

2.4.1 Freely Diffusing Particles

In the simplest case of freely diffusing particles, the EoM of a system can be formulated in terms of a GLE without any conservative interactions. For simplicity, we will consider one-dimensional systems. The GLE then takes the form

$$m\dot{v} = F(t) = -\int_0^t \mathrm{d}s\ \Gamma(t-s)\, v(s)\ + F^R(t). \tag{2.24}$$

It describes the CoM dynamics of a tagged particle with velocity v in an isotropic solvent. As discussed earlier, in the limit of large particle mass, Eq. (2.24) can be reduced to a Markovian LE, which describes the motion of a heavy Brownian particle. In the Markovian case, the dynamics is governed by the scalar friction coefficient γ, which determines the diffusion coefficient via the Stokes-Einstein relation, and leads to a VACF that shows an exponential decay and determines the MSD. In a similar way, the memory kernel $\Gamma(t)$ determines the dynamics of a single tagged particle with memory. According to Eq. (2.20), the VACF obeys the relation

$$m\,\langle v(t)v(0)\rangle = m\langle v^2\rangle - \int_0^t \mathrm{d}s\, \gamma(s)\,\langle v(t-s)v(0)\rangle, \tag{2.25}$$

where $\gamma(s) = \int_0^s \mathrm{d}s'\ \Gamma(s')$. Using $\left\langle \Delta x^2(t)\right\rangle = \int_0^t \mathrm{d}t' \int_0^t \mathrm{d}t''\, \langle v(t')v(t'')\rangle$ and the equipartition relation $m\langle v^2\rangle = k_B T$, one can derive an equation for the mean square displacement (MSD)[81]

$$m\left\langle \Delta x^2(t)\right\rangle = k_B T t^2 - \int_0^t \gamma(s)\left\langle \Delta x^2(t-s)\right\rangle \mathrm{d}s. \tag{2.26}$$

On long time scales, once the memory function has fully decayed, the dynamics becomes uncorrelated, thus fulfilling the Stokes-Einstein relation. The friction coefficient governing the diffusion on long time scales is then given by $\gamma = \int_0^\infty \Gamma(t)\mathrm{d}t$. The MSD for a memoryless LE exhibits a ballistic regime at time scales $t \approx 0$ and smoothly transitions into a linear regime for larger time scales. Anomalous diffusion with different scaling exponents can thus be attributed to the memory kernel, as given by Eq. (2.26). It is known that sub-diffusive dynamics, in which the MSD scales as $\left\langle \Delta x^2(t)\right\rangle \propto t^\alpha$ with $\alpha < 1$, can be described in terms of a GLE with a memory kernel of the form $\Gamma(t) \propto t^{-\alpha}$ at large times. [84] This especially occurs in viscoelastic materials such as polymer melts, in which stresses relax very slowly.

Over the last couple of decades, different methods have been proposed to extract the memory kernel of a tagged particle from trajectories based on higher resolution (FG) models. [39, 80, 81, 85–91] One

approach is to discretize Eqs. (2.25) or (2.26), calculate $\gamma(t)$ from the time evolution of the position of a tagged particle,[81] and then take the time derivative. Another widely used approach [27, 80, 92] is based on the Volterra equations (2.18) and (2.19), which here can be written in the form

$$\langle F(t)v(0)\rangle = -\int_0^t \Gamma(t-s)\,\langle v(s)v(0)\rangle\,\mathrm{d}s. \tag{2.27}$$

and

$$\langle F(t)F(0)\rangle = \int_0^t \Gamma(s)\,\langle F(t-s)v(0)\rangle\,\mathrm{d}s + m\;\Gamma(t)\left\langle v^2\right\rangle. \tag{2.28}$$

The force-velocity correlation function (FVCF) and the FACF can be computed directly from the FG trajectories. Subsequently, $\Gamma(t)$ can be calculated from Eq. (2.28) by discretization in the time-domain [80, 89, 92] or by exploiting the convolution theorem to extract $\Gamma(t)$ in the Fourier or Laplace space. [57, 88, 93–95] Additional relations can be formulated in the Fourier space such as

$$\tilde{\Gamma}(\omega) = 2Re\left(\frac{k_BT}{\tilde{C}_+^{vv}}\right), \tag{2.29}$$

and[96]

$$\tilde{C}_{FF}(\omega) = \frac{k_BT\;\tilde{\Gamma}(\omega)}{|1 - i\omega\,\tilde{\Gamma}_+(\omega)/(m\omega^2)|^2}. \tag{2.30}$$

where $\tilde{C}_+^{vv}$ is the one-sided Fourier transform of the VACF and $\tilde{C}_{FF}(\omega)$ is the Fourier transform of the FACF.

While $\Gamma(t)$ can be obtained from Eq. (2.29) by means of an inverse Fourier transform, Eq. (2.30) can be solved by assuming a functional form of $\Gamma(t)$ and optimizing the fitting parameters, which reproduce $\tilde{C}_{FF}(\omega)$. [96] Kowalik *et al.* [81] compared the performance of approaches derived from Eqs. (2.25) through Eq. (2.30) for calculating the memory kernel of a freely diffusing methane particle in water. The authors found that the methods described by Eqs. (2.25, 2.26, 2.29, 2.30) perform equally well, while methods based on Eqs. (2.27) and (2.28) are prone to numerical instabilities at long times. In general, the high-frequency contributions of the memory kernel are usually better reconstructed by methods that are directly based on the force autocorrelation function, while discretization errors in the long-time dynamics can commonly be reduced using slower decaying correlation functions such as the VACF. Recently, this observation has been used to construct a high-precision hybrid method. [97]

While the memory kernel at thermal equilibrium can be described in terms of the FDT, $k_BT\,\Gamma(t) = \left\langle F^R(t)F^R(0)\right\rangle$, the above mentioned methods to extract the memory kernel do not require the direct calculation of the projected dynamics defined in the MZ formalism. They rather exploit general properties of the GLE which are independent of its MZ theory background. Carof *et al.* derived a method to explicitly calculate the projected force correlation function from the FG trajectories based on a rigorous application of the MZ theory. [85] The original numerical schemes applied first order approximations for numerical discretizations, while second order schemes were shown to be significantly more accurate. [39, 86] While the extracted memory kernels should be the same as those obtained with the other methods discussed above (within the numerical error), the projected dynamics scheme by Carof *et al.* offers more general insight as it also allows to calculate the projected dynamics for other dynamical variables that depend on the chosen CG variables. This allows, for example, to separate interactions into different contributions and independently calculate their contributions to the memory kernel and thus, to the total friction. This was applied in the same study to calculate the contributions of short range repulsive and long range attractive interactions and their cross-correlations to the memory kernel. Based on their results, the authors concluded that friction in LJ fluids is dominated by the short range interactions, which is expected as the repulsive interactions are much steeper and thus contribute to dissipation through a stronger transfer of momentum.

Recently, two works have explored the possibility of using fine-grained trajectories to extract extended Markov models[32, 98] from which the memory kernel can be calculated. The idea of extended Markov models is to artificially include a coupling of the CG variables to additional degrees of freedom with Markovian interactions, which mimic the non-Markovian dynamics of the system. This approach thus directly combines reconstruction of memory with the construction of models that can be integrated very efficiently, as will be discussed in detail in Section 2.6.2.

2.4.2 Particles Diffusing in Harmonic Potentials

Studies of particles diffusing in harmonic potentials are of special interest, because such potentials can model typical setups of single-molecule force spectroscopy and/or microrheological experiments. In such experiments, optical or magnetic tweezers are used to trap large molecules such as DNA, proteins, or colloids. The tweezers can be calibrated such that effectively, a harmonic external potential is applied to the trapped tracer particle. Monitoring the trajectory allows to calculate the rheological properties of the fluid in which they are suspended. However, the temporal resolution in experiments is typically limited to a timescale of $\approx$ 0.1 ms, which is too large to resolve atomistic fluctuations, therefore an interpretation in terms of GLEs is appropriate.

In the analysis of experimental data, the motion is typically taken to be overdamped. If the mass of the tracer particles is large, memory effects can be neglected. This approximation is well justified for tracer particles of size around $\approx$ 0.25-0.5 μm.[99] The standard procedure in the analysis of force spectroscopy measurements is thus to fit the power spectrum of positional noise by a Lorentzian function, from which the viscosity of the fluid can be deduced. Taking memory effects into account in the analysis of the experimental data can give further information on the properties of the fluid. For example, the measurement of the frequency-dependent viscosity gives insight into the viscoelastic properties such as the storage and the loss moduli.[100] In order to understand such experiments, one must understand the effect of confinement on the measured rheological properties.

Daldrop *et al.*[96] and Kowalik *et al.*[81] have studied memory effects of solutes whose CG EoM is given by the GLE

$$m\frac{\mathrm{d}\,v(t)}{\mathrm{d}t} = F(t) = F^C(t) - \int_0^t \mathrm{d}s\,\Gamma(t-s)\,v(s)ds + F^R(t), \tag{2.31}$$

where $F^C(t)$ is the force due to an external harmonic potential, $F^C(t) = k\,x(t)$. The case $k = 0$ describes a freely diffusing particle and the case of $k = \infty$ can be implemented by constrained dynamics. In Ref. [96] the authors carried out atomistic MD simulations of a single methane molecule in water, wherein a harmonic confinement potential was applied to the CoM of the molecule. To extract the memory kernel, they derived a generalized variant of Eq. (2.30)

$$\tilde{C}_{FF}(\omega) = \frac{k_BT\ \tilde{\Gamma}(\omega)}{|1 - i\omega\,\tilde{\Gamma}_+(\omega)/(m\omega^2 - k)|^2} \tag{2.32}$$

from which the friction coefficient for $k \neq 0$ can be evaluated as

$$\gamma = \frac{\tilde{\Gamma}(0)}{2} = \frac{\tilde{C}_{FF}(0)}{2k_BT} = \frac{1}{k_BT}\int_0^\infty \mathrm{d}t\,C_{FF}(t). \tag{2.33}$$

Here $\tilde{\Gamma}(0)$ and $\tilde{C}_{FF}(0)$ are the Fourier transforms of the memory kernel and the FACF at frequency $\omega = 0$, which can be evaluated as the time integrals over $\Gamma(t)$ and $C_{FF}(t)$. Eq. (2.33) shows that the friction coefficient can be extracted directly from the integral of the FACF for weak confinement forces. As mentioned in Section 2.3, this is not possible for unconfined dynamics due to the plateau problem. By

varying the strength k of the confining potential, its influence on the friction coefficient can be evaluated. It is important to stress that Eq. (2.33) only holds for the frequency $\omega = 0$ and thus only relates the integrals of the memory kernel and the FACF, but not the functional form itself.

Daldrop *et al.*[96] analyzed the influence of the confinement on the form of the FACF and the memory kernel independently. For weak confinement, the integral over the FACF exhibits a distinct maximum value followed by a decay to zero similar to the unconfined case. On larger time scales, the weak confining forces induce a long lived positive tail in the FACF which generates a finite plateau in the running integral over the FACF on large time scales. Harmonic potentials were shown to slow down the relaxation of the FACF on intermediate time scales. This leads to an increase in the plateau value of the integral in confined simulations, and thus to an increase in the apparent friction coefficient. In the limiting case of a constrained particle, the friction coefficient was found to be overestimated by a factor of ≈ 1.5. The authors note that this enhancement of the friction due to confinement does not result from any structural changes in the solvation shell, as the confinement forces do not affect the equilibrium structural properties. However, the confinement of the methane molecule influences the relaxation of the water molecules in the hydration shell, effectively increasing the local viscosity in the first hydration shell. They observed a similar effect when artificially increasing the mass of the methane molecule.[101] Higher solute masses also resulted in a slowdown of hydration shell dynamics and a local increase of the viscosity.

In the above approach the memory kernel $\Gamma(t)$ was extracted by parameterization, which allowed a separation of contributions to the memory kernel on different time scales. The authors could attribute them to distinct molecular processes[96] and concluded that the imposed confinement mainly affects the hydrogen bond breaking processes. The time scale analysis furthermore suggested that the impact of confinement on the local viscosity is only significant if the inertial time scale of the tagged particle is comparable to or smaller than the time scale of the memory kernel. In the Markovian limit of heavy particles, confinement is not expected to influence the measured friction.

In a follow-up study,[81] the authors studied the influence of harmonic potentials on the memory kernel for a broader set of solutes and solvents with varying viscosities. The solutes under study were methane, water, sodium cations, "sodium" anions and glycerol, while the viscosity of the solvent was varied by changing the composition of a water-glycerol mixture. When comparing different solutes for a fixed solvent, the confinement effects on the friction were found to be negatively correlated with the amplitude of the friction coefficient of the free solute. On the other hand, when varying the solvent for a fixed solute (i.e., a confined glycerol molecule), the correlation was positive. This can be understood in terms of time scale separation due to size effects: The larger the solute and the less viscous the solvent, the clearer is the time scale separation and hence, the smaller the memory-induced confinement effects on the friction.

As mentioned above, the computational studies of Daldrop and Kowalik *et al.*[81, 96] can give insight into the dynamical processes in typical single-molecule force spectroscopy experiments. The numerical findings[81] suggest that significant confinement effects are unlikely in typical optical trap experiments, as the applied harmonic potentials are too weak and thus introduce modes which have larger time scales than the memory kernel. However, the spring constants applied in atomic force microscopy experiments can be orders of magnitude higher and thus can couple with the dynamical modes of the solvent, thereby introducing confinement-dependent frictional effects.

2.4.3 Iterative Reconstruction

The memory reconstruction methods described above are restricted to freely diffusing particles and particles in harmonic potentials. Jung *et al.* introduced two techniques for the iterative reconstruction of memory kernels (IMR) from FG simulations, [39] which can be applied more generally.

The methods take their inspiration from the iterative Boltzmann inversion (IBI) method, which was

introduced for structural coarse-graining.[9] The memory reconstruction methods use either the force correlation function (IMRF) or the velocity correlation function (IMRV) as the target function in the iterative schemes. The IMRF method is based on the fact that in the infinite mass limit the force correlation function is exactly proportional to the memory kernel. This can be used to motivate an iterative optimization scheme for the memory kernel which is linear in the deviations of the force correlation functions determined from the FG input and CG simulations using the current guess for the memory kernel. The iterative procedure is initialized using the Q-approximation, i.e. the memory kernel is initialized as the FACF. Starting from the IMRF method, the IMRV method exploits the fact that the second derivative of the VACF is proportional to the FACF, hence the FACF is replaced by the finite-difference representation of the second derivative of the VACF in the IMRV scheme. To enhance convergence of the optimization procedure, a time dependent and adaptive choice for the step size of any given iteration was introduced.

The method was evaluated using the example of a freely diffusing colloid in a LJ particle bath. Both IMRV and IMRF were applied for the reconstruction of the memory kernel starting with the FACF as the initial guess. Both schemes reasonably converged after 100 iterations. The IMRV was found to be more stable, i.e., exhibiting less noise in the resulting memory kernel and resulted in a better representation of the VACF in the final model. The memory kernel obtained by the IMRV was also compared to the memory kernel as calculated from inverting the Volterra equation (Eq. (2.27)) or determining the projected force correlation function following Carof *et al.*, [85] and the results were found to be virtually equivalent. In terms of reproducing the VACF of the underlying system, the IMRV scheme, by construction, proved to be less prone to errors due to discretization. Moreover, the IMRV method optimizes, also by construction, the representation of the memory kernel in the target GLE integration scheme, and thus automatically accounts for time-discretization effects at the GLE level. In the example above, the time step in the GLE simulations could be chosen 200 times larger than that in the FG simulations, making the integration of the GLE efficient, despite the need of explicitly calculating the convolution integral (see also Section 2.6). In a follow-up paper, Jung *et al.* applied their method to the reconstruction of pair memory kernels.[30] This work will be discussed in more detail in Section 2.5.

The recent work by Wang *et al.* [32] is based on a similar iterative approach and optimizes the CG model via a Bayesian optimization scheme.

2.4.4 Generalized Variables

The Mori-Zwanzig formalism and the memory reconstruction methods quoted above are clearly not restricted to particle-based descriptions, but can similarly be applied to generalized coordinates. Some popular examples are molecular hydrodynamic or fluctuating hydrodynamics descriptions[102–105], in which the distinguished variables are density, energy density, and longitudinal current modes and the corresponding correlation functions are, e.g., intermediate scattering functions (ISF). In this subsection we will briefly discuss such techniques.

Deriving molecular hydrodynamic equations is one of the oldest applications of the memory function formalism.[102, 103] Originally, it was believed that certain correlation functions (i.e. the VACF) must decay exponentially in time due to the molecular chaos assumption, which states that collisions experienced by a particle in a fluid are uncorrelated. However, in a pioneering work in the 70s, Alder and Wainwright unmistakably demonstrated the existence of long-time tails already in hard-sphere fluids.[106] Their observation could be explained based on a molecular hydrodynamic description, in which the memory kernel is approximated using mode-coupling theory.[107] Similar anomalous properties of various important transport coefficients have been studied extensively since then, also in the context of the glass transition.[108] For detailed discussions we refer to recent reviews and standard textbooks on related topics such as anomalous transport,[109] molecular hydrodynamics [103] and memory in glassy systems.[108,

110, 111]

Amati *et al.*[112, 113] used the Mori-Zwanzig formalism to study memory effects in the density fluctuations of a Fermi-Pasta-Ulam model, i.e., a linear chain with anharmonic bond potential. The reconstruction technique was based on a series expansion of the numerically calculated ISF. The detailed analysis of the short-time behavior of both the classical and the quantum mechanical versions of the Fermi-Pasta-Ulam model revealed zero-point energy effects that affect the mobility of the particles.

Chen *et al.* investigated the non-Markovian conformational motion of large proteins such as HIV-1 protease, which consists of nearly 200 residues, [114] showing that the conformational motion of proteins, which is usually modeled via Markov models, can exhibit memory effects, depending on the degree of coarse-graining. This study was based on an analysis of the potential energy of the protein only and did not yet include solvent effects. Later, Ma *et al.*[115] and Lee *et al.* [116] used molecular simulations to reconstructed the non-Markovian conformational motion of chignolin[115] and Alanine dipeptide.[116]

Memory kernels have also been reconstructed for non-equilibrium non-stationary GLEs.[54] Meyer *et al.* used their memory reconstruction methods (Eq. (2.22)) to study the fundamental problem of nucleation. [82, 117] In this case, the time-dependence of the nucleation-cluster size was chosen to be the relevant generalized variable. The authors found intriguing non-Markovian effects in the dynamics of the cluster size, which explicitly depend on the age of the sample.

2.5 GLE-based Coarse-Graining and Multiscale Modeling

In the previous section, we have discussed how FG systems can be mapped onto (mostly low-dimensional) GLEs in order to study the non-local effects in the friction (memory kernel) and properties of colored noise. In dynamic coarse-graining, the goal is often to construct dynamically consistent high-dimensional CG models with many interacting CG variables. Such efforts will be discussed in this section.

Smith *et al.* [118, 119] and Tuckerman *et al.*[120] were among the first to derive effective GLE type EoM from MD simulations and employ it in CG simulations. While the foundations of this approach were thus already laid quite some time ago, in recent years increasing efforts have been dedicated to deriving methods for non-Markovian CG models using bottom-up approaches. So far, successful models in this direction include models on freely diffusing Brownian particles with single-particle friction kernels, [27, 92] dilute and dense particle systems with pairwise friction interactions, [26, 27, 30, 121] and also models based on generalized CG variables that do not have a (CG) particle interpretation such as density fields. [122, 123]

2.5.1 Particle-based Coarse-Graining

The earliest attempts to solve stochastic differential equations with interactions that are non-local in time date back to the beginning of the 80s with the works of Ermak and Buckholz[124] and Ciccotti and Ryckaert.[125] Details of the numerical implementations will be discussed in Sec. 2.6. Smith *et al.* [118, 119] were the first to apply these ideas to real systems and to thus propose a systematic dynamic coarse-graining procedure. They applied their methods to the vibrational relaxation of iodine suspended in LJ Xenon at $T = 300$K. The integration of the generalized Langevin equation is based on an autoregression model, which has been shown to be equivalent to the method of Ciccotti and Ryckaert [125] and related to the auxiliary variable approaches discussed in Section 2.6.2. They compared the results of their GLE model to MD simulations, showing that such a simple model is indeed able to describe the FG dynamics in full detail, thus laying the foundation for future works on dynamic coarse-graining. One year later, Tuckerman and Berne[120] used methods derived earlier by Berne *et al.* [90, 91] to extract the memory kernel of a constrained diatomic LJ harmonic oscillator immersed in a LJ particle bath. Later, they generalized this

to anharmonic coupling,[126] thus providing the first dynamically consistent coarse-grained model in a complex energy landscape.

Only recently, this idea was brought back to life and generalized to multi-particle systems. The simplest approach is to neglect particle correlations in the friction terms and assume that the motion of CG particles can be described by a single effective "self-friction kernel" according to the EoM [27, 31, 92]

$$\frac{\mathrm{d}\boldsymbol{P}_I(t)}{\mathrm{d}t} = \boldsymbol{F}_I^C([\boldsymbol{X}(t)]) - \int_0^t \mathrm{d}s\, \boldsymbol{\Gamma}_I(t-s)\boldsymbol{V}_I(s) + \boldsymbol{F}_I^R(t), \tag{2.34}$$

where $\boldsymbol{\Gamma}(t)$ is a single-particle memory kernel and particles can only interact *via* the conservative forces $\boldsymbol{F}_I^C([\boldsymbol{X}(t)])$.

Recently, Wang *et al.*[32] showed that for star polymer systems, Eq. (2.34) suffices to reproduce dynamical properties of the underlying FG system over density ranges from dilute solutions to a melt. In this study, all memory effects were described by an average scalar self-friction memory kernel, which can be modeled by the auxiliary variable approach (see Section 2.6.2). The authors used a Gaussian process based Bayesian optimization scheme[127] to optimize the memory kernel to match the VACF of a single particle. The fundamental idea is comparable to the IMRV scheme, however, it is better suited for the auxiliary variable approach, because the parameters of the integrator are optimized directly instead of being fitted *a* posteriori to a memory kernel. A similar Bayesian approach was used to parameterize CG DPD models in Ref. [128].

While these models can well reproduce the tagged-particle motion, it is expected that pair diffusion will not be appropriately described. Already in 1990, Straub *et al.* showed that the relative motion between two bounded LJ particles can be described by a GLE with a memory kernel that strongly depends on the particle distance.[129] An alternative approach is thus to assume that the friction forces can be decomposed into pair friction terms that solely depend on the relative velocity $\boldsymbol{V}_{IJ}$ of the interacting particles I and J, [27, 129] resulting in the approximation (cf. Eq. (2.14))

$$\frac{\mathrm{d}\boldsymbol{P}_I(t)}{\mathrm{d}t} = \sum_{J\neq I}\left[\boldsymbol{F}_{IJ}^C(\boldsymbol{X}_{IJ}(t)) - \int_0^t \mathrm{d}s\, \boldsymbol{\Gamma}_{IJ}^{\mathrm{DPD}}(t-s)\boldsymbol{V}_{IJ}(s) + \boldsymbol{F}_{IJ}^R(t)\right]. \tag{2.35}$$

As discussed in Section 2.2, this corresponds to a non-Markovian extension of DPD like models. For such models an additional fundamental problem arises: Pair memory kernels typically depend on the distance between particles, which changes with time. Therefore, the problem of determining pair frictions is only well-defined in cases where the distance between the particles is confined by a potential, e.g., a bond potential or if the CG sites belong to the same molecule.[129] In all other cases, one must make the additional approximation that the particle distance is roughly constant on the time scale of memory decay – i.e., one must assume that the time scales of the memory kernel and the characteristic diffusion time of particles are well separated. If this is indeed the case, pair memory kernels can be extracted from FG simulations in the same way as single particle memory kernels [27, 28, 129] (Section 2.4).

Li *et al.* considered a GLE of the form of Eq. (2.35) and introduced a pairwise decomposition of conservative interaction and the memory kernel. [26–28] The EF-CG approach[76] and the IBI [9] method were used to derive the conservative interactions, while a pairwise variant of the Volterra equation (2.27) was used for the derivation of the pairwise memory kernels. Furthermore, for numerical simplicity, the time and distance dependence of the memory kernels were assumed to be separable. In all cases, the star polymer systems were considered with varying polymer sizes and densities.

In Ref. [26], Li *et al.* considered star polymers consisting of 11 beads interacting through Weeks-Chandler-Andersen interactions at reduced densities of 0.4 and 0.7. They found that at both densities, the non-Markovian DPD approach performed well in reproducing the VACF of the underlying FG system (see

Fig. 2.2). A comparison with Markovian DPD simulations further showed that the improvement due to the incorporation of memory effects was stronger for the dense systems, which lacked time scale separation. However, the Markovian DPD simulations also performed relatively well at both densities, which highlighted the possibility of using Markovian approximations in a wide range of implicit solvent polymer systems, depending on the desired accuracy. Only for high frequencies (i.e., small times), one can observe clear deviations between the non-Markovian and the Markovian DPD models, as highlighted in the insets in Fig. 2.2.

Yoshimoto *et al.*[28] combined a non-Markovian DPD model with the IBI [9] and EF-CG[76] methods and applied it to a dense system of LJ colloids. They found that the dynamic properties did not depend on the specific coarse-graining strategy for the conservative interactions. Furthermore, they compared two different approaches for extracting the memory kernel: First, approximating the memory kernel by the force autocorrelation function (Q-approximation), and second, by inverting the Volterra equation. Since the chosen system was dense, a time scale separation cannot be assumed and the memory kernel extracted from the Volterra equation led to a better representation of the dynamics. Being exact for $t = 0$, the Q-approximation shows good agreement for the short-time behavior, however, for long times, the force autocorrelation function significantly deviates from the real memory kernel and also suffers from the plateau problem[66, 68] as discussed earlier.

Another interesting more qualitative approach to include memory on the pairwise level to coarse-grained simulations has been suggested in Ref. [130] and applied several times since then in the context of star polymer melts [131] and polymer solutions [132]. The idea is to include additional, physically motivated degrees of freedom to the system which mimic the slow structural relaxation of the orthogonal variables. This approach is thus connected to the data-driven auxiliary variable approach, in which these additional degrees of freedom, however, usually do not have any physical interpretation.

The "pure self-friction kernel" models (Eq. (2.34)) and the non-Markovian DPD models (Eq. (2.35)) discussed so far can be implemented efficiently, but they impose rather severe restrictions on the form of the multi-particle memory kernel, compared to Eq. (2.12). Moreover, they are not even compatible with each other. In particular, the self-friction contribution of the memory kernel in non-Markovian DPD model

$$\mathbf{\Gamma}_I = \sum_{J \neq I} \mathbf{\Gamma}_{IJ}^{\mathrm{DPD}}(r_{IJ}), \tag{2.36}$$

depends solely on the surrounding particles and may either become very large (in dense systems) or very small (in dilute systems). This causes problems, e.g., when looking at colloidal suspensions where the dominant friction stems from the interaction with the (implicit) solvent, but collective memory effects[133] (frequency-dependent hydrodynamic interactions) may, nevertheless, not be neglected. Theoretical and numerical studies of a system containing two colloids only reveal an intriguing dependence of both the pair- and the self-memory on the inter-particle distance. [133] Methods that are purely based on self-memory or on DPD-type pair-friction are thus expected to fail. To solve this problem, Jung *et al.* [30] proposed a generalization of the non-Markovian DPD models. In this study, the memory matrix as defined in Eq. (2.12) consists of a self memory matrix coupling to the velocity of the particle and a set of pair matrices coupling to the velocities of the other particles in the system.

$$\mathbf{\Gamma}_{IJ}(t) = \begin{cases} \mathbf{\Gamma}^{\mathrm{self}}[\{\boldsymbol{R}_{IK}(t)\}, t] & : \quad I = J \\ \mathbf{\Gamma}^{\mathrm{p}}[\boldsymbol{R}_{IJ}(t), t] & : \quad I \neq J. \end{cases} \tag{2.37}$$

The self memory matrix is assumed to depend on the configuration, as the friction with respect to the background medium can be altered by nearby particles.[133] It thus has a configuration-independent

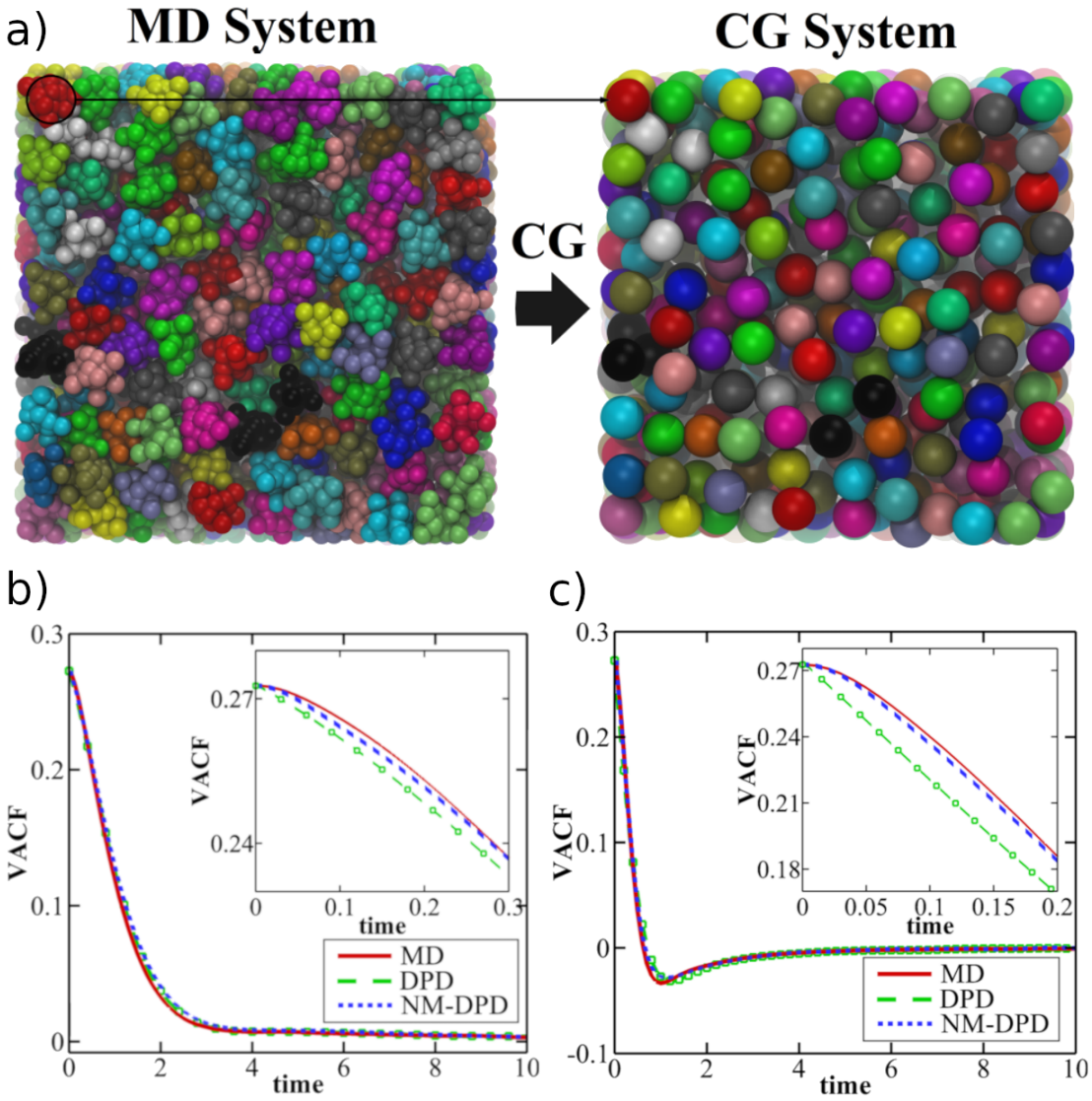

Figure 2.2: Non-Markovian coarse-graining procedure for a star polymer melt.[26] a) Illustration of the coarse-graining procedure in which each polymer is replaced by a single CG particle, which interacts with the other particles via the EoM (2.35). b, c) VACF for the non-Markovian DPD (NM-DPD) model in comparison to the MD results and a Markovian DPD model for low (b) and high density (c). Reproduced from *J. Chem. Phys.* **2015**, *143*, 243128, with the permission of AIP Publishing.

"bare" component and a contribution that depends on the relative positions of other particles in the vicinity

$$\mathbf{\Gamma}^{\text{self}}[\{\boldsymbol{R}_{IK}(t)\},\tau] = \mathbf{\Gamma}^{\text{s}}(\tau) + \sum_{K\neq I} \Delta\mathbf{\Gamma}^{\text{s}}[\boldsymbol{R}_{IK}(t),\tau]. \tag{2.38}$$

The set of Eqs. (2.37, 2.38) is still less general than Eq. (2.12), but it can interpolate between Eqs. (2.34) and (2.35) and includes them both as special cases. Using this framework, Jung *et al.* studied a dilute system of repulsive nanocolloids (radius $R_c = 3\,\sigma$) in a LJ liquid (diameter $d = 1\,\sigma$) as illustrated in Fig. 2.3. The memory kernel was reconstructed using the iterative reconstruction.[39] As an initial guess for the memory kernel, a generalization of the Volterra equation (2.27) including distance-dependent velocity auto- and cross-correlations for a system containing only two particles was used, similar to Ref. [133]. Effective many-body effects in multiparticle systems were then implicitly introduced by optimizing the memory matrix via the IMRV method. In order to validate and test the approach, the authors compared the distance-dependent velocity autocorrelation and crosscorrelation functions from the original FG system to those in their model, with excellent results, as shown in Fig. 2.3 b) and c). The authors also compared the reconstructed memory kernel to fluid dynamics theory, obtained by analytically solving the linearized Navier-Stokes equation for two embedded spheres [133]. The simulation and theoretical results are in quantitative agreement (see Fig. 2.3d), which not only validates the assumptions made for the simulation model but also highlights the importance of using distance-dependent memory kernels to capture the relevant physics of the fluid. Moreover, for the first time, the authors also analyzed the *transferability* of the CG model to different colloid densities. They found that the model not only describes the dynamic properties of one particular system, but indeed captures the fundamental non-Markovian interactions of colloids suspended in a Lennard-Jones fluid over a wide range of colloid densities. A significant gain in performance could be achieved for colloid number densities corresponding to dilute systems compared to FG simulations, not only due to the reduction of the number of particles, but also because the time step could be chosen about 50 times larger than that in the reference FG simulations.

The portfolio of methods for bottom-up non-Markovian CG simulations with consistent dynamics has grown quite substantially over the last decade. The choice of the method strongly depends on the system under study and the properties of interest. The general method proposed by Jung *et al.* [30] can be applied to a large set of systems, and is most efficient in cases where the relevant particles only represent a very small fraction of the microscopic degrees of freedom, e.g. in implicit solvent models. In the opposite case, in which the coarse-grained system incorporates most of the microscopic degrees of freedom, as is the case, for example for the coarse-graining of polymer melts, the non-Markovian DPD approach by Li *et al.*[27] might, however, be more suitable due to its numerical efficiency. Both methods are clearly less efficient compared to the pure self-friction models that have been applied in Refs. [26, 31, 76]. These simplified models are able to describe tagged-particle motion in a numerically efficient and dynamically consistent manner. Many physical and chemical processes, such as hydrodynamic motion or diffusion in complex environments, however, crucially depend on the relative motion of molecules. An additional problem is the transferability of these models. Since the single-particle memory does not include any information on the (local) density of the system, one would expect that the models can only reproduce the correct dynamics in exactly the same system in which they were reconstructed, and that any change of state variables will require a re-evaluation of the memory kernel. Furthermore, any information on dynamic heterogeneities in the system will be lost due to the averaging over all particles. These problems will have to be discussed in the future in order to improve the practical use of dynamically consistent coarse-grained models.

2.5.2 Coarse-Graining with Generalized Collective Variables

Much of the work on GLE-based coarse-graining so far has addressed particle-based CG models. In Sec. 2.4.4, we have discussed some recent works where memory kernels were reconstructed for GLEs operating

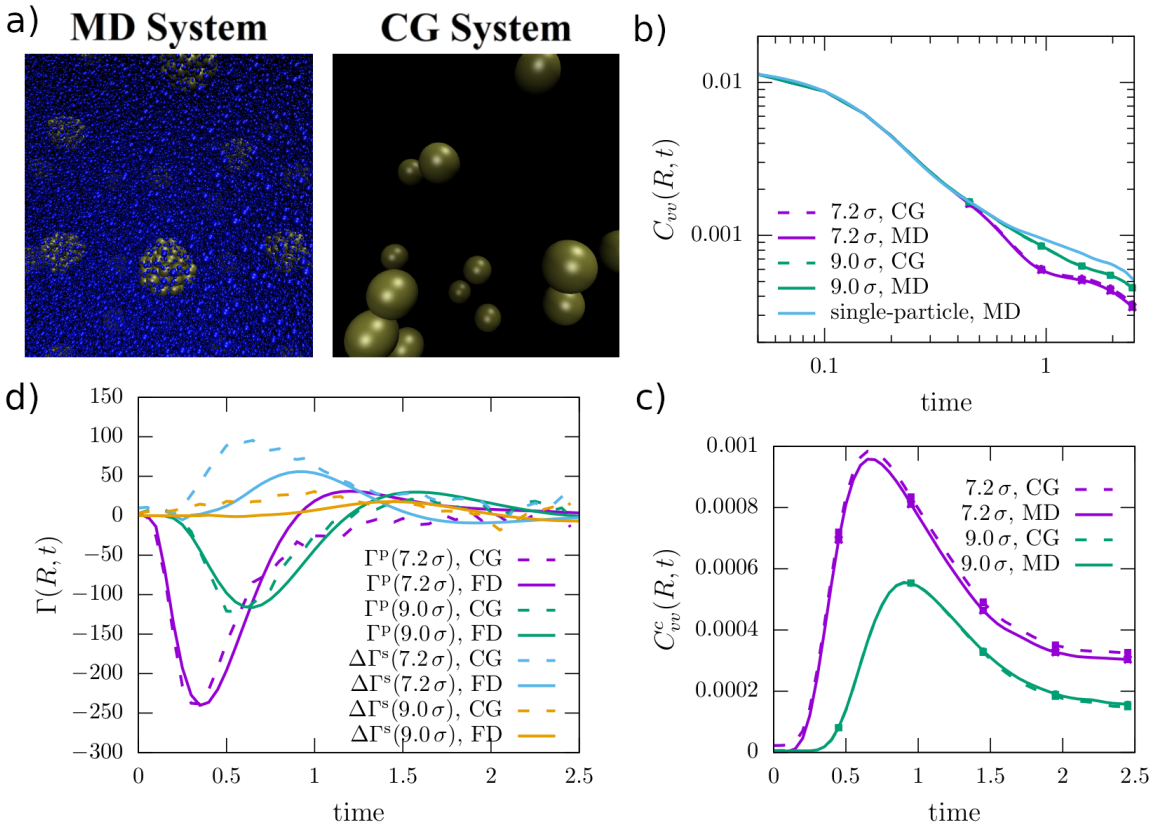

Figure 2.3: Non-Markovian coarse-graining procedure for a colloidal suspension. a) Illustrates the coarse-graining procedure, in which every colloid is represented by a single CG particle, and the interaction with the solvent is incorporated purely implicitly. b) Shows the velocity auto-correlation function, $C_{vv}(R,t)$, for colloids which have a nearest neighbor at a distance R. c) Shows the velocity cross-correlation function, $C^{c}_{vv}(R,t)$ for pairs of colloids at distance R. Results in b)+c) are compared between MD results and the non-Markovian coarse-grained model (CG) d) Compares the reconstructed memory kernels $\Gamma(R,t)$ of the CG model (see Eqs. (2.37) and (2.38)) with fluid dynamics (FD) theory [133]. This also shows the importance of the introduction of distance-dependent memory kernels. Figure adapted from Ref. [30] with permission from The Royal Society of Chemistry.

with generalized collective variables, focusing on the interpretation of memory effects in dynamics, and not on the construction of CG models for actual non-Markovian simulations. In the following we will highlight a few examples where GLE-based coarse-graining was applied to derive CG models with generalized CG variables.

One example is the set of non-Markovian models that were constructed to describe the conformational motion in proteins, [114–116] which were already mentioned in Sec. 2.4.4. Chen *et al.* studied a high-dimensional model, where the coarse-grained variables correspond to low frequency eigenmodes of HIV-I protease (the authors also provided results for more standard, particle-based coarse-graining). In terms of complexity, the model operates on a similar level as Ref. [30], introducing dissipative forces for both the self- and the pair-interactions in the system.

Other examples are the non-Markovian dynamic density functionals, which are attracting growing attention. Very recently, Russo *et al.* [134] developed a multiscale framework for describing reacting multi-species fluids in equilibrium and non-equilibrium. They started from an already coarse-grained GLE-system of particles with pure self-memory, and then performed ensemble averages over local densities, momenta, and reaction sources, applying a local equilibrium assumption. The resulting theory had the form of a fluctuating non-Markovian dynamic density functional and was used to study, e.g., the diffusion of a gas in a double well potential and the influence of memory on Turing patterns.

Memory effects are particularly prominent in polymer systems where the dynamics of density fluctuations is governed by chain relaxation processes on multiple time scales. [135–137] Wang *et al.* [138] recently investigated the influence of memory on the kinetics of relaxation and structure formation in copolymer melts and polymer blends. They derived an analytic expression for the memory kernel in random-phase approximation and constructed a non-Markovian dynamic density functional theory (NM-DDFT) based on this kernel. They showed that NM-DDFT calculations can quantitatively reproduce the collective disordering dynamics of particle-based reference simulations. Based on this work, Rottler and Müller[139] used the method of Meyer *et al.*[82] (Eq. (2.22)) and further approximations regarding the collective dynamic structure factor to derive a memory kernel for block copolymer melts, and applied it to study pattern formation in thin block copolymer films.

Memory is also a central ingredient in the recently proposed hydrodynamic models for fluctuating viscoelasticity. [140–142] The Oldroyd-B and related models for viscoelastic flow of polymeric melts are examples of multiscale models with memory, where the memory is approximated by a physically motivated auxiliary variable, which is usually denoted as an extension tensor that basically "memorizes" the local extension of polymers. This description has been generalized to a GLE-based model in two works by Hohenegger *et al.*.[122, 123] Instead of applying a single mode Maxwell model for the stress tensor (which would result in the Oldroyd-B model), they assumed that the memory can be expressed as a series of exponentials (see also Sec. 2.6). In this way they were able to describe, in very general terms, the movement of passive tracers in a viscoelastic medium.

2.6 Implementation of GLE Simulations and Efficient Integration

In the previous section we have introduced and discussed various different models to incorporate non-Markovian dynamics into complex coarse-grained models. We have mostly skipped details of the numerical implementation and efficient integration of the equations of motion. These will be discussed in this section.

The first papers on the integration of stochastic differential equations based on the GLE date back to the 80s. In a seminal contribution, Ermak and Buckholz proposed two novel approaches for the integration of a GLE in an arbitrary external potential.[124] The first is based on a direct integration scheme that can be applied to arbitrary memory kernels, in which the memory integral is discretized in time using a standard mid-point rule and the noise is calculated using a convolution approach, similar to the Fourier

transform method which will be introduced below.[143] The second approach is based on the assumption that the memory kernel is exponential, which allows to replace it by an equivalent extended Markovian model with one additional variable. This method is based on an idea presented one year earlier by Ferrario and Grigolini [144] and it is the precursor of the auxiliary variable technique discussed below (see Section 2.6.2). In the same year, Ciccotti *et al.* published two works [125, 145] in which they integrated the GLE by assuming a truncation of the continued fraction representation of the memory kernel, [146] which is equivalent to the autoregression model used by Marchesoni *et al.* [147] and Smith *et al.*.[118]

Generally, one faces two main issues when trying to integrate a GLE: First, the integration of the friction force which, in principle, requires the storage and evaluation of the entire past of all coarse-grained particles, and second, the generation of suitably correlated random numbers. In the most complex situation, where the system is governed by non-Markovian interactions between different particles, these random numbers must be correlated in *space and time*. [30, 114] Two distinct types of approaches have been used to solve these problems, the direct integration and the auxiliary variable methods. Both have their advantages and disadvantages, which we will discuss in the following.

2.6.1 Direct Integration

In the direct integration approach, the convolution integral appearing in the friction force is integrated numerically using a time cutoff t_{cut}, which effectively corresponds to multiplying the memory kernel with a Heaviside Theta function $\Theta(t_{\text{cut}} - t)$. This allows for a straightforward and easy evaluation, however, it can introduce artifacts. The most obvious artifact is that any long-time tails in the dynamics will be disregarded, which can be problematic in situations involving hydrodynamic tails (see discussion in Ref. [30]). In most applications, however, in which the introduction of memory is supposed to be an improvement compared to the idealistic Markovian assumption, the cutoff is not expected to lead to serious errors.

One major challenge in direct integration methods is to produce suitably correlated random forces. The most popular approach is based on the original idea of Ermak *et al.*[124] to express the colored noise as a convolution of an unknown function with a white noise variable. The method was successfully applied by Barrat *et al.*[143] using a Fourier transform approach, but the function can also be determined by autoregressive techniques[118] or optimization.[27] For non-interacting particles, the scaling of the method is similar to that of the direct integrator of the friction force, i.e., the computational costs increase linearly with the particle number N and the number of memory steps, $N_t = t_{\text{cut}}/\Delta t$ (where Δt is the time step) with the scaling $\mathcal{O}(N_t \cdot N)$.

Producing colored random numbers becomes much more problematic when simulating interacting particles or integrating multi-dimensional GLEs, in which the random force also has cross-correlations, described by the off-diagonal terms in the memory kernel matrix. This problem was addressed by Chen *et al.* [114] and Jung *et al.* [30] and, in both cases, was solved using the Lanczos method. [148] In short, the Lanczos method can be used to approximate highly-dimensional matrices by tridiagonal matrices in Krylov subspaces with significantly reduced dimension, thus allowing for efficient matrix inversion and Cholesky decomposition. If one can further assume that every coarse-grained dimension only interacts with a fixed number of "connected" variables (e.g. neighbors in particle-based descriptions), this method allows to reduce the computational time to $\mathcal{O}(N_t \cdot N)$, making it suitable for applications in large-scale simulations.

The last remaining problem is the choice of an efficient GLE integrator. Generally, one can use any standard Langevin integrator, since the time-retarded contributions to the force can just be added to the total force on the coarse-grained variables. Addressing specifically GLEs, Tuckerman and Berne have derived a multiple time-stepping algorithm in 1991, which can be used in cases where the typical frequencies related to the conservative forces differ very much from the time scale of the memory. [120] Jung *et al.*[30, 39] derived an alternative integrator which generalizes the Grønbech-Jensen/Farago Langevin (GJ-F)

thermostat [149] and was found to perform very well for both non-interacting and interacting particles.

The direct integration method is thus very flexible and can be applied to basically all non-Markovian models that were discussed in the literature. However, in cases where N_t is large, the computational overhead for the evaluation of the friction and the random force is significant.

2.6.2 Methods Based on Auxiliary Variables

The central idea of auxiliary variable approaches is to introduce additional stochastic variables and replace a GLE by an equivalent extended system of Markovian LEs. Let us consider a Markovian LE for two coupled degrees of system. As we will show below, integrating out one of them automatically results in the emergence of a memory kernel in the dynamical equation for the other.[23] Inverting this procedure, one can transform a system with exponential memory into an *extended Markovian* system with an additional, auxiliary variable that mimics the effect of the memory. The auxiliary variable approaches use this fact to construct extended Markovian models for the GLE. The idea is to expand the memory kernel into multiple exponentials, and then represent each one by an additional auxiliary variable.

Related approaches were already proposed in some of the very first works on numerical GLE integrators[144, 147]. In these studies, the auxiliary variables were constructed by a truncation of Mori's continued fraction expansion. [146] The method was revived about 10 years ago, mainly due to the work of Ceriotti *et al.* who used it as a practical numerical tool, in which the expansion is determined by a fitting procedure. [150–159] Recently, two works have also extracted extended Markov models directly from fine-grained trajectories, with great success [32, 98].

To introduce the technique, let us consider the following two-dimensional linear differential equation, [23]

$$\frac{\partial}{\partial t}\begin{pmatrix} a_1 \\ a_2 \end{pmatrix} = \begin{pmatrix} L_{11} & L_{12} \\ L_{21} & L_{22} \end{pmatrix}\begin{pmatrix} a_1 \\ a_2 \end{pmatrix}. \tag{2.39}$$

Solving Eq. (2.39) for the variable a_2 and putting the result back in the equation for a_1 gives

$$\frac{\partial}{\partial t}a_1 = L_{11}a_1(t) + L_{12}\int_0^t \mathrm{d}s \exp\left(L_{22}(t-s)\right) L_{21}a_1(s) + L_{12}\exp(L_{22}t)a_2(0) \tag{2.40}$$

In Eq. (2.40), the dynamics of a_1 now only depends on the initial conditions of a_2 and not its time evolution. Instead, an integral term appears, which involves the history of a_1. This procedure is exact and reversible. Since the Markovian Eq. (2.39) and the non-Markovian Eq. (2.40) are equivalent, it is evident that it should in many cases be possible to rewrite non-Markovian integro-differential equations such as GLEs in a Markovian form by the introduction of additional variables. Such a procedure allows to describe the evolution of the convolution integral in a GLE in terms of a set of auxiliary variables, thus rendering the EoM Markovian.

This method was used by Ceriotti *et al.* to introduce a general framework for exploiting the GLE as a flexible thermostat in MD simulations. [150–155] Following their scheme, a non-Markovian GLE of the form

$$m\dot{v} = F(t) = F^C(t) - \int_0^t \Gamma(t-s)\, v(s)\, \mathrm{d}s + F^R(t), \tag{2.41}$$

can be rewritten in a Markovian form as

$$\begin{pmatrix} F \\ \dot{\boldsymbol{s}} \end{pmatrix} = \begin{pmatrix} F^C \\ \mathbf{0} \end{pmatrix} - \boldsymbol{A}\begin{pmatrix} v \\ \boldsymbol{s} \end{pmatrix} + \boldsymbol{B}\left(\boldsymbol{\xi}\right) = \begin{pmatrix} F^C \\ \mathbf{0} \end{pmatrix} - \begin{pmatrix} a_{pp} & -\boldsymbol{a}_p^T \\ \boldsymbol{a}_p & \boldsymbol{a}_s \end{pmatrix}\begin{pmatrix} v \\ \boldsymbol{s} \end{pmatrix} + \begin{pmatrix} b_{pp} & \mathbf{0}^T \\ \mathbf{0} & \boldsymbol{b}_s \end{pmatrix}\left(\boldsymbol{\xi}\right), \tag{2.42}$$

where, $\boldsymbol{A}$ and $\boldsymbol{B}$ are the drift and the diffusion matrices, respectively. For canonical sampling $\boldsymbol{B}$ is fully determined by $\boldsymbol{A}$ in terms of the FDT. The noise term $\boldsymbol{\xi}$ is a vector of uncorrelated Gaussian random numbers with zero mean and variance one, which can be implemented rather efficiently compared to correlated noise. The vector $\boldsymbol{s}$ is a set of auxiliary variables, which effectively "stores" the dynamical history of v, while the drift matrix $\boldsymbol{A}$ includes the self- and cross coupling of the momentum and the auxiliary variables. The matrix $\boldsymbol{A}$ must satisfy the requirement that $\boldsymbol{A} + \boldsymbol{A}^T$ is positive (semi-)definite to ensure that $\boldsymbol{B}$ can be chosen in a manner consistent with the FDT, and that a stationary distribution of $(v, \boldsymbol{s})$ exists. This can be ensured by choosing the non-diagonal elements in the drift matrix to be antisymmetric and the diagonal elements to be positive, $A_{ii} > 0$.

As long as this specific condition is met, one has some freedom in the choice of $\boldsymbol{A}$. For certain functional forms of the memory kernel $\Gamma(t)$, equivalent parameterizations for Eq. (2.42) were proposed. Ceriotti *et al.* proposed parameterizations for exponential memory kernels and memory kernels that are δ-correlated in Fourier space. [151] The total memory kernel can also be constructed as a sum of contributions, which allows, for example, to use a sum of exponentials to describe memory decaying on different time scales [160] or to approximate a power-law memory kernel. [155] The δ-like memory kernel is defined by its amplitude, mean value and a line width in Fourier space, which allows to define a memory kernel with an arbitrary power spectrum by a sum of δ-like functions. [151]

As a side note, we remark that Ceriotti *et al.* did not have dynamic coarse graining in mind in their work, but rather the development of enhanced sampling schemes for MD simulations. Applying thermostats with memory and colored noise allows to control and optimize the correlation times of modes with different frequencies independently.[151] Ceriotti *et al.* also proposed to use nonequilibrium GLEs (with colored noise that does not fulfill the FDT) to mimic the effect of nuclear quantum fluctuations.[152]

Similar approaches can be used to parameterize memory kernels in GLE simulations.[27, 32, 92] Li *et al.* considered a star polymer melt with the dynamics of a single star polymer mapped on to a GLE and exploited the Volterra inversion method (Eq. (2.27)) for the extraction of the memory kernel.[27] In the CG simulations, they compared the results obtained using a discretized calculation of the convolution kernel with those using the auxiliary variable approach due to Ceriotti.[151] Both methods were found to reproduce the VACF with small deviations on large time scales, which were, however, more pronounced in the discretized convolution integral approach. The direct calculation of the convolution integral necessarily involves cutting off the number of time steps considered in the evaluation of the GLE. In particular, if the memory kernel exhibits a slowly decaying tail, this will always lead to a overestimation of the dynamics due to the truncation of the long time friction. The auxiliary variable approach shows a similar but slightly lower deviation. For the parameterization of the auxiliary variable approach, a set of damped oscillators was used. This fitting procedure allows to represent the memory kernel for larger time scales, which can enhance the representability of the long time scale behavior. Even though the memory kernel is not truncated in the auxiliary variable approach, approximating long tail memory kernels by a finite sum of exponentials still implicitly results in a, though less severe, truncation error.

The same approach was also applied to solutions ranging from generic star polymer solutions to a solution of tri-n-butyl phosphate in chloroform.[92] In these systems, it was possible to capture the long time scaling of the memory kernel accurately enough to match the VACF over all time scales with a reasonable number of fitting functions for the memory kernel. Furthermore, the authors established a GJ-F integrator[149] for the auxiliary variable approach, thus enhancing the performance of the CG simulation due to larger time steps.

Li *et al.* also extended the auxiliary variable approach for the case of non-Markovian DPD equations and derived it in a pairwise-decomposed form, including also complex exponentials which allows for a better representation of the memory kernel.[27] Here, the auxiliary variables were coupled to the relative velocities of the bead pairs, instead of the absolute velocity of a single particle. This leads to an increase in

the computational cost compared to the GLE-thermostat, as auxiliary variables must now be introduced for each bead pair. Nonetheless, it was found that this approach is roughly 20 times more efficient than the direct evaluation of the convolution integral in the same system.[26] The authors demonstrated that both approaches can well capture the dynamical properties of the underlying FG system.

The auxiliary variable approach is thus clearly more efficient than the direct integration technique which we have discussed in Section 2.6.1. One challenge is an accurate reconstruction of the non-Markovian dynamics, which often requires fitting of memory kernels with a series of (complex) exponentials. This problem, however, might be not very severe, because it is often not necessary to reproduce memory kernels in full detail. Furthermore, recent work on direct optimization has demonstrated that it is possible to faithfully represent self-friction memory kernels over several orders of magnitude in time with auxiliary variables.[32]

On the other hand, when looking at multidimensional memory kernels with distance-dependent pair memory contribution, the approach may also fail and it may not be possible to find an equivalent representation of the form Eq. (2.42). The problem is that the different entries in the memory kernel matrix then depend on the relative distances between all particles in the system, and there is no (obvious) way to ensure that this memory kernel matrix is always positive (semi)-definite (see discussion in the Appendix of Ref. [30]).

2.7 Physical Impact of Memory

From the point of view of dynamic coarse-graining, it is clear that memory effects should be included in CG models in many cases in order to *quantitatively* reproduce the dynamics of the underlying FG model. In addition, memory can have a significant impact on the *qualitative* behavior of materials. One particularly prominent example is the glass transition, which has been the subject of intense research for almost a century now and will not be discussed here (see Refs. [108, 110, 161–165] for recent advances and reviews). Another important field where memory plays a central role is anomalous diffusion (see Sec. 2.4.1), which has also attracted enormous interest due to its many applications in physics and biology and will also not be discussed here (for Reviews see, e.g., Refs. [84, 109, 166]). There are many other cases where memory has a physical impact on systems, and we will now illustrate this using a few selected examples.

Mankin and coworkers studied the influence of memory on the motion of trapped Brownian particles in oscillatory viscoelastic shear flow with a power-law-type memory kernel.[167, 168] Among other things, they discovered a dynamic phase transition from a trapped to a diffusive state when increasing the memory exponent. Moreover, the cross-correlation of the particle motion in flow and shear direction changed sign twice with increasing exponent.

Lesnicki *et al.*[86] gave a beautiful example of how the analysis of memory kernels can enhance the understanding of physical phenomena. They performed an accurate calculation of the memory kernel of a tagged LJ particle in a bath consisting of equivalent particles on long time scales, using the method of Carof *et al.*[85], and numerically derived the algebraic long-time tail for the memory kernel. They related this result to the Basset-Boussinesq hydrodynamic force equation, which is typically used to model colloidal spheres in suspension.[169, 170] Thus, they showed that the Basset-Boussinesq equation is also applicable in the microscopic regime, with parameters that can be directly derived from the memory function.[86] Seyler and Presset[171, 172] investigated the influence of this "Basset history force" on the motion of microspheres in oscillatory flow and a periodic potential. They showed that hydrodynamic memory significantly enhances the mobility of microspheres and helps them to escape potential wells in which they would otherwise remain trapped for much longer times.

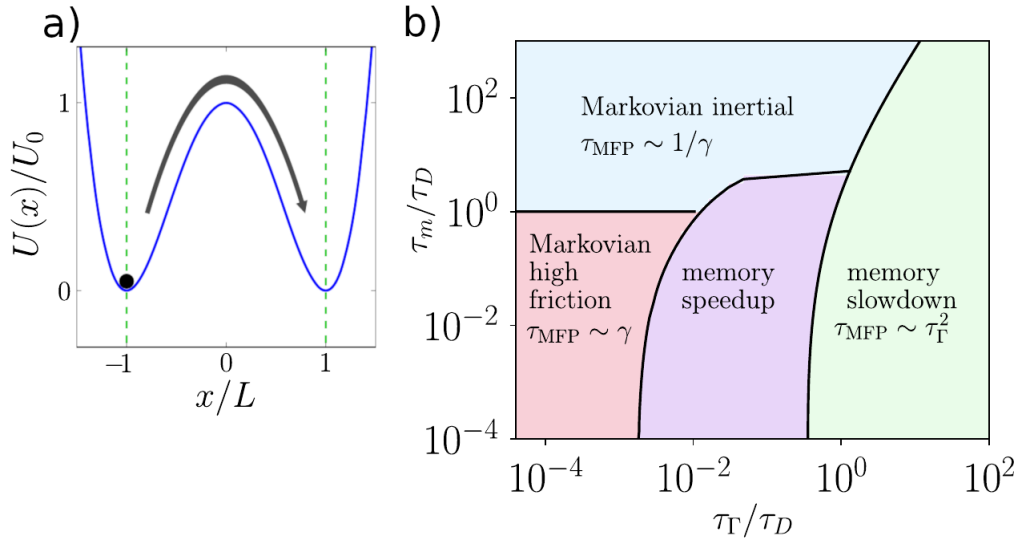

Figure 2.4: The effect of memory on the barrier crossing dynamics of a single particle.[75] a) Illustrates the simulation setup. b) Highlights the important regimes for the mean first passage time, τ_{MFP}: the Markovian regimes for overdamped and underdamped dynamics in which the memory has no effect, as well as the regimes in which the memory introduces a speedup or a slowdown compared to the Markovian results. τ_m and τ_D: inertial and diffusive time scales, τ_Γ: time scale of the memory kernel. Reproduced from *J. Chem. Phys.* **2018**, *148*, 014903, with the permission from AIP Publishing.

Goychuk[173, 174] considered the effect of hydrodynamic memory on the diffusion in so-called washboard potentials, where the diffusion is enhanced by orders of magnitude already in the absence of any memory.[175] He showed that hydrodynamic forces can enhance the diffusion even further in such systems and induce a transient, but long-lived superdiffusion regime, where the mean-square displacement scales with t^3.

The above situations have in common that the memory kernels were long-range in time. However, memory effects may also qualitatively affect the dynamics of systems if the memory kernels are short-range, i.e., decay exponentially. One such example was recently discussed by Kappler *et al.*,[75] who analyzed the influence of memory with an exponentially decaying memory kernel on the mean first passage time (MFPT), τ_{MFP} in a generic symmetric double well potential (see Fig. 2.4). For fixed inertial and diffusive time scales, τ_m and τ_D, they reported an intriguing non-monotonous behavior as a function of the time scale τ_Γ of the memory kernel, where the MFPT first decreases with τ_Γ ("memory speedup" regime in Fig. 2.4) and then grows as τ_Γ^2 for large τ_Γ ("memory slowdown" regime in Fig. 2.4). If multiple memory time scales $\tau_{\Gamma,i}$ with different associated friction constants γ_i are involved, then the behavior of the MFPT is dominated by the time scale $\tau_{\Gamma,j}$ for which $\gamma_j/\tau_{\Gamma,j}^2$ is the largest.[160, 176] This study demonstrated that, remarkably, memory effects in the presence of conservative interactions can affect the long time dynamics far beyond the time scale of the memory. It further showed that this effect strongly depends on the chosen barrier height.

The findings of Kappler and coworkers might provide a possible explanation for the observation that Markovian DPD models can capture the long time dynamics rather well in simple liquids with low viscosity, in which energy barriers are significantly smaller than k_BT, whereas they tend to overestimate the diffusion coefficient in systems, in which energy barriers due to conservative interactions are rather high – as is the case for polymer melts and solutes in polymer networks.[65] In both cases, the separation of time

scales is incomplete. However, the diffusion of the polymer should not depend much on the local relaxation processes in dilute polymer solutions and thus can be well captured by a Markovian approximation after appropriate time scale mapping.[65] In the case of penetrant diffusion in a polymer matrix, which is closely related to the MFPT problem in a double-well potential, one observes significant deviations from Markovian DPD models. A potential enhancement of the barrier crossing rate resulting from the Markovian approximation can accumulate over time and effectively translate into an enhanced diffusion coefficient, as was observed by Deichmann and Van der Vegt. [65]

Memory effects can also be prominent in driven and active systems. Russo *et al.*[134] derived a generalized dynamic density functional framework for reactive multicomponent fluids with memory and showed that reaction-diffusion equations for components with dissimilar memory kernels exhibit novel Turing patterns. Two examples of memory effects in systems of microswimmers were recently discovered by Nagai and coworkers[177] and by Narinder and coworkers.[178] Nagai *et al.*[177] investigated the effect of memory (colored noise) on the pattern formation in fluids of microswimmers and showed that memory can induce a whole spectrum of novel patterns in such systems, including vortex lattices and laning. Narinder *et al.*[178] studied the motion of colloidal microswimmers in a viscoelastic fluid both experimentally and theoretically and showed that memory can induce spontaneous circular motion.

These examples show how memory can fundamentally influence the dynamical behavior of systems. In many cases, properly accounting for memory effects in coarse-grained simulations is not just necessary to establish a proper quantitative link between the fine-grained and coarse-grained systems. It may also be crucial to capture the essential characteristics of the dynamics at the coarse-grained level.

2.8 Outlook

Over the last decade a lot of progress has been made toward improving dynamical consistency in CG simulations based on the Mori-Zwanzig theory. While the Markovian approach has been exploited with varying success, in most cases the systems under study were chosen such that the approximation is evidently valid. In such cases, even though the methodology could be validated, its applicability to real physical systems remains questionable. In general, for moderate level of coarse-graining at a high density, the Markovian approximation is not valid. Interestingly, the approximation could still capture the long time dynamics of simple liquids where the time scales are not well separated. [65] For multi-bead mapping schemes in polymer systems at high densities the approximation introduces errors in the long time dynamics, probably due to the comparable timescales of memory effects and chain relaxation processes that govern diffusion. In principle, this could be circumvented by choosing a higher degree of coarse-graining, which would enhance the time scale separation. However, such models will ultimately loose their predictive capabilities as the mapping scheme for a given physical question is chosen based the corresponding length and time scales of interest.

On the other hand, non-Markovian CG models are more flexible and can be applied to a broad range of physical problems, with an obvious increase in computational overhead. Among the existing methods, the generalized Langevin dynamics method [30] proposed by Jung *et al.* is rather general and can be applied to any physical system with arbitrary mapping schemes, however, at a relatively high computational cost. The assumption of pairwise-additivity of the frictional forces as proposed by Li *et al.* allows to formulate non-Markovian DPD-type models, which can be integrated more efficiently using auxiliary variable approaches. [27] While this circumvents the computational overhead of explicit memory evaluation to a large extent, the non-Markovian DPD models with moderate degree of coarse-graining can still be less efficient compared to fine-grained MD simulations, again limiting their applicability to coarser models.

Unfortunately, there are no studies yet in which the predictive capabilities of non-Markovian DPD models are demonstrated conclusively. If the corresponding memory kernels (which only depend on the

direct interactions and thus, local correlations) can be assumed to be short lived compared to the diffusive time scales and the dynamics on longer time scales are partially encoded in the conservative interactions, it is reasonable to assume that non-Markovian DPD models can be parameterized with relatively short fine-grained MD simulations, while the dynamics on long time scales can be sampled with the CG models. One possible application of this kind would be the penetrant diffusion in polymer melts or polymer networks, for which it was shown that Markovian DPD approaches do not correctly reproduce diffusion. [65] However, to the best of our knowledge, no study has applied any of the discussed non-Markovian CG approaches to predict dynamical properties of such materials or related molecular processes. One possible reason is the nontrivial derivation of the memory kernels and the rather complicated and computationally expensive implementation of the CG model.

Transferability of CG models is another important issue that requires future attention, in particular with respect to dynamical properties. In the field of systematic polymer coarse-graining, transferable pair potentials have been developed based on approaches that minimize the contributions of average, and strongly state-dependent, multibody effects. The CRW pair potential[73, 74], as well as the EF-CG pair potential,[76] represent the free energy associated with the interactions among the internal DoF of two beads at a fixed distance, excluding contributions of the non-bonded environment of the two beads. CRW models for linear alkanes are shown to be transferable between the melting and boiling points of the materials,[74] reproduce the liquid surface tension, have been used to study wetting problems [179], and, applied to syndiotactic polystyrene [180], have been successfully used to study crystallization in the bulk [181] and at the surface of a thin polymer film [182]. These studies rely on the transferability of the potential and have been applied to static aspects of problems whose dynamics is of significant interest, too. The Markovian MZ-DPD approach of Deichmann and Van der Vegt has, with an eye to transferability, been derived based on EF-CG interactions, while neglecting (state-dependent) multibody contributions to the DPD pair frictions.[65] This approach, in principle, requires time scale separation, i.e. distances between beads are fixed on the time scale of the memory kernel, and is expected to work for polymer-based systems such as polystyrene in which rotations of side groups occur on time scales where the monomeric units hardly move. This system is also a good example for testing the temperature transferability of memory kernels employed in a non-Markovian extension of the work in Ref. [65] , e.g. with respect to reproducing temperature dependent segmental and chain dynamics of polystyrene. [183]

While the parameterization of the original DPD model, which is often applied to simple bead-spring polymer systems, is generic (not chemistry specific), it can still capture some fundamental dynamical properties of well known theoretical models in polymer physics, even though it fails to capture reptation dynamics for long polymer chains in melts.[184] In this line, it is conceivable that an in-depth understanding of friction and memory kernels and its coupling to the conservative interactions can be utilized to establish a similar top-down procedure to derive CG models with realistic dynamics. The realm of non-Markovian simulations, in principle, allows to tune dynamical properties of generic CG models with a greater flexibility, opening new possibilities in the development of empirical models with a broader range of possible applications.

Beyond the realm of equilibrium systems, the MZ theory and the application of GLEs has been extended to non-equilibrium and non-stationary processes [82, 83]. For example, non-Markovian dynamics emerges naturally when looking at ”hot Brownian motion”, i.e., the motion of heated colloids in a fluctuating thermodynamic environment[185, 186]. Non-Markovian interactions with time delay offer interesting opportunities for a feedback control of Brownian motion and create intriguing novel equilibrium states [187, 188]. These examples illustrate that a modification of dissipative and stochastic interactions in non-equilibrium can have a qualitative impact on the *structural* properties of the system (see, e.g., Ref. [177]). One problem along this line will be that in nonequilibrium, a clear distinction between systematic and random forces is missing [189, 190], which makes it challenging to establish a meaningful, systematic

dynamic coarse-graining procedure.

In the following an (incomplete) list of open questions and problems is given, that could potentially guide future research towards practical applications of non-Markovian models.

- Understanding the transferability and predictive power of (equilibrium) non-Markovian models.
- Implementation of (distance-dependent) pairwise friction kernels could be essential to achieve a high level of transferability. Potential issues of currently proposed (particle-based) techniques that should be addressed are
  - the assumption of a time-scale separation between the decay of the memory kernel and the characteristic diffusion time of the particles,
  - the usage of auxiliary variable approaches for models with self- and pair-memory kernels,
  - and the handling of long-range and long-time interactions.
- The practical application of the coarse-graining techniques in non-stationary and non-equilibrium systems. This will include
  - analysis of the FDT for non-equilibrium processes and in non-stationary situations,
  - the development of practical computational tools for the time-integration of non-equilibrium coarse-grained models,
  - and further development of reconstruction techniques for non-stationary memory kernels.
- The application of state-of-the-art techniques to the problem of non-Markovian coarse-graining. This mainly includes the usage of machine-learning tools[32], which have the potential to be a powerful methodology to approach some of the above listed open problems.

A multi-disciplinary, collaborative effort will be needed to standardize the methodologies and exploit their potential, while reaching a broader community of researchers. Concrete application to relevant physical questions would help drive continuous improvements on the methodological front and broaden their capabilities.

Acknowledgment

We wish to thank Niklas Bockius, Emiliano Brini, Gregor Deichmann, Martin Hanke-Bourgeois, Florian Müller-Plathe, and Jeanine Shea for inspiring discussions and enjoyable collaborations on topics presented in this review. Financial support for this work was granted by the Deutsche Forschungsgemeinschaft (DFG) via SFB TRR 146 (Grant 233630050, projects A2 and A3). GJ also gratefully acknowledges funding by the Austrian Science Fund (FWF): I 2887.

List of Acronyms

ACF: Autocorrelation function
CG: Coarse-grained
CRW: Conditional reversible work
DoF: Degrees of freedom
DPD: Dissipative particle dynamics
EF-CG: Effective force - coarse-graining

EoM: Equation of motion
FACF: Force autocorrelation function
FDT: Fluctuation-dissipation theorem
FG: Fine-grained
GF/F: Grønbech-Jensen/Farago integrator
GLE: Generalized Langevin equation
IBI: Iterative Boltzmann inversion
IMR: Iterative memory reconstruction
IMRF: IMR based on FACV
IMRV: IMR based on VACF
ISF: Intermediate scattering function
LE: Langevin equation
LJ: Lennard-Jones
MD: Molecular dynamics
MFPT: Mean first-passage time
MSD: Mean square displacement
MZ: Mori-Zwanzig
NM-DDFT: non-Markovian dynamic density functional theory
RDF: Radial distribution function
VACF: Velocity autocorrelation function

3 Theoretical Background and General Approach

In this chapter, the most relevant technical aspects necessary to understand the following chapters are condensed and a description of the general workflow for the parametrization of Eq. 1.1 is provided. Basic aspects of molecular dynamics (MD) simulations and of coarse-graining for static properties are not covered, as there are well established literature on them. [2–7, 191, 192]

3.1 Defining Coarse-grained Degrees of Freedom: Mapping of Fine-Grained Trajectories

Consider a typical FG molecular dynamics model for which the phase space is defined in terms of the positions and momenta of n particles, $\boldsymbol{r} = \{\boldsymbol{r}_1, ...\boldsymbol{r}_n\}$ and $\boldsymbol{p} = \{\boldsymbol{p}_1, ...\boldsymbol{p}_n\}$. The canonical probability distribution of the FG DoFs are determined by a Hamiltonian

$$\mathcal{H}(\boldsymbol{r}, \boldsymbol{p}) = \sum_{i=1}^{n} \frac{1}{2m_i}\boldsymbol{p}_i^2 + U^{FG}(\boldsymbol{r}) \tag{3.1}$$

with the particles masses m_i and a potential energy function $U^{FG}(\boldsymbol{r})$ encompassing all bonded and non-bonded interactions in the system. The canonical probability density is then given by

$$p_r(\boldsymbol{r}) \propto \exp\left(-U^{FG}(\boldsymbol{r})/k_B T\right) \tag{3.2}$$

$$p_p(\boldsymbol{p}) \propto \exp\left(-\sum_{i=1}^{n} \frac{1}{2m_i k_b T}\boldsymbol{p}_i^2\right) \tag{3.3}$$

where k_B is the Boltzmann constant and T is the temperature.

In systematic bottom-up coarse-graining, a mapping operator $\hat{\boldsymbol{M}}$ determines how to define positions and momenta of N coarse-grained beads ($\boldsymbol{R} = \{\boldsymbol{R}_1, ...\boldsymbol{R}_N\}$ and $\boldsymbol{P} = \{\boldsymbol{P}_1, ...\boldsymbol{P}_N\}$), such that

$$\hat{\boldsymbol{M}}\{\boldsymbol{r}, \boldsymbol{p}\} = \{\boldsymbol{R}, \boldsymbol{P}\}. \tag{3.4}$$

A typical choice for an mapping operator is a linear combination of FG DoFs, as e.g. a center of mass mapping, where

$$\boldsymbol{R}_I = \frac{\sum_{i \epsilon I} m_i \boldsymbol{r}_i}{M_I} \tag{3.5}$$

$$\boldsymbol{P}_I = \sum_{i \epsilon I} \boldsymbol{p}_i \tag{3.6}$$

whereby $i \epsilon I$ picks out all FG atoms which are part of the CG bead I. Applying $\hat{\boldsymbol{M}}$ on a FG trajectory yields a *mapped trajectory* in terms of CG DoFs governed by the FG Hamiltonian. The corresponding FG canonical probability densities of CG DoFs are given via

$$p_R(\boldsymbol{R}) \propto \exp\left(-W(\boldsymbol{R})/k_b T\right) \tag{3.7}$$

$$p_P(\boldsymbol{P}) \propto \exp\left(-\sum_{I=1}^{N} \frac{1}{2M_I k_b T} \boldsymbol{P}_I^2\right). \tag{3.8}$$

where

$$W(\boldsymbol{R}) = -k_B T \ln \int d\boldsymbol{r} \exp\left(-U^{FG}(\boldsymbol{r})\right) \delta(\boldsymbol{R} - \hat{\boldsymbol{M}}(\boldsymbol{r})) \tag{3.9}$$

is the multibody potential of mean force (MB-PMF), a free energy function governing the probability density $p_R(\boldsymbol{r})$.

In constructing typical CG molecular models, a CG potential $U^{CG}(\boldsymbol{R})$ applied in CG simulations has to be defined. In CG simulations, $U^{CG}(\boldsymbol{R})$ governs the canonical probability density via

$$P_R(\boldsymbol{R}) \propto \exp\left(-U^{CG}(\boldsymbol{R})/k_b T\right). \tag{3.10}$$

For the CG model to be consistent with the underlying reference the to probability density $P_R(\boldsymbol{R})$ and $p_R(\boldsymbol{R})$ have to coincide and thus the goal of a constructing $U^{CG}(\boldsymbol{R})$ is to mimic the MB-PMF $W(\boldsymbol{R})$.[193] In practice, for many-body systems the MB-PMF cannot be computed, nor be represented in CG simulations in terms of pair-potentials. Also, this consistency criterion only holds for static properties. Dynamic consistency is a distinct problem and the main topic of this thesis. At the same time, the discrepancies between $U^{CG}(\boldsymbol{R})$ and $W(\boldsymbol{R})$ influence both static and dynamic properties, and therefore, the CG potential has to be parameterized carefully. In Eq. 1.1 and throughout this thesis conservative interactions due to a coarse-grained potential are denoted as $\boldsymbol{F}_I^C = -\frac{\partial U^{CG}(\boldsymbol{R})}{\partial \boldsymbol{R}_I}$.

3.2 Hierarchy of Non-Markovian Generalized Langevin Equations for Coarse-Grained Simulations

As discussed in chapter 2, different forms of GLEs have been explored for coarse-graining with the aim to faithfully represent dynamic properties of the reference FG system. These GLEs can be roughly organized in a hierarchy along the dimension of complexity and accordingly the incorporation of physical details. Fig. 3.1 summarizes this hierarchy.

Eq. (M1) in Fig. 3.1 represents a very general form of a GLE for a many-body CG description, which can be derived with the application of a non-linear projection operator.[58] The the total force $\boldsymbol{F}_I(t)$ on some CG bead I consists of three distinct contributions. The first term, the conservative force $\boldsymbol{F}_I^C(t)$, represents a systematic force determined by the configuration of the total system $\boldsymbol{R}$ at time t, associated with the (in general non-linear) potential of mean force. The second term represents a non-Markovian frictional force which depends on the history of all velocities $\boldsymbol{V}$. The third term, $\delta \boldsymbol{F}_I^Q$, represents the so called $\mathcal{Q}$-projected force, a force contribution, which is statistically independent of the relevant DoFs $\{\boldsymbol{R}, \boldsymbol{V}\}$ and thus is interpreted as a random force contributions. In Eq. (M1), $\boldsymbol{K}_{IJ}(t, \boldsymbol{R})$ is a complex high-dimensional memory(friction) tensor, encoding the coupling of all the systems velocities $\boldsymbol{V}$ (or momenta $\boldsymbol{P}$). For modeling purposes, Eq. (M1) is in general too complex due to the high dimensionality of the memory tensor in which (in principle) every entry depends on the configuration of the whole system. The most direct implementation of Eq. (M1) is found in the work of Jung *et al.*.[30] To make Eq. (M1) tractable, Jung *et al.*

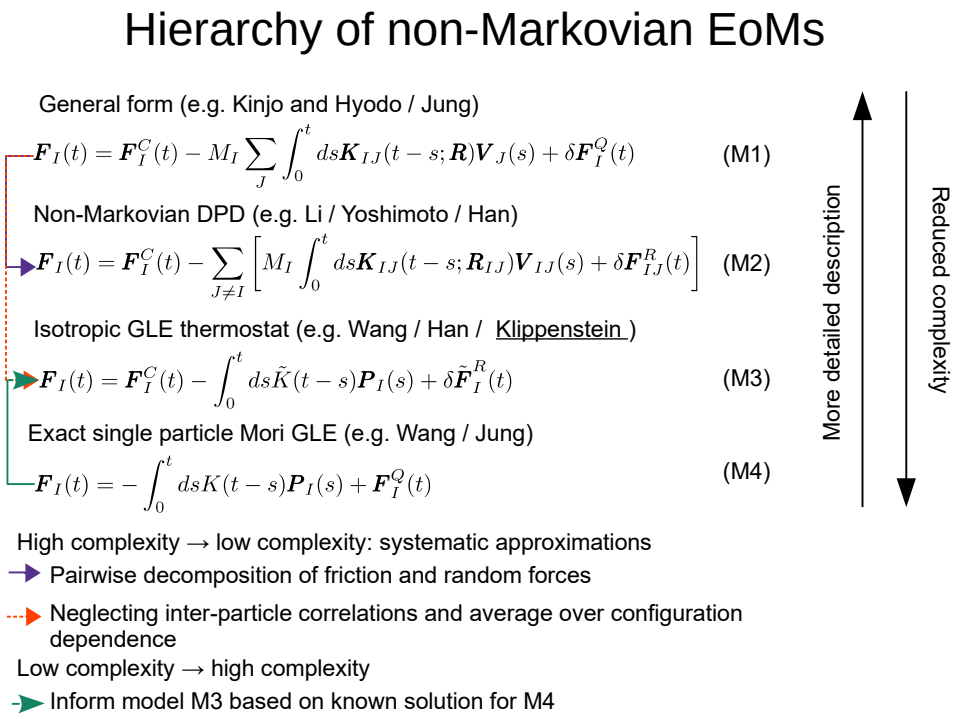

Figure 3.1: Overview of GLEs for non-Markovian CG modeling. In parenthesis, examples for authors discussing or utilizing the corresponding EoMs are noted. The corresponding references are: Kinjo and Hyodo[58], Jung[30, 39], Li[27], Yoshimoto[28], Han[29, 31], Wang[32, 92] and Klippenstein[33, 34, 194] / the current work.

proposed to construct the memory tensor by only considering its dependence on pair-distances. This idea was successfully applied for deriving an implicit-solvent model of a dilute system of colloids, whereby the friction due to the solvent DoFs was modeled in terms of a self memory kernel ($-\int_0^t ds M_I \boldsymbol{K}_{II}(t-s,\{R_{IJ}\})\boldsymbol{V}_I(s)$). Hydrodynamic interactions, i.e. solvent mediated interactions due to the motion of particle J on particle I, were modeled via a pair memory kernel ($-\int_0^t ds M_I \boldsymbol{K}_{IJ}(t-s,R_{IJ})\boldsymbol{V}_J(s)$).

It has to be noted that the validity of the derivation of (M1) in Ref. [58] is debated in literature,[25] but recent derivations by Vroylandt and Monmarché[195] seem to indicate that, in equilibrium, CG EoMs following the form of (M1) can be derived, as long as the memory tensor is considered to be configuration dependent.

By applying a pairwise decomposition to Eq. (M1), assuming $\boldsymbol{K}_{II} = -\sum_{J\neq I}\boldsymbol{K}_{IJ}$ and enforcing Newton's third law, the momentum conserving non-Markovian dissipative particle dynamics (NM-DPD) model (Eq. (M2)) can be derived.[26] In NM-DPD, the random forces $\delta\boldsymbol{F}_{IJ}$ and $\delta\boldsymbol{F}_{IK}$ are uncorrelated for $J \neq K$, which simplifies the construction of random forces in CG simulations.[30] NM-DPD is particularly useful for mapping schemes where momentum is conserved in mapped FG trajectories. In such a case, assuming $\boldsymbol{K}_{II} = -\sum_{J\neq I}\boldsymbol{K}_{IJ}$ is not a limitation. The main approximation on the level of the EoM is the neglect of many-body correlations. NM-DPD has been successfully tested for coarse-graining generic star-polymer melts.[26, 27] The limitation in NM-DPD lies in the fact that it is computationally expensive. This can to some extent be alleviated by applying the auxiliary variable approach,[27] a technique to render non-Markovian EoMs Markovian,[151] but for molecular coarse-graining where only few FG DoFs are mapped onto CG DoFs, the computational overhead due to the complexity of the CG EoM might outweigh

the computational gain due to the reduced number of DoFs.

The computationally least complex non-Markovian EoM which can be used for CG modeling of many-body systems is given by Eq. (M3). To derive Eq. (M3) from Eq. (M1), it has to be assumed that $\boldsymbol{K}_{IJ} = 0$ for $I \neq J$. By doing so, hydrodynamic interactions in implicit solvent systems, or more generally, inter bead correlations of friction and noise, are neglected. Lei *et al.* tested this approach by deriving CG models of Markovian analogs of Eq. (M2) (DPD) and Eq. (M3) (Markovian Langevin thermostat), and found that the explicit neglect of these correlations yields too low diffusion coefficients in CG Markovian Langevin models[36] while DPD models yield better results.

To construct models of the form of Eq. (M3) such that dynamic properties are faithfully represented, the effects of the cross-terms of the memory tensor ($\boldsymbol{K}_{IJ}$ for $I \neq J$) have to be incorporated into $\tilde{K}$ in an averaged sense.

The problem with going from complex to more simple (Eq. (M1)→Eq.(M3)) is that contributions with a significant effect on the overall dynamics have to be neglected. The alternative approach, chosen in this thesis, is to start with an even simpler EoM, which is the single-particle GLE due to the Mori projection, given by Eq. (M4). Eq. (M4) can be, contrary to Eq. (M3), formally exactly derived and thus the memory kernel K is numerically accessible. In the following sections, strategies are presented, which allow to derive parametrizations of $\tilde{K}$ in Eq. (M3), with the aim to be consistent with the single-particle EoM Eq. (M4).

3.3 Single Particle Dynamics in Equilibrium: The Mori-Projection Operator

This section is an adaptation from the supporting information (SI) of Ref. [34]. The respective section in the SI of chapter 5 is accordingly removed.

A prototypical coarse-graining problem is the dynamics of a single heavy Brownian particle immersed in a solvent consisting of molecules of much smaller size. In the absence of external forces the total force acting upon the Brownian particle can then be described as drag, exerting friction upon the movement of the particle, and random collisions of the solvent molecules due to thermal fluctuations. The phenomenological EoM often used to describe this type of dynamics is the Langevin equation (LE).

$$\boldsymbol{F}_I(t) = -\gamma \boldsymbol{P}_I(t) + \boldsymbol{F}_I^R(t) \tag{3.11}$$

Here $\boldsymbol{F}_I(t)$, $\boldsymbol{F}_I^R(t)$ and $\boldsymbol{P}_I(t)$ are the total force, the random force and the momentum of the Brownian particle at time t, respectively and γ is the friction coefficient. To describe the dynamics of a Brownian particle in thermal equilibrium, γ and $\boldsymbol{F}_I^R(t)$ have to be related via the fluctuation-dissipation theorem[69]

$$\frac{\left\langle \boldsymbol{F}_I^R(t) \boldsymbol{F}_I^R(t') \right\rangle}{3 M_I k_B T} = 2\gamma\delta(t - t'). \tag{3.12}$$

Eq. 3.11 can be formally justified in terms of the Mori-Zwanzig theory. The main ideas behind the the projection operator formalism, following the description in Ref.[23], are summarized in the following paragraph.

Consider the EoM of the vector of "relevant" (for the purpose of this thesis, real valued) dynamical variables $\boldsymbol{A}_0 \equiv \boldsymbol{A}(t = 0)$ in terms of the Liouville equation

$$\frac{d\boldsymbol{A}_t}{dt} = i\mathcal{L}\boldsymbol{A}_t \tag{3.13}$$

with the formal solution

$$\boldsymbol{A}_t = e^{i\mathcal{L}t}\boldsymbol{A}_0. \tag{3.14}$$

Different projection operators $\mathcal{P}$ can be defined such that $\mathcal{P}\mathcal{P} = \mathcal{P}$. In this work the projection operator as defined by Mori is considered, which, applied on a vector of real valued observables $\boldsymbol{B}_t \equiv \boldsymbol{B}(t)$, reads

$$\mathcal{P}\boldsymbol{B}_t = \left\langle \boldsymbol{B}_t \boldsymbol{A}_0^T \right\rangle \left\langle \boldsymbol{A}_0 \boldsymbol{A}_0^T \right\rangle^{-1} \boldsymbol{A}_0. \tag{3.15}$$

The superscript T denotes transposed vectors and $\langle ... \rangle$ denotes the canonical ensemble average.

The projection operator for the orthogonal projection can be defined as

$$\mathcal{Q} = (1 - \mathcal{P}) \tag{3.16}$$

with which the Liouville operator can be split up as

$$i\mathcal{L} = \mathcal{P}i\mathcal{L} + \mathcal{Q}i\mathcal{L}. \tag{3.17}$$

Additionally one has to introduce the following operator identity:[23]

$$e^{i\mathcal{L}t} = e^{\mathcal{Q}i\mathcal{L}t} + \int_0^t ds e^{i\mathcal{L}(t-s)} \mathcal{P}i\mathcal{L}e^{\mathcal{Q}i\mathcal{L}s}. \tag{3.18}$$

By applying both sides of Eq. 3.18 to $\mathcal{Q}i\mathcal{L}\boldsymbol{A}_0$, the left-hand side reads

$$\begin{aligned} e^{i\mathcal{L}t}\mathcal{Q}i\mathcal{L}\boldsymbol{A}_0 &= e^{i\mathcal{L}t} i\mathcal{L}\boldsymbol{A}_0 - e^{i\mathcal{L}t}\mathcal{P}i\mathcal{L}\boldsymbol{A}_0 \\ &= \frac{\partial}{\partial t} e^{i\mathcal{L}t}\boldsymbol{A}_0 - e^{i\mathcal{L}t} \left\langle (i\mathcal{L}\boldsymbol{A}_0)\boldsymbol{A}_0^T \right\rangle \left\langle \boldsymbol{A}_0 \boldsymbol{A}_0^T \right\rangle^{-1} \boldsymbol{A}_0 \\ &= \frac{\partial}{\partial t}\boldsymbol{A}_t - \left\langle (i\mathcal{L}\boldsymbol{A}_0)\boldsymbol{A}_0^T \right\rangle \left\langle \boldsymbol{A}_0 \boldsymbol{A}_0^T \right\rangle^{-1} \boldsymbol{A}_t \\ &= \frac{\partial}{\partial t}\boldsymbol{A}_t - i\boldsymbol{\Omega}\boldsymbol{A}_t. \end{aligned} \tag{3.19}$$

In the first step, it is exploited that $\mathcal{Q} = (1 - \mathcal{P})$; in the second step, $\mathcal{P}$ is applied and noted that $\frac{\partial}{\partial t} e^{i\mathcal{L}t}\boldsymbol{A}_0 = e^{i\mathcal{L}t} i\mathcal{L}\boldsymbol{A}_0$. In the third step, the propagator is applied to $\boldsymbol{A}_0$ and in the last step the frequency matrix is defined as follows:

$$i\boldsymbol{\Omega} = \left\langle (i\mathcal{L}\boldsymbol{A}_0)\boldsymbol{A}_0^T \right\rangle \left\langle \boldsymbol{A}_0 \boldsymbol{A}_0^T \right\rangle^{-1}. \tag{3.20}$$

The right-hand side reads

$$\begin{aligned} & e^{i\mathcal{L}t}\mathcal{Q}i\mathcal{L}\boldsymbol{A}_0 \\ &= e^{\mathcal{Q}i\mathcal{L}t}\mathcal{Q}i\mathcal{L}\boldsymbol{A}_0 \\ &+ \int_0^t ds e^{i\mathcal{L}(t-s)} \left\langle \left(i\mathcal{L}e^{\mathcal{Q}i\mathcal{L}s}\mathcal{Q}i\mathcal{L}\boldsymbol{A}_0\right) \boldsymbol{A}_0^T \right\rangle \left\langle \boldsymbol{A}_0 \boldsymbol{A}_0^T \right\rangle^{-1} \boldsymbol{A}_0 \\ &= e^{\mathcal{Q}i\mathcal{L}t}\mathcal{Q}i\mathcal{L}\boldsymbol{A}_0 \\ &+ \int_0^t ds \left\langle \left(i\mathcal{L}e^{\mathcal{Q}i\mathcal{L}s}\mathcal{Q}i\mathcal{L}\boldsymbol{A}_0\right) \boldsymbol{A}_0^T \right\rangle \left\langle \boldsymbol{A}_0 \boldsymbol{A}_0^T \right\rangle^{-1} \boldsymbol{A}_{t-s} \\ &= e^{\mathcal{Q}i\mathcal{L}t}\mathcal{Q}i\mathcal{L}\boldsymbol{A}_0 \\ &- \int_0^t ds \left\langle \left(e^{\mathcal{Q}i\mathcal{L}s}\mathcal{Q}i\mathcal{L}\boldsymbol{A}_0\right) i\mathcal{L}\boldsymbol{A}_0^T \right\rangle \left\langle \boldsymbol{A}_0 \boldsymbol{A}_0^T \right\rangle^{-1} \boldsymbol{A}_{t-s} \\ &= \dot{\boldsymbol{A}}_t^{\mathcal{Q}} - \int_0^t ds \left\langle \left(\dot{\boldsymbol{A}}_s^{\mathcal{Q}}\right) \dot{\boldsymbol{A}}_0^T \right\rangle \left\langle \boldsymbol{A}_0 \boldsymbol{A}_0^T \right\rangle^{-1} \boldsymbol{A}_{t-s}. \end{aligned} \tag{3.21}$$

First $\mathcal{P}$ is applied, followed by the application of the propagator $e^{i\mathcal{L}(t-s)}$ in the integral. In the third step it is noticed that $i\mathcal{L}$ is an anti-hermitian operator, so for any two vectors of observables $\boldsymbol{A}$ and $\boldsymbol{B}$ one can write:

$$\left\langle \boldsymbol{A} i\mathcal{L}\boldsymbol{B}^T \right\rangle = -\left\langle (i\mathcal{L}\boldsymbol{A})\boldsymbol{B}^T \right\rangle. \tag{3.22}$$

In the last step, a $\mathcal{Q}$-projected time derivative of $\boldsymbol{A}_t$ (which later will be a $\mathcal{Q}$-projected force) is defined as

$$\dot{\boldsymbol{A}}_t^{\mathcal{Q}} = e^{\mathcal{Q}i\mathcal{L}t}\mathcal{Q}i\mathcal{L}\boldsymbol{A}_0. \tag{3.23}$$

Eqs. 3.19 and 3.21 can be combined and reordered to give

$$\frac{\partial}{\partial t}\boldsymbol{A}_t = i\boldsymbol{\Omega}\boldsymbol{A}_t - \int_0^t ds \left\langle \left(\dot{\boldsymbol{A}}_{t-s}^{\mathcal{Q}}\right) \dot{\boldsymbol{A}}_0^T \right\rangle \left\langle \boldsymbol{A}_0\boldsymbol{A}_0^T \right\rangle^{-1} \boldsymbol{A}_s + \dot{\boldsymbol{A}}_t^{\mathcal{Q}} \tag{3.24}$$

The derivation can now be finalized by choosing the relevant DoFs. For a single diffusive Brownian particle, its position is unbound. Thus it cannot be used as a relevant variable in the Mori-projection, as the normalization matrix $\left\langle \boldsymbol{A}_0\boldsymbol{A}_0^T \right\rangle^{-1}$ is not defined for that case. Choosing $\boldsymbol{A}_0 \equiv \boldsymbol{P}_{I,0}$ for a single tagged particle I, the frequency matrix $i\boldsymbol{\Omega} = \left\langle \boldsymbol{F}_{I,0}\boldsymbol{P}_{I,0}^T \right\rangle \left\langle \boldsymbol{P}_{I,0}\boldsymbol{P}_{I,0}^T \right\rangle^{-1}$ vanishes and Eq. 3.24 reads

$$\boldsymbol{F}_I(t) = -\int_0^t ds\boldsymbol{K}(t-s)\boldsymbol{P}_I(s) + \boldsymbol{F}_I^{\mathcal{Q}}(t) \tag{3.25}$$

with $\boldsymbol{K}(t) = \left\langle \boldsymbol{F}_{I,t}^{\mathcal{Q}}\boldsymbol{F}_{I,0}^T \right\rangle \left\langle \boldsymbol{P}_{I,0}\boldsymbol{P}_{I,0}^T \right\rangle^{-1}$. In this thesis only isotropic systems are considered, in which case all Cartesian coordinates are equivalent and independent. Thus $\boldsymbol{K}(t)$ will be a diagonal matrix with equivalent entries along the diagonal. This allows to replace the memory kernel matrix by a scalar memory kernel, which yields

$$\boldsymbol{F}_I(t) = -\int_0^t dsK(t-s)\boldsymbol{P}_I(s) + \boldsymbol{F}_I^{\mathcal{Q}}(t). \tag{3.26}$$

From Eq. 3.24 and Eq. 3.26 the fluctuation-dissipation relation is defined:

$$K(t) = \frac{\left\langle \boldsymbol{F}_I^{\mathcal{Q}}(t)\boldsymbol{F}_I^{\mathcal{Q}}(0) \right\rangle}{3M_I k_B T}. \tag{3.27}$$

Eq. 3.26 can be interpreted as a non-Markovian version of Eq. 3.11. To recover Eq. 3.11 from Eq. 3.26, a separation of time scales between the memory kernel and the momentum has to be assumed. The memory kernel $K(t)$ and the friction coefficient γ are then related via

$$\gamma = \lim_{t\to\infty}\int_0^t dsK(s) = \lim_{t\to\infty} G(t), \tag{3.28}$$

where γ determines the diffusion coefficient D of the Brownian particle via the Einstein relation:

$$D = \frac{k_B T}{M_I \gamma}. \tag{3.29}$$

3.4 Extracting the Single-Particle Memory Kernel from Volterra Equations

The previous section described how one can derive an effective CG EoM for a diffusing particle, using the Mori projection operator. In Eq. 3.26 all information from the FG reference is condensed into the memory kernel $K(t)$, which can be easily extracted from FG simulations. First, by multiplying Eq. 3.26 with $\boldsymbol{P}_I(0)$, taking the ensemble average, and using the relation

$$\left\langle \boldsymbol{F}_I^{\mathcal{Q}}(t)\boldsymbol{P}_I(0)\right\rangle = 0 \tag{3.30}$$

a Volterra equation of the following form can be derived:

$$C_{FP}(t) = \dot{C}_{PP}(t) = -\int_0^t dsK(t-s)C_{PP}(s). \tag{3.31}$$

Here, $C_{PP}(t) = \langle \boldsymbol{P}_I(t)\boldsymbol{P}_I(0)\rangle /3$ and $C_{FP}(t) = \langle \boldsymbol{F}_I(t)\boldsymbol{P}_I(0)\rangle /3$ are the momentum autocorrelation function and the force-momentum correlation function, respectively. By dividing Eq. 3.31 twice by the mass M_J of the relevant particle J, the Volterra equation can be rewritten as

$$\dot{C}_{VV}(t) = -\int_0^t dsK(t-s)C_{VV}(s). \tag{3.32}$$

As $C_{VV}(t)$ and $\dot{C}_{VV}(t) = C_{FV}(t)/M_I$ are easily accessible from FG trajectories, the effective single particle memory kernel $K(t)$ can be numerically derived through inversion of Eq. 3.31 or 3.32.[81]

Alternatively, for numerical stability, Eq. 3.32 can be integrated, yielding

$$C_{VV}(t) = C_{VV}(0) - \int_0^t dsG(t-s)C_{VV}(s). \tag{3.33}$$

As Eq. 3.33 involves only $C_{VV}(t)$, which is typically less noisy than $\dot{C}_{VV}(t)$, its numerical inversion tends to yield numerically more stable results. [81]

3.5 Defining Dynamic Consistency and Friction and Memory due to Conservative Interactions

Whichever way $\tilde{K}(t)$ is chosen in CG GLE simulations, one can always evaluate the VACF $C_{VV}^{CG}(t)$, whereby CG here indicates the evaluation based on a CG trajectory. As shown in sec. 3.4, the knowledge of a VACF is sufficient to extract some memory kernel $K^{CG}(t)$ via

$$\dot{C}_{VV}^{CG}(t) = -\int_0^t dsK^{CG}(t-s)C_{VV}^{CG}(s), \tag{3.34}$$

whereby a single-particle GLE simulation parameterized with $K^{CG}(t)$ would reproduce $C_{VV}^{CG}(t)$. This suggests a straight forward definition of dynamic consistency in CG GLE models following Eq. 1.1, that is

$$K^{CG}(t) \approx K(t). \tag{3.35}$$

So the aim of finding an optimal $\tilde{K}(t)$, is to satisfy Eq. 3.35, as this will simultaneously yield an accurate representation of e.g. the VACF. This is a harder problem than the direct evaluation of $K(t)$ from a FG VACF, as, in contrast to Eq. 3.26, Eq. 1.1 cannot be exactly derived from first principles. The reason for that is that $\boldsymbol{F}_I^C(t)$ is due to some CG potential approximating the MB-PMF. This conservative force, in

general, is highly non-linear. The combination of non-linear conservative forces with a linear frictional forces can formally only be an approximation to the "exact" CG EoM,[35] and in the context of this work has to be considered a modeling tool. The implication of the approximate nature of Eq. 1.1 is that there is no formally exact way to find a memory kernel $\tilde{K}(t)$ directly from a FG trajectory, such that the dynamics of the FG model can be recovered exactly in CG simulations.

To circumvent these limitations and to derive at least a good approximate *a-priori* tool for estimating an optimal $\tilde{K}(t)$, it is insightful to consider the role of conservative interactions in CG GLE models.

From Eq. 1.1, an alternative Volterra equation can be derived which reads

$$\dot{C}^{CG}_{VV}(t) = C^{CG}_{F^CV}(t)/M_I - \int_0^t ds\tilde{K}(t-s)C^{CG}_{VV}(s). \tag{3.36}$$

By equating Eq. 3.34 and 3.36, it follows:

$$C^{CG}_{F^CV}(t)/M_I = -\int_0^t ds(K^{CG}(t-s) - \tilde{K}(t-s))C_{VV}(s) = -\int_0^t ds\Delta K^{CG}(t-s)C_{VV}(s). \tag{3.37}$$

Herein, $\Delta K^{CG}(t)$ is the memory kernel contribution which is not explicitly modeled through the thermostat and thus can be interpreted as the friction and memory induced on particle I in CG simulations due to conservative forces $\boldsymbol{F}^C_I(t)$. So in many-body CG simulations subject to an isotropic GLE thermostat and conservative interactions, the effective single-particle memory kernel $K^{CG}(t)$ consists of two distinct contributions, namely the memory kernel of the GLE-thermostat ($\tilde{K}(t)$) and the memory kernel from conservative interactions ($\Delta K^{CG}(t)$) and thus $K^{CG}(t) = \tilde{K}(t) + \Delta K^{CG}(t)$.

In order to find an estimate for the optimal choice of $\tilde{K}(t)$ in an a-priori bottom-up approach, i.e. solely based on the analysis of a FG trajectory of the underlying reference system, a method to predict $\Delta K^{CG}(t)$ is needed. A method to do so is described in sec. 3.6.2, and is tested throughout chapters 4-6 for different systems.

Alternatively, $\tilde{K}(t)$ can be optimized iteratively in successive CG GLE simulations, until Eq. 3.35 is satisfied. A systematic procedure is described in sec. 3.7 and tested in chapters 5 and 6.

3.6 Bottom-up Estimation of Memory Kernels for Many-Body Coarse-Grained Models

3.6.1 Parameterizing Generalized Langevin Thermostats from Volterra Equations

In sec. 3.4 it is described how to derive a the single-particle memory kernel $K(t)$ from a FG trajectory using Volterra equations of different forms. A similar approach has been suggested to parameterize $\tilde{K}(t)$ for Eq. 1.1 and was applied both for the derivation of Markovian[196] and non-Markovian[31] models. Under the assumption that Eq. 1.1 is formally exact, following the same rationale as in sec. 3.4, the following Volterra equation can be derived:

$$\dot{C}_{VV}(t) = C_{F^CV}(t)/M_I - \int_0^t ds\tilde{K}(t-s)C_{VV}(s). \tag{3.38}$$

Note that the form of Eq. 3.38 is analogue to Eq. 3.36. The difference lies in the trajectories used for the analysis evaluation of the time correlation functions. Where Eq. 3.36 relies on time correlation functions from CG simulations due to Eq. 1.1, Eq. 3.38 relies on time correlation functions from mapped FG trajectories. To evaluate $C_{F^CV}(t)$, a rerun of the mapped trajectory has to be carried out. In the rerun

a time series for the conservative forces $\boldsymbol{F}_I^C(t)$ is evaluated based on a predetermined coarse-grained potential. By defining $\delta\boldsymbol{F}_I(t) = \boldsymbol{F}_I(t) - \boldsymbol{F}_I^C(t)$, Eq. 3.38 can be rewritten as

$$C_{\delta FV}(t)/M_I = -\int_0^t ds\tilde{K}(t-s)C_{VV}(s). \tag{3.39}$$

Eq. 3.39 can be numerically solved for $\tilde{K}(t)$ in the same way as Eq. 3.32.

Due to the approximate nature of Eq. 1.1, Eq. 3.39 typically does not yield an optimally accurate memory kernel for dynamic consistency. The problems which arise due to the approximate nature of Eq. 1.1 are demonstrated and discussed in chapters 4 and 5.

3.6.2 Direct Evaluation of Projected Time-Correlation Functions: the Backward-Orthogonal Dynamics Method

This section is an adaptation from the SI of Ref. [34]. The respective section in the SI of chapter 5 is accordingly removed.

In chapter 4, an approach to fully account for the cross correlations between $\boldsymbol{F}_I^C$ and $\delta\boldsymbol{F}_I$ is proposed and tested. This approach is based on the backward orthogonal dynamics (BOD) method due to Carof *et al.*[85]. The BOD method allows to evaluate $\mathcal{Q}$-projected time correlation functions based on Mori's GLE (Eq. 3.26), using Mori's linear projection operators $\mathcal{P}$ and $\mathcal{Q}$ as defined in sec. 3.3.

As will be discussed below, the BOD method allows to get a good estimate of $\Delta K^{CG}(t)$ and thus yields an alternative route to a bottom-up parameterization of Eq. 1.1.

The $\mathcal{Q}$-projected time-correlation function of two observables A and B is defined as

$$\tilde{C}_{AB}(t) = \left\langle A_0 e^{i\mathcal{Q}\mathcal{L}t} B_0 \right\rangle = \left\langle e^{-i\mathcal{L}\mathcal{Q}t} A_0 B_0 \right\rangle = \left\langle A_t^- B_0 \right\rangle \tag{3.40}$$

where $A_t \equiv A(t)$ and $A_t^- = e^{-i\mathcal{L}\mathcal{Q}t}A_0$, i.e. A_0 is propagated backwards over a time t according to the orthogonal dynamics. Due to stationary of the time correlation function in equilibrium one can write

$$\tilde{C}_{AB}(t) = \left\langle \left(e^{i\mathcal{L}t}A_t^-\right)\left(e^{i\mathcal{L}t}B_0\right)\right\rangle = \left\langle \tilde{A}_t^- B_t \right\rangle, \tag{3.41}$$

where $\tilde{A}_t^- = e^{i\mathcal{L}t}A_t^-$. Carof *et al.* have shown,[85] that this auxiliary variable evolves as

$$\frac{d\tilde{A}_t^-}{dt} = i\mathcal{L}e^{i\mathcal{L}t}(\mathcal{P})e^{-i\mathcal{L}t}\tilde{A}_t^-. \tag{3.42}$$

Applying the definition of the projection operator $\mathcal{P}$ yields

$$\begin{aligned}
\frac{d\tilde{A}_t^-}{dt} &= i\mathcal{L}e^{i\mathcal{L}t}\boldsymbol{P}_{I,0}\frac{\left\langle \boldsymbol{P}_{I,0}e^{-i\mathcal{L}t}\tilde{A}_t^- \right\rangle}{\left\langle \boldsymbol{P}_{I,0}^2 \right\rangle} \\
&= i\mathcal{L}e^{i\mathcal{L}t}\boldsymbol{P}_{I,0}\frac{\left\langle e^{i\mathcal{L}t}\boldsymbol{P}_{I,0}\tilde{A}_t^- \right\rangle}{\left\langle \boldsymbol{P}_{I,0}^2 \right\rangle} \\
&= \frac{\left\langle \boldsymbol{P}_{I,t}\tilde{A}_t^- \right\rangle}{\left\langle \boldsymbol{P}_{I,0}^2 \right\rangle}\boldsymbol{F}_{I,t}.
\end{aligned} \tag{3.43}$$

In Eq. 3.43, while applying the projection operator, the notation is simplified by assuming an isotropic system, in which all Cartesian components are equivalent and independent. This allows to replace $\left\langle \boldsymbol{P}_{I,0}\boldsymbol{P}_{I,0}^{T}\right\rangle$ by the scalar product $\left\langle \boldsymbol{P}_{I,0}^{2}\right\rangle$.

The variable $\tilde{A}_t^-$ cannot be directly evaluated for any given point in phase space, as it depends on the chosen initial conditions. Thus it has to be iteratively propagated following Eq. 3.43 for a sufficiently large set of time origins to evaluate $\left\langle \boldsymbol{P}_{I,t}\tilde{A}_t^-\right\rangle$. In practice, different numerical strategies can be employed. A first-order scheme proposed in the original publication reads

$$\tilde{A}_{t+\delta t}^- = \tilde{A}_t^- + \frac{\left\langle \boldsymbol{P}_{I,t}\tilde{A}_t^-\right\rangle}{\left\langle \boldsymbol{P}_{I,0}^2\right\rangle}\boldsymbol{F}_{I,t}\delta t. \tag{3.44}$$

In this thesis a second order scheme, as proposed by Jung *et al.*[39], is employed:

$$\tilde{A}_{t+\delta t}^- = \tilde{A}_t^- + \alpha(t)\boldsymbol{F}_{I,t}\frac{\delta t}{2} + \frac{\boldsymbol{F}_{I,t+\delta t}}{1-\frac{\delta t}{2}\kappa}\left[\zeta(t)+\epsilon\alpha(t)\frac{\delta t}{2}\right]\frac{\delta t}{2}, \tag{3.45}$$

with

$$\alpha(t) = \frac{\left\langle \boldsymbol{P}_{I,t}\tilde{A}_t^-\right\rangle}{\left\langle \boldsymbol{P}_{I,0}^2\right\rangle} \tag{3.46}$$

$$\zeta(t) = \frac{\left\langle \boldsymbol{P}_{I,t+\delta t}\tilde{A}_t^-\right\rangle}{\left\langle \boldsymbol{P}_{I,0}^2\right\rangle} \tag{3.47}$$

$$\kappa = \frac{\langle \boldsymbol{P}_{I,0}\boldsymbol{F}_{I,0}\rangle}{\left\langle \boldsymbol{P}_{I,0}^2\right\rangle} \tag{3.48}$$

$$\epsilon = \frac{\langle \boldsymbol{P}_{I,\delta t}\boldsymbol{F}_{I,0}\rangle}{\left\langle \boldsymbol{P}_{I,0}^2\right\rangle}. \tag{3.49}$$

By choosing $A = B = \boldsymbol{F}_I$, the memory kernel $K(t)$ can be evaluated as

$$\tilde{C}_{FF}(t) = \left\langle \boldsymbol{F}_I(0)\boldsymbol{F}_I^{\mathcal{Q}}(t)\right\rangle = 3M_I k_B T K(t) \tag{3.50}$$

While the BOD approach described in this section and the Volterra-inversion approach described in Sec. 3.4, yield the same memory kernel,[33, 39, 85] the BOD-method can be used to evaluate any arbitrary $\mathcal{Q}$-projected correlation function.[85] In particular, by choosing $A = B = \boldsymbol{F}_I^C$, $A = B = \delta\boldsymbol{F}_I = \boldsymbol{F}_I - \boldsymbol{F}_I^C$ or $A = \boldsymbol{F}_I^C$ and $B = \delta\boldsymbol{F}_I$, the total memory kernel can be split into different contributions as in Eq. 3.51.

$$\begin{aligned} K(t) &= \frac{\left\langle \boldsymbol{F}_I^{C,\mathcal{Q}}(t)\boldsymbol{F}_I^{C,\mathcal{Q}}(0)\right\rangle}{3M_I k_B T} \\ &\quad + \frac{\left\langle \delta\boldsymbol{F}_I^{\mathcal{Q}}(t)\delta\boldsymbol{F}_I^{\mathcal{Q}}(0)\right\rangle}{3M_I k_B T} + 2\frac{\left\langle \boldsymbol{F}_I^{C,\mathcal{Q}}(t)\delta\boldsymbol{F}_I^{\mathcal{Q}}(0)\right\rangle}{3M_I k_B T} \\ &= K_C(t) + K_\delta(t) + 2K_X(t) \end{aligned} \tag{3.51}$$

The three contributions $K_C(t)$, $K_\delta(t)$ and $K_X(t)$ can be interpreted as the memory and friction due to effective conservative interactions between the CG DoFs, due to interactions with the lost DoFs, and due to the cross-correlations between these interactions. Due to the analogue physical interpretation, it can be assumed that

$$\Delta K^{CG}(t) \approx K_C(t). \tag{3.52}$$

This suggests that for a purely bottom-up approach the optimal choice of $\tilde{K}(t)$ to ensure dynamic consistency in the sense of Eq. 3.35 is given by

$$\tilde{K}(t) \equiv K_\delta(t) + 2K_X(t). \tag{3.53}$$

3.7 Iterative Optimization of Memory Kernels (IOMK)

An alternative to a purely bottom-up informed parametrization of Eq. 1.1, is to iteratively optimize the parameterization of the memory kernel $\tilde{K}(t)$ in CG GLE simulations, such that the FG reference dynamics is approached in successive steps. By explicitly tuning the memory kernel $\tilde{K}(t)$ to match the FG dynamics, such an approach circumvents the main problem of bottom-up approaches, which is the need for a set of more or less justified assumptions. The challenge herein lies in finding an appropriate recipe for a systematic procedure, which determines how to choose an update scheme. This approach is well established in structural coarse-graining for the optimization of pair-potentials, and gave rise to several methods as IBI,[9] IMC,[10] REM[197] and HNC-N.[12] Jung *et al.*, inspired by the IBI method for structural coarse-graining, proposed several update schemes for the optimization of memory kernels. In these methods, the target function, with respect to which the memory kernel is optimized, is either the force autocorrelation function ("IMRF")[39] or the VACF ("IMRV")[30, 39].

In particular in many-body simulations with conservative interactions and memory, the relation between the memory kernel of the GLE thermostat and dynamical quantities, for example the VACF, can be quite complicated. Thus, the IMRV method can suffer from numerical instabilities. In order to optimize the stability in the IMRV method the step size has to be tuned by empirical parameters. If done carefully, this can yield good results. Still, the number of iterations needed for sufficient convergence can be quite high.(See Refs. [30, 39] and chapter 6 in this thesis.) Slow convergence in terms of the number of CG iterations is of little concern as long as the degree of coarse-graining is high and thus CG simulations are efficient compared to FG simulations. If however a mapping scheme is chosen such that the resolution is only moderately reduced, the computational overhead due to the need of many iterations can be significant.

An alternative iterative scheme, which allows to define an update step which is simultaneously stable, efficient (fast convergence) and generic (no empirical tuning parameters) would greatly simplify the parametrization process and improve the applicability as a out of the box tool for dynamic CG. The main problem of the IMRV method for parametrizing $\tilde{K}(t)$ is that the relation between the VACF and $\tilde{K}(t)$ is quite complicated and potentially highly non-linear. (See sec. 6.6.2 for a detailed discussion.) The consistency condition given by Eq. 3.35 suggests an alternative choice for the target function, which is $K^{CG}(t)$. This choice is in principle equivalent to targeting the VACF directly. The advantage lies in the fact that the memory kernels $\tilde{K}(t)$ and $K^{CG}(t)$ are related via simpler relations than $\tilde{K}(t)$ and the VACF. Thus it is easier to derive iterative schemes with favorable convergence behavior.

In the following, three novel iterative procedures are presented. For their formulation, it is useful to reformulate the consistency condition Eq. 3.35 in terms of integrated memory kernels:

$$G^{CG}(t) \approx G(t) = G^{tgt}(t). \tag{3.54}$$

Arguably, the most straight-forward approach to construct an iterative update scheme, is to derive an (approximate) Newton scheme of the form

$$\tilde{G}_{i+1}(t) = \tilde{G}_i(t) + (G_i^{CG'}(t))^{-1}(G^{tgt}(t) - G_i^{CG}(t)) \tag{3.55}$$

whereby

$$G_i^{CG'}(t) = \frac{\partial G_i^{CG}(t)}{\partial \tilde{G}_i(t)}. \tag{3.56}$$

Note, that this formulation is not of the most general form, but already assumes that $G_i^{CG}(t)$ at time t is only affected by $\tilde{G}_i(t)$ at the same time t. This is an assumption, which will be made throughout all three of the methods presented below.

The task now is to find a reasonable approximation for $G_i^{CG'}(t)$.

The first approach

Consider a CG simulation using Eq. 1.1 with a integrated memory kernel $\tilde{G}_i(t)$ used in the parametrization of the GLE thermostat. The total integrated memory kernel is given by

$$G_i^{CG}(t) = \Delta G_i^{CG}(t) + \tilde{G}_i(t). \tag{3.57}$$

If one assumes that $\Delta G_i^{CG}(t) \neq f(\tilde{G}_i(t))$, so that the friction and memory introduced through conservative interactions do not depend on the parameterization of the GLE thermostat, then the derivative $G_i^{CG'}(t)$ is given by

$$G_i^{CG'}(t) = 1 \tag{3.58}$$

and the approximate Newton scheme reads

$$\tilde{G}_{i+1}(t) = \tilde{G}_i(t) + (G^{tgt}(t) - G_i^{CG}(t)). \tag{3.59}$$

With this update scheme one attempts to compensate for any deviations from the target just by changing the GLE-thermostat parameterization. Eq. 3.59 will always yield the correct direction for the update. But as the parametrization of the GLE thermostat affects the structural relaxation in many-body simulations, it will simultaneously affect the friction induced through conservative interactions, typically in the same direction. This can, as will be demonstrated in chapter 5, yield to oscillatory convergence.

At the same time, this approach very clearly demonstrates the advantage of constructing an iterative scheme from the consistency condition 3.54: in the limit where conservative interactions are weak and their influence on the total effective friction is negligible, Eq. 3.59 converges trivially within one iteration. In contrast, the IMRV method can take up to hundreds of iterations, even in an idealized case.[39]

The second approach

For the second approach, assume that $G_i^{CG}(t) \propto \tilde{G}_i(t)$, such that

$$G_i^{CG}(t) \approx b(t)\tilde{G}_i(t). \tag{3.60}$$

In this case, the derivative $G_i^{CG'}(t)$ is given by

$$G_i^{CG'}(t) = b(t). \tag{3.61}$$

In practice, it would be tedious to derive $b(t)$ from a linear regression. It is easier, to let $b(t)$ depend on the current iteration i and to utilize Eq. 3.60 to get

$$G_i^{CG'}(t) = \frac{G_i^{CG}(t)}{\tilde{G}_i(t)}, \tag{3.62}$$

from which the approximate Newton scheme is given by

$$\tilde{G}_{i+1}(t) = \tilde{G}_i(t) + \frac{\tilde{G}_i(t)}{G_i^{CG}(t)}(G^{tgt}(t) - G_i^{CG}(t)). \tag{3.63}$$

Eq. 3.63 can be further simplified to

$$\tilde{G}_{i+1}(t) = \frac{G^{tgt}(t)}{G_i^{CG}(t)}\tilde{G}_i(t). \tag{3.64}$$

As can be seen, this update scheme applies a rescaling of the thermostat memory kernel according the the ratio of the target to the current effective integrated memory kernel. The implications, in comparison the the first update scheme, are the following: as in the first approach, if friction and memory due to conservative interactions are negligible, Eq. 3.64 converges within a single iteration as in such a case $\frac{\tilde{G}_i(t)}{G_i^{CG}(t)} = 1$ and thus, the first update scheme is recovered. Whenever the contribution of friction due to conservative interactions becomes significant (this means $G_i^{CG}(t) > \tilde{G}_i(t)$), $G_i^{CG'}(t)$ increases and accordingly the stepsize decreases automatically. Thus, this update scheme can circumvent oscillations in the update procedure with the drawback of smaller stepsizes and thus potentially slower convergence in some cases.

Adding some physical intuition: iterative optimization of memory kernels (IOMK)

The approximations on which Eqs. 3.59 and 3.64 are based, are clearly not optimal. While the former case neglects the dependence of $\Delta G_i^{CG}(t)$ on $\tilde{G}_i(t)$, the latter case can, in principle, yield infinitesimally small stepsizes when $\Delta G_i^{CG}(t)$ is very large compared to $\tilde{G}_i(t)$. To derive a better approximate Newton scheme, an accurate approximation for the dependence of $\Delta G_i^{CG}(t)$ on $\tilde{G}_i(t)$ is needed. As already indicated, $\Delta G_i^{CG}(t)$ should be positively correlated with $\tilde{G}_i(t)$, but is non-zero for $\tilde{G}_i(t) = 0$. Thus one can assume

$$\Delta G_i^{CG}(t) \approx a(t) + b(t)\tilde{G}_i(t). \tag{3.65}$$

Herein, $a(t)$ is the effective integrated memory kernel in a CG-MD simulation, if $\tilde{G}(t)$ is set to zero. From that, the full approximation for $G_i^{CG}(t)$ is given by

$$G_i^{CG}(t) \approx a(t) + (1 + b(t))\tilde{G}_i(t), \tag{3.66}$$

from which the derivative $G_i^{CG'}(t)$ can be derived as

$$G_i^{CG'}(t) = (1 + b(t)). \tag{3.67}$$

Again, the need for performing a linear regression can be circumvented by reordering of Eq. 3.66, which yields

$$G_i^{CG'}(t) = \frac{G_i^{CG}(t) - a(t)}{\tilde{G}_i(t)}. \tag{3.68}$$

Thus, the third update scheme reads

$$\tilde{G}_{i+1}(t) = \tilde{G}_i(t) + \frac{\tilde{G}_i(t)}{G_i^{CG}(t) - a(t)}(G^{tgt}(t) - G_i^{CG}(t)). \tag{3.69}$$

Eq. 3.69 can be further simplified to yield

$$\tilde{G}_{i+1}(t) = \frac{G^{tgt}(t) - a(t)}{G_i^{CG}(t) - a(t)}\tilde{G}_i(t). \tag{3.70}$$

This method, referred to as the iterative optimization of memory kernels (IOMK) method, in contrast to Eq. 3.64, accounts for the fact that even for $\tilde{G}_i(t) \to 0$, the total integrated memory kernel $G_i^{CG}(t)$ has a lower bound of $a(t)$. This effectively increases the stepsize compared to Eq. 3.64, while still reducing oscillations compared to Eq. 3.59. A thorough comparison of all three schemes is carried out in chapter 5, while a comparison of the IOMK and the IMRV method due to Jung *et al.*[30] is provided in chapter 6.

3.8 General Approach

3.8.1 Modeling Non-Markovian Dynamics Through Markovian Equations: The Auxiliary Variable Approach

This section is partially an adaptation from the SI of Ref. [34]. The respective section in the SI of chapter 5 is accordingly removed.

To correct the dynamics in CG-MD simulations, a dissipative EoM of motion has to be employed. This work focuses on the application of a non-Markovian GLE thermostat of the form

$$\boldsymbol{F}_I(t) = \boldsymbol{F}_I^C(t) - \int_0^t ds\tilde{K}(t-s)\boldsymbol{P}_I(s) + \tilde{\boldsymbol{F}}_I^R(t). \tag{3.71}$$

With this particular choice for the CG EoM, thermostatting by means friction and noise is employed independently on every CG DoF. More complex non-Markovian models have been explored in this context[26, 27, 30], but these come with the drawback of high computational complexity and thus reduced efficiency.

Eq 3.71 can be efficiently integrated by casting it into a Markovian Langevin EoM in extended phase space[150]

$$\begin{aligned}\begin{pmatrix} F_I \\ \dot{\boldsymbol{s}}_I \end{pmatrix} &= \begin{pmatrix} F_I^C \\ \boldsymbol{0} \end{pmatrix} - \boldsymbol{A}\begin{pmatrix} P_I \\ \boldsymbol{s}_I \end{pmatrix} + \boldsymbol{B}\boldsymbol{\xi} \\ &= \begin{pmatrix} F_I^C \\ \boldsymbol{0} \end{pmatrix} - \begin{pmatrix} 0 & \boldsymbol{A}_{Ps}^T \\ -\boldsymbol{A}_{Ps} & \boldsymbol{A}_{ss} \end{pmatrix}\begin{pmatrix} P_I \\ \boldsymbol{s}_I \end{pmatrix} + \begin{pmatrix} 0 & \boldsymbol{0} \\ \boldsymbol{0} & \boldsymbol{B}_{ss} \end{pmatrix}\boldsymbol{\xi},\end{aligned} \tag{3.72}$$

For notational simplicity, Eq. 3.72 represents the EoM for a single CG DoF, for one Cartesian dimension, and can be trivially extended to three dimensions in isotropic systems. The DoF of interest is P_I, so the EoM of motion of P_I can be singled out as

$$F_I = F_I^C - \boldsymbol{A}_{Ps}^T\boldsymbol{s}_I. \tag{3.73}$$

To show how Eq. 3.72 relates to Eq. 3.71, the auxiliary variables have to be integrated.[155]

$$\boldsymbol{s}_I(t) = \int_0^t e^{-(t-t')\boldsymbol{A}_{ss}} \left[\boldsymbol{A}_{Ps} P_I(t') + \boldsymbol{B}_{ss}\xi(t')\right] dt' \tag{3.74}$$

Eq. 3.74 can now be plugged into Eq. 3.73, which yields

$$F_I(t) = F_I^C(t) - \int_0^t K(t-t')P_I(t')dt' + \tilde{F}^R(t) \tag{3.75}$$

with

$$\tilde{K}(t) = -\boldsymbol{A}_{Ps}^T e^{-t\boldsymbol{A}_{ss}} \boldsymbol{A}_{Ps} \tag{3.76}$$

and

$$\tilde{F}_I^R(t) = -\int_0^t \boldsymbol{A}_{Ps} e^{-(t-t')\boldsymbol{A}_{ss}} \boldsymbol{B_{ss}}\xi(t')dt'. \tag{3.77}$$

From Eq. 3.76 it is evident that the choice of the coupling matrix A in the auxiliary variable EoM determines the functional form of the memory kernel which it effectively mimics. As a simple example, consider

$$\boldsymbol{A} = \begin{pmatrix} 0 & -\sqrt{\frac{\gamma}{\tau}} \\ \sqrt{\frac{\gamma}{\tau}} & \frac{1}{\tau} \end{pmatrix}. \tag{3.78}$$

Using this definition in Eq. 3.76,

$$\tilde{K}(t) = \sqrt{\frac{\gamma}{\tau}} e^{-\frac{t}{\tau}} \sqrt{\frac{\gamma}{\tau}} = \frac{\gamma}{\tau} e^{-\frac{t}{\tau}}, \tag{3.79}$$

thus a exponentially decaying memory kernel with a time scale of τ and a total integral corresponding to the total, long time, friction coefficient of $\gamma = \int_0^\infty \tilde{K}(t)dt$.

In principle, the coupling matrix $\boldsymbol{A}$ can be chosen to model more complex functions. Its dimensionality NxN, determines the number of auxiliary momenta which is given by $N-1$. For canonical sampling the fluctuation dissipation theorem[151]

$$\boldsymbol{B}\boldsymbol{B}^T = k_B T(\boldsymbol{A} + \boldsymbol{A}^T) \tag{3.80}$$

has to be satisfied. This limits the choice of the coupling matrix $\boldsymbol{A}$ to cases where $\boldsymbol{A} + \boldsymbol{A}^T$ is positive-(semi)definite. The easiest way to enforce that is by using a skew symmetric matrix with positive diagonal entries.

In molecular systems memory kernels, even in the case of simple single particle systems, typically exhibit quite complicated behavior and cannot be easily represented in a closed analytical form. Even less is it possible to give an exact analytical prescription to construct the matrix A to represent arbitrary memory kernels with an unknown functional form. A numerical scheme, based on which the $\boldsymbol{A}$ matrix for, in principle, arbitrary (well behaved) memory kernels can be reconstructed for one dimensional problems, was given by Bockius *et al.*.[98] Their approach cannot be trivially extended to the purpose of the current work, that is for CG simulations of many particle systems. An alternative approach, chosen in the current work, is to represent the memory kernel in terms of basis functions for which the form of the $\boldsymbol{A}$ matrix is known.

Herein, for CG simulations the desired memory kernel can be fitted by as sum N_{osc} of dampened oscillators

$$\tilde{K}(t) \approx \sum_{i=1}^{N_{osc}} \tilde{K}_i = \sum_{i=1}^{N_{osc}} \exp\Big(-\frac{a_i}{2}t\Big)(b_i \cos(d_i t) + c_i \sin(d_i t)), \tag{3.81}$$

which allows to model a broad range of memory kernels. A single dampened oscillator corresponds to the coupling to two auxiliary momenta with a coupling matrix given by

$$\boldsymbol{A} = \begin{pmatrix} 0 & \sqrt{\frac{b}{2} - \frac{cd}{a}} & \sqrt{\frac{b}{2} + \frac{cd}{a}} \\ -\sqrt{\frac{b}{2} - \frac{cd}{a}} & a & \frac{1}{2}\sqrt{4d^2 + a^2} \\ -\sqrt{\frac{b}{2} + \frac{cd}{a}} & -\frac{1}{2}\sqrt{4d^2 + a^2} & 0 \end{pmatrix}. \tag{3.82}$$

For a sum of dampened oscillators, two respective auxiliary variables per dampened oscillator are coupled to P_I and uncoupled to the auxiliary variables of the other dampened oscillators. Thus, $\boldsymbol{A}_{Ps}^T = (\boldsymbol{A}_{Ps,1}^T, \boldsymbol{A}_{Ps,2}^T, ..., \boldsymbol{A}_{Ps,N}^T)$ is a vector of length $2N$ and

$$\boldsymbol{A}_{ss} = \begin{pmatrix} \boldsymbol{A}_{ss,1} & \boldsymbol{0} & \dots & \boldsymbol{0} \\ \boldsymbol{0} & \boldsymbol{A}_{ss,2} & \dots & \boldsymbol{0} \\ \vdots & \vdots & \ddots & \vdots \\ \boldsymbol{0} & \boldsymbol{0} & \dots & \boldsymbol{A}_{ss,N} \end{pmatrix} \tag{3.83}$$

is a skew-symmetric, block diagonal matrix with N blocks of size 2×2.

In practice, the fitting process can be improved by considering the integrated memory kernel $\tilde{G}(t) = \int_0^t \tilde{K}(t')dt'$ and the fitting function accordingly reads

$$\begin{aligned} \tilde{G}(t) \approx \sum_{i=1}^{N} \Bigg(& 2\frac{a_i b_i + 2c_i d_i}{a_i^2 + 4d_i^2} \\ & - \frac{2e^{-\frac{a_i t}{2}}\left((a_i b_i + 2cd)\cos(d_i t) + (a_i c_i - 2b_i d_i)\sin(d_i t)\right)}{a_i^2 + 4d_i^2} \Bigg). \end{aligned} \tag{3.84}$$

3.8.2 General Workflow

In this section, the general workflow for development of dynamic CG, as applied in Chapters 4-6 is shortly summarized.

As the current work addresses systematic approaches, the first step is to choose the reference fine-grained (FG), often all-atom (AA) model. Standard molecular dynamics simulations are carried out with the reference model. Then a mapping with the desired resolution is chosen and applied on FG reference trajectories. This results in mapped trajectories governed by the references Hamiltonian, from which structural and dynamic properties can be computed on the desired CG level.

In the next step, the CG conservative potential has to be chosen. To do so, in principle any available systematic coarse-graining method, as e.g. IBI,[9] IMC,[10] REM,[197] HNCN,[12] FM,[193] EFCG,[76] CRW[74] etc., can be used to directly use information from the reference model to parameterize the CG conservative potential. In principle, also top-down parameterized models can be chosen. While the overall workflow does not prescribe a strict strategy for the choice of the conservative CG potential, its choice can greatly affect the the representation of dynamic properties in CG model and thus a judicious choice has to be made in practice, as is discussed throughout chapters 4-6.

In the next step, the memory kernel for the GLE thermostat has to be derived. In the current work, two distinct strategies are applied: a purely bottom-up informed approach and an iterative optimization approach.

For the bottom-up approach, the BOD-method due to Carof *et al.*[85] is applied to analyze mapped reference trajectories. Therein the total memory kernel $K(t)$ is separated into different contributions, as described in Sec. 3.6.2. Based on the argument that $K_C(t)$ will be implicitly contributed due to conservative interactions in CG simulations, it is found that

$$\tilde{K}(t) = K(t) - K_C(t) = K_\delta(t) + 2K_X(t) \tag{3.85}$$

yields the best results. The BOD-method allows for different choices of contributions to explicitly include in the thermostat memory kernel. For comparison, $K_\delta(t)$ and $K_{\delta,X}(t) = K_\delta(t) + K_X(t)$ can also be considered as potential parameterization for the GLE-thermostat. In passing, it should be noted that the memory $K_{\delta,X}(t)$ is equivalent to the memory kernel which can be derived based on Eq. 3.39. This is demonstrated numerically in chapter 4 and has recently been confirmed based on theoretical considerations by Vroylandt.[198]

For an iterative approach, an initial guess has to be made, from which the memory kernel can be optimized in successive iterations of CG simulations. In Chapters 5 and 6, different prescriptions for the the update step are tested and discussed.

As described in Sec. 3.8.1, the memory kernel for the GLE thermostat has to be translated into a coupling matrix for the auxiliary variable thermostat due to Ceriotti.[150, 151] This step, naturally, can be omitted if the non-Markovian GLE models is directly integrated as e.g. in Ref. [31].
Finally, the FG and CG models can be analyzed.

4 Cross-Correlation Corrected Friction in (Generalized) Langevin Models

Abstract

We propose a route for parameterizing isotropic (generalized) Langevin ((G)LE) thermostats with the aim to correct the dynamics of coarse-grained (CG) models with pairwise conservative interactions. The approach is based on the Mori-Zwanzig formalism and derives the memory kernels from Q-projected time correlation functions. Bottom-up informed (GLE and LE) thermostats for a CG star-polymer melt are investigated and it is demonstrated that the inclusion of memory in the CG simulation leads to predictions of polymer diffusion in quantitative agreement with fine-grained simulations. Interestingly, memory effects are observed in the diffusive regime. We demonstrate that previously neglected cross correlations between the "irrelevant" and the CG degrees of freedom are important and lie at the origin of shortcomings in previous CG simulations.

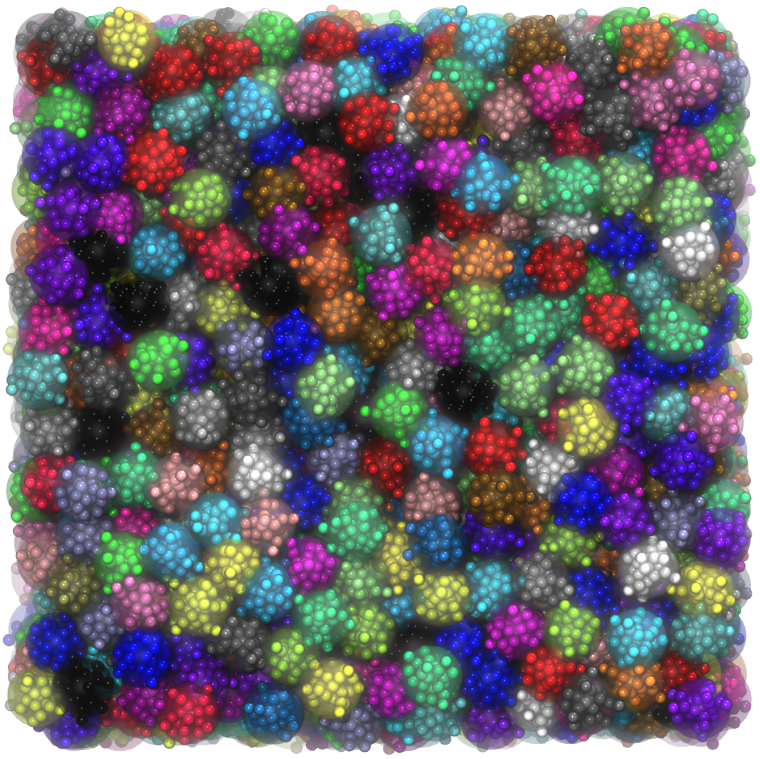

4.1 Introduction

To reduce the numerical complexity in computer simulations of soft matter, coarse-grained (CG) models are commonly used. The systematic derivation of these models frequently targets at structural and thermodynamical properties based on procedures that map a high-dimensional space of atomistic degrees of freedom (DoF) on a lower dimensional space of CG DoF. The interaction sites ("beads") of the resulting CG models usually correspond to the centers of mass of several atoms grouped together to represent, e.g., a small molecule, functional group, monomer, thermal blob, or an entire macromolecule.[9, 10, 44, 57, 73, 193, 197, 199] Contrary to static properties, the dynamic properties of these CG models are usually poorly represented in standard molecular dynamics simulations.[15, 19, 200, 201] Despite progress made in recent years, challenges remain, in particular in representing the dynamic properties of material-specific CG models on all relevant time scales.

The Hamiltonian dynamics of a fine-grained (FG) system can be represented with a CG model when non-Markovian interactions, represented by friction and noise terms, are introduced in the equation of motion (EoM). The Mori-Zwanzig theory[22, 23, 51] provides an exact theoretical framework to link the FG and CG dynamics and has been explored in recent years with varying success.[26, 27, 60, 62–65, 121] The difficulties encountered are usually caused by incomplete time scale separation of the relevant (CG) and the removed DoF. Therefore, configuration-dependent frictions, e.g, pairwise, distance-dependent and time-independent friction coefficients in dissipative particle dynamics (DPD) models, cannot readily be computed. A conceptually simpler approach involves the use of configuration-independent friction coefficients or memory kernels in a Langevin (LE) or a generalized Langevin (GLE) thermostat coupled to the CG DoF.[32, 36]

Methods for constructing (G)LE thermostats, which do not rely on a *a posteriori* optimization scheme,[30, 32, 39] have in common that FG trajectories are analyzed by separating forces into contributions from an assumed conservative force-field, governing structure and thermodynamical properties, and fluctuating contributions which are assigned to frictional and random interactions.[26, 27, 60, 62–65, 121] In early studies Lei *et al.*[36] attempted by this approach to correct the self-diffusivity of a liquid composed of CG fluid particles representing clusters of Lennard-Jones (LJ) particles. A Markovian Langevin thermostat was applied where the friction coefficient was parameterized based on the integral of the force auto-correlation function (FACF) of the fluctuating forces. This approach was derived based on the EoM derived by Kinjo and Hyodo[58] by neglecting cross-correlations between different CG beads and subsequently assuming Markovian behavior. The authors found that the self-diffusion coefficient was underestimated by a factor of four in the CG Langevin models while DPD-type models performed significantly better for the same system,[36] indicating that the mismatch was due to missing configuration dependency in the frictional and random forces. In the following years, the same research group focused their efforts on improving the methodology to derive more accurate DPD-type models by e.g. the introduction of memory effects.[26, 27, 121] Yet the magnitude of the mismatch in self-diffusion coefficients in the Langevin models is intriguing as one could reasonably assume that configuration dependencies would average out in isotropic systems, similar to the case of single-particle implicit solvent GLE models which can capture the underlying FG dynamics exactly in the absence of conservative interactions.[92] In principle, the parametrization of (generalized) Langevin models can be optimized iteratively until the fine-grained dynamics is matched.[30, 32, 39] While this is a valid approach and widely used in the derivation of conservative interactions for CG models,[9, 10, 202] such methods obscure the origin of the poor performance of bottom-up derived friction coefficients and memory kernels for LE and GLE models.

Herein, we will demonstrate that through the splitting of interactions into conservative and fluctuating forces on the CG level, frictional contributions arise, which were not accounted for in earlier studies. The calculation of these contributions from Q-projected time correlation functions provides a route to compute

memory kernels with which dynamic consistency is achieved in GLE simulations. It furthermore provides improved insight in interactions that lead to memory effects in soft matter systems manifested on diffusive timescales.

We shall be interested in a GLE of the form

$$F(t) = F^C(t) - m\int_0^t ds\tilde{K}(t-s)v(s) + \tilde{F}^R(t), \tag{4.1}$$

in which $F(t)$ is the total force on a CG particle, $F^C(t)$ is a conservative force corresponding to a CG force field, m is the particle mass, and $v(t)$ its velocity. One-dimensional descriptions are used throughout, which for isotropic systems trivially hold for all Cartesian dimensions. The random force $\tilde{F}^R(t)$ and the memory kernel $\tilde{K}(t)$ are related through the fluctuation-dissipation theorem (FDT)[23, 69] and represent the GLE thermostat. The question of interest herein is how the microscopic interactions encode $\tilde{K}(t)$.

To this end, it is instructive to first consider the GLE for a single particle in an isotropic medium. Expressed in the Mori-Zwanzig formulation, the EoM is

$$F(t) = -m\int_0^t dsK(t-s)v(s) + F_Q(t), \tag{4.2}$$

in which $F_Q(t)$ denotes the Q-projected total force on the particle.[23, 85] Its relation to $K(t)$ is provided by the FDT according to

$$K(t) = \langle F_Q(t)F_Q(0)\rangle / mk_BT, \tag{4.3}$$

where k_B is the Boltzmann constant, T the temperature, and $\langle ...\rangle$ denotes averaging over configurations of the microscopic (FG) system. To make the evaluation of Eq. 4.2 tractable in computer simulations, $F_Q(t)$ has to be interpreted to be a random force $F^R(t)$, in which case the EoM reads

$$F(t) = -m\int_0^t dsK(t-s)v(s) + F^R(t). \tag{4.4}$$

The Q-projected total force in Eq. 4.3 can be written as $F_Q(t) = F_Q^C(t) + \delta F_Q(t)$. The kernel can therefore be expressed as

$$\begin{aligned} mk_BTK(t) &= \langle F_Q(t)F_Q(0)\rangle \\ &= \left\langle F_Q^C(t)F_Q^C(0)\right\rangle + \langle \delta F_Q(t)\delta F_Q(0)\rangle + 2\left\langle F_Q^C(t)\delta F_Q(0)\right\rangle \\ &= mk_BTK_C(t) + mk_BTK_\delta(t) + 2mk_BTK_X(t). \end{aligned} \tag{4.5}$$

A similar splitting of contributions to $K(t)$ in terms of attractive and repulsive interactions in a LJ fluid was carried out by Carof *et al.*.[85] The above splitting of $F_Q(t)$ in Eq. 4.2, generally leads to correlated Q-projected conservative- and fluctuating forces, i.e. $\left\langle F_Q^C(t)\delta F_Q(0)\right\rangle \neq 0$. The *r*andom force, $\tilde{F}^R(t)$, in Eq. 4.1 is often interpreted to stem from the same fluctuations that determine $\delta F_Q(t)$.[36] This however leads to the tacit assumption that $\left\langle F_Q^C(t)\delta F_Q(0)\right\rangle = 0$, and, correspondingly, $K_X(t) = 0$, which can only be assumed if $F_Q^C(t)$ and $\delta F_Q(t)$ evolve on separated time scales.

The above analysis of the single-particle model has consequences for interpreting the memory kernel in Eq. 4.1. The CG conservative forces are explicit in Eq. 4.1 and, therefore, do not contribute to the friction represented by the kernel $\tilde{K}$. We may therefore approximate $\tilde{K}(t)$ as

$$\tilde{K}(t) \approx K_\delta(t), \tag{4.6}$$

Table 4.1: Summary of important definitions and relations of the memory kernels considered.

backward orthogonal dynamics	Volterra equations	auxiliary relations
$K(t) = \langle F_Q(t)F_Q(0)\rangle / mk_BT$	$\langle F(t)v(0)\rangle = -m\int_0^t dsK^V(t-s)\langle v(s)v(0)\rangle$	$K_{\delta,X}(t) = K_\delta(t) + K_X(t)$
$K_C(t) = \left\langle F_Q^C(t)F_Q^C(0)\right\rangle / mk_BT$	$\langle \delta F(t)v(0)\rangle = -m\int_0^t ds\tilde{K}^V(t-s)\langle v(s)v(0)\rangle$	$\tilde{K}(t) = K_\delta(t) + 2K_X(t)$
$K_\delta(t) = \langle \delta F_Q(t)\delta F_Q(0)\rangle / mk_BT$	$\left\langle F^C(t)v(0)\right\rangle = -m\int_0^t dsK_C^V(t-s)\langle v(s)v(0)\rangle$	$K_{C,X}(t) = K_C(t) + K_X(t)$
$K_X(t) = \left\langle F_Q^C(t)\delta F_Q(0)\right\rangle / mk_BT$		$K^V(t) = K(t)$
		$\tilde{K}^V(t) = K_{\delta,X}(t)$
		$K_C^V(t) = K_{C,X}(t)$

if we assume that $K_X(t) = 0$. In the Markovian limit, the Q-projected forces may be replaced with the real forces ("Q-approximation") so that

$$\tilde{K}(t) \approx \langle \delta F(t)\delta F(0)\rangle / mk_BT. \tag{4.7}$$

Based on these approximations, Lei *et* al.[36] performed Langevin dynamics simulations of CG LJ clusters in which the applied friction coefficient γ_{FACF} was obtained from

$$\gamma_{\mathrm{FACF}} = \int_0^\tau dt\,\langle \delta F(t)\delta F(0)\rangle / mk_BT. \tag{4.8}$$

In the general case, Eq. 4.5 however suggests that the kernel $\tilde{K}$ in Eq. 4.1 should be written as

$$\tilde{K}(t) = K_\delta(t) + 2K_X(t). \tag{4.9}$$

It thus contains a contribution of Q-projected correlations between fluctuating forces, encoded by the term $K_\delta(t) = \langle \delta F_Q(t)\delta F_Q(0)\rangle / mk_BT$, and a contribution corresponding to Q-projected cross-correlations of fluctuating and the conservative forces, encoded by $K_X(t) \equiv \left\langle F_Q^C(t)\delta F_Q(0)\right\rangle / mk_BT$. The remaining contribution $K_C(t) = \left\langle F_Q^C(t)F_Q^C(0)\right\rangle / mk_BT$ encodes the friction and memory due to the conservative interactions $F^C(t)$. The Q-projected time correlation functions are herein computed on the basis of the backward orthogonal dynamics method proposed by Carof *et al.*[85] while using the second order integration scheme proposed by Jung *et al.*[39] for numerical evaluation.

Alternatively, different memory kernels can be defined by multiplying Eq. 4.1 or 4.4 with $v(0)$ and subsequent averaging, leading to Volterra equations. These equations can be numerically inverted to derive memory kernels from time correlation functions of mapped FG trajectories. In particular we define the memory kernels $K^V(t)$, $\tilde{K}^V(t)$ and $K_C^V(t)$ linked to the force-velocity correlations functions $\langle F(t)v(0)\rangle$, $\langle \delta F(t)v(0)\rangle$ and $\left\langle F^C(t)v(0)\right\rangle$, respectively. The Volterra inversion approach is discussed in more detail in the Supporting Information (SI). In Tab. 4.1 definitions of memory kernels both in terms of the backward orthogonal dynamics method and the Volterra inversion method are listed, as are their interrelations. Memory kernels derived from the inversion of Volterra equations are denoted by the superscript V. We note that a Volterra inversion applied to Eq. 4.4 provides $K^V(t) = K(t)$.[80, 89, 92, 94, 95] Solving the Volterra equation corresponding to Eq. 4.1 however yields $\tilde{K}^V(t) = K_\delta(t) + K_X(t) \neq \tilde{K}(t)$. This will be demonstrated numerically in Sec. 4.2.1 and discussed analytically in the SI.

4.2 Results

As a test case for the proposed methods we consider a generic star-polymer melt system, where every star-polymer in the microscopic (FG) description consists of one central bead with ten arms and three

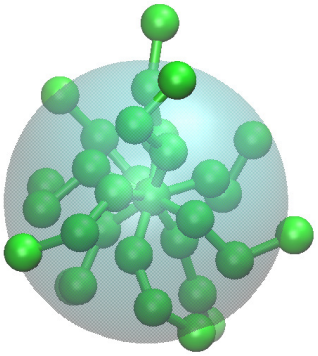

Figure 4.1: The FG and CG representation of a single star-polymer molecule. In the CG process all 31 beads are mapped on the center of mass as $\boldsymbol{R}_I = \sum_i \frac{m_i}{m_I} \boldsymbol{R}_{I,i}$, and accordingly the CG velocity and the total force are calculated as $\boldsymbol{v}_I = \sum_i \frac{m_i}{m_I} \boldsymbol{v}_{I,i}$ and $\boldsymbol{F}_I = \sum_i \boldsymbol{F}_{I,i}$ respectively, where the sum runs over the FG beads and $m_I = \sum_i m_i$. Here the subscript I refers the a CG to the Ith star-polymer molecule and I, i to the ith monomer bead within molecule I.

beads per arm, following Wang *et al.*.[32] We use the iterative Boltzmann inversion (IBI) method for the derivation of conservative CG model in which every star polymer is represented as a single interaction site. A visualization of a single star-polymer in its FG and CG representation is shown in Fig. 4.1. Further details can be found in the SI.

4.2.1 Memory Kernels

We first demonstrate the equivalence of the derived memory kernels based on Volterra equations and the backward orthogonal dynamics method. In particular we want to validate that the cross contribution $K_X(t)$ contributes equivalently to $K_C^V(t)$ and $\tilde{K}^V(t)$ obtained by a Volterra equation approach (see SI). The memory kernels obtained by these methods are compared in Fig. 4.2. Except for small numerical deviations we find that $K^V(t) = K(t)$, $K_C^V(t) = K_{C,X}(t)$ and $\tilde{K}^V(t) = K_{\delta,X}(t)$ holds.

Fig. 4.3 shows all memory kernels evaluated based on the backward orthogonal dynamics method and their respective integrals $\Gamma(t)$. It can be seen that on small time scales the total memory kernel $K(t)$ is mainly governed by the fast degrees of freedom, i.e. $K_\delta(t)$. On longer time scales, the conservative CG interaction, i.e. $K_C(t)$, dominates. The contributions from cross-correlations, i.e. $K_X(t)$, overall are small in amplitude. Yet, over long time scales, the mainly negative contributions accumulate giving rise to an effective decrease of the total friction. A similar behavior was found for the cross-correlations of long-ranged and short-ranged interactions in LJ fluids.[85]

For the parameterization of the GLE-thermostat models we fit the integrals of the memory kernels $K(t)$, $K_\delta(t)$, $K_{\delta,X}(t)$ and $\tilde{K}(t)$ with 6 damped oscillators respectively (see SI for details). We chose to fit the the integrals rather then the memory kernels to account for the accumulative nature of memory effects which effectively govern the qualitative behavior. Furthermore, we want to emphasize the long time dynamics. In Fig. 4.4 the fitted functions are overlayed as dotted lines. For $K(t)$, $K_\delta(t)$, $K_{\delta,X}(t)$ the fitted functions well reproduce the integral of the memory kernels up to a time of $t = 50$. For $\tilde{K}(t)$ we chose to fit the function only up to $t \approx 20$. The reason for that is that the cross contributions $K_X(t)$ show a long

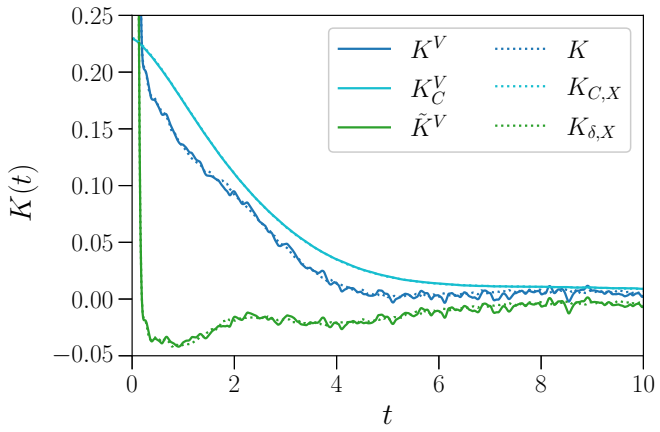

Figure 4.2: Comparison of the memory kernels obtained from Volterra equations (K^V, K_C^V, $\tilde{K}^V$) and the corresponding kernels obtained from the backward orthogonal dynamics method of Carof *et al.*[85] (K, $K_{C,X}$, $K_{\delta,X}$).

lived negative tail, leading to divergence in the plateau of the integral. All memory kernels which can be derived from Volterra equations seem not to suffer from that problem.

4.2.2 Langevin Dynamics Simulations

For the parameterization of Markovian LE models, we chose to derive the friction coefficient from the plateau value of the fit functions. By that the effective friction coefficient employed in the Markovian LE models is consistent with the memory kernels of the non-Markovian GLE models discussed in Sec. 4.2.3, which allows for an analysis of the relevance of memory effects. We will below refer to the different Markovian LE models as "γ-models" and adjust the notation for "γ" according to the corresponding kernels (i.e. γ-model $\leftrightarrow K$, γ_δ-model $\leftrightarrow K_\delta$, $\gamma_{\delta,X}$-model $\leftrightarrow K_{\delta,X}$, $\tilde{\gamma}$-model $\leftrightarrow \tilde{K}$, γ_{FACF}-model $\leftrightarrow \langle \delta F(t) \delta F(0) \rangle / m k_B T$).

In Fig. 4.5 the mean square displacement (MSD), scaled by $\frac{1}{6t}$ is plotted in the linear regime and compared to the FG results. The scaled MSD is constant for the shown time scale for all models and represents the self-diffusion coefficient. As expected, the γ-model, for which all interactions are encoded in γ obtained by integrating $K(t)$, accurately reproduces the self-diffusion coefficient of the FG system and can be seen as a validation of the method for calculating the memory kernels. For the remaining models the LE-thermostat is used in conjunction with CG conservative interactions based on the IBI method. For the γ_{FACF}-model (Eq. 4.8) we find that the self-diffusion coefficient is underestimated by $\approx 25\%$. This is in line with the findings of Lei *et al.*,[36] who found an even larger deviation of approximately a factor of 4 for LJ-clusters. The finding that LE models based on the FACF of the fluctuating forces $\delta F(t)$ show significantly too slow dynamics appears to be quite general. Comparing the result for the γ_{FACF}-model with the γ_δ-model shows that the main error source for the deviation does not lay in the Q-approximation, as the γ_δ-model predicts even lower self-diffusion coefficients. The $\gamma_{\delta,X}$-model, in which the friction coefficient is identical to the one obtained by integrating the kernel $\tilde{K}^V(t)$ obtained from the Volterra equation (cf. Table 4.1), improves the result significantly, but still leads to an underestimation of the self-diffusion coefficient. The $\tilde{\gamma}$-model further enhances the dynamics compared to the $\gamma_{\delta,X}$-model, but is found to overshoot, effectively leading to an overestimation of the self-diffusion coefficient by a similar margin as the $\gamma_{\delta,X}$-model shows an underestimation of the self-diffusion coefficient.

The too fast self-diffusion of the $\tilde{\gamma}$-model can be understood in terms of memory effects, which are

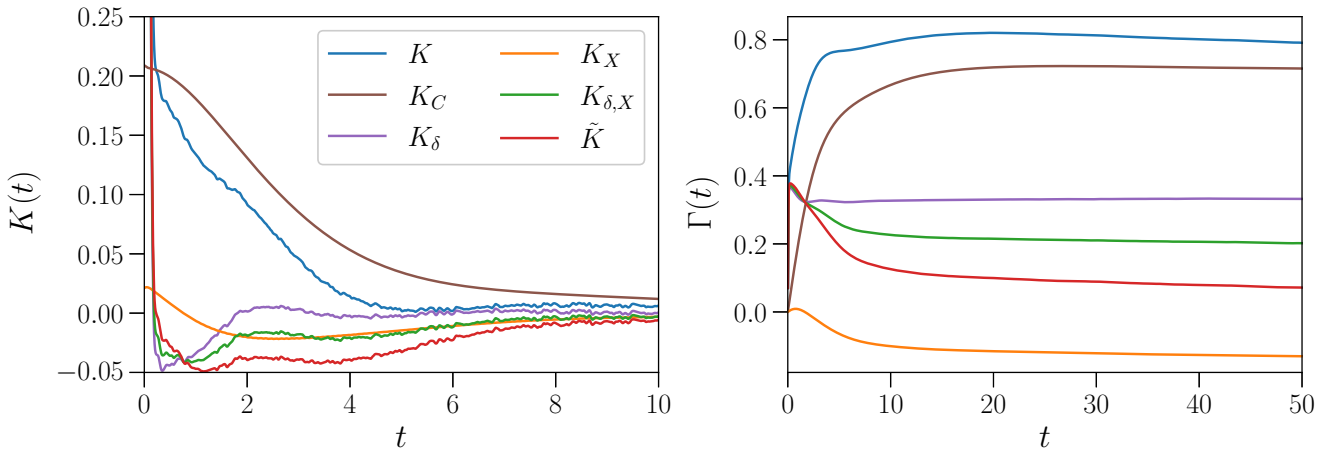

Figure 4.3: Left: The memory kernel $K(t)$ and all its contributions derived from the backward orthogonal dynamics method. Contributions from fluctuating forces (K_δ) decay quite fast, giving rise to quasi-instantaneous friction, while contributions from CG interactions (K_C) show a slow decay. Contributions from cross-correlations (K_X) are small in amplitude on all time scales, being positive on short time scales with a negative slowly decaying tail on long time scales. Right: Integrals $\Gamma(t) = \int_0^t dsK(s)$ of the memory kernel and its contributions. For $t \to \infty$ these integrals represent the friction coefficients in the Markovian approximation. The total integral of $K_X(t)$ is negative, effectively reducing the total friction. The inclusion of $K_X(t)$ in the parameterization of CG models thus should increase the self-diffusion coefficient.

neglected in Markovian models. Generally, when applying a non-Markovian GLE-thermostat the effects on the dynamics depend on the density of states governed by the conservative interactions. [154, 203] In a simple model system this feature of GLE-thermostats was nicely demonstrated by Kappler *et al.* by applying a GLE-thermostat to a particle in a one-dimensional double well potential.[75, 160] They showed that the application of an exponential memory kernel, which decays on much longer time scales than the typical time scale of fluctuations within one minimum of the double well, leads to a slow down of the barrier crossing dynamics. Especially the introduction of a second exponential term in the memory kernel has shown that the effects of the shorter lived memory kernel dominate.[160] This underlines the feature that dynamic modes in the system more strongly couple to a memory kernel which relaxes on comparable time scales.

Differences in the self-diffusion coefficients obtained from Markovian and non-Markovian models parameterized based on the same memory kernel provide indications for memory effects in the long time dynamics. The preceding arguments applied to the CG model used in this work can be used to explain the role of memory. The IBI-model is effectively purely repulsive. As we consider a dense star-polymer melt, the overall dynamics is dominated by short-lived collisions of the beads with their nearest neighbors. The positive amplitudes of the memory kernel on short time scales couple strongly to the dominant dynamic modes. The introduction of the cross contributions $K_X(t)$ in the memory kernel, as demonstrated in Fig. 4.3 and Fig. 4.4, introduces negative amplitudes on long time scales, which should mostly decouple from the short-lived fluctuations due to collisions. Including contributions on all time scales indiscriminately in the derivation of the friction coefficient of the LE-thermostat leads to an increase of the diffusion coefficient compared to non-Markovian models which correctly account for the frequency or time scale dependence of dissipative interactions. We will validate this interpretation of the data in the next section.

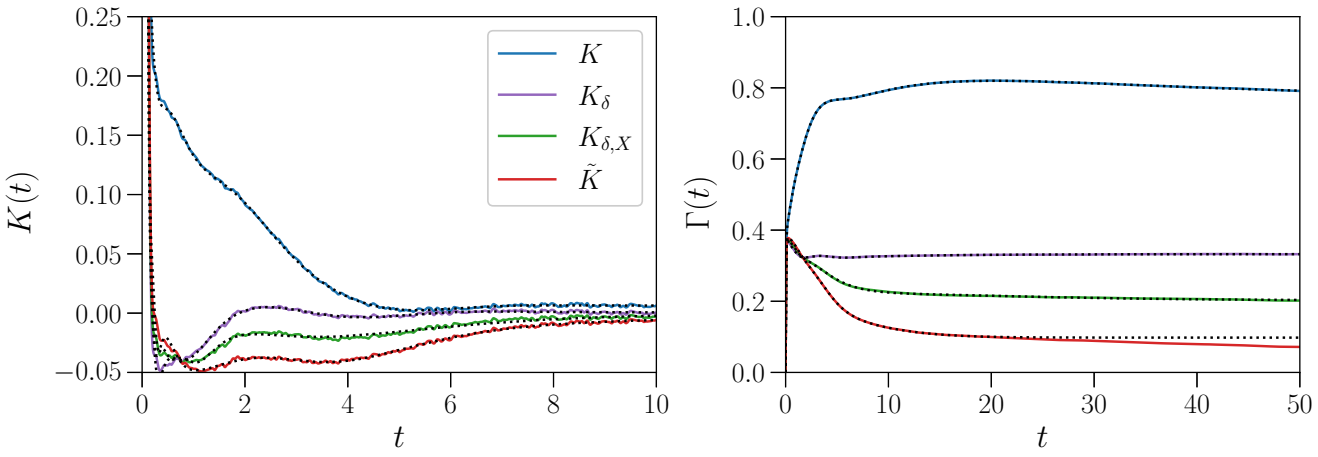

Figure 4.4: Left: Memory kernels applied in CG simulations. The black dotted lines represent the fit functions used for the parameterization of the GLE-thermostat. Right: Respective integrals of the memory kernels and their fit functions (black dotted lines).

4.2.3 Generalized Langevin Dynamics Simulations

The dynamics of the non-Markovian models are evaluated based on the velocity auto-correlation function (VACF) and compared to the FG model in Fig. 4.6. We do not show the non-Markovian counterpart of the γ_{FACF}-model for which the functional form of the memory kernel is assumed not to be physically meaningful due to a lack of time scale separation. The model without conservative interaction (K, blue line) reproduces the FG VACF and its integral $D(t) = \int_0^t ds\, \langle v(s)v(0)\rangle$ on all time scales and is shown here to validate the method for the calculation and fitting of the memory kernel $K(t)$. For the non-Markovian models we again find that the models not including the cross-correlation contributions ($K_\delta(t)$) or including it only once ($K_{\delta,X}(t)$) lead to an underestimation of the self-diffusion coefficient. The self-diffusion coefficient is well matched for $\tilde{K}(t)$. With this kernel, the VACF is also better matched in terms of its amplitudes on small time scales compared to $K_\delta(t)$ and $K_{\delta,X}(t)$. The origin of the remaining deviations from the FG VACF can be attributed to errors in the conservative interactions and are discussed in the SI.

A comparison of the derived self-diffusion coefficients between the Markovian and non-Markovian models allows to asses the importance of memory effects in the models at hand. Most evidently we find that the $\tilde{K}(t)$-model shows a significantly slower self diffusion than the Markovian $\tilde{\gamma}$-model. The same holds true to a lesser extent when comparing the $K_{\delta,x}(t)$-model and the $\gamma_{\delta,x}$-model, while the self-diffusion coefficients for the $K_\delta(t)$-model and the γ_δ-model are comparable. This finding is exactly in line with the discussion presented in Sec. 4.2.2.

4.3 Conclusion

In this work we have presented a new method for the parameterization of LE-thermostats and GLE-thermostats for dynamic consistency in CG models. Recently it was demonstrated that GLE-thermostat models can be parameterized by means of optimization schemes,[32, 39] which ensure that dynamical properties such as the VACF of CG beads are reproduced. We instead aimed to illuminate the main origins of the deficiencies in early attempts[36] of constructing Langevin-thermostat based CG models based on Mori-Zwanzig theory. We have found that cross-correlations of CG and FG degrees of freedom must be considered to consistently model friction and memory effects on a CG level. In non-Markovian models,

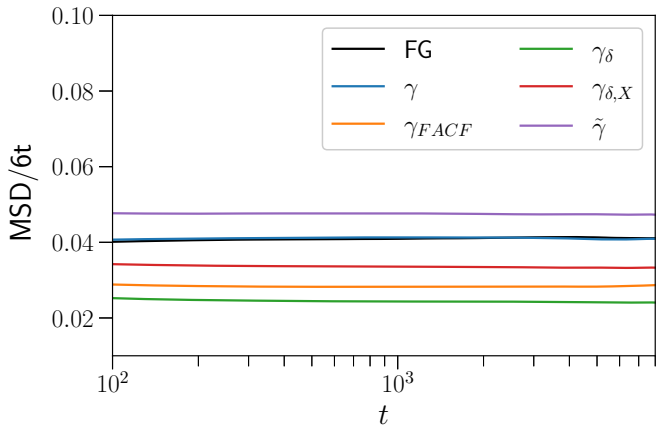

Figure 4.5: Scaled MSD for the evaluation of self-diffusion coefficients in CG LE models. FG denotes the evaluation based on the mapped all-atom trajectory.

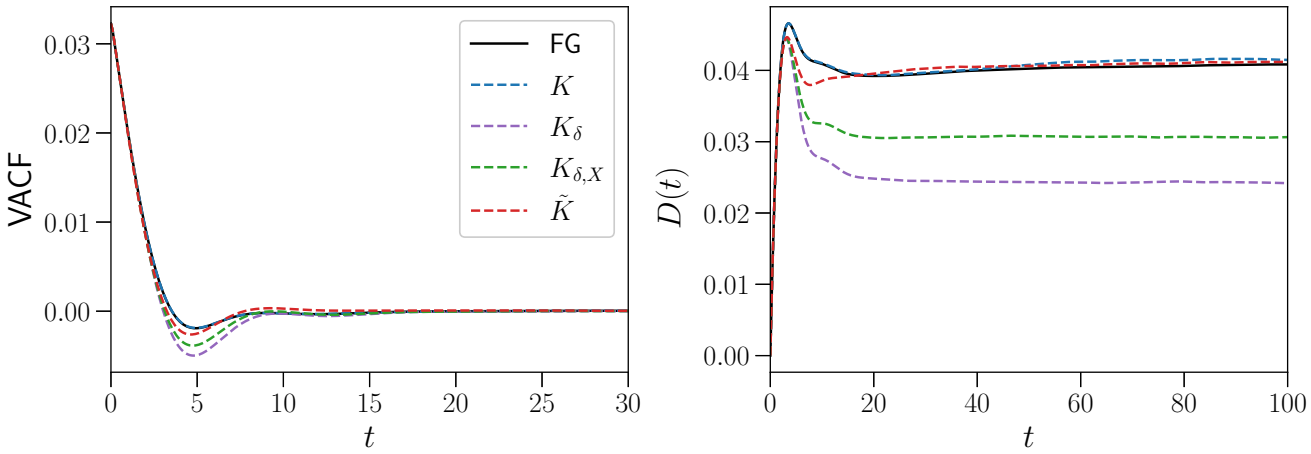

Figure 4.6: VACFs and their integrals $D(t) = \int_0^t ds\, \langle v(t)v(0)\rangle$ for the FG simulation compared to the GLE CG models.

inclusion of the cross-correlated contribution to the memory leads to improved representability of the dynamics, also on short time scales. Neglecting the cross-correlated contribution to the memory kernel leads to dynamic inconsistencies of the CG model and fully accounts for the too slow dynamics predicted with methods solely based on correlations of fluctuating forces.

Additionally, the comparison of Markovian and non-Markovian models has shown that in the CG system studied in this work memory effects manifest on the diffusive timescale. This has shown to be only the case for memory kernels which exhibit a significant negative contribution on large time scales. In the SI we demonstrate that this memory effect is inverted for positive long-lived memory kernels and is less pronounced in dilute (implicit solvent) CG systems.

For the proposed approach to perform optimally, in principle the conservative interactions would have to represent the exact multi-body potential of mean force. Deviations can lead to a discrepancy of the friction caused by the CG conservative interactions in sampling governed by the CG force-field compared to the sampling of the microscopic (FG) system (see SI). Generally, the loosest requirement to have a fully dynamically consistent model, independent of the choice of how to model friction and random

interactions, is an exact representation of the multi-body potential of mean force on the CG level.[15, 204] This is, of course, not generally feasible and compromises have to be made. While an iterative optimization technique[32, 39] can be used to optimally reproduce a single measure such as the VACF, this procedure does not guarantee that all conceivable dynamical properties are reproduced. This is related to the representability problem of CG conservative interactions,[205–207] where, e.g., the IBI-method only guarantees the reproduction of the radial distribution function (RDF), but is known to, e.g., overestimate the pressure, underestimate isothermal compressibilities,[208, 209] and does not guarantee to represent higher-order correlations.

In cases in which the exact reproduction of the VACF is required, the memory kernel obtained with the method proposed in this work can be used as an optimal initial guess for the memory kernel in iterative reconstruction methods, which have shown to need up to hundreds of iterations to reach convergence, when the initial guess is far from the optimal solution.[39]

While in the past a lot of effort has been put into the development of new methods for parameterizing CG methods with conserved dynamical properties,[15] predictive modeling of the dynamic properties of material-specific soft matter system still poses challenges. For non-Markovian models, the form of Eq. 4.1 is computationally the least demanding in both derivation and implementation with a Mori-Zwanzig based CG modeling approach. These type of models are not as rigorous as formulations including configuration dependent memory kernels,[30] but the ease of its implementation in principle allows for the application to more complex problems. For future endeavors within this field of research, it is desirable to extend the efforts to more complex systems, such that predictive capabilities of the existing approaches can be tested.

SUPPLEMENTARY MATERIAL

See supplementary material for more details on the setup of the simulations and the derivation of the coarse-grained models. In the supplementary material we also provide complementary data and discussions on memory effects, the origin of remaining inaccuracies in the coarse-grained models and the Markovian, high mass limit for coarse-grained generalized Langevin models.

Data Availability

The data that supports the findings of this study are available within the article and its supplementary material. Input parameters for simulations, analysis scripts and raw data of the shown figures are available from the corresponding author upon reasonable request.

4.4 Supporting Information

4.4.1 Evaluation of Memory Kernels

Backward Orthogonal Dynamics

In the main text we defined a set of memory kernels based on correlation functions of Q-projected forces as

$$K(t) = \frac{\langle F_Q(t) F_Q(0) \rangle}{m k_B T} \tag{4.10}$$

$$K_\delta(t) = \frac{\langle \delta F_Q(t) \delta F_Q(0) \rangle}{m k_B T} \tag{4.11}$$

$$K_C(t) = \frac{\left\langle F_Q^C(t) F_Q^C(0) \right\rangle}{m k_B T} \tag{4.12}$$

$$K_X(t) = \frac{\left\langle F_Q^C(t) \delta F_Q(0) \right\rangle}{m k_B T} \tag{4.13}$$

$$K_{C,X}(t) = K_C(t) + K_X(t) \tag{4.14}$$

$$K_{\delta,x} = K_\delta(t) + K_X(t) \tag{4.15}$$

$$\tilde{K}(t) = K_\delta(t) + 2K_X(t) \tag{4.16}$$

Q-projected correlation functions can be calculated from an analysis of Hamiltonian trajectories as described by Carof *et al.*[85]. In particular in this study we have applied the backward orthogonal dynamics method, which will be summarized below. For an in depth derivation the original publication should be consulted.

For two arbitrary Q-projected dynamic variables $A(t)$ and $B(t)$ the Q-projected correlation function has the symmetry

$$\langle A(0) B_Q(t) \rangle = \langle A_Q(-t) B(0) \rangle \tag{4.17}$$

where we made use of the fact that $A_Q(0) = A(0)$ and $B_Q(0) = B(0)$. The backward orthogonal dynamics method builds on the right hand sight of Eq. 4.17. By defining a auxiliary property $\tilde{A}(t) = e^{i\mathcal{L}t} A_Q(-t)$ we can rewrite the Q-projected correlation function as

$$\left\langle A^Q(-t) B(0) \right\rangle = \left\langle \tilde{A}(t) B(t) \right\rangle. \tag{4.18}$$

$\tilde{A}(t)$ is propagated in time through

$$\tilde{A}(t) = A(0) + \int_0^t ds F(s) \frac{\left\langle mv(s) \tilde{A}(s) \right\rangle}{\langle m^2 v(0)^2 \rangle}. \tag{4.19}$$

The value of $\tilde{A}(t)$ is not solely determined by the state of the system at time t but depends on the choice of the time origin when evaluating Eq. 4.19. For the numerical evaluation of Eq. 4.19 we applied the second order discretization scheme derived by Jung *et al.*[39].

$$\tilde{A}(t + \Delta t) = \tilde{A}(t) + F(t)\alpha(t)\frac{\Delta t}{2} + \frac{F(t + \Delta t)}{1 - \frac{\Delta t}{2}\kappa} \left[\zeta(t) + \epsilon\alpha(t)\frac{\Delta t}{2} \right] \frac{\Delta t}{2} \tag{4.20}$$

$$\kappa = \frac{\langle mvF \rangle}{\langle m^2 v(0)^2 \rangle} \tag{4.21}$$

$$\epsilon = \frac{\langle mv(\Delta t) F(0) \rangle}{\langle m^2 v(0)^2 \rangle} \tag{4.22}$$

$$\alpha(t) = \frac{\left\langle mv(t) \tilde{A}(t) \right\rangle}{\langle m^2 v(0)^2 \rangle} \tag{4.23}$$

$$\zeta(t) = \frac{\left\langle mv(t+\Delta t)\tilde{A}(t)\right\rangle}{\langle m^2 v(0)^2\rangle} \tag{4.24}$$

A and B can now be replaced by any of the force contributions to calculate the respective Q-projected correlations functions. For the numerical evaluation we chose $\Delta t = 0.01$ (ten time steps of the simulation) and in total 9000 time origins with a spacing of 0.1 time units (100 time steps). We calculated the correlation functions up to a time of $t_{cut} = 50$ (50000 time steps). The averages in Eqs. 4.21 and 4.22 were evaluated from the respective time window from $t = 0$ to $t = t_{cut}$, while also averaging over all particles and spatial dimensions. For Eqs. 4.23 and 4.24 the averaging was carried out only over all particles and dimensions. We note here that the averages can also be evaluated over the time dimension, but we found that our scheme leads to good results, especially to a good consistency between $K^V(t)$ and $K(t)$ as demonstrated in the main text.

The Volterra Equation Approach

For the single particle GLE

$$F(t) = -m\int_0^t dsK(t-s)v(s) + F^R(t) \tag{4.25}$$

a Volterra equation can be derived by multiplying Eq. 4.25 with $v(0)$ and taking the average.

$$\langle F(t)v(0)\rangle = -m\int_0^t dsK(t-s)\,\langle v(s)v(0)\rangle \tag{4.26}$$

Eq. 4.26 can be evaluated by discretizing the integral, which gives a solvable linear system of equations.[92] In our work we employed the convolution theorem to Eq. 4.26. The convolution theorem states that in general a function of the form of Eq. 4.26

$$y(t) = \int_0^t dsh(t-s)x(t) = (h * x)(t), \tag{4.27}$$

where $*$ is the convolution operator, can be equivalently written in Fourier space

$$Y(\nu) = H(\nu)\cdot X(\nu), \tag{4.28}$$

where we denote Fourier transforms in capital letters. By simple reordering we get

$$X(\nu) = \frac{Y(\nu)}{H(\nu)} \tag{4.29}$$

which by an inverse Fourier transform gives $x(t)$ in the time domain. Similar to the approach by discretizing Eq. 4.26,[92] in this approach $K(0)$ is not well defined, but can be either evaluated by interpolation or by noting that $K(0) = \frac{\langle F^2\rangle}{mk_BT}$.

In the main text we refer to $K(t)$ calculated through Eq. 4.26 as $K^V(t)$.

Further Volterra type equations can be derived by considering GLE-models including conservative interactions $F^C(t)$.

$$F(t) = F^C(t) - m\int_0^t ds\tilde{K}(t-s)v(s) + \tilde{F}^R(t) \tag{4.30}$$

By subtracting $F^C(t)$ and defining $\delta F(t) = F(t) - F^C(t)$ we get

$$\delta F(t) = -m \int_0^t ds \tilde{K}(t-s) v(s) + \tilde{F}^R(t) \tag{4.31}$$

from which a Volterra equation can be derived as

$$\langle \delta F(t) v(0) \rangle = -m \int_0^t ds \tilde{K}^V(t-s) \langle v(t) v(0) \rangle . \tag{4.32}$$

As described in the main text, $\tilde{K}^V(t)$ in Eq. 4.32 does not give the optimal parameterization for $\tilde{K}(t)$ in Eq. 4.30, which is why we do make the distinction in nomenclature.

A third Volterra equation can be derived by rewriting Eq. 4.32 as

$$\langle F(t) v(0) \rangle = \left\langle F^C(t) v(0) \right\rangle - m \int_0^t ds \tilde{K}^V(t-s) \langle v(t) v(0) \rangle . \tag{4.33}$$

and equating Eq. 4.33 with Eq. 4.26. Some restructuring leads to

$$\left\langle F^C(t) v(0) \right\rangle = -m \int_0^t ds (K(t-s) - \tilde{K}^V(t-s)) \langle v(s) v(0) \rangle . \tag{4.34}$$

We define $K_C^V(t) = K(t) - \tilde{K}^V(t)$ to emphasize its relation to the conservative interactions $F^C(t)$.

$$\left\langle F^C(t) v(0) \right\rangle = -m \int_0^t ds K_C^V(t-s) \langle v(s) v(0) \rangle . \tag{4.35}$$

Now we want to shortly motivate analytically that $\tilde{K}^V(t) = K_{\delta,X}(t)$ and $K_C^V(t) = K_{C,X}(t)$ as numerically demonstrated in the main text. This can be done by taking the time derivative of Eq. 4.32 which yields

$$\langle \delta F(t) F(0) \rangle = m k_B T \tilde{K}^V(t) + m \int_0^t ds \tilde{K}^V(t-s) \langle F(s) v(0) \rangle \tag{4.36}$$

If time scale separation can be assumed, the integral on the right-hand side vanishes. We can then write

$$\langle \delta F(t) F(0) \rangle \approx m k_B T \tilde{K}^V(t) \tag{4.37}$$

Eq. 4.37 suggests that in the Markovian limit

$$\tilde{K}^V(t) = K_{\delta,X}(t) = K_\delta(t) + K_X(t). \tag{4.38}$$

The same argumentation can be made for the equivalence of $K_C^V(t)$ and $K_{C,X}(t)$. We note that this is not a strict proof for the case in which a time scale separation cannot be assumed, but in conjunction with the numerical evidence shown in the main text it indicates that the relation does hold in general.

4.4.2 Computational Details

Microscopic Model

As microscopic model we set up the same system as used by Wang *et al.* for parameterization of GLE-thermostat models based on an optimization scheme.[32] The microscopic system consists of a star-polymer melt consisting of beads interacting by a Weeks-Chandler-Anderson (WCA) potential given by[210]

$$U_{WCA}(r) = \begin{cases} 4\epsilon \left[\left(\frac{\sigma}{r}\right)^{12} - \left(\frac{\sigma}{r}\right)^{6} \right] + \epsilon, & r \leq r_c \\ 0, & r > r_c \end{cases} \tag{4.39}$$

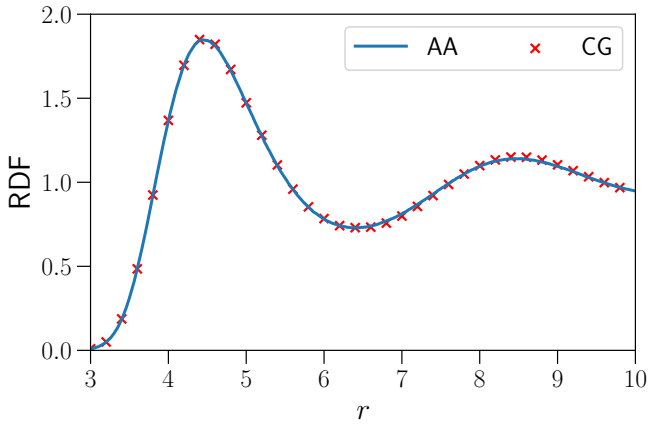

Figure 4.7: Radial distribution function of the center of mass of the star-polymers in the FG and CG model.

with a cutoff radius $r_c = 2^{1/6}\sigma$. Reduced units are defined such that the mass of a bead is $m = 1$, and the LJ-parameters are $\sigma = 1$ and $\epsilon = 1$. Every star-polymer consists of 31 beads, where one central bead is connected to 10 arms with 3 beads each. The beads within a star-polymer are connected through FENE-bonds[211].

$$U_{FENE}(r) = \begin{cases} -\frac{1}{2}kr_0^2 \ln\left[1 - \left(\frac{r}{r_0}\right)^2\right], & r \leq r_0 \\ \infty, & r > r_0 \end{cases} \tag{4.40}$$

The spring constant for the FENE-bonds are set to $k = 30$ and the maximum length to $r_0 = 1.5$.

The total system consists of 2500 star-polymers in a cubic box of length 57.8647. Simulations were carried out using GROMACS version 2018.2[212–214] at a temperature of $k_BT = 1$ using the Nosé-Hoover thermostat and time step of 0.001.

Coarse-Grained Models

Coarse-Grained Conservative Interactions

Conservative interactions for the CG models were derived using the iterative Boltzmann inversion (IBI)[9] method implemented in the VOTCA-package.[202, 215, 216] Starting from well equilibrated configurations the RDF was calculated from runs consisting of 10^7 time-steps where every 1000th time step was saved. The RDF was calculated based on the center of mass of the star-polymers, with a spatial discretization of 0.02. The conservative interactions were iteratively optimized for 600 iterations. The cutoff radius for the IBI model as set to 6.4. To validate the resulting conservative interactions, we compare the RDF of the atomistic simulations with the CG model in Fig. 4.7.

Langevin Thermostat Models

The CG Markovian LE-thermostat simulations were carried out with GROMACS version 2018.2[212–214] and the stochastic dynamics implementation. In total we derive 5 Markovian LE models. The relaxation time for the stochastic dynamics integrator are derived from the inverse of the integrals of the respective memory kernel or of the FACF given by Eqs. 4.41 - 4.45. Due to the softer interactions in the CG model, a higher time step of 0.01 was used for CG simulations and each run consists of 10^6 time steps. The friction coefficients were calculated from integrals of the respective memory kernels or force correlation function.

$$\gamma = \int_0^\infty dt K(t) \tag{4.41}$$

$$\gamma_\delta = \int_0^\infty dt K_\delta(t) \tag{4.42}$$

$$\gamma_{\delta,X} = \int_0^\infty dt K_{\delta,X}(t) \tag{4.43}$$

$$\tilde{\gamma} = \int_0^\infty dt \tilde{K}(t) \tag{4.44}$$

$$\gamma_{\mathrm{FACF}} = \int_0^\tau dt \left\langle \delta F(t) \delta F(0) \right\rangle / m k_B T \tag{4.45}$$

In the γ-model no conservative interactions were considered, as all interactions of the fine-grained model are incorporated in the friction coefficient.

Generalized Langevin Thermostat Models

For the evaluation of the memory kernel the total force $F(t)$ for every star-polymer and in every dimension is evaluated based on a mapped FG trajectory. The force contribution $F^C(t)$ is evaluated based on a rerun of the mapped FG trajectory and $\delta F(t)$ is evaluated by the difference $\delta F(t) = F(t) - F^C(t)$ of the mapped FG trajectory and the rerun evaluating $F^C(t)$ based on the IBI interactions.

In total we derive 4 non-Markovian CG models with the memory kernels given by Eqs. 4.46 - 4.49.

$$K(t) = \frac{\langle F_Q(t) F_Q(0) \rangle}{m k_B T} \tag{4.46}$$

$$K_\delta(t) = \frac{\langle \delta F_Q(t) \delta F_Q(0) \rangle}{m k_B T} \tag{4.47}$$

$$K_{\delta,X}(t) = \frac{\langle \delta F_Q(t) \delta F_Q(0) \rangle}{m k_B T} + \frac{\left\langle F_Q^C(t) \delta F_Q(0) \right\rangle}{m k_B T} \tag{4.48}$$

$$\tilde{K}(t) = \frac{\langle \delta F_Q(t) \delta F_Q(0) \rangle}{m k_B T} + 2\frac{\left\langle F_Q^C(t) \delta F_Q(0) \right\rangle}{m k_B T} \tag{4.49}$$

In Eq. 4.46, all interactions are incorporated in the memory kernel, such that the FG dynamics is reproduced in simulations without conservative interactions. The other memory kernels were applied in conjunction with conservative interactions due to the IBI model.

The Auxiliary Variable GLE-thermostat

The simulations with a the various GLE-thermostat models were performed using the auxiliary variables approach derived by Ceriotti [150, 151, 155] in its current implementation in LAMMPS.[217] For a thorough discussion of the auxiliary variables approach the reader should consult the original publications by Ceriotti *et al.*.[150, 151, 155]

The basic idea is to render the non-Markovian contributions in Eq. 4.30 Markovian, by the coupling of a set of auxiliary variables to the velocities (or momenta) of any single particles. This means

$$F(t) = F^C(t) - m\int_0^t dsK(t-s)v(s) + F^R(t), \tag{4.50}$$

can be rewritten in a Markovian form as

$$\begin{pmatrix} F \\ \dot{\boldsymbol{s}} \end{pmatrix} = \begin{pmatrix} F^C \\ \mathbf{0} \end{pmatrix} - \boldsymbol{A}\begin{pmatrix} mv \\ \boldsymbol{s} \end{pmatrix} + \boldsymbol{B}\boldsymbol{\xi} \tag{4.51}$$

Here $\boldsymbol{s}$ is a vector of auxiliary variables with the unit of momentum. $\boldsymbol{A}$ is referred to as drift-matrix, giving rise to defining the coupling between $\boldsymbol{s}$ and v. The frictional force on a given particles thus does not only depend on the velocity of the particle but on the state of the auxiliary variables, which implicitly encodes memory effects in a Markovian equation of motion. The diffusion matrix $\boldsymbol{B}$ determines the coupling strength of the vector of Gaussian random numbers $\boldsymbol{\xi}$, which consists of random numbers with zero mean and a unit variance. The formulation in terms of Eq. 4.51 has two main advantages compared to the direct evaluation of Eq. 4.50. Firstly, a direct numerical evaluation of the non-Markovian formulation of Eq. 4.50 necessitates the storage of historical data, which is costly in terms of storage and computation. Secondly, this implies a cut-off in time for the evaluation of the integral term, which can lead to truncation errors.[26]

Fitting of Memory Kernels and Parameterization of the Drift Matrix

To make the Markovian description of GLEs given by Eq. 4.51 practical, a relation between the memory kernel and the drift matrix has to be established. For that a functional form of the memory kernel has to be assumed. In the original formulation Ceriotti *et al.* established formulations of the drift matrix such that exponentially decaying memory kernels and $\delta-$like memory kernels in Fourier space can be represented.[150, 153] In the realm of coarse-graining the functional form of memory kernels can have quite complex forms. It was found that a sum of exponentially damped oscillators can be related to the drift matrix and is a good choice to fit to arbitrary memory kernels.[27, 32, 92]

For our systems we assumed a sum of exponentially damped oscillators of the form

$$K(t) = e^{-\frac{at}{2}}\left(b\cos(dt) + c\sin(dt)\right) \tag{4.52}$$

which can be translated to a drift matrix as[32]

$$\boldsymbol{A} = \begin{pmatrix} 0 & \sqrt{\frac{b}{2} - \frac{cd}{a}} & \sqrt{\frac{b}{2} + \frac{cd}{a}} \\ -\sqrt{\frac{b}{2} - \frac{cd}{a}} & a & \frac{1}{2}\sqrt{4d^2 + a^2} \\ -\sqrt{\frac{b}{2} + \frac{cd}{a}} & -\frac{1}{2}\sqrt{4d^2 + a^2} & 0 \end{pmatrix}. \tag{4.53}$$

In practice we found that it is simpler to fit the integrals of memory kernels with

$$\Gamma(t) = \int_0^t dsK(s) = 2\frac{ab + 2cd}{a^2 + 4d^2} - \frac{2e^{-\frac{at}{2}}\left((ab + 2cd)\cos(dt) + (ac - 2bd)\sin(dt)\right)}{a^2 + 4d^2}, \tag{4.54}$$

instead of the memory kernel itself. This can introduce small errors in the representation of the memory kernel on small time scales, but allows for a more accurate representation of the accumulative effect of the memory kernel over larger time scales.

The fitting parameters have to obey the boundary conditions $a > 0$, $\frac{b}{2} + \frac{cd}{a} > 0$ and $\frac{b}{2} - \frac{cd}{a} > 0$. For fitting the memory kernels shown in the main text, 6 damped oscillators were used respectively.

4.4.3 Memory Effects in Dense and Dilute Systems

In the main text we discuss that fast fluctuations governed by conservative interactions in coarse-grained models lead to a partial decoupling from the long time scales of the memory kernels. In the case of a negative long lived tail in the memory kernel, this effectively leads to a decrease in the diffusion coefficient compared to its Markovian approximation. To further corroborate that the memory effects observed in the bottom-up coarse-grained models are due to the long tail, memory kernels with long lived positive tails can be considered which should invert the effect. To that end we consider exponential memory kernels of the form

$$K(t) = \frac{\gamma}{\tau} \exp\left(-\frac{t}{\tau}\right) \tag{4.55}$$

where we fix $\gamma = 0.097815$ and vary τ. In Fig. 4.8, the memory kernels considered are shown. $\tilde{K}_{melt}$ denotes the fit to $\tilde{K}$ of the main text. For $\tau = 0.1$ the GLE is quasi-Markovian. From $\tilde{K}_{melt}$ to $\tau = 50$ the amplitude of the memory kernel on short time scales decreases while the amplitude on long time scales increases. In Fig. 4.9, the VACF and its integral for all memory kernels in the CG star-polymer melts are shown. Comparing the plateau of $D(t) = \int_0^t ds\, \langle v(s)v(0)\rangle$ of the $\tilde{K}_{melt}$-model with $\tau = 0.1$ shows the behavior already described in the main text. An increase in τ leads to an further increase in the diffusion coefficient. This corroborates the finding that in the CG star-polymer melt model the overall coupling strength of a memory kernel can depend on its functional form when its integral is fixed. In particular, a positive long-lived tail shows an inversion of the memory effects compared to a memory kernel with a negative long-lived tail.

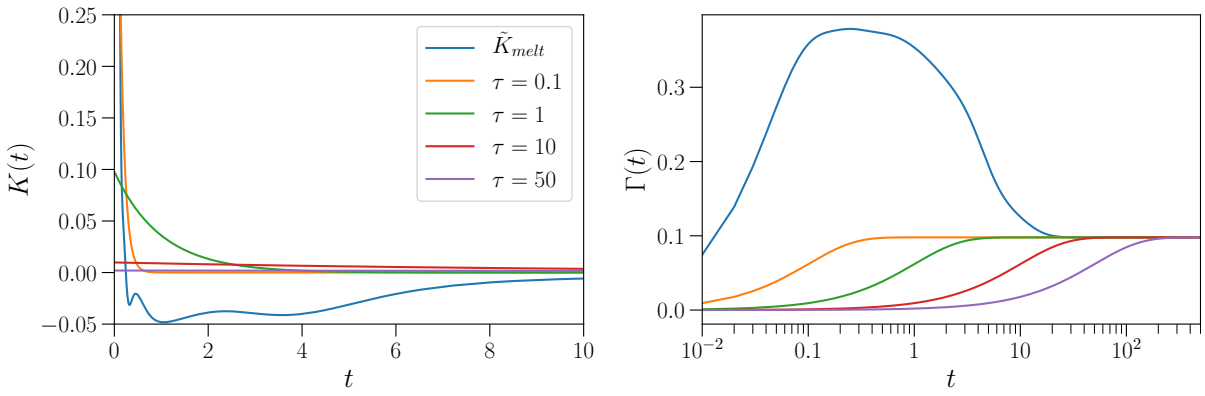

Figure 4.8: Memory kernels and its integrals considered for the demonstration of the effect of long lived tails on the diffusion coefficient.

In the main text we made the argument that the coupling to long tails in memory kernels in the CG star-polymer melt systems is reduced due to the dominance of fast fluctuations governed by the conservative CG force-field. To test that, we derived a CG IBI model for a star-polymer solution in which we coarse-grained 1000 star-polymers which are desolved in 46500 single WCA-beads, following Wang *et al.*.[32] In this implicit solvent model, the time scale of collisions is enhanced due to the lower polymer number density. The resulting VACFs and polymer diffusion coefficients $D(t)$ are shown in Fig. 4.10. These results were obtained applying the same memory kernels as in the case of the melt. While in the polymer melt the change in the self-diffusion coefficient comparing $\tilde{K}_{melt}$ and $\tau = 50$ is $\approx 35\%$, this is reduced to $\approx 20\%$ in the implicit solvent model. The total difference in the diffusion coefficient is higher in the implicit solvent model due to the overall higher diffusion coefficient. To evaluate the extent of memory effects it is more meaningful to compare the change in the effective friction coefficient in terms of the Stokes-Einstein

relation $\gamma_{eff} = \frac{k_B T}{D}$. Here we find a relative change of $\approx 27\%$ and an absolute change of ≈ 6.5 in γ_{eff} in the melt, while we find a relative change of $\approx 17\%$ and an absolute change of ≈ 1.2 in γ_{eff} in the implicit solvent model. This is in line with the interpretation that an increase of the time scale of collisions should increase the coupling to long lived tails of the memory kernel and thus mitigate memory effects. Overall the implicit solvent model is still quite dense. In the fine-grained representation, the system still consists to 40% of the star-polymer particles. For that reason, memory effects still alter the diffusion coefficient significantly in the implicit solvent model. In Fig. 4.11, the VACFs and $D(t)$ for an implicit-solvent system with 100 star-polymers is shown. The particle density is now reduced to 4%. For this system the polymer diffusion coefficient does not significantly change with the form of the memory kernel and memory effects are negligible on long time scales.

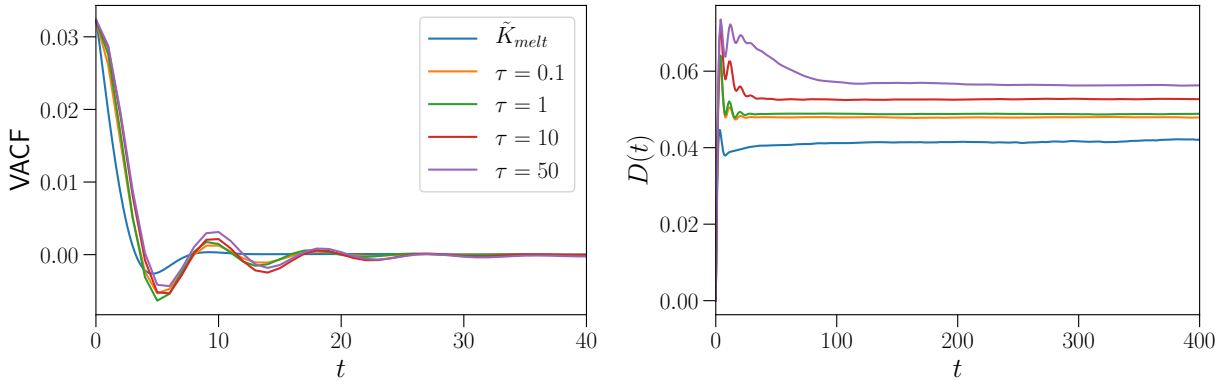

Figure 4.9: VACFs and its integrals for a CG star-polymer system with using the same conservative interactions as in the model discussed in the main text. The parameterization of the GLE-thermostat is varied such that the integral of the memory kernel is equivalent for all models.

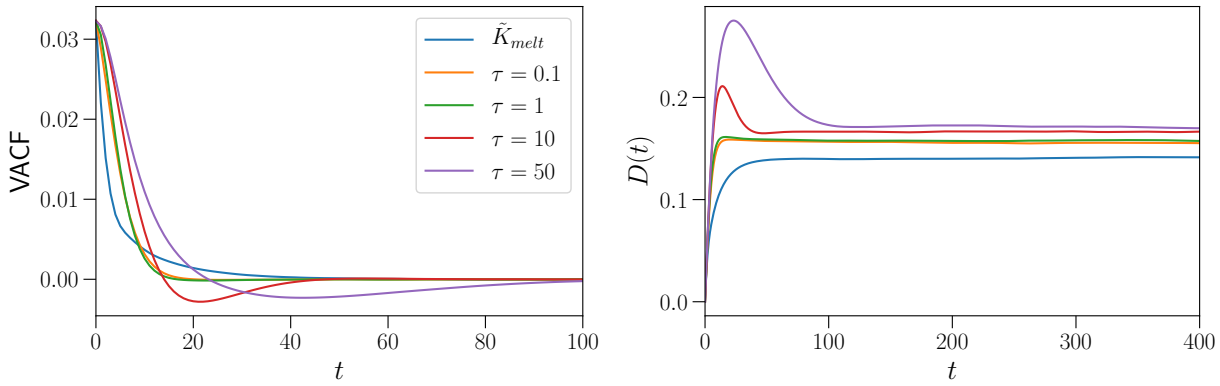

Figure 4.10: VACFs and its integrals for a implicit solvent CG star-polymer system with 1000 CG beads. The conservative interactions were derived from the IBI-method. The parameterization of the GLE-thermostat is varied such that the integral of the memory kernel is equivalent for all models.

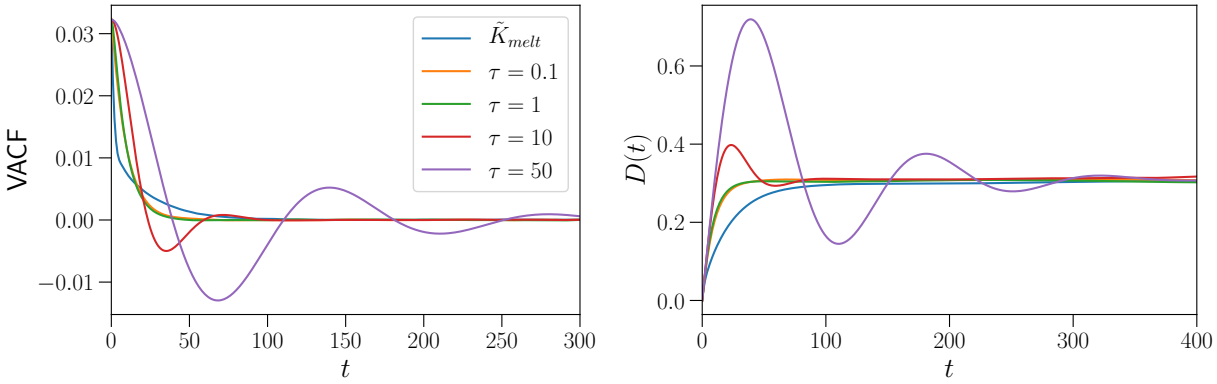

Figure 4.11: VACFs and its integrals for an implicit solvent CG star-polymer system with 100 CG beads. The conservative interactions applied in this model were taken from the 1000-bead implicit solvent model. The parameterization of the GLE-thermostat is varied such that the integral of the memory kernel is equivalent for all models.

4.4.4 Origin of Remaining Inaccuracies

In the main text we demonstrated that physics based methods, that means methods which do not rely on *a posteriori* optimization of parameters, for the parameterization of CG LE and GLE models have to take into account cross-correlations between FG and CG interactions in Q-space. The question is, if it is possible to further pin down the origin of the remaining inaccuracies.

The formulation in the main text assumes that the frictional effects on the CG scale in the FG system (governed by the memory kernel $K_C(t)$), is the same as in the CG-GLE model. That, of course, can only by true if the conservative interactions in the CG GLE model represent the multi-body potential of mean force. That suggests that the proposed method assumes

$$\left\langle F_C^Q(t)F_C^Q(0)\right\rangle_{FG} = \left\langle F_C^Q(t)F_C^Q(0)\right\rangle_{CG-GLE} \tag{4.56}$$

where the subscripts FG and CG refer to sampling of the FG and CG model, respectively.

While the particular form of the correlation functions defined by Eq. 4.56 in principle are prone to a several different error sources, a more loose requirement is $\left\langle F_C^Q F_C^Q\right\rangle_{FG} = \left\langle F_C^Q F_C^Q\right\rangle_{CG-GLE}$. This requirement is independent of time and thus of the dynamics of the model. In Fig. 4.12 we compare the memory kernel $K_C(t)$ from the conservative interactions in the CG-GLE-model with $K_C(t)$ and $K_X(t)$ and $K_{C,X}(t)$ from the FG model. Due to proportionality this is equivalent to comparing Q-projected force correlation functions.

We find that in fact at time $t = 0$ the memory kernel calculated from the CG-GLE-model differs significantly from $K_C(0)$ calculated from FG trajectories. In particular the memory Kernel $K_C(t)$ for the CG-GLE-model has a higher magnitude than $K_C(t)$ at times lower than $t \approx 5$ while it is lower on larger time scales. This is in line with the finding that the VACF in CG-GLE-model is slightly too strongly damped at times smaller than ≈ 6 while it exhibits slightly to high values at times larger than ≈ 6.

An additional curious finding of Fig. 4.12 is that $K_{C,X}(t) = K_C(t) + K_X(t)$ for $t = 0$, within numerical accuracy, is equivalent to $K_C(0)$ from the CG-GLE-model. The findings of this sections indicate that assuming the IBI-potentials as an approximation for the multi-body potential of mean force leads to an incomplete decoupling of the CoM and the internal degrees of freedom of the star-polymers. In this particular case,

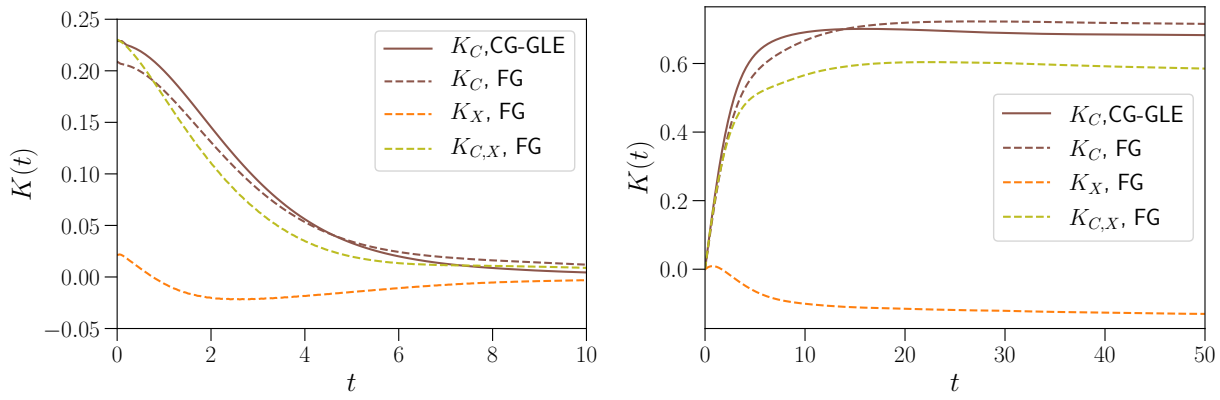

Figure 4.12: Memory kernels calculated from different contributions from the FG simulation and the CG GLE simulation.

the fact that $K_C(0)$, and thus the variance in coarse-grained forces, is larger in the CG-GLE-model than in the FG model indicates that the FG system does not sample the full configuration space accessible in the IBI-model for the same temperature.

4.4.5 Analysis of the High-Mass Limit

In the main text we discuss that the cross-correlation contribution $K_X(t)$ to the memory kernel should decline for systems in which the timescales of the FG and CG degrees of freedom are separated. This implies that for systems in which time scales are separated the memory kernel derived based on the Volterra inversion technique ($\tilde{K}^V(t)$) should yield dynamics of the CG models of comparable quality as the approach explicitly including cross-correlations ($\tilde{K}(t) = K_\delta(t) + 2K_X(t)$). This can be, in principle, studied by considering very coarse mapping schemes. The coarseness of the mapping scheme has its natural upper boundary by the size of the considered molecules. Here, as a proof of concept, we artificially enforce a better time scale separation by increasing the mass of the central bead of every star polymer in the melt. By doing so, we preserve the time scale of the fluctuations on a FG level while slowing down the center of mass dynamics and thus the dynamics on a coarse-grained level. We consider 4 different systems with different masses m_c =1, 10, 100, 1000 for the central bead. For $m_c = 1$ we reuse the data for the system discussed in the main text. For $m_c \neq 1$ we again constructed conservative interactions applying the IBI-method and derive $K_\delta^V(t)$ based on the Volterra equation Eq. 4.32. For $m_c = 1$ we consider the data gathered for $K_{\delta,X}(t)$ as it was demonstrated to be equivalent to $\tilde{K}^V(t)$.

In FIG. 4.13, we show the VACFs for the different systems. We find that for $m_c = 1$ and $m_c = 10$ the VACF decays significantly faster in the CG GLE-model, indicating slower dynamics. This effect is found to be less pronounced for $m_c = 100$ and very weak for $m_c = 1000$.

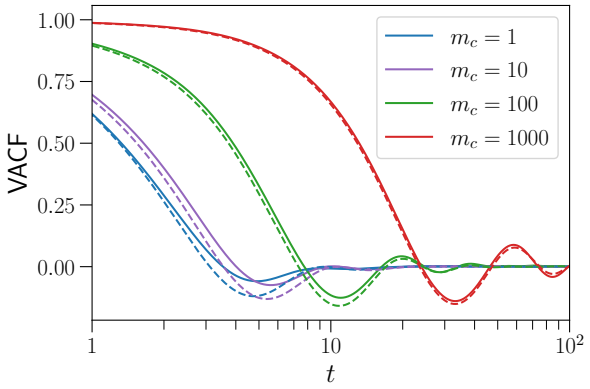

Figure 4.13: VACF for FG (solid lines) and CG GLE simulations (dashed lines) for star polymer melts with $\tilde{K}^V(t)$ as input memory kernel and varying central bead mass m_c.

5 Cross-Correlation Corrected Friction in Generalized Langevin Models: Application to the Continuous Asakura-Oosawa Model

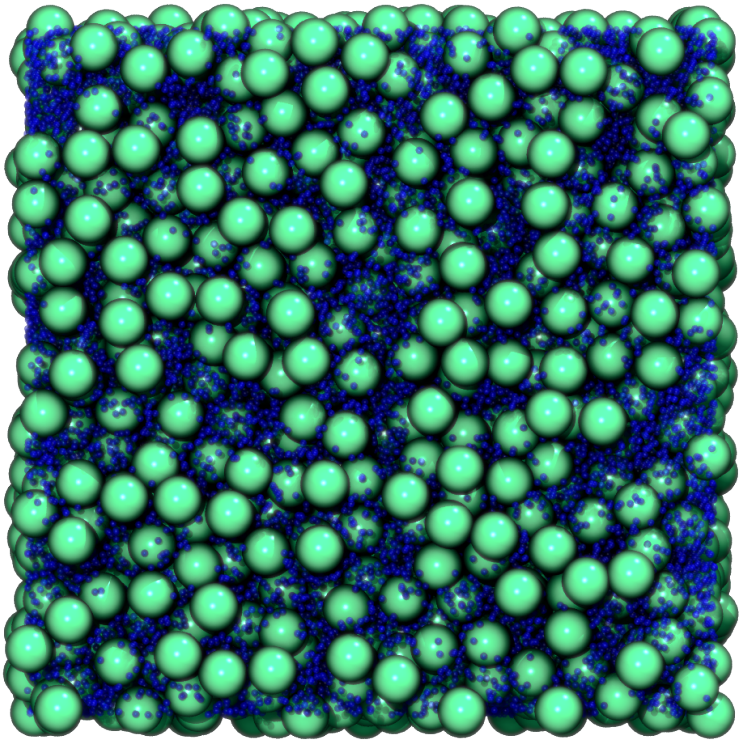

Abstract

The development of dynamically consistent coarse-grained models for molecular simulations is often based on generalized Langevin equations, motivated by the application of the projection-operator formalism (Mori-Zwanzig theory). While Mori's projection operator yields linear generalized Langevin equations which can be computationally efficiently implemented in numerical simulations, the downside is that Mori's generalized Langevin equation does not encompass the multi-body potential of mean force required to correctly encode structural and thermodynamic properties in coarse-grained many-body systems. Zwanzig's projection operator yields non-linear generalized Langevin equations including the multi-body potential of mean force, while remaining force-contributions are not as cheaply to implement in molecular simulation

without making formally hard to justify approximations. For many-particle coarse-grained models, due to computational and conceptual simplicity, an often used approach is to combine non-linear conservative interactions with linear expressions to model dissipation. In a previous study (J. Chem. Phys. **154**, 191102 (2021)), we proposed a method to parameterize such models to achieve dynamic consistency in coarse-grained models, allowing to reconcile Mori's and Zwanzig's approach for practical purposes. In the current study, by applying the same strategy, we develop coarse-grained implicit solvent models for the continuous Asakura-Oosawa model, which under certain conditions allows to develop very accurate coarse-grained potentials. By developing coarse-grained models for different reference systems with varying parameters, we test the broader applicability of the proposed procedure and demonstrate the relevance of accurate coarse-grained potentials in bottom-up derived dissipative models. We study how different system parameters affect the dynamic representability of the coarse-grained models. In particular, we find that the quality of the coarse-grained potential is crucial to correctly model the backscattering effect due to collisions on the coarse-grained scale. As hydrodynamic interactions are not explicitly modeled in the presented coarse-graining approach, deviations are observed in the long-time dynamics. The Asakura-Oosawa model allows a tuning of system parameters to gain an improved understanding of this limitation. We also propose three new iterative optimization schemes to fine tune the generalized Langevin thermostat to exactly match the reference velocity-autocorrelation function.

5.1 Introduction

In recent years there has been an increasing interest in developing methods to systematically derive coarse-grained (CG) models for molecular simulations which reproduce dynamic properties.[15, 25, 201] Several systematic approaches have been proposed to derive CG force-fields in a systematic way,[4, 41, 218] which (ideally) allow to describe specific fine-grained (FG) reference systems. Applying CG force-fields in standard equilibrium molecular dynamics (MD) simulations allows to reproduce structural and thermodynamic properties of the FG reference system, if the CG force-field sufficiently well represents the multi-body potential of mean force (MB-PMF).[193] Independent of the quality of the CG force-field, standard MD methods however do not correctly represent dynamical properties, as coarse graining leads to a reduction of the number of degrees of freedom (DoFs) and to a corresponding reduction in friction and noise.[15]

With an eye to representing both structure and dynamics, the coarse-graining process can be split up into two separate tasks. The first task is to derive the conservative interactions in the CG model and construct a potential, $U_{CG}(\boldsymbol{R})$, that closely approximates the equilibrium probability distribution in the space of CG configurational variables $\boldsymbol{R}$,[193]

$$\begin{aligned} e^{-U_{CG}(\boldsymbol{R})/k_BT} &\approx e^{-W(\boldsymbol{R})/k_BT} \\ &\propto \int d\boldsymbol{r} \exp(-U_{FG}(\boldsymbol{r})/k_BT)\delta(\hat{M}_R(\boldsymbol{r}) - \boldsymbol{R})). \end{aligned} \tag{5.1}$$

Here, $W(\boldsymbol{R})$ is the MB-PMF. The quantity $\hat{M}_R(\boldsymbol{r})$ represents a mapping operator, which defines the CG configurational DoFs $\boldsymbol{R} = \{\boldsymbol{R}_1, ..., \boldsymbol{R}_N\}$ and usually is a linear function of FG (i.e. atomic) Cartesian coordinates $\boldsymbol{r} = \{\boldsymbol{r}_1, ..., \boldsymbol{r}_n\}$ with $n > N$. Multiple points in the FG configurational space spanned by $\boldsymbol{r}$ map onto a single point in the CG space spanned by $\boldsymbol{R}$. The FG potential energy is denoted by $U_{FG}(\boldsymbol{r})$, and k_B is the Boltzmann constant and T the temperature. Bottom-up coarse-graining methods implicitly or explicitly aim to construct a CG potential that best approximates $W(\boldsymbol{R})$. For non-bonded interactions, the CG potential, due to computational and conceptional simplicity, is usually modeled in terms of two-body potentials.

$$U_{CG}(\boldsymbol{R}) = \sum_{I}^{N} \sum_{J<I}^{N} U_{IJ}(R_{IJ}) \tag{5.2}$$

Here $U_{IJ}(R_{IJ})$ is a CG pair-potential for a pair of CG particles I and J, and R_{IJ} is the distance between particles I and J. The force evaluation for standard CG-MD simulations is then

$$\boldsymbol{F}_I^C(\boldsymbol{R}) = -\frac{\partial U_{CG}(\boldsymbol{R})}{\partial \boldsymbol{R}_I} = -\sum_{J \neq I} \frac{\partial U_{IJ}(R_{IJ})}{\partial R_{IJ}} \hat{\boldsymbol{e}}_{IJ}, \tag{5.3}$$

where $\hat{\boldsymbol{e}}_{IJ}$ is the unit vector parallel to the distance vector between particle I and J.

The second task is to account for the effects of the FG DoFs removed by the coarse-graining process on the dynamics of the remaining CG DoFs. To this end, the total force, $\boldsymbol{F}_I$, on the CG particle I is augmented with a dissipative and random force according to

$$\boldsymbol{F}_I = \boldsymbol{F}_I^C + \boldsymbol{F}_I^D + \boldsymbol{F}_I^R \tag{5.4}$$

The superscripts C, D and R denote conservative, dissipative and random forces, respectively. In practice Eq. 5.4 can be realized by augmenting standard MD algorithms with a dissipative thermostat which simultaneously controls the temperature and adjusts the dynamics. To this end, different types of models

have been proposed, such as Markovian Langevin[36, 196] or Markovian dissipative particle dynamics (DPD) models,[36, 61, 63, 65]and non-Markovian isotropic generalized Langevin,[32, 33] non-Markovian DPD[26, 27, 29] or non-isotropic generalized Langevin models.[30] The strategies for the parametrization of the dissipative and random forces are typically based on either an iterative optimization strategy[30, 32, 219, 220] (comparable to IBI,[9] IMC,[10] HNCN[12] methods in structural coarse-graining) or the direct reconstruction of friction coefficients or memory kernels from time-correlation functions.[26, 27, 29, 33, 36, 196]

The phenomenologically intuitive form of Eq. 5.4 is often motivated by the Mori-Zwanzig theory,[22, 23, 25] which formalizes the coarse-graining process in terms of the projection operator formalism. The mathematical form the terms in Eq. 5.4 formally take depends on the choice of the projection operator.[25] While the projection operator of Mori leads to a CG equation in which all terms are linear in the CG DoFs, applying Zwanzig's projection operator leads to a CG EoM in which both the terms $\boldsymbol{F}_I^C$ and $\boldsymbol{F}_I^D$ can be non-linear in the CG DoFs.[25]

In fact, Zwanzig's projection operator allows to derive an EoM in which the conservative force $\boldsymbol{F}_I^C$ is the negative gradient of the MB-PMF.[35] This makes it a good candidate to use in conjunction with established coarse-graining methods, but simultaneously the non-linearity of the dissipative term in general complicates the justification of computationally tractable models.[35]

Mori's projection operator allows to derive a linear generalized Langevin equation (GLE) for which the dissipative and random forces can be efficiently implemented in molecular dynamics simulations as a non-Markovian GLE-thermostat.[151, 221] This comes with the drawback that the conservative forces in Mori's GLE are not in general equivalent to the negative gradient of the MB-PMF and thus structural and thermodynamic properties generally can not be modeled purely based on this approach.

From a modeling perspective, a combination of both approaches would be optimal. In this study we parameterize models of the form

$$\boldsymbol{F}_I(t) = \boldsymbol{F}_I^C(t) - \int_0^t ds \tilde{K}(t-s)\boldsymbol{P}_I(s) + \tilde{\boldsymbol{F}}_I^R(t), \tag{5.5}$$

where $\boldsymbol{P}_I(t)$ is the momentum of the CG particle I and $\tilde{K}(t)$ is an isotropic, configuration independent memory kernel, which is related to the random force $\tilde{\boldsymbol{F}}_I^R(t)$ via the fluctuation-dissipation relation

$$\tilde{K}(t) = \frac{\left\langle \tilde{\boldsymbol{F}}_I^R(t)\tilde{\boldsymbol{F}}_I^R(0)\right\rangle}{3M_I k_B T}, \tag{5.6}$$

where M_I is the mass associated with the Ith CG DoF.

In Ref.[33], we proposed a method to parameterize $\tilde{K}(t)$, which is motivated based on the single particle GLE

$$\boldsymbol{F}_I(t) = -\int_0^t ds K(t-s)\boldsymbol{P}_I(s) + \boldsymbol{F}_I^{\mathcal{Q}}(t), \tag{5.7}$$

which can be rigorously derived using Mori's linear projection operator for a freely diffusing particle in an isotropic environment. We keep the subscript I, as we will use Eq. 5.7 to motivate the parametrization of many-body models following Eq. 5.5, while de facto Eq. 5.7 arises as CG EoM for a single tagged particle. $\boldsymbol{F}_I^{\mathcal{Q}}(t)$ is called $\mathcal{Q}$-projected force, which is propagated in time in the subspace which is orthogonal to the CG momentum at the time origin $\boldsymbol{P}_I(0)$ and is related to the memory kernel $K(t)$ via

$$K(t) = \frac{\left\langle \boldsymbol{F}_I^{\mathcal{Q}}(t)\boldsymbol{F}_I^{\mathcal{Q}}(0)\right\rangle}{3M_I k_B T}. \tag{5.8}$$

Eq. 5.7 is an exact CG EoM and the memory kernel $K(t)$ can be readily obtained from a reference trajectory of a single tagged particle.[39, 81, 85, 92, 95, 96, 101] The $\mathcal{Q}$-projected force in Eq. 5.7 is often interpreted as random force, which allows to construct a single particle CG model reproducing e.g. the velocity auto-correlation function (VACF) of the reference.[39, 92]

In general, models of the form of Eq. 5.5 with a non-linear conservative force term and linear friction can only under certain conditions be derived exactly from microscopic dynamics,[35, 222] while the validity of assuming these conditions can in principle be numerically assessed as recently demonstrated by Ayaz *et al.*.[222]

In a recent study we have proposed a link between the exact EoM Eq. 5.7 and Eq. 5.5, which allows to parameterize $\tilde{K}(t)$ such that single-particle dynamic properties are well reproduced in many-body CG simulations following Eq. 5.5, which we have shown for a star-polymer melt system.[33]

The proposed parametrization scheme is based a method called backward orthogonal dynamics (BOD), introduced by Carof *et al.*,[85] which allows to directly evaluate $\mathcal{Q}$-projected correlation functions. This method can be used to determine the effective single particle memory kernel $K(t)$ by analyzing the trajectory of a tagged particle. The crucial difference to other methods is that the BOD-method allows to derive $\mathcal{Q}$-projected correlation functions for any observable. For our purpose, we analyze a mapped FG (e.g. atomistic) trajectory, i.e. we apply $\hat{M}_R(\boldsymbol{r})$ to a FG trajectory. Hence, we track the evolution of the CG DoFs in a many-body FG system, in which we split the total force on any CG DoF I as $\boldsymbol{F}_I(t) = \boldsymbol{F}_I^C(t) + \delta\boldsymbol{F}_I(t)$. Here $\boldsymbol{F}_I(t)$ is the total force on the CG DoF I in the mapped FG reference trajectory, $\boldsymbol{F}_I^C(t)$ is the force a priory defined CG potential would yield for the same CG configurations and $\delta\boldsymbol{F}_I(t)$ is the residual force, not captured by the CG potential. For each force contribution, and for their cross correlation, a $\mathcal{Q}$-projected correlation function can be calculated following the BOD-method. This allows to split the total memory kernel in Eq.5.8 into different contributions, as shown in Eq.5.9.

$$\begin{aligned} K(t) &= \frac{\left\langle \boldsymbol{F}_I^{C,\mathcal{Q}}(t)\boldsymbol{F}_I^{C,\mathcal{Q}}(0)\right\rangle}{3M_I k_B T} \\ &+ \frac{\left\langle \delta\boldsymbol{F}_I^{\mathcal{Q}}(t)\delta\boldsymbol{F}_I^{\mathcal{Q}}(0)\right\rangle}{3M_I k_B T} + 2\frac{\left\langle \boldsymbol{F}_I^{C,\mathcal{Q}}(t)\delta\boldsymbol{F}_I^{\mathcal{Q}}(0)\right\rangle}{3M_I k_B T} \\ &= K_C(t) + K_\delta(t) + 2K_X(t) \end{aligned} \tag{5.9}$$

In the CG target model, Eq. 5.5, the conservative forces will effectively exert friction on any particle I, in addition to the friction due to the GLE-thermostat. This has to be taken into account in the parametrization of $\tilde{K}(t)$. Eq. 5.9 suggests a relation between $K_C(t)$ and the conservative interactions. Assuming that the additional friction and memory effects due to the conservative interactions in the multi-body CG simulations is well estimated by $K_C(t)$, we suggest[33] that

$$\tilde{K}(t) \equiv K(t) - K_C(t) = K_\delta(t) + 2K_X(t) \tag{5.10}$$

should yield an optimal parametrization for dynamic consistency. One requirement for this approach to work optimally is that the CG model samples the same distribution $\rho(\boldsymbol{R}) \propto e^{-W(\boldsymbol{R})/k_B T}$ as the FG reference, as only then the overall force fluctuations can be consistent.

We applied the sketched approach to coarse-grain a star-polymer melt system and were able to reproduce the overall mobility and the form of the velocity auto-correlation function (VACF) reasonably well.[33] Still, some deviations were observed, especially around the first minimum of the VACF. We argued that the residual deviations of the VACF in our CG model compared to the reference were mainly due to the fact that the conservative forces in the CG model did not optimally represent the MB-PMF, as higher

order correlations cannot be accounted for in CG force-fields based on pairwise potentials. This is the main hypothesis we want to test in the current work, for which we need a CG particle based model, with an accurate representation of the the MB-PMF in terms of pairwise interactions.

To this end, we herein study the (continuous) Asakura–Oosawa[37, 38, 223, 224] (AO) model for which we parameterize a GLE-thermostat for the CG representation. The AO model by itself is a generic CG representation which models a colloidal suspension in a polymer solution. Both colloids and polymers are modeled as purely repulsive single beads. Due to entropic effects, the colloid beads effectively attract each other. It was shown that these effective interactions can be exactly described in terms of pairwise interactions if the size ratio of polymer beads to colloid beads is small enough.[37, 223] For this case an implicit solvent model, only resolving the colloid beads, can be derived for which the MB-PMF can be exactly reproduced. By changing the polymer-colloid bead size ratio, the quality of the CG model can be readily tuned and our main hypothesis can be tested.

The remainder of this paper is structured as follows: Sec. 5.2.1 describes some routes to evaluate the effective single particle memory kernel based on the inversion of Volterra equations. Sec. 5.2.2 sketches the main ideas behind the BOD-method.[85] In Sec. 5.2.3, we elaborate more detailed the choice for the parametrization of $\tilde{K}(t)$. In Sec. 5.2.4, we propose three different iterative optimization schemes to optimize the parametrization of GLE-thermostats to correct for residual deviations in the VACF from its reference. In Sec. 5.2.5, we provide a summary of the general coarse-graining procedure. In Sec. 5.3, we summarize how we model the FG and CG continuous AO-model. In Sec. 5.4, we report the main results. In particular we compare dynamic properties of the FG reference and CG GLE models for three different AO models with different polymer-colloid bead size ratios. We also demonstrate the performance of the newly proposed iterative optimization schemes for memory kernels. In Sec. 5.5, we discuss our findings and its implications and conclude with a short summary and outlook in Sec. 5.6.

5.2 Theory

5.2.1 Evaluation of the Memory Kernel Through Inversion of Volterra Equations

In order to evaluate the memory kernel in the exact single-particle EoM Eq. 5.7, we multiply both sides of the equation with $\boldsymbol{P}_I(0)$ and subsequently take the canonical average. Due to the definition of the projection operator

$$\left\langle \boldsymbol{F}_I^{\mathcal{Q}}(t)\boldsymbol{P}_I(0)\right\rangle = 0 \tag{5.11}$$

and thus

$$C_{FP}(t) = -\int_0^t dsK(t-s)C_{PP}(s), \tag{5.12}$$

or equivalently

$$C_{FV}(t) = -M_I\int_0^t dsK(t-s)C_{VV}(s), \tag{5.13}$$

where we have defined the time correlation functions $C_{FP}(t) = \frac{1}{3}\left\langle \boldsymbol{F}_I(t)\boldsymbol{P}_I(0)\right\rangle$, $C_{PP}(t) = \frac{1}{3}\left\langle \boldsymbol{P}_I(t)\boldsymbol{P}_I(0)\right\rangle$, $C_{FV}(t) = \frac{1}{3}\left\langle \boldsymbol{F}_I(t)\boldsymbol{V}_I(0)\right\rangle$ and the VACF $C_{VV}(t) = \frac{1}{3}\left\langle \boldsymbol{V}_I(t)\boldsymbol{V}_I(0)\right\rangle$. These correlation functions can be directly evaluated from molecular dynamics trajectories and thus allow to evaluate $K(t)$ through inversion of Eq. 5.13. This can be done by discretization.[81, 92] In our previous study,[33] we exploited the convolution theorem to recover $K(t)$ in Fourier-space.

Generally, schemes to derive $K(t)$ from Eq. 5.13 tend to be numerically unstable. This can be improved by integrating Eq. 5.13.[95]

$$C_{VV}(t) = C_{VV}(0) - \int_0^t ds G(t-s) C_{VV}(s) \tag{5.14}$$

Here, $G(t)$ is the integrated memory kernel

$$G(t) = \int_0^t ds K(s). \tag{5.15}$$

Following Ref.[95], Eq. 5.14 is discretized as

$$G_i = \frac{1 - C_{VV,i}/C_{VV,0}}{\delta t/2} - 2\sum_j^{i-1} G_j C_{VV,i-j}/C_{VV,0} \tag{5.16}$$

where $G_i \equiv G(i\delta t)$ and $C_{VV,i} \equiv C_{VV}(i\delta t)$, with δt being the discretization step of the VACF. To further increase the numerical stability, a predictor-corrector scheme is employed as

$$G_i := (G_{i-1} + 3G_i^* + G_{i+1}^*)/5 \tag{5.17}$$

where the superscript $*$ indicates values calculated in the predictor step and Eq. 5.17 is the corrector step. In addition to improved numerical stability, this scheme has the advantage that it can be used to evaluate the memory kernel from trajectories in which the total force is not stored, which is often the case in standard MD software when stochastic thermostats are used. We apply it to derive reference memory kernels, against which the results of the BOD-method can be compared and to derive effective single-particle memory kernels for CG-GLE trajectories.

5.2.2 Direct Evaluation of Projected Time-Correlation Function: The Backward-Orthogonal Dynamics Method

Two alternative routes to evaluate memory kernels based on the GLE in Eq. 5.7 were proposed by Carof *et al.*,[85] called the forward and backward orthogonal dynamics (BOD) method. As in Ref.[33], we apply the BOD method in this study, which is summarized in the SI. The main idea behind the BOD-method is to express $\mathcal{Q}$-projected correlation functions in terms of properties which are easily accessible form FG MD trajectories. Accordingly, arbitrary projected correlation functions of the form

$$\tilde{C}_{AB}(t) = \left\langle A(0) B^{\mathcal{Q}}(t) \right\rangle \tag{5.18}$$

can be evaluated.

By choosing $A = B = \boldsymbol{F}_I$, the memory kernel $K(t)$ can be evaluated as

$$\tilde{C}_{FF}(t) = \left\langle \boldsymbol{F}_I(0) \boldsymbol{F}_I^{\mathcal{Q}}(t) \right\rangle = 3 M_I k_B T K(t). \tag{5.19}$$

While the BOD-method and the Volterra-inversion approach described in the previous section yield the same memory kernel,[33, 39, 85] the BOD-method can be used to evaluate any arbitrary $\mathcal{Q}$-projected correlation function.[85] In particular, by choosing $A = B = \boldsymbol{F}_I^C$, $A = B = \delta\boldsymbol{F}_I = \boldsymbol{F}_I - \boldsymbol{F}_I^C$ or $A = \boldsymbol{F}_I^C$ and $B = \delta\boldsymbol{F}_I$, the total memory kernel can be split into different contributions (Eq. 5.9) as described in the introduction.

The three contributions to $K(t)$, namely $K_C(t)$, $K_\delta(t)$ and $K_X(t)$, can be interpreted as the memory and friction due to effective conservative interactions between the CG DoFs, due to interactions with the lost DoFs, and due to the cross-correlations between these interactions.

5.2.3 Definition of Dynamic Consistency

In this work we define dynamic consistency in terms of the reproduction of single particle correlation functions. In practice we can map the dynamics of any single particle I onto a GLE of the form of Eq. 5.7, where the memory kernel $K(t)$ determines all other time-correlation functions. By replacing $\boldsymbol{F}_I^Q(t)$ with a random force $\boldsymbol{F}_I^R(t)$, which fulfills the fluctuation-dissipation theorem, single-particle CG simulations, in which, e.g., the VACF is correctly reproduced, can be readily carried out.[39, 92] The EoM for such a model is

$$\boldsymbol{F}_I(t) = -\int_0^t dsK(t-s)\boldsymbol{P}_I(t) + \boldsymbol{F}_I^R(t) \tag{5.20}$$

with $3M_I k_B T K(t) = \left\langle \boldsymbol{F}_I^R(t)\boldsymbol{F}_I^R(0)\right\rangle$. Equivalently, the memory kernel $K(t)$ can always be represented by a sum of n functions with n independent random forces,

$$\boldsymbol{F}_I(t) = -\int_0^t ds\sum_{i=1}^n K_i(t-s)\boldsymbol{P}_I(s) + \sum_{i=1}^n \boldsymbol{F}_{I,i}^R(t) \tag{5.21}$$

where every random force term has to fulfill its own fluctuation-dissipation relation $3Mk_BTK_i(t) = \left\langle \boldsymbol{F}_{I,i}^R(t)\boldsymbol{F}_{I,i}^R(0)\right\rangle$. As long as $K(t) = \sum_{i=1}^n K_i(t)$, Eq. 5.20 and Eq. 5.21 are equivalent in the sense that they yield the same single particle time-correlation functions, such as the VACF.

Analogously, we interpret the target model, Eq. 5.5, as a many-particle model in which the dynamics of any particle I is governed by the memory and friction due to the sum of two contributions, namely due to the conservative interactions and due to the memory kernel $\tilde{K}(t)$. Considering such a CG simulation based on Eq. 5.5, the trajectory of any particle in the system can be mapped onto a GLE of the form of Eq. 5.7, and an effective single-particle memory kernel $K^{CG}(t)$ can be derived from the Volterra equation

$$C_{FP}^{CG}(t) = -\int_0^t dsK^{CG}(t-s)C_{PP}^{CG}(s), \tag{5.22}$$

(or its integrated form as in Eq. 5.14) where the superscript CG denotes evaluation from a CG trajectory. From Eq. 5.5 we can also derive,

$$C_{FP}^{CG}(t) = C_{F^CP}^{CG}(t) - \int_0^t ds\tilde{K}(t-s)C_{PP}^{CG}(s). \tag{5.23}$$

Equating Eq. 5.22 and 5.23, and reordering yields

$$C_{F^CP}^{CG}(t) = -\int_0^t ds\Delta K^{CG}(t-s)C_{PP}^{CG}(s). \tag{5.24}$$

Inversion of Eq. 5.24 allows to evaluate $\Delta K^{CG}(t) = K^{CG}(t) - \tilde{K}(t)$, which is the memory and friction effectively added through the conservative interaction $\boldsymbol{F}_I^C(t)$. The question now is how to parameterize $\tilde{K}(t)$ such that $K^{CG}(t) \approx K(t)$. Here the BOD-method described in Sec. 5.2.2 can be exploited.

The physical interpretation that $\Delta K^{CG}(t)$ is due to conservative interactions suggests

$$\Delta K^{CG}(t) \approx K_C(t), \tag{5.25}$$

if $K^{CG}(t) \approx K(t)$. Because of the additivity of memory kernels implied by Eq. 5.21, this furthermore suggests, that

$$\tilde{K}(t) \equiv K_\delta(t) + 2K_X(t) \tag{5.26}$$

should be an optimal a-priori choice for the parametrization of the target model, which we will validate in Sec. 5.4.

One might be tempted to replace the CG correlation functions in Eq. 5.23 with correlation functions from reference simulations to derive a memory kernel for the target model. This approach was used in the past to parameterize a Markovian Langevin thermostat.[196] The assumption in the derivation of Eq. 5.23 is $\left\langle \boldsymbol{F}_I^R(t)\boldsymbol{P}_I(0)\right\rangle = 0$, similar to the assumption in Eq. 5.11, and holds true for the GLE-thermostat by construction. Contrary to the single particle GLE, the target EoM Eq. 5.5 from which Eq. 5.23 is derived is not equivalent to a formally exact CG EoM[35] and thus the link between the Volterra equation Eq. 5.23 and the FG dynamics, without further justification,[222] is at least ambiguous.

5.2.4 Iterative Optimization

Similar to structural coarse-gaining,[9, 10] memory kernels in GLE-models can be iteratively optimized to match certain target properties, where the VACF is the most prominent target to this day.[32, 39] As the VACF is a single particle property, it can always be related to an effective (integrated) single particle memory kernel following Eq. 5.14. For an iterative optimization scheme, $G(t)$ can be directly used as target. The rationale is that the relation between the optimal memory kernel $\tilde{K}(t)$, or its integrated form $\tilde{G}(t) = \int_0^t ds\tilde{K}(s)$, to the effective integrated single-particle memory kernel $G^{CG}(t)$ is less complex and thus straight forward, hopefully stable, iterative schemes, can be established. Here we want to present three different update schemes for the task. First we notice that in a CG simulation

$$G^{CG}(t) = \Delta G^{CG}(t) + \tilde{G}(t). \tag{5.27}$$

Assuming that the residual between the integrated target memory kernel $G^{tgt}(t) \equiv G(t)$ and the CG integrated effective single particle memory kernel $G^{CG}(t)$, both evaluated based on the VACF using Eq. 5.14, can be compensated by a change in $\tilde{G}(t)$ suggests the update scheme

$$\tilde{G}_{i+1}(t) = \tilde{G}_i(t) + \left(G^{tgt}(t) - G_i^{CG}(t)\right). \tag{5.28}$$

In the limit where conservative interactions are negligibly weak, we have

$$G_i^{CG}(t) \approx \tilde{G}_i(t) \tag{5.29}$$

and thus Eq. 5.28 would converge within a single step. When conservative interactions play a significant role in the dynamics of the system, Eq. 5.28 would converge within a single step, only if $\Delta G^{CG}(t)$ is independent of $\tilde{G}(t)$.

As we will demonstrate in Sec. 5.4.4, $\Delta G^{CG}(t)$ in fact depends on $\tilde{G}(t)$, which can lead to an oscillatory approach of the target. To prevent that, a step-size parameter can be included in Eq. 5.28 to increase the stability. As the optimal step parameter is not known a-priori, an update scheme which is generally less prone to suffer from oscillations might be preferable. We therefore consider

$$\tilde{G}_{i+1}(t) = \frac{G^{tgt}(t)}{G_i^{CG}(t)}\tilde{G}_i(t) \tag{5.30}$$

or by using $G_i^{CG}(t) = \Delta G_i^{CG}(t) + \tilde{G}_i(t)$

$$\tilde{G}_{i+1}(t) = \frac{G^{tgt}(t)}{\Delta G_i^{CG}(t) + \tilde{G}_i(t)}\tilde{G}_i(t). \tag{5.31}$$

In a case where $\Delta G_i^{CG}(t) = 0$ this update scheme again should trivially converge within one step. For the case of large $\Delta G_i^{CG}(t)$ we expect that also the absolute change of $\Delta G_i^{CG}(t)$ will be large. The formulation

of Eq. 5.30 automatically decreases the step size in this case, and thus should prevent oscillatory behavior. As will be demonstrated in Sec. 5.4.4, Eq. 5.30 can yield slow convergence in some cases.

We consider a third update scheme to further improve the convergence by approximately quantifying the dependence of $\Delta G^{CG}(t)$ on the GLE-thermostat parametrization due to $\tilde{G}(t)$. We start from $G^{CG}(t) = \Delta G^{CG}(t) + \tilde{G}(t)$, and assume the linear relation $\Delta G^{CG}(t) \approx a(t) + b(t)\tilde{G}(t)$. In this expression, $b(t)$ accounts for the fact that application of a GLE-thermostat affects the friction due to particle collisions (conservative interactions). Without a GLE-thermostat, the approximation yields $\Delta G^{CG}(t) = a(t)$, with $a(t)$ corresponding to the overall single-particle friction in a CG-MD simulation, i.e. $a(t) = G_{CG-MD}(t)$. To derive an iterative scheme, we apply these assumptions and write

$$G_i^{CG}(t) \approx a(t) + (b(t) + 1)\tilde{G}_i(t) \tag{5.32}$$

for each iteration and

$$G^{tgt}(t) \approx a(t) + (b(t) + 1)\tilde{G}^{tgt}(t) \tag{5.33}$$

for the target. Solving Eq. 5.32 for $b(t)$, using the result in Eq. 5.33 and replacing $\tilde{G}^{tgt}(t)$ by $\tilde{G}_{i+1}(t)$ yields

$$\tilde{G}_{i+1}(t) = \frac{G^{tgt}(t) - a(t)}{G_i^{CG}(t) - a(t)}\tilde{G}_i(t). \tag{5.34}$$

For this third update scheme an additional CG-MD simulation has to be carried out to predetermine $a(t)$.

For negligible conservative interactions $a(t)$ vanishes, in which limit Eq. 5.34 is equivalent to Eq. 5.30 and again should converge within one iteration step. For strong conservative interactions, the correction term $a(t)$ takes care of the case where friction due to conservative interactions is quite dominant. This effectively leads to larger steps close to the target, while still preventing oscillatory behavior.

5.2.5 Summary of the Bottom-up Coarse-Graining Procedure and of Notations

Here we want to shortly summarize the procedure needed to derive coarse-grained models for the target EoM Eq 5.5. The first step is always to derive a conservative CG potential. For the parametrization of the GLE-thermostat the following steps need to be carried out.

1. Generate trajectories for the FG reference model.
2. Generate a mapped trajectories, representing the reference dynamics in terms of CG DoFs.
3. Analyze the mapped trajectory to compute $K_C(t)$, $K_\delta(t)$ and $K_X(t)$ according to the BOD-method.
4. Run CG simulations following Eq. 5.5, with $\tilde{K}(t) = K_\delta(t) + 2K_X(t)$.
5. Evaluate dynamic properties from CG trajectories, as e.g. $\Delta K^{CG}(t)$ from Eq. 5.24 to test the assumption $K_C(t) \approx \Delta K^{CG}(t)$.

The above summary is generic. In practice, before carrying out step 4., we fit the respective memory kernel with dampened oscillators to parameterize the auxiliary variable GLE-thermostat due to Ceriotti.[221] (See SI for a detailed description.) To study the relevance of the cross-correlation term, $K_X(t)$, in step 4. we also consider $K_\delta(t)$ and $K_{\delta,X}(t) = K_\delta(t) + K_X(t)$ for the parametrization of the GLE-thermostat.

As we have introduced many different memory kernels with slightly differing notations, a short recap follows:

- $K(t)$, $K_\delta(t)$, $K_C(t)$ and $K_X(t)$ always refers to the single particle memory kernel and its different contributions, as defined by Mori's linear single particle EoM (Eq. 5.7). These memory kernels are always evaluated from FG trajectories based on the BOD-method.
- $\tilde{K}(t)$ refers to the proposed optimal bottom-up parametrization of the target EoM Eq. 5.5.
- $\Delta K^{CG}(t)$ refers to the memory added through conservative interactions in CG simulations following Eq. 5.5. $\Delta K^{CG}(t)$ is evaluated based on the inversion of Eq. 5.24.
- $K^{CG}(t)$ refers to the effective single-particle memory kernel in CG simulations. In practice, we evaluate only its integral, $G^{CG}(t)$, directly from CG VACFs, following Eq. 5.14.
- G generally refers to integrated memory kernels, with the respective subscripts, superscripts, etc. denoting the particular memory kernel we refer to.

For the iterative optimization schemes we additionally introduced the following notations:

- $G^{tgt}(t)$ refers to the target integrated memory kernel, equivalent to $G(t)$, but evaluated from the FG reference VACF following Eq. 5.14.
- $\tilde{G}_i(t)$ refers to the parametrization of the GLE-thermostat of the ith iteration. In particular $\tilde{G}_0(t)$ is the initial guess, which can be chosen in different ways.
- $G_i^{CG}(t)$ refers to the integrated effective single-particle memory kernel, evaluated based on the VACF from the ith CG simulation.
- $\Delta G_i^{CG}(t)$ refers to integrated memory implicitly introduced due to conservative interactions in the ith CG simulation. (Has not to be explicitly evaluated.)

5.3 Models

5.3.1 Fine-Grained Reference: The Continuous Asakura-Oosawa Model

The Asakura-Oosawa (AO) model[37, 38] is a well known generic model for the description of colloid-polymer mixtures.[223] In this model, colloids and polymers are described respectively by single beads of different radii σ_{cc} and σ_{pp}, where $\sigma_{pp} < \sigma_{cc}$. The colloid-colloid and the colloid-polymer interactions are described by hard-sphere interactions, while there are no polymer-polymer interactions. While all interactions in this model are repulsive, the *e*ffective (depletion) interaction between the colloids is attractive and related to the translational entropy of the polymer. For a sufficiently small size-ratio $q = \sigma_{pp}/\sigma_{cc} < 0.1547$,[223, 225] it can be shown that these effective interactions can be described exactly in terms of pair-interactions. This means that a CG implicit-solvent model can be derived, for which the MB-PMF can be exactly represented with pairwise CG potentials.

For our purpose the hard-sphere description is not very useful, which is why we use a continuous variant of the AO-model, similar to Ref. [224]. We model the colloid-colloid and colloid-polymer interaction via purely repulsive Weeks-Chandler-Andersen (WCA)-interactions,[226] i.e.,

$$U_{cc}(R) = 4\epsilon_{cc}\left[(\sigma_{cc}/R)^{12} - (\sigma_{cc}/R)^6 + \frac{1}{4}\right], \qquad R < 2^{1/6}\sigma_{cc}, \tag{5.35}$$

$$U_{cp}(R) = 4\epsilon_{cp}\left[(\sigma_{cp}/R)^{12} - (\sigma_{cp}/R)^6 + \frac{1}{4}\right], \qquad R < 2^{1/6}\sigma_{cp}, \tag{5.36}$$

q	n_c	n_p	ρ_c	ρ_p	η_c	η_p	m_p
0.15	2000	60000	0.73	21.87	0.38	0.039	1
0.15	**2000**	**60000**	**0.73**	**21.87**	**0.38**	**0.039**	**3**
0.4	**2000**	**10000**	**0.73**	**3.64**	**0.38**	**0.122**	**3**
0.6	**2000**	**1000**	**0.73**	**0.36**	**0.38**	**0.041**	**3**

Table 5.1: System parameters for all AO systems discussed in the main text. The bold entries represent the systems discussed in Sec. 5.4.3-5.4.3. The systems for which we applied iterative optimizations, discussed in Sec. 5.4.4, are underlined. The parameters for all studied systems (in total 19) can be found in the SI.

and

$$U_{pp}(R) = 0. \tag{5.37}$$

Throughout this work, we use a system of reduced units by defining the energy, length, mass and time units as $\epsilon = \sigma = m = 1$ and $\tau = \sigma\sqrt{m/\epsilon}$. Furthermore we set the Boltzmann constant $k_B = 1$. (In this section we will make the choice of the unit system explicit. In the following sections, tables and figures we will omit the units.) For all systems we set $k_BT = 1\epsilon$, $\sigma_{cc} = 1\sigma$, $\sigma_{cp} = 0.5(\sigma_{cc} + \sigma_{pp})$. For the 4 reference systems reported in the main text we always use a cubic simulation box of length $14\ \sigma$, yielding a box volume of $V = 2744\ \sigma^3$, and $n_c = 2000$ colloid particles, which amounts to a colloid number density $\rho_c = 0.73\ \sigma^{-3}$. The colloid-bead mass is chosen as $m_c = 10m$. We summarize the parameters which are discussed in the main text in Tab. 5.1, where we also report the volume fractions $\eta_{c/p} = (\pi\sigma^3_{cc/pp}/6)\rho_{c/p}$. In total we studied 19 different systems. The parameters and results for the systems not discussed in detail in the main text, are reported in the SI. In the remainder of this paper we refer to the three bold systems in Tab. 5.1 as $q = 0.15$-, $q = 0.4$- and $q = 0.6$-system respectively.

The FG reference simulations were carried out using GROMACS version 2018.2..[212, 214] We used a simulation step of $\Delta t = 0.0005\tau$. Trajectories, which were used for the calculation of radial distribution functions and as input for the coarse-graining procedure, were run for $4 \cdot 10^6$ steps, generated using the stochastic dynamics integrator with a time constant of 4 τ while snapshots were saved every 1000 steps. For the evaluation of VACFs simulations were run for $2 \cdot 10^6$ steps using the velocity-verlet integrator and the Nosé-Hoover thermostat with a time constant of 4 τ. Snapshots were taken after every 20 simulation steps. For the application of the BOD-method, we generated 5 independent trajectories per system with $2 \cdot 10^5$ steps per trajectory and snapshots were taken after every 2 steps. Memory kernels derived based on the BOD-method were averaged over these 5 trajectories.

5.3.2 Coarse-Grained Asakura-Oosawa Model

Conservative Interactions

The CG AO model can be understood as an implicit solvent model, in which the DoFs of the polymer beads are removed and effective colloid-colloid interactions are employed. Thus the mapping operator is defined as

$$\hat{M}_R(\boldsymbol{r}) = \boldsymbol{R}, \tag{5.38}$$

with $\boldsymbol{r} = \{\boldsymbol{r}_1, ..., \boldsymbol{r}_{n_c}, \boldsymbol{r}_{n_c+1}, ..., \boldsymbol{r}_{n_c+n_p}\}$, $\boldsymbol{R} = \{\boldsymbol{R}_1, ..., \boldsymbol{R}_{n_c}\}$ and $\boldsymbol{R}_I = \boldsymbol{r}_I$. The CG momenta and masses are accordingly equivalent to the FG colloids momenta and masses. While the exact analytical effective interactions for small values of q are known for the hard-sphere AO model,[223] in principle it should also be possible to describe the MB-PMF for the continuous AO-model in terms of pairwise interactions. The CG force-field can be derived by any established coarse-graining method for conservative interactions. A

natural choice for the system at hand is the force-matching (FM) (also referred to as multi-scale coarse-graining)[193] method, which optimizes the pairwise-interactions such that the MB-PMF is optimally represented.[193] For small values of q, the FM-method should yield exact (within numerical accuracy) CG potentials. We derived effective pair-potentials for the three studied systems, using the FM-method implemented in the VOTCA software package.[202] For the FM-method we set the cut-off distance to 1.31, 2.6 and 2.0 for the $q = 0.15$-, $q = 0.4$-, $q = 0.6$-system, respectively.

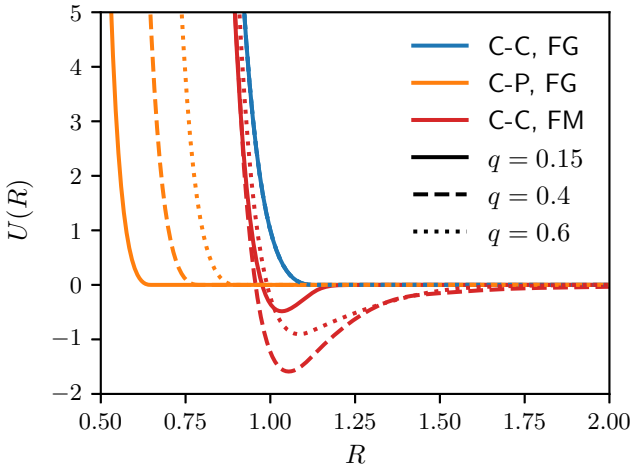

Figure 5.1: Summary of FG and CG (FM) potentials for the $q = 0.15$-, the $q = 0.4$- and the $q = 0.6$-system. Note that the colloid-colloid interactions in all FG systems are equivalent.

In Fig. 5.1 we show show the FG colloid-colloid and colloid-polymer interactions, alongside the CG potentials derived via FM. As expected, in the CG picture, the colloid-colloid interactions are effectively attractive.

Coarse-Grained Simulations

To test the CG potentials and the calculation of radial-distribution functions we generated trajectories again using GROMACS version 2018.2..[212, 214] The stochastic dynamics integrator was used with a smaller time constant of 0.625, to efficiently obtain uncorrelated snapshots.

All CG trajectories used to evaluate time-correlation functions were obtained using LAMMPS.[227] CG-MD trajectories were generated using the Nosé-Hoover thermostat with a time-constant of 5. GLE-thermostat simulations were carried out using the auxiliary-variable GLE-thermostat by Ceriotti[151] as implemented in LAMMPS. After equilibration, CG simulations for the calculation of VACFs were carried out for a total simulation time of 1000 with a spacing between frames of 0.01. Additional trajectories were generated to evaluate $\Delta K^{CG}(t)$ based on Eq. 5.24 with a total simulation time of 100 and a spacing between frames of 0.001.

For the application of the iterative schemes discussed in Sec. 5.4.4 the simulation time was reduced to 500 to save computational costs.

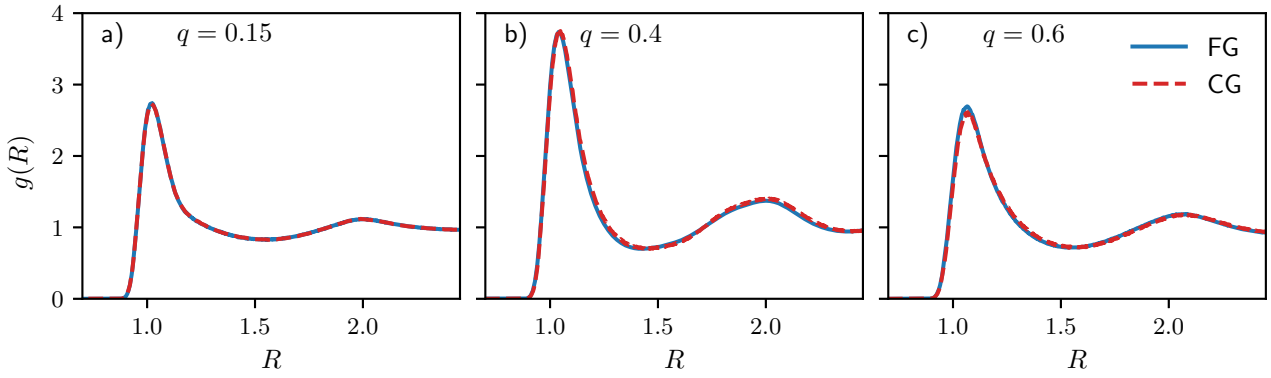

Figure 5.2: Radial distribution functions $g(R)$ for FG and CG simulations of the AO-model for the a) $q = 0.15$-, b) $q = 0.4$- and c) $q = 0.6$-system.

5.4 Results

5.4.1 Accuracy of Conservative Interactions and Structure

In the CG AO model, we assume that the FM method yields accurate conservative interactions as long as $q \leq 0.15$. For larger q values, multi-body correlations contribute to the MB-PMF which cannot be captured in terms of pairwise interactions. In Fig.5.2 we compare the radial distribution functions $g(R)$ from FG and CG simulations for the considered systems. For $q = 0.15$ we find that the FM-method yields a potential which perfectly reproduces the $g(R)$, as expected. For $q = 0.4$ the structure is also very accurately represented. Only minor deviations can be found. This indicates that for the system with $q = 0.4$ many-body effects might be present, but they still might be comparably weak. While the RDF is also quite well reproduced for the $q = 0.6$-system, we find a slightly too small first peak in this case. By varying the value of q we can thus control the accuracy of the representation of the MB-PMF, while still reproducing the main structural features, and thus test the relevance of the quality of the conservative interactions on the representability of dynamic properties in the CG models.

5.4.2 Memory due to Conservative Interactions

Here we want to test the hypothesis that $K_C(t) \approx \Delta K^{CG}(t)$, to further justify our strategy for the parametrization of $\tilde{K}(t)$.

In the supporting information of Ref. [33] we have made the equivalent comparison for a star-polymer melt. While we found a qualitatively good agreement, quantitatively the two functions showed some non-trivial deviations. Accordingly, small but significant deviations have been found in the VACF of the CG model. We suggested that the deviations stem from inaccuracies in the conservative interactions.

The comparison between $K_C(t)$ and $\Delta K^{CG}(t)$ for the systems discussed in Sec. 5.4.1 is shown in Fig. 5.3. Indeed, overall a good agreement between $K_C(t)$ and $\Delta K^{CG}(t)$ is found for all the three systems. In the $q = 0.15$- and the $q = 0.4$-system the initial decay matches perfectly. For the $q = 0.6$ system we, find the most significant deviations on short time scales. In particular the mismatch $K_C(0) \neq \Delta K^{CG}(0)$ directly indicates, that different probability distributions $\rho(\boldsymbol{R})$ are sampled in the FG and CG simulations, which is in line with the small deviations in the radial distribution function found in Fig.5.2. From Fig. 5.3 it can be inferred that the VACF will be well reproduced on short time scales for $q = 0.15$ and $q = 0.4$. For $q = 0.6$ deviations, especially on short time scales, can be expected.

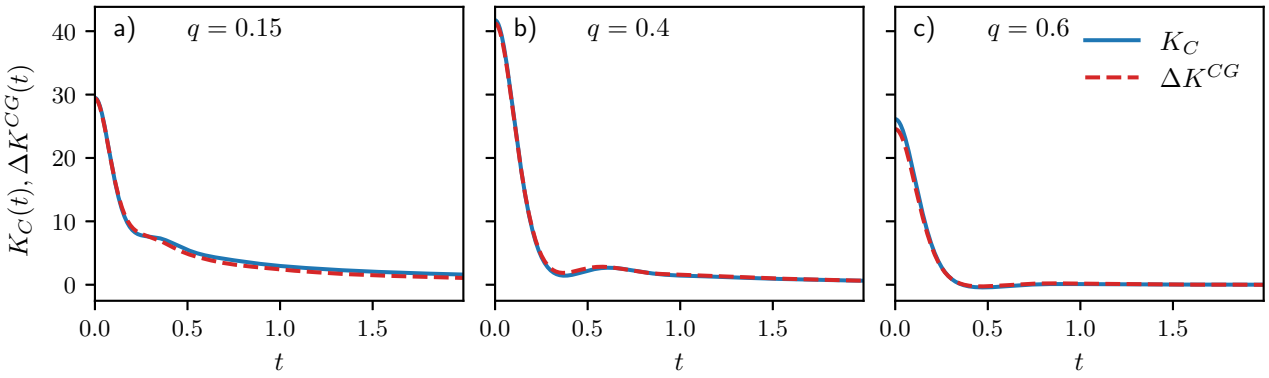

Figure 5.3: Comparison of the memory kernel contribution $K_C(t)$ from FG and $\Delta K^{CG}(t)$ from CG simulations with a GLE thermostat parameterized with $\tilde{K}(t)$ for the a) $q = 0.15$-, b) $q = 0.4$- and c) $q = 0.6$-system.

An interesting finding is, that in the $q = 0.15$-system, the tail behavior of $K_C(t)$ and $\Delta K^{CG}(t)$ differs noticeably. We will discuss this finding and its implication in more detail in Sec. 5.4.3.

5.4.3 Dynamic Properties in Coarse-Grained Models

In the previous section we have shown that the validity of the assumption that $K_C(t) \approx \Delta K^{CG}(t)$ depends on the accuracy of the conservative interactions and is more generally system dependent on longer time scales. The AO model has some free parameters which can be independently chosen. A detailed study of the full parameter space is out of the scope of this study and we only sparsely screen the bead-size ratio q in the main text. Varying colloid density, polymer density and mass of the polymer beads are reported in the SI.

The $q = 0.15$-system

As a first example we study a system with accurate CG conservative interactions ($q = 0.15$), high colloid density ($\rho_c = 0.73$), high polymer density ($\rho_p = 21.87$) and a polymer bead mass of $m_p = 3$. For this system it can be expected, that the overall friction on a single colloid particle is neither dominated by the colloid-colloid collisions nor solely by its collision with the polymer beads. This ensures that both the conservative and dissipative interactions in the CG model are relevant to accurately represent dynamics.

In Fig. 5.4 the full memory kernel $K(t)$, and its contributions as defined by Eq. 5.9, are shown. We also show the integrals $G(t) = \int_0^t dsK(s)$ to evaluate the contributions to the total friction. We find that the total memory kernel on very short time scales is dominated by $K_\delta(t)$, which is mostly decayed at $t = 1$. While the amplitude of $K_C(t)$ is smaller on short time scales, it is the dominant contribution already at $t = 0.15$. The cross-correlation contribution $K_X(t)$ is the smallest in amplitude. At times $t < 0.5$ it shows some complex behavior, while it exhibits a long lived negative tail.

One interesting feature of the full memory kernel is that it is purely positive, and thus retarding on all time scales. Especially in dilute colloid suspensions this is typically not the case. In Ref. [39], correlations at larger time scales were found for the single-particle memory kernel of colloids, modeled by Lennard-Jones interactions. A negative, persistent tail of the memory kernel in colloids is induced by a backflow effect in the solvent. For the AO model, with the chosen parameters, we do not find this feature in the full memory kernel. The $K_\delta(t)$ and $K_X(t)$ contributions indicate that a similar correlation enhancing mechanism is present but counteracted by the retarding effect of colloid-colloid collisions. The fit functions for $K_\delta(t)$ and

$\tilde{K}(t)$ are shown as dotted black lines. The integrals of the memory kernel and its contributions are shown in inset. At long times the integrals represent the effective friction coefficient and its contributions. For this system, the overall contributions to the total friction due to $K_\delta(t)$ and $K_C(t)$ are comparable. As also found in Ref. [33], $K_X(t)$ effectively reduces the overall friction.

We have already discussed the physical interpretation of $K_C(t)$. Now we can try to infer the physical meaning of $K_\delta(t)$ and $K_X(t)$ by considering the data shown in Fig. 5.4, while noting, that this can only provide a qualitative picture. $K_\delta(t)$ can be straight-forwardly interpreted as being the actual solvent contribution, as it is explicitly related to the orthogonal projection of the residual forces $\delta F_I(t)$ and it encodes for the viscoelastic response due to the lost DoFs. The definition of the $K_X(t)$ indicates that it is physically not only linked to the lost DoFs, but it describes the coupling between the irrelevant and the relevant DoFs. The physical interpretation of this coupling somewhat depends on the type of system and the mapping scheme. In the current system, we consider the dynamics of some colloid-particle I. Its motion will induce a sound wave in the solvent DoFs, which will interact with other colloid particles in the vicinity. On short time scales (but not instantaneous) this solvent mediated colloid-colloid coupling will modulate the dynamics of colloid-particle I in some complex way. On longer time scales it will yield persistent coherent collective motion of the colloids and the solvent, effectively increasing the diffusivity of particle I. In Fig. 5.4 we find that $K_X(t)$ on short time scales shows some complex fluctuations and on long time scales ultimately has a long lived negative tail, which would fit the described physical picture. In our CG model, we do not include solvent mediated hydrodynamic colloid-colloid interactions explicitly, instead the incorporation of $K_X(t)$ in the GLE-thermostat accounts for these phenomena in an averaged way.

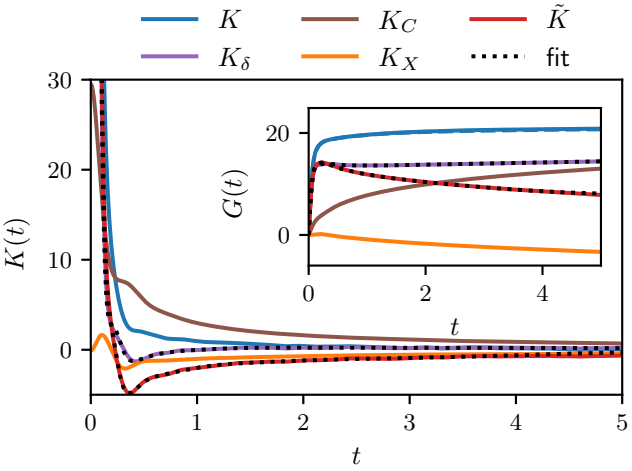

Figure 5.4: The memory kernel $K(t)$ and its contributions for the $q = 0.15$-system. Inset: Integrals of the memory kernels. We plot $G(t)$ evaluated from Eq. 5.14 as dashed blue line. The fit functions used for the parametrization of the GLE-thermostat are shown as black dotted lines.

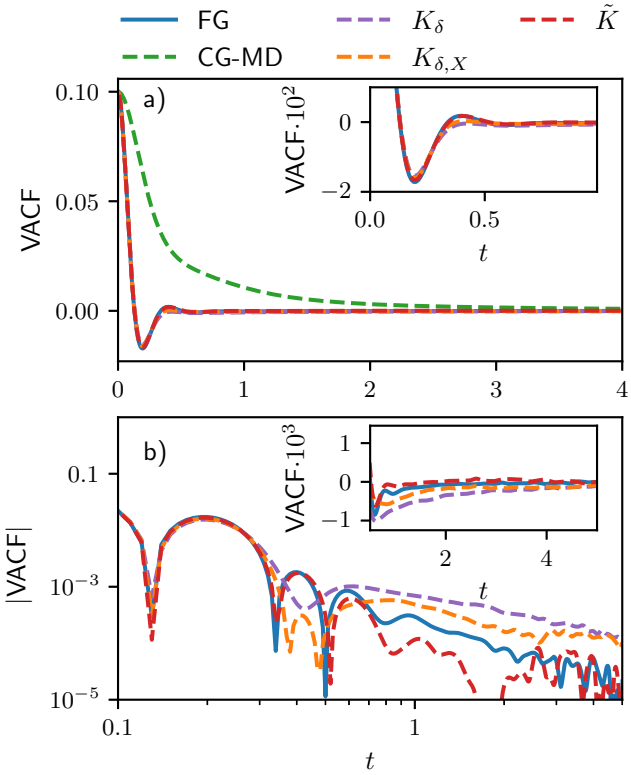

Figure 5.5: VACFs for FG and CG AO models with $q = 0.15$. a) Overview of the VACFs up to $t = 4$. Inset: Detailed plot of the first minimum of the VACFs. b) Log-log-plot of the absolute values of the VACFs to emphasize the hydrodynamic scaling of the tail. Inset: Detailed plot of the tail region up to $t = 4$.

In Fig. 5.5 the VACFs from CG simulations and FG reference simulations are shown. We find that the VACF is almost perfectly reproduced when using $\tilde{K}(t)$ as defined by Eq. 5.26 in the GLE thermostat. We find that even zooming into the data by about a factor of 10, as found in the inset of Fig. 5.5 a), does not reveal any significant deviations. The FG VACF shows a pronounced backscattering effect, indicated by a negative region of the VACF. While this behavior is qualitatively captured by all three parametrizations, using $K_\delta(t)$, $K_{\delta,X}(t) = K_\delta(t) + K_X(t)$ and $\tilde{K}(t)$, it is best captured with $\tilde{K}(t)$, demonstrating that the cross-correlation contribution $K_X(t)$ has to be taken into account to capture the VACF accurately. In this system we see two sign changes in the VACF, and accordingly two local extrema. In $K_X(t)$ we find similar features, exhibiting first a local maximum, which shifts the local minimum in the VACF to smaller values, and a local minimum, which shifts the local maximum in the VACF to higher values. While the initial decay can be well captured without taking $K_X(t)$ into account, the intermediate fluctuations are modulated through the cross-correlations.

While in our earlier study on a star-polymer melt[33] the back scattering effect was not as well reproduced as in the AO model, it was also found that taking $K_X(t)$ into account strongly improves the representation of the backscattering effect and in particular a neglection of $K_X(t)$ leads to too slow dynamics. This was previously indirectly shown in a study by Lei *et al.*[36] and is now confirmed for the AO model.

As discussed in e.g. Refs. [35, 195, 222], Eq. 5.5 can only be an approximate EoM and we do expect to find some discrepancies in the CG dynamics. The inset of Fig. 5.5 b) shows the data zoomed in by another order of magnitude on a larger time scale. On a time scale on which the VACF is almost fully decayed (by more than 99%), small but persistent deviations can be found in the tail region. In Fig. 5.5 b) the log-log plot reveals that in fact the hydrodynamic tail is not described accurately in the CG systems.

The $q = 0.4$-system

By varying the bead size ratio q multi-body effects can be introduced into the effective colloid-colloid interactions and the quality of the CG potentials based on pair-interactions can be investigated in a controlled way. In this section we study the dynamic properties of the $q = 0.4$-system. In Fig. 5.2 we have shown that despite the increased bead-size ratio q the RDF can be accurately captured by the FM-potentials. While many-body effects should in theory be present, the volume per polymer bead is still only 6.4% of the volume per colloid bead and the pairwise potential seems to be a good approximation of the MB-PMF.

This is also reflected in Fig. 5.3, where we have found that $\Delta K^{CG}(t)$ in CG GLE models matches $K_C(t)$ from the reference simulations quite well on all time scales. In particular, we do not see the divergence in the tail region as found in the $q = 0.15$-system and it can be assumed that the CG GLE model parameterized with $\tilde{K}(t)$ should capture the reference VACF on short and long time scales.

In Fig. 5.6 we compare the memory kernel $K(t)$ and its contributions. Qualitatively, the contributions show a comparable behavior as in the $q = 0.15$-system, but we find that $K_C(t)$ yields a more significant contribution to the total friction. This is firstly due to the more attractive and longer ranged CG potential, and secondly due to the reduced number of polymer beads in the reference system. Still the contribution to the total friction due to the removed DoFs is far from negligible and the reproduction of dynamic properties in CG simulations is non-trivial.

In Fig. 5.7 we compare the FG and CG VACFs and find, as one would expect, a slower decay in the CG-MD simulations without a GLE-thermostat, indicating overall faster dynamics. While the parametrization with $K_\delta(t)$, $K_{\delta,X}(t)$ and $\tilde{K}(t)$ all lead to a significant improvement in the reproduction of the reference VACF, zooming into the the first minimum and into the tail region reveals again that neglecting the cross-correlation contribution $K_X(t)$ in the parametrization of the GLE-thermostat leads to errors is the representation on intermediate time scales. For this particular system, even the long time tail is very well

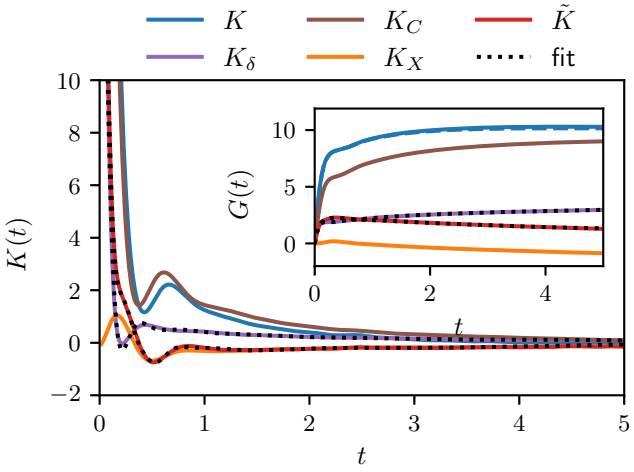

Figure 5.6: The memory kernel $K(t)$ and its contributions for the $q = 0.4$-system. Inset: Integrals of the memory kernels. We plot $G(t)$ evaluated from Eq. 5.14 as dashed blue line. The fit functions used for the parametrization of the GLE-thermostat are shown as black dotted lines.

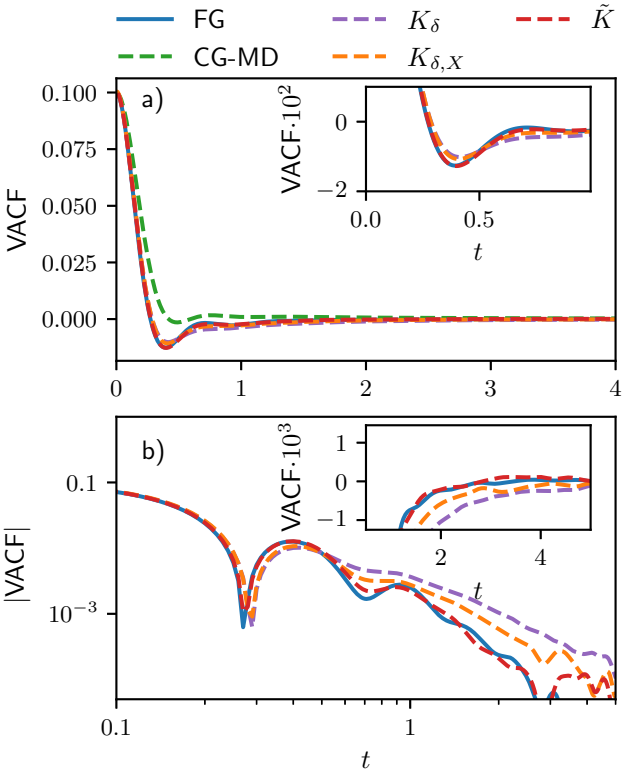

Figure 5.7: VACFs for FG and CG AO models with $q = 0.4$. a) Overview of the VACFs up to $t = 4$. Inset: Detailed plot of the first minimum of the VACFs. b) Log-log-plot of the absolute values of the VACFs to emphasize the hydrodynamic scaling of the tail. Inset: Detailed plot of the tail region up to $t = 4$.

captured with $\tilde{K}(t)$ which can be best seen in the log-log representation.

The $q = 0.6$-system

In this section we study the dynamic properties of the $q = 0.6$-system. In Fig. 5.8 we show the memory kernel $K(t)$ and its contributions. In this system, the $K_C(t)$-contribution decays significantly faster, while the $K_\delta(t)$-contribution shows a more persistent tail, compared to the other systems. Overall $K_C(t)$ accounts for the most part of the total friction.

For this system the volume of a polymer bead is about 22% of a colloid bead, and multi-body effects can be assumed to be more relevant.

As shown in Fig. 5.2 the radial distribution function is not perfectly matched in CG simulations, which indicates that the MB-PMF is not exactly reproduced in this system. In Fig. 5.3 we have found, that while the overall form of $K_C(t)$ and $\Delta K^{CG}(t)$ qualitatively still match quite well a discrepancy at time zero is found. As both $K_C(t)$ and $\Delta K^{CG}(t)$ are proportional to the variance of the forces due to the CG potential in the FG reference simulation and the CG simulation, respectively, this, additionally to slight deviations

in the RDF, directly indicates that the CG simulations do not sample the correct probability distribution $\rho(\boldsymbol{R})$. If the hypothesis we proposed in the introduction and in Ref. [33] is true, this should introduce some deviations in the VACF in the $\tilde{K}$-model.

In Fig. 5.9 we compare the VACF of CG simulations with the FG reference. Even though the overall friction should be dominated by the conservative interactions, we find that the CG-MD simulation still leads to a too slow decay of the VACF in CG simulations, indicating too fast dynamics, and thus necessitates the introduction of friction. We again find that all three GLE-models lead to an improvement of the representation of the VACF, but for this system by zooming into the first minimum and the tail, we find that the $\tilde{K}(t)$ cannot fully capture the VACF on short and intermediate time scales. Still the $\tilde{K}$-model performs significantly better than the K_δ- and $K_{\delta,X}$-model, which show a strong underestimation of the VACF at times $t > 1$, and is thus found to be the optimal purely bottom-up informed choice for the parametrization of the isotropic GLE-thermostat.

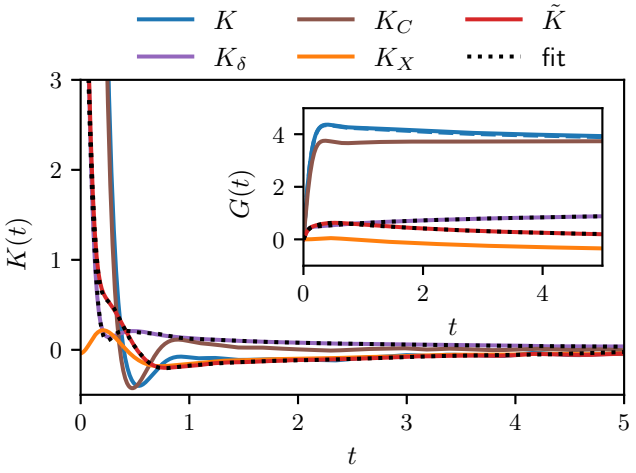

Figure 5.8: The memory kernel $K(t)$ and its contributions for the $q = 0.6$-system. Inset: Integrals of the memory kernels. We plot $G(t)$ evaluated from Eq. 5.14 as dashed blue line. The fit functions used for the parametrization of the GLE-thermostat are shown as black dotted lines.

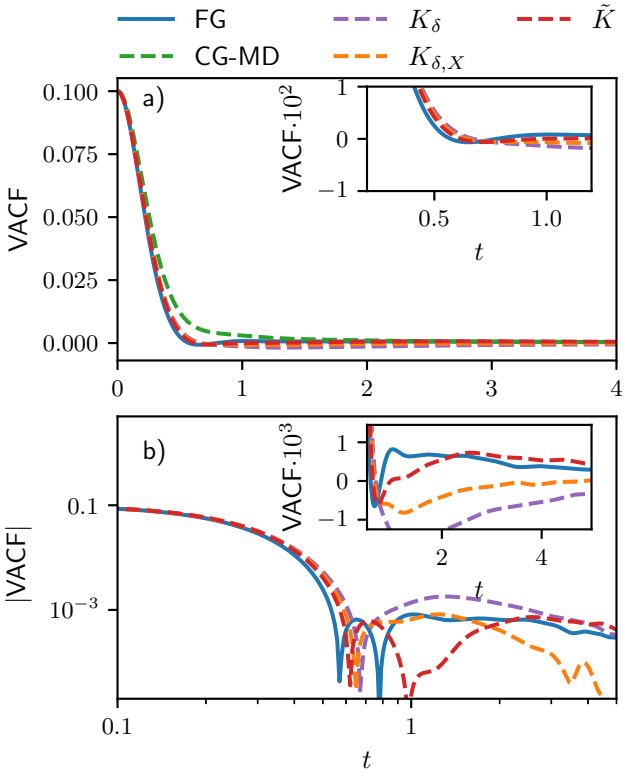

Figure 5.9: VACFs for FG and CG AO models with $q = 0.6$. a) Overview of the VACFs up to $t = 4$. Inset: Detailed plot of the first minimum of the VACFs. b) Log-log-plot of the absolute values of the VACFs to emphasize the hydrodynamic scaling of the tail. Inset: Detailed plot of the tail region up to $t = 4$.

5.4.4 Iterative Optimization

Here we want to apply the three iterative optimization schemes for memory kernels as described in Sec. 5.2.4 (see Eqs. 5.28, 5.30 and 5.34). We start with the first system in Tab. 5.1. This system is equivalent to the $q = 0.15$-system discussed in Sec. 5.4.3, except for the reduced polymer bead mass $m_p = 1$. We made this choice, as we have found that the deviations in the tail in the VACF are more pronounced with reduced polymer bead mass and thus an optimization is more relevant.

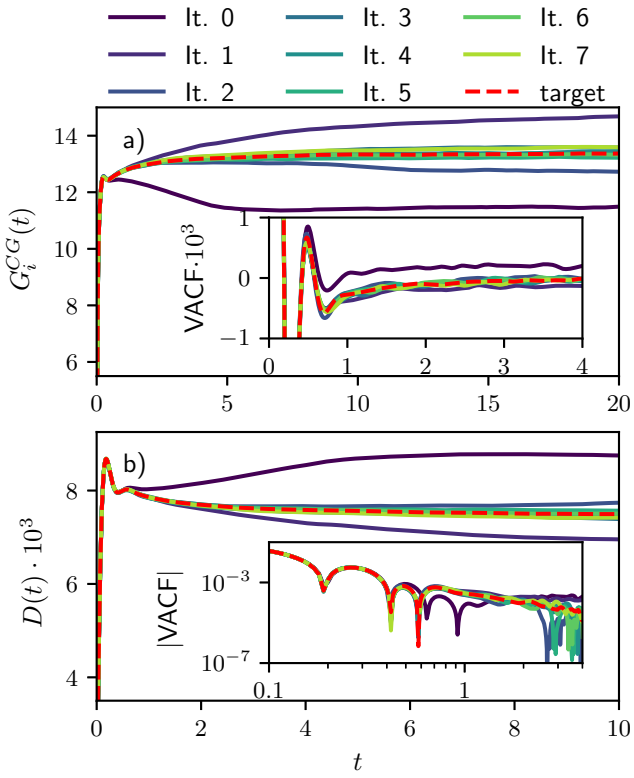

Figure 5.10: Iterative optimization of the parametrization of the CG GLE-thermostat model for $q = 0.15$ with $m_p = 1$ using the update scheme described by Eq. 5.28. $\tilde{G}_0(t) \equiv \tilde{G}(t)$ is used as initial guess. a) Integrated effective single particle memory kernel $G_i^{CG}(t)$. Inset: Tail region of the VACFs up to $t = 4$. b) Integral of the VACFs $D(t) = \int_0^t dsC_{VV}(s)$, where the plateau value represents the diffusion coefficient. Inset: Log-log-plot of the absolute values of the VACFs to emphasize the hydrodynamic tail.

In Fig. 5.10 we show that the first update scheme (Eq. 5.28) improves the tail behavior of the VACF, while it maintains the previously already accurate dynamics on shorter time scales. But we also find that the residual in the effective kernel $G_i^{CG}(t)$ is overcompensated in the first steps. The reason for this behavior is found in the fact that $\Delta G^{CG}(t)$ depends on $\tilde{G}(t)$. To get an intuition on how the effective friction and memory due to conservative interactions is affected by friction added through a thermostat, we can compare the integrals of $G_\delta(t) = \int_0^t dsK_\delta(s)$, which is related to the friction due to collisions with polymer beads, and $G_C(t) = \int_0^t dsK_C(s)$, related to the friction due to effective interactions with colloid beads.

In Fig. 5.11 we plot $G_C(\tau)$ against $G_\delta(\tau)$, with $\tau = 4$ for 18 different systems. For otherwise equivalent systems, an increase in the polymers mass naturally leads to an increase in the friction due to colloid-

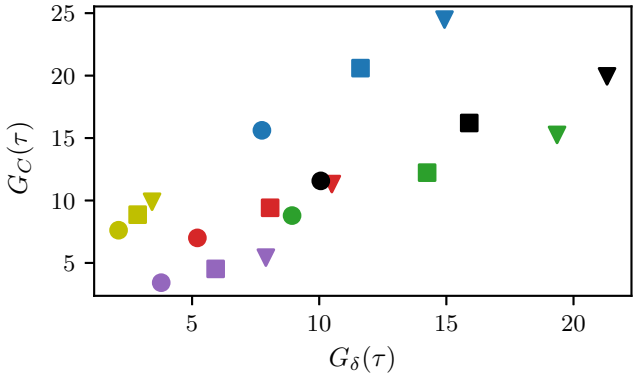

Figure 5.11: Here we plot $G_C(\tau) = \int_0^\tau dt K_C(t)$ against $G_\delta(\tau) = \int_0^\tau dt K_\delta(t)$, with $\tau = 4$ for 18 different systems, as defined in the SI. Data points with the same color indicate equivalent systems for which only the polymer bead mass m_p was varied. The symbols, circle, square and triangle, represent systems with polymer bead mass of 1,3 and 6, respectively.

polymer collisions and thus the plateau value of $G_\delta(t)$ increases. We find that at the same time also the other contributions to the total memory get more pronounced. In particular the plateau values of $G_C(t)$ are increased. This indicates that an increase in the viscosity of the implicit solvent also increases the effective friction exerted due to effective colloid-colloid interactions. This is not surprising as the reduction in the mobility of the colloids leads to a slower decorrelation of the conservative interactions, and thus increases the friction due to these interactions. The relation between $G_C(\tau)$ and $G_\delta(\tau)$ seems to be almost linear if only the polymer mass is changed. This qualitatively explains the oscillatory nature of the iterative scheme due to Eq. 5.28. In CG simulations, $\Delta G^{CG}(t)$ will dominantly change in the same direction as the correction applied to $\tilde{G}(t)$.

In Sec. 5.2.4, with Eq. 5.30, we proposed an update scheme which should be less prone to oscillations. We show the first iterations using Eq. 5.30 in Fig. 5.12, and indeed, both the effective memory kernel and the VACF smoothly approach the target.

The results for the third update scheme (Eq. 5.34) are found in Fig. 5.13. Here the target is approaches faster than with Eq. 5.30 and simultaneously does not show any oscillatory behavior, indicating that Eq. 5.34 constitutes the most promising optimization scheme.

The choice $\tilde{G}_0(t) \equiv \tilde{G}(t)$ already provides a good initial guess. Jung *et al.*[39] in their iterative scheme based the initial guess on force-autocorrelation functions. To test our schemes for an initial guess which is not as close to the optimal parametrization, we also started from $\tilde{G}_0(t) \equiv \int_0^t ds \frac{C_{\delta F \delta F}(s)}{M_I k_B T}$. The results obtained with this choice are summarized in the SI. While the initial guess in this case is not as close to the optimal choice, all three iteration schemes yield quite good results within the first few steps.

In summary, all three iterative schemes perform quite well for the $q = 0.15$-system with $m_p = 1$. As already discussed, this is a system in which the contribution to the total friction due to conservative interactions is highly relevant, but not dominant. We would expect to see a stronger difference in the performance of the different schemes in a case in which the conservative interactions yield the dominant part of the overall friction. This is the case in the $q = 0.6$-system. Furthermore, the deviations in the $q = 0.6$ are not limited to the tail region in the VACF, which makes it a good complementary test case. For reference we show the results for $\tilde{G}_0(t) = \tilde{G}(t)$ as initial guess in the SI. We find that all three update schemes yield good corrections. Yet, as in this system friction due conservative interactions are more dominant, for the scheme of Eq. 5.30 the target is approached quite slowly, which is not the case for Eq. 5.28 and Eq. 5.34. This becomes more evident by again using $\tilde{G}_0(t) \equiv \int_0^t ds \frac{C_{\delta F \delta F}}{M_I k_B T}(s)$ as initial guess. The results

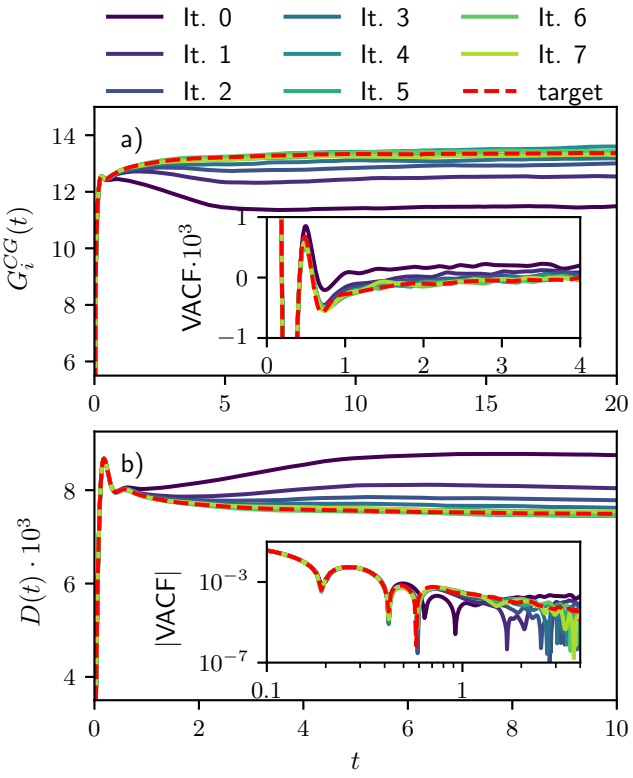

Figure 5.12: Iterative optimization of the parametrization of the CG GLE-thermostat model for $q = 0.15$ with $m_p = 1$ using the update scheme described by Eq. 5.30. $\tilde{G}_0(t) \equiv \tilde{G}(t)$ is used as initial guess. a) Integrated effective single particle memory kernel $G_i^{CG}(t)$. Inset: Tail region of the VACFs up to $t = 4$. b) Integral of the VACFs $D(t) = \int_0^t dsC_{VV}(s)$, where the plateau value represents the diffusion coefficient. Inset: Log-log-plot of the absolute values of the VACFs to emphasize the hydrodynamic tail.

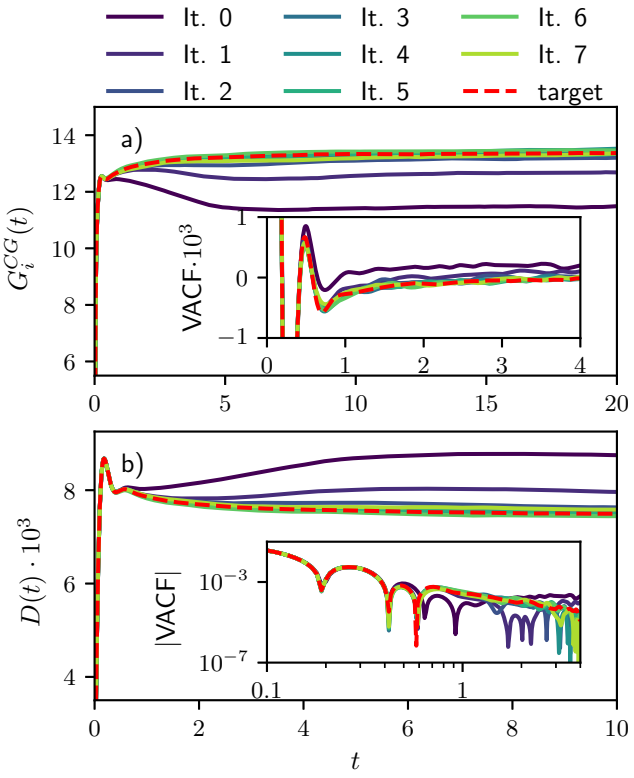

Figure 5.13: Iterative optimization of the parametrization of the CG GLE-thermostat model for $q = 0.15$ with $m_p = 1$ using the update scheme described by Eq. 5.34. $\tilde{G}_0(t) \equiv \tilde{G}(t)$ is used as initial guess. a) Integrated effective single particle memory kernel $G_i^{CG}(t)$. Inset: Tail region of the VACF up to $t = 4$. b) Integral of the VACF $D(t) = \int_0^t dsC_{VV}(s)$, where the plateau value represents the diffusion coefficient. Inset: Log-log-plot of the absolute values of the VACF to emphasize the hydrodynamic tail.

for optimization following Eq. 5.30 and Eq. 5.34 are shown in Fig. 5.14 and Fig. 5.15, respectively. We find that for Eq. 5.30 the target is approached only slowly, while Eq. 5.34 automatically optimizes the step size, such that the target is well reproduced within 3-4 iterations.

5.5 Discussion

In the previous sections we have demonstrated that a parametrization of a CG model following Eq. 5.5 based on the splitting of contributions to the single particle memory kernel as introduced in Ref. [33] and

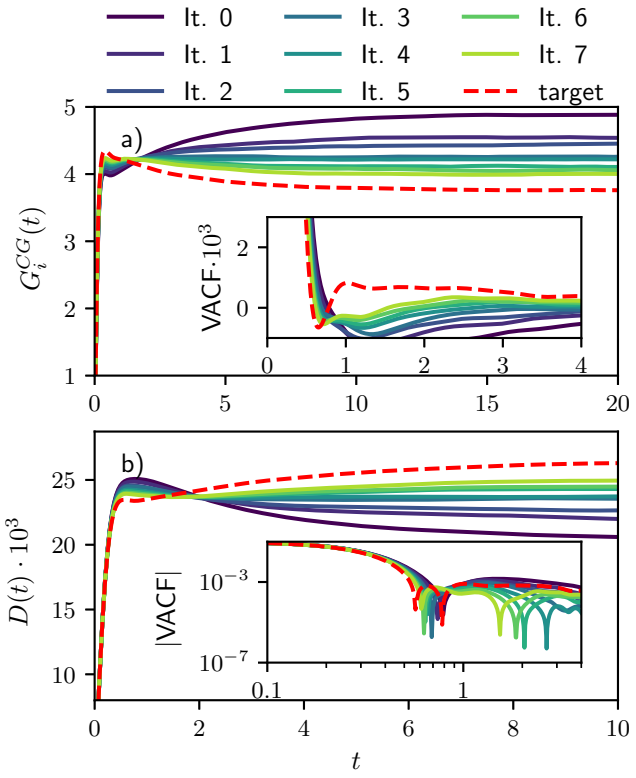

Figure 5.14: Iterative optimization of the parametrization of the CG GLE-thermostat model for $q = 0.6$ using the update scheme described by Eq. 5.30. $\tilde{G}_0 = \int_0^t dsC_{\delta F\delta F}(s)/(M_I k_B T)$ is used as initial guess. a) Integrated effective single particle memory kernel $G_i^{CG}(t)$. Inset:Tail region of the VACFs up to $t = 4$. b) Integral of the VACFs $D(t) = \int_0^t dsC_{VV}(s)$, where the plateau value represents the diffusion coefficient. Inset: Log-log-plot of the absolute values of the VACFs to emphasize the hydrodynamic tail.

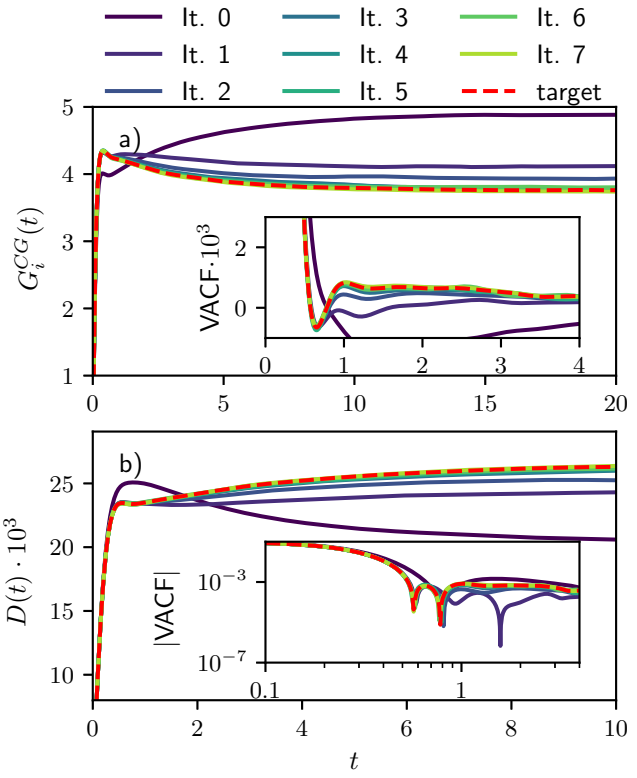

Figure 5.15: Iterative optimization of the parametrization of the CG GLE-thermostat model for $q = 0.6$ using the update scheme described by Eq. 5.34. $\tilde{G}_0 = \int_0^t dsC_{\delta F\delta F}(s)/(M_I k_B T)$ is used as initial guess. a) Integrated effective single particle memory kernel $G_i^{CG}(t)$. Inset: Tail region of the VACFs up to $t = 4$. b) Integral of the VACFs $D(t) = \int_0^t dsC_{VV}(s)$, where the plateau value represents the diffusion coefficient. Inset: Log-log-plot of the absolute values of the VACFs to emphasize the hydrodynamic tail.

Sec. 5.2.3, generally yields a good representation of the VACF in coarse-grained implicit solvent continuous AO models.

We have found that the assumption that $\Delta K^{CG}(t) \approx K_C(t)$ is generally well justified in the studied systems, and reinforces the interpretation of $K_C(t)$ as the memory and friction introduced by the CG potential in multi-body simulations. The results of the $q = 0.6$-system have shown that indeed this assumption is less accurate if the MB-PMF is not fully captured by the CG potential.

This confirms our interpretation of the data in Ref. [33]. An increase in q introduces errors in the radial distribution function and accordingly our CG models cannot exactly reproduce FG VACFs on short time scales. The reason lies in the assumption Eq. 5.25. In the evaluation of $K_C(t)$ trajectories which sample the

actual MB-PMF are used. When the conservative interactions in the CG model do not reproduce the MB-PMF well enough, the CG model will sample different structures and subsequently different force fluctuations. A change in the force-fluctuations directly translates to a change in the effective friction introduced by the conservative interactions. While this point is typically not deeply discussed in the literature on CG dissipative models, in other contexts the importance of accurate CG force-fields for dynamical properties is discussed. For example, the relevance of accurate energy barriers in CG models is discussed in Ref. [204]. This is particularity crucial, as this fact does not specifically apply to our approach, but to any parametrization scheme of dissipative models, which is based on the analysis of mapped reference trajectories, as e.g. in Refs. [27, 29, 61, 65].

In Ref. [61] the authors derived different types of Markovian DPD models for star-polymer melts with different numbers of beads per molecule. The authors found that the quality of their DPD models depends on the number of beads per molecule. In particular, in these models the VACF could be very well reproduced for small star-polymers, in which also the structural properties were well reproduced. For a similar star-polymer-system as used in our previous study,[33] the minimum of the VACF could not be matched while simultaneously also structural properties were less accurately reproduced. The authors mentioned the potential relevance of many-body correlations[61] and our findings reinforce this interpretation.

In Ref. [29] the authors derived Markovian and non-Markovian CG DPD models for fluid blobs with an adaptive mapping scheme. They were able to reproduce the pair-structure quite accurately by employing local-density dependent potentials. While their non-Markovian models reproduce the initial decay and the long time scale of the VACF of the reference model accurately, the back-scattering effect could only be reproduced qualitatively.[29] While the complexity of the model complicates the interpretation of this finding, we propose that our method of comparing $K_C(t)$ and $\Delta K^{CG}(t)$ could in principle be used as an indirect test for the origin of the mismatch in the VACF on intermediate time scales for such models.

The bottom-up derivation of dynamically consistent particle based CG models is thus not only complicated by finding an appropriate, tractable EoM and its formal relation to the FG reference, but in some sense also limited by the quality of the CG potential.

We have found that for the $q = 0.15$-system the long time tail cannot be fully captured without a-posteriori optimization of the parametrization, while the $q = 0.4$-system does not suffer from this problem. In the SI we report the results for a broader spectrum of parameters of the reference AO model. We find that the accuracy of our CG models, in particular with respect to the hydrodynamic tail, is strongly system dependent. In particular the discrepancy in the tail behavior is less severe for high polymer-bead density and for high polymer mass. So an increase in the viscosity of the "solvent" improves the long tail representability in our CG models. This finding reflects the screening of hydrodynamic interactions: In the FG reference systems the collision of colloid beads with polymer beads induces a flow of polymer beads, which can subsequently transfer momentum to other colloid beads. These hydrodynamic interactions are not explicitly encoded in our CG models. At high viscosity these hydrodynamic interactions are dampened and thus less relevant.[228] Both the increase in the polymer beads mass or the increase of the polymer beads number density leads to an effective increase in viscosity. It can thus be assumed that the indirect momentum transfer through hydrodynamic interactions is reduced and the modeling in terms of independent friction and fluctuating forces on the colloid beads is better justified.

We want to stress that the averaged effects of hydrodynamic interactions, which typically lead to an increase in diffusivity through collective motion, is implicitly included in $\tilde{K}(t)$ via $K_X(t)$. The origin of the mismatch in the tail behavior for some systems comes from the fact that the friction and noise is modeled independently for each bead. This potentially reduces the inter-bead correlations, which leads to a change in the temporal fluctuations in the structure. This in turn determines the fluctuations in conservative interactions and on long time scales can lead to errors in the induced contribution to the total effective

memory kernel.

Qualitatively the question if the hydrodynamic tail can be correctly modeled by Eq. 5.5 following our parametrization scheme, boils down to the question if the colloid-colloid momentum transfer is dominated through the conservative interactions or through colloid-colloid hydrodynamic interactions. If the former is the case, the inter-bead correlations should be less dependent on the choice of the form of the thermostat. If the latter is the case, the loss of cross-correlations will be evident in the tail of the VACF.

To validate this intuition we can calculate velocity cross-correlation function $C^X_{VV}(t; R_{cut})$ between pairs of particles as defined by

$$C^X_{VV}(t; R_{cut}) = \langle \boldsymbol{V}_I(0)\boldsymbol{V}_J(t)\rangle_{R_{IJ}(0)<R_{cut}} \,. \tag{5.39}$$

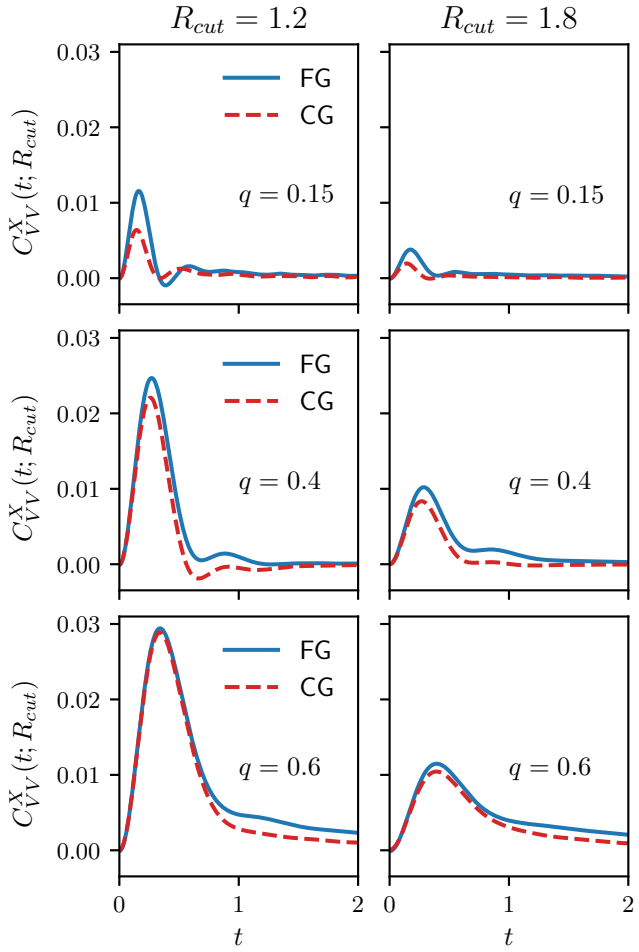

Figure 5.16: Here we plot the the velocity cross-correlation function as defined by Eq. 5.39 for the $q = 0.15$-, $q = 0.4$- and $q = 0.6$-system, respectively for two cut-off values $R_{cut} = 1.2$ and $R_{cut} = 1.8$ for FG reference simulations and CG GLE-thermostat simulations parameterized with $\tilde{K}(t)$.

In Fig. 5.16 we compare $C^x_{VV}(t; R_{cut})$ for $R_{cut} = 1.2$ and $R_{cut} = 1.8$ for all three systems. In the $q = 0.15$-system we find that in the CG model the maximal cross-correlations are approximately half of the reference, while in the $q = 0.4$-system and the $q = 0.6$-system, the CG model captures the cross-correlations significantly better. This is not surprising, as the depth and range of the CG conservative potential in the $q = 0.4$- and $q = 0.6$-system are larger, which allows for an increase in correlations between neighboring

beads due to conservative forces. Thus in the $q = 0.15$ the colloid-colloid momentum transfer through hydrodynamic interactions is more prominent than in the other systems and cannot be fully captured in CG models without explicit hydrodynamic interactions. Thus the modeling errors evident in the VACFs in the $q = 0.15$- and the $q = 0.6$ are of different origin and affect different time scales. In either case the proposed iterative optimization schemes, especially Eq. 5.34, can be applied to correct these residual deviations to match the target correlation functions.

5.6 Conclusion

In this article, we bottom-up derived CG implicit solvent models for different continuous AO models. For the derivation of CG pair-potentials we used the FM-method. We applied an isotropic GLE-thermostat based on the auxiliary variable approach to correctly represent single particle time-correlation functions. The parametrization of the GLE-thermostat to achieve dynamic consistency is based on the splitting of the effective single particle memory kernel into different contributions. We have shown that our scheme generally leads to a good representation of single particle dynamics. By deliberately choosing the parameters in the reference AO models we have shown that an accurate representation of the MB-PMF in terms of the CG potential is crucial in purely bottom-up derived models, as only then the collision and back-scattering dynamics can be accurately captured. We have shown that the application of an isotropic, configuration independent thermostat in many-body simulations can lead to errors in the long tail of VACFs, as such a thermostat does not explicitly consider inter-bead correlations in dissipation and random forces. This implies a lack of inter-bead momentum transfer, which can lead to a reduction in collective motion. Based on inter-bead velocity cross-correlations functions we have have shown that this limitation of isotropic thermostats applies to different extents for different systems, and can be expected to be most crucial when the momentum transfer between the CG DoFs in the FG reference models is dominantly mediated through the removed DoFs. In implicit solvent models, as in the studied systems, this is the momentum transfer mediated by an induced flow in the solvent. More generally one cannot expect to capture all dynamic properties in full detail when using a CG model of the form of Eq. 5.5. This is not unique to dynamic coarse-graining as also in structural coarse-graining e.g. the reliance on non-bonded pair potentials limits the accuracy of CG models and the interpretation of results from CG simulations have always to be assessed carefully. For practical purposes always a balance between feasibility and accuracy has to be found. In particular, in molecular coarse-graining, in which few atomistic degrees of freedom are mapped onto CG beads, and the molecular structure is maintained in the CG representation, a perfect representation of the MB-PMF with simple CG potentials is not possible due to e.g. the representation of non-symmetric molecule segments in term of spherically symmetric interactions. This fact alone poses limitations to the derivation of dynamically consistent coarse-grained models in a purely bottom-up manner. For the case in which single particle time correlation functions need to be reproduced accurately despite of the intrinsic limitations of the target model, we have proposed three different iterative optimization schemes for the parameterization of the optimal memory kernel. We used the integrated effective single-particle memory kernel, which can be readily obtained from a VACF, as the target property, as this memory kernel fully determines other correlation functions and allows the usage of very simple update schemes.

In future it is of interest to investigate how well the CG models of the form studied in this paper can perform for realistic molecular systems. For example the speed-up upon coarse-gaining in mixtures can lead to inconsistent relative diffusivities in different species,[48] which could be accounted for by coupling different CG DoFs to distinctly parameterized GLE-thermostats. Another example where non-Markovian dissipative models might be particularly useful is the study of the dynamics of polymer chains, as anomalous diffusion found in e.g. polymer melts is an intrinsically non-Markovian process,[137] which cannot be fully captured through Markovian models.

SUPPLEMENTARY MATERIAL

See supplementary material for complementary data and discussion on additional systems not discussed in the main text. We also provide short summaries of Mori's projection operator, the BOD-method and the parametrization of the auxiliary variable GLE-thermostat.

Data Availability

The data that supports the findings of this study are available within the article and its supplementary material. Input parameters for simulations, analysis scripts and raw data of the shown figures are available from the corresponding author upon reasonable request.

5.7 Supporting Information

5.7.1 Auxiliary Variable Generalized Langevin Thermostat

A generalized Langevin thermostat can be implemented by explicitly integrating the convolution term for the evaluation of the friction and by constructing correlated noise.[39] Alternatively the non-Markovian GLE can be rendered Markovian in an extended phase space, by introducing auxiliary variables (auxiliary momenta).[33, 92, 151]

The target equation of motion in the main text can be rewritten in terms of the Markovian equation

$$\begin{aligned}\begin{pmatrix} F \\ \dot{\boldsymbol{s}} \end{pmatrix} &= \begin{pmatrix} F^C \\ \mathbf{0} \end{pmatrix} - \boldsymbol{A} \begin{pmatrix} P \\ \boldsymbol{s} \end{pmatrix} + \boldsymbol{B}\boldsymbol{\xi} \\ &= \begin{pmatrix} F^C \\ \mathbf{0} \end{pmatrix} - \begin{pmatrix} 0 & \boldsymbol{A}_{Ps}^T \\ -\boldsymbol{A}_{Ps} & \boldsymbol{A}_{ss} \end{pmatrix} \begin{pmatrix} P \\ \boldsymbol{s} \end{pmatrix} + \begin{pmatrix} 0 & \mathbf{0} \\ \mathbf{0} & \boldsymbol{B}_{ss} \end{pmatrix} \boldsymbol{\xi},\end{aligned} \tag{5.40}$$

where the matrix $\boldsymbol{A}$ defines the coupling of the auxiliary momenta $\boldsymbol{s}$ to the particles momentum, $\boldsymbol{\xi}$ is a Gaussian noise vector, and $\boldsymbol{A}$ and $\boldsymbol{B}$ are related through the fluctuation dissipation theorem

$$\boldsymbol{B}\boldsymbol{B}^T = k_B T(\boldsymbol{A} + \boldsymbol{A}^T) \tag{5.41}$$

This formulation allows to model different functional forms of memory kernels. E.g. for a memory kernel of the form of a dampened oscillator

$$K(t) = \exp\Big(-\frac{a}{2}t\Big)(b\cos(dt) + c\sin(dt)) \tag{5.42}$$

the matrix $\boldsymbol{A}$ takes the form[92]

$$\boldsymbol{A} = \begin{pmatrix} 0 & \sqrt{\frac{b}{2} - \frac{cd}{a}} & \sqrt{\frac{b}{2} + \frac{cd}{a}} \\ -\sqrt{\frac{b}{2} - \frac{cd}{a}} & a & \frac{1}{2}\sqrt{4d^2 + a^2} \\ -\sqrt{\frac{b}{2} + \frac{cd}{a}} & -\frac{1}{2}\sqrt{4d^2 + a^2} & 0 \end{pmatrix}. \tag{5.43}$$

Eq. 5.43 implies, that two auxiliary variables are needed to represent a dampened oscillator memory kernel. For the parametrization of our CG models, we can fit the memory kernel $\tilde{K}(t)$ with N dampened oscillators, i.e.,

$$\tilde{K}(t) \approx \sum_{i=1}^{N} \tilde{K}_i = \sum_{i=1}^{N} \exp\Big(-\frac{a_i}{2}t\Big)(b_i \cos(d_i t) + c_i \sin(d_i t)). \tag{5.44}$$

Thus, $\boldsymbol{A}_{Ps} = (\boldsymbol{A}_{Ps,1}, \boldsymbol{A}_{Ps,2}, ..., \boldsymbol{A}_{Ps,N})$ is a vector of length $2N$ and

$$\boldsymbol{A}_{ss} = \begin{pmatrix} \boldsymbol{A}_{ss,1} & \mathbf{0} & \dots & \mathbf{0} \\ \mathbf{0} & \boldsymbol{A}_{ss,2} & \dots & \mathbf{0} \\ \vdots & \vdots & \ddots & \vdots \\ \mathbf{0} & \mathbf{0} & \dots & \boldsymbol{A}_{ss,N} \end{pmatrix} \tag{5.45}$$

is a skew-symmetric, block diagonal matrix with N blocks of size 2×2.

In practice, for the parametrization of $\boldsymbol{A}$ for CG simulations, we fitted $\tilde{G}(t) = \int_0^t ds \tilde{K}(s)$ rather then $\tilde{K}(t)$. The fitting function then reads

$$\begin{aligned} \tilde{G}(t) \approx \sum_{i=1}^{N} \Bigg(& 2\frac{a_i b_i + 2c_i d_i}{a_i^2 + 4d_i^2} \\ & - \frac{2e^{-\frac{a_i t}{2}} \left((a_i b_i + 2cd)\cos(d_i t) + (a_i c_i - 2b_i d_i)\sin(d_i t) \right)}{a_i^2 + 4d_i^2} \Bigg) \end{aligned} . \tag{5.46}$$

The parameter space is limited by two boundary conditions: the matrix $(\boldsymbol{A} + \boldsymbol{A}^T)$ has to be positive (semi-)definite, such that matrix $\boldsymbol{B}$ can be determined. Furthermore, matrix $\boldsymbol{A}$ has to be real valued. We thus use three different constraints on the parameter space: $a_i > 0$, $\frac{b_i}{2} - \frac{c_i d_i}{a_i} \geq 0$ and $\frac{b_i}{2} + \frac{c_i d_i}{a_i} \geq 0$.

For the studied systems $N \leq 6$ dampened oscillators were sufficient to accurately fit the memory kernels. In practice we applied the curvefit function of the scipy library,[229] and applied the trust region reflective algorithm[230] for the constrained optimization of the parameters.

5.7.2 Overview of All Studied AO-Systems

Here we report the memory kernels and VACFs for FG and CG simulations of all studied AO systems. In Tab. 5.2 we present the parameters for every reference system. In the main text we have mainly discussed the influence of the bead size ratio q and thus of the accuracy of the CG potentials. Through a sparse but broader screening of other parameters as the polymer beads mass m_p, the number of colloid and polymer beads, n_c and n_p, we can qualitatively asses the system dependency of the quality of our GLE-thermostat models.

In Figs. 5.17-5.21 we report the results for systems in which we have $q = 0.15$. As one would expect an increase in the number density of colloids and of polymers increases the overall friction, indicated by the plateau of the integral of the total memory kernel. A sole increase in the density of colloids increases the dominance of $K_C(t)$ over $K_\delta(t)$ while a sole increase in the density of polymer beads has the opposite effect. In any case, the overall form of the VACF is well matched for every system, and only a detailed look at the tail behavior reveals system dependent deviations. In particular we find that an increase of the polymer bead mass leads to a better match of the long-time tail. The same holds true for an increase of the number of polymer beads. In both cases this is due to an overall increase of the viscosity of the "solvent" which dampens hydrodynamic interactions and thus improves the applicability of models which do not explicitly include hydrodynamic interactions.

The main additional insight from the results of Figs. 5.22-5.26 is, that the longer range interactions and reduced number of polymer beads in $q = 0.4$-systems allow for an quite accurate match of the long-time tail in the VACF, while maintaining accurate short-time dynamics.

	q	n_c	n_p	ρ_c	ρ_p	η_c	η_p	m_p
a	0.13	2500	30000	0.91	10.93	0.48	0.013	1
b	0.13	2500	30000	0.91	10.93	0.48	0.013	3
c	0.13	2500	30000	0.91	10.93	0.48	0.013	6
a	0.15	1500	30000	0.55	10.93	0.29	0.019	1
b	0.15	1500	30000	0.55	10.93	0.29	0.019	3
c	0.15	1500	30000	0.55	10.93	0.29	0.019	6
d	0.15	2000	30000	0.73	10.93	0.38	0.019	1
e	0.15	2000	30000	0.73	10.93	0.38	0.019	3
f	0.15	2000	30000	0.73	10.93	0.38	0.019	6
g	**0.15**	**2000**	**60000**	**0.73**	**21.87**	**0.38**	**0.039**	**1**
h	**0.15**	**2000**	**60000**	**0.73**	**21.87**	**0.38**	**0.039**	**3**
i	0.15	2000	60000	0.73	21.87	0.38	0.039	6
d	0.15	2200	60000	0.80	21.87	0.42	0.039	1
e	0.15	2200	60000	0.80	21.87	0.42	0.039	3
f	0.15	2200	60000	0.80	21.87	0.42	0.039	6
g	0.4	2000	10000	0.73	3.64	0.38	0.122	1
h	**0.4**	**2000**	**10000**	**0.73**	**3.64**	**0.38**	**0.122**	**3**
i	0.4	2000	10000	0.73	3.64	0.38	0.122	6
	0.6	**2000**	**1000**	**0.73**	**0.36**	**0.38**	**0.041**	**3**

Table 5.2: Parameters for all studied AO-models. The results for the red systems are reported in Figs. 5.17-5.21. The results for the black systems (except for the $q = 0.6$-system) are reported in Figs. 5.22-5.26. The letter in the very first column denotes the sub-figure in which the results for the system are reported in the respective figures. The systems, the iterative optimization schemes were tested on, are underlined.

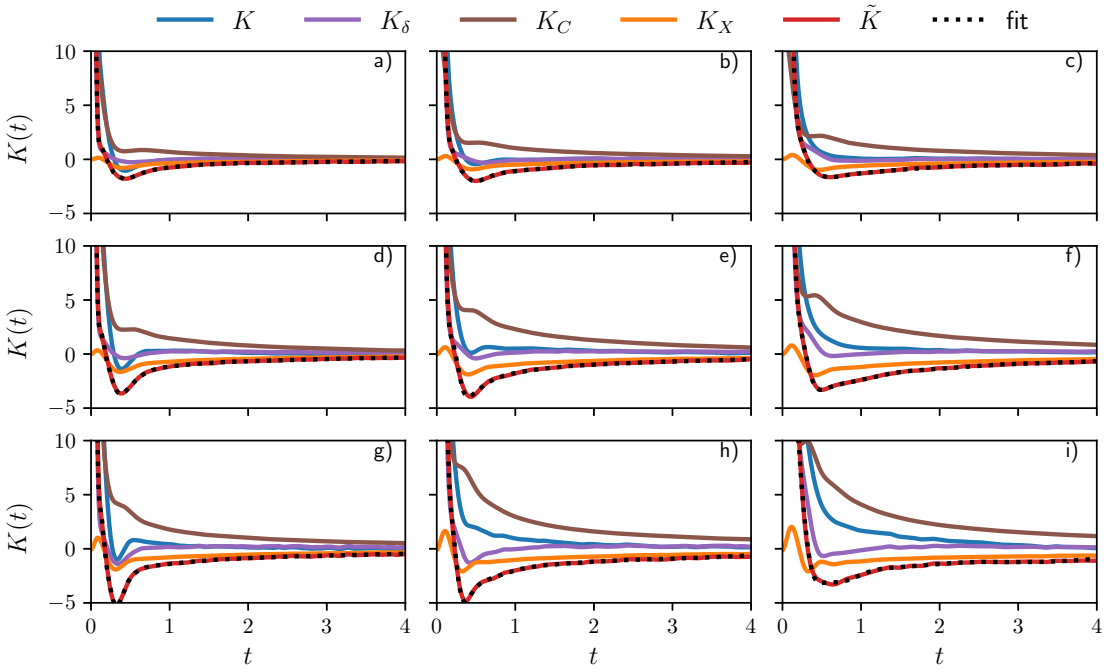

Figure 5.17: Memory kernels and its contributions, obtained via the BOD-method. The respective parameters and the assignment to the respective sub-figure are denoted in red in Tab. 5.2.

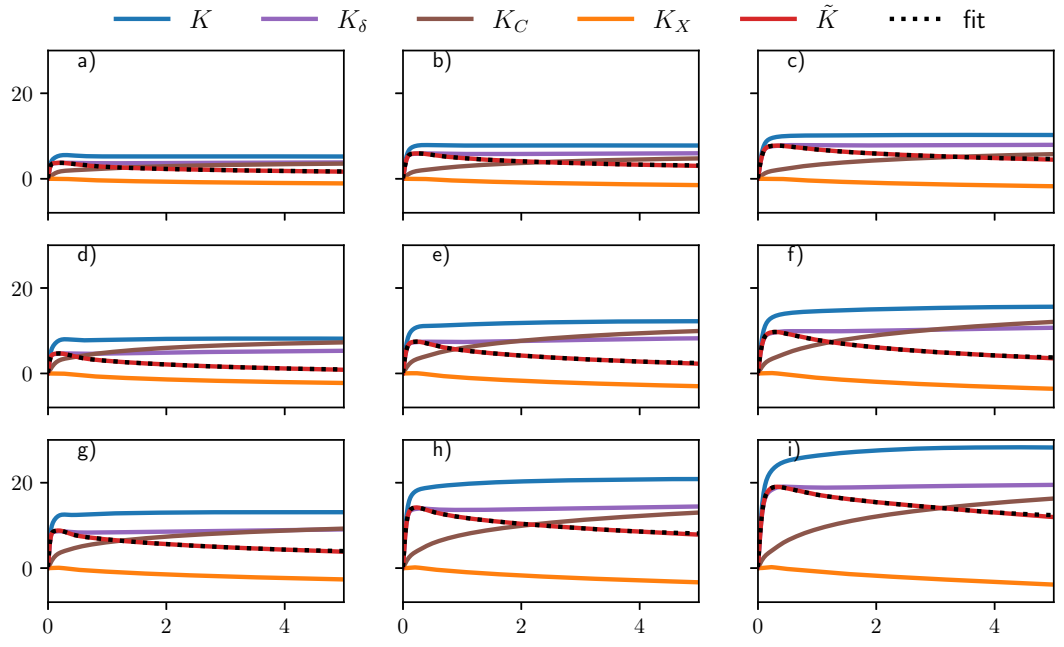

Figure 5.18: Integrated memory kernels and its contributions, obtained via the BOD-method. The respective parameters and the assignment to the respective sub-figure are denoted in red in Tab. 5.2.

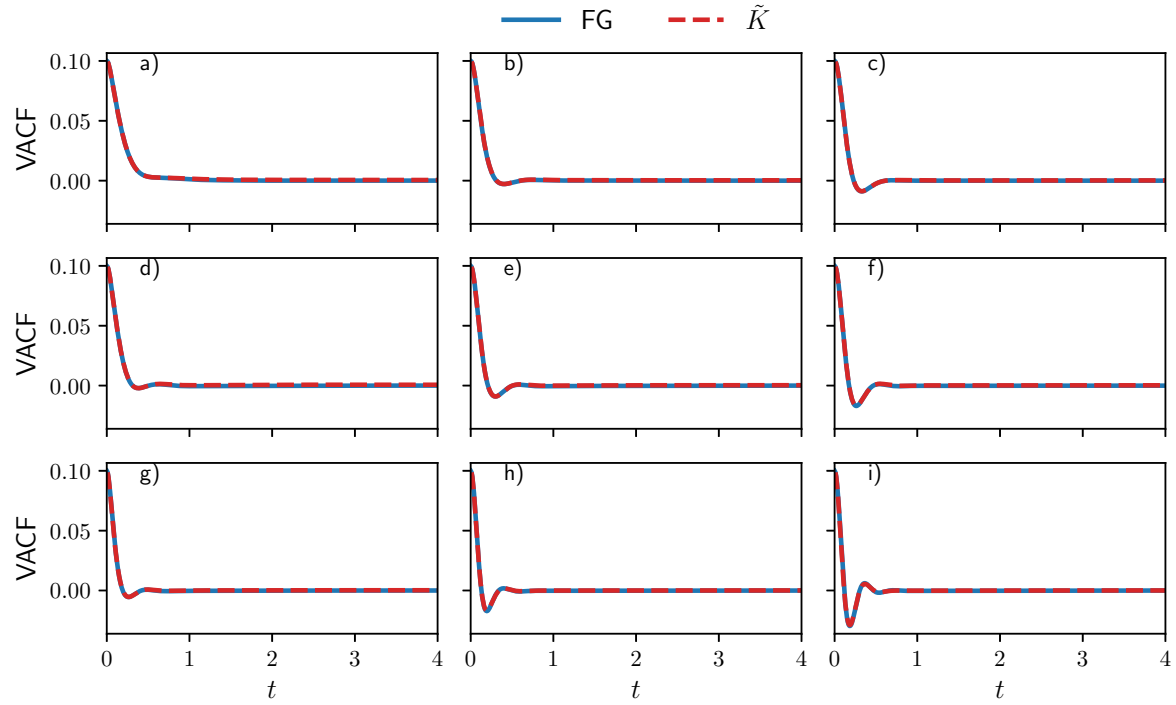

Figure 5.19: VACFs for FG and CG AO models. The respective parameters and the assignment to the respective sub-figure are denoted in red in Tab. 5.2.

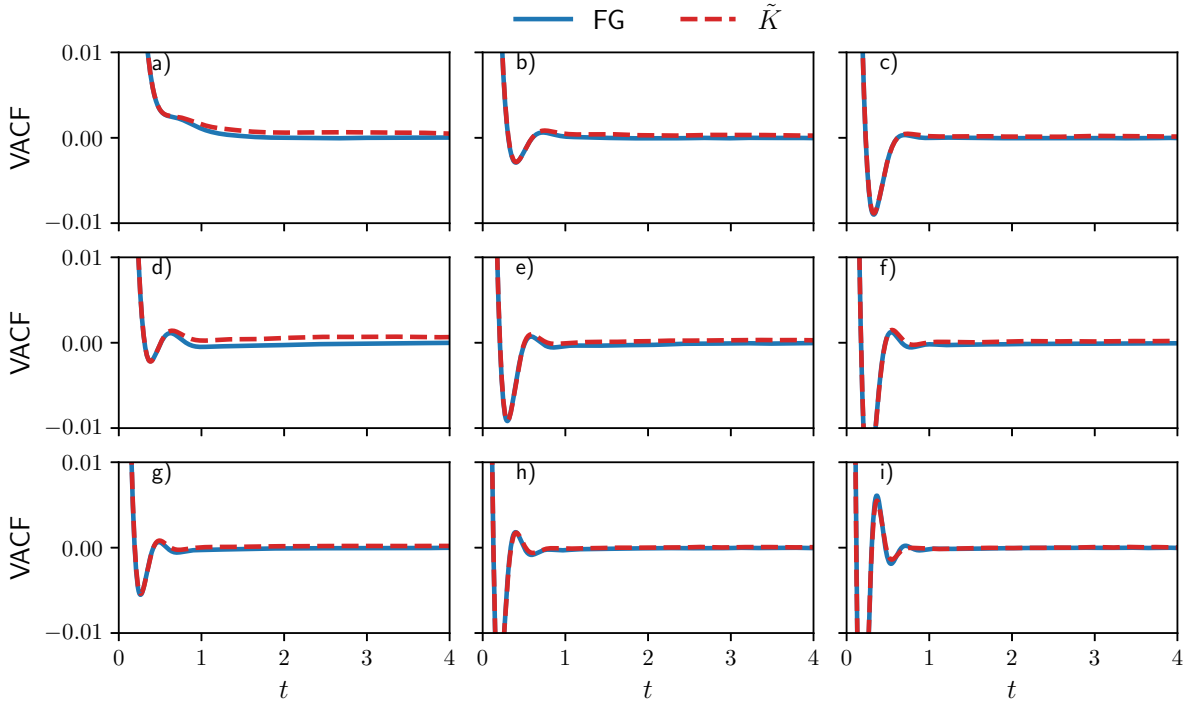

Figure 5.20: VACFs for FG and CG AO models highlighting the tail region. The respective parameters and the assignment to the respective sub-figure are denoted in red in Tab. 5.2.

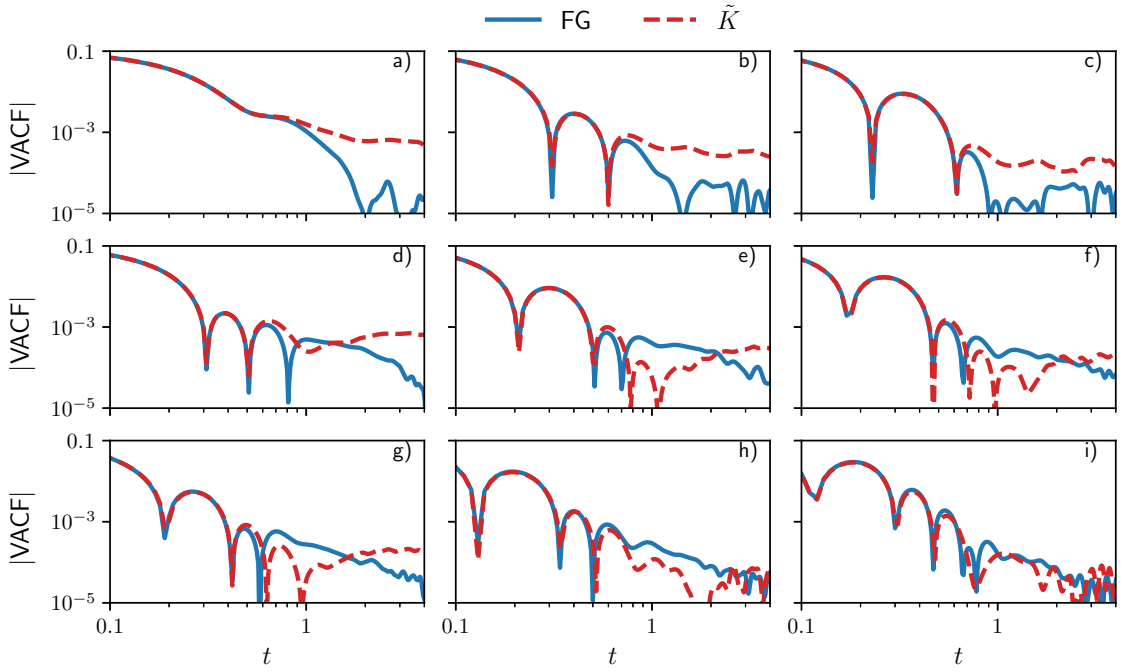

Figure 5.21: Log-log-plot of absolute values of the VACFs for FG and CG AO models. The respective parameters and the assignment to the respective sub-figure are denoted in red in Tab. 5.2.

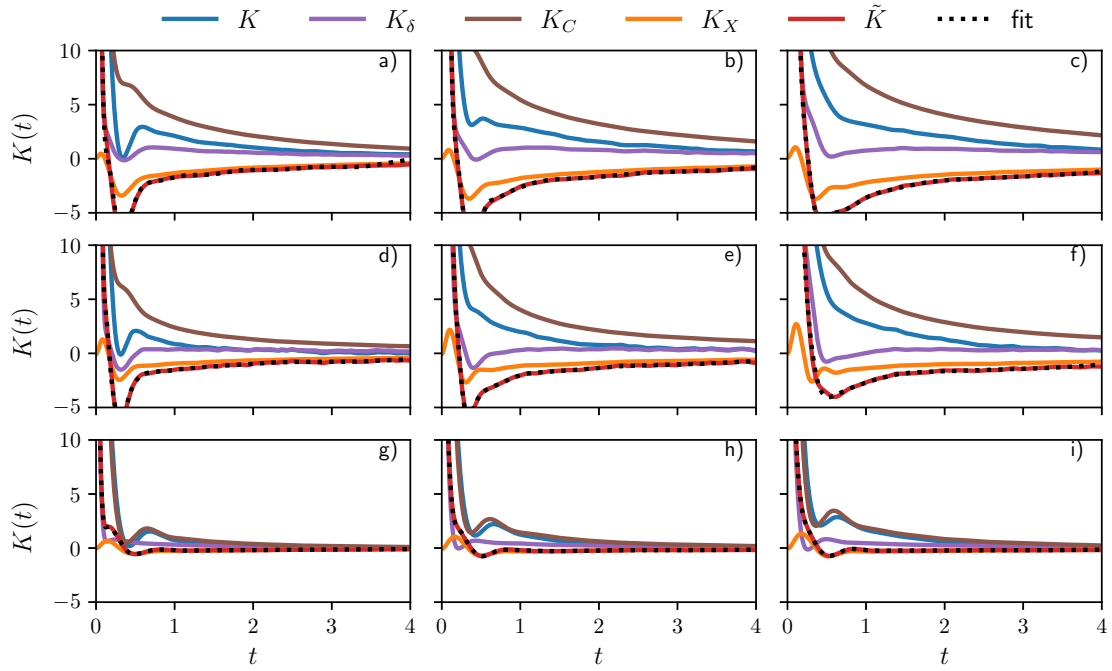

Figure 5.22: Memory kernels and its contributions, obtained via the BOD-method. The respective parameters and the assignment to the respective sub-figure are denoted in black in Tab. 5.2.

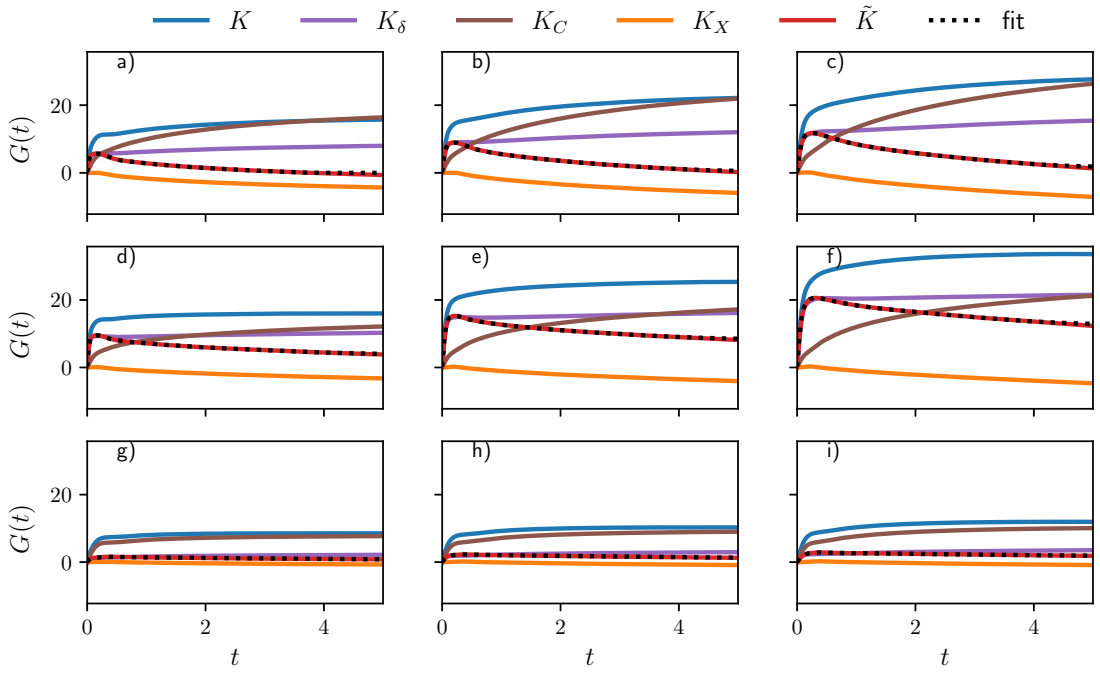

Figure 5.23: Integrated memory kernels and its contributions, obtained via the BOD-method. The respective parameters and the assignment to the respective sub-figure are denoted in black in Tab. 5.2.

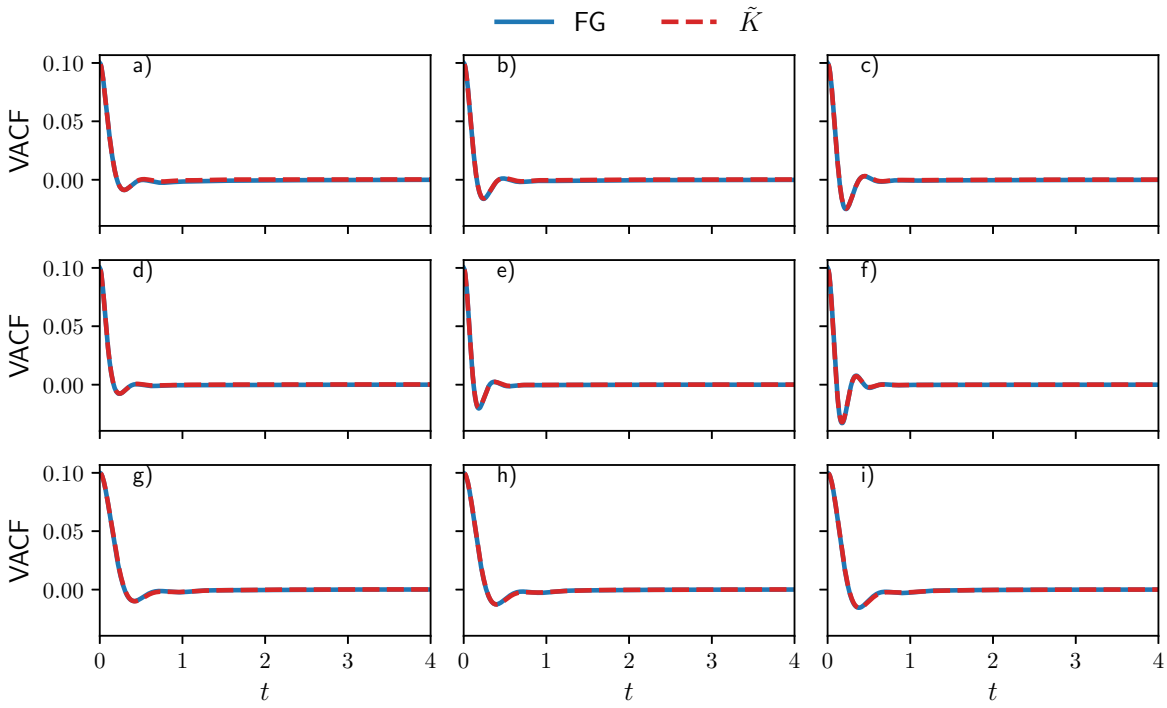

Figure 5.24: VACFs for FG and CG AO models. The respective parameters and the assignment to the respective sub-figure are denoted in black in Tab. 5.2.

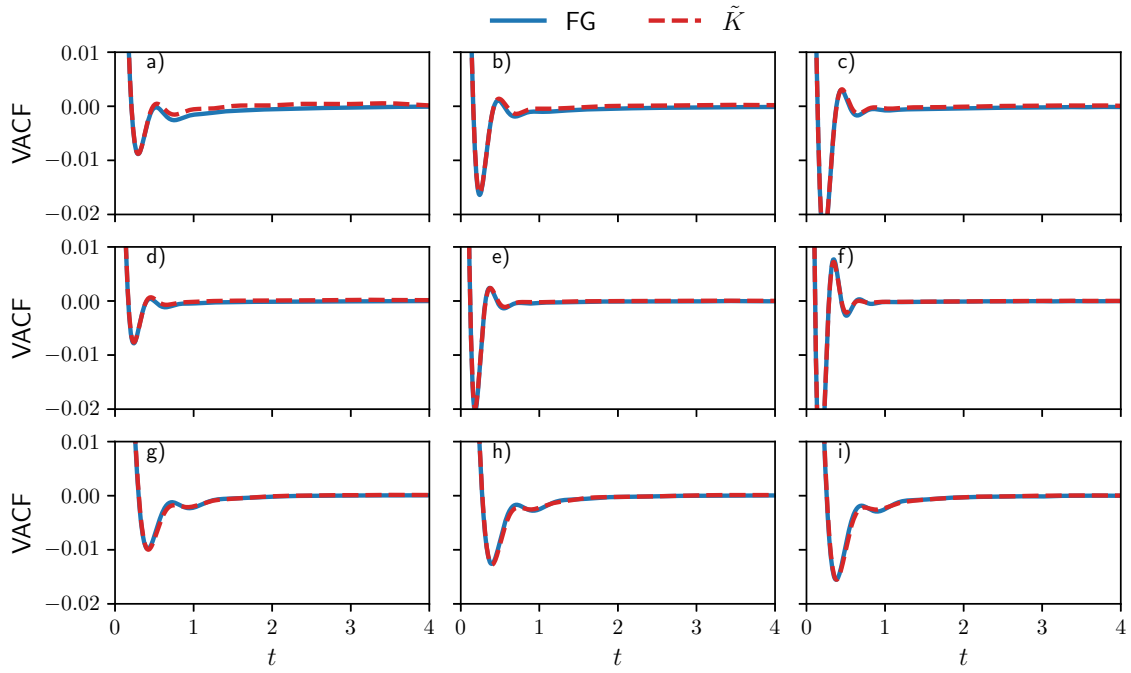

Figure 5.25: VACFs for FG and CG AO models highlighting the tail region. The respective parameters and the assignment to the respective sub-figure are denoted in black in Tab. 5.2.

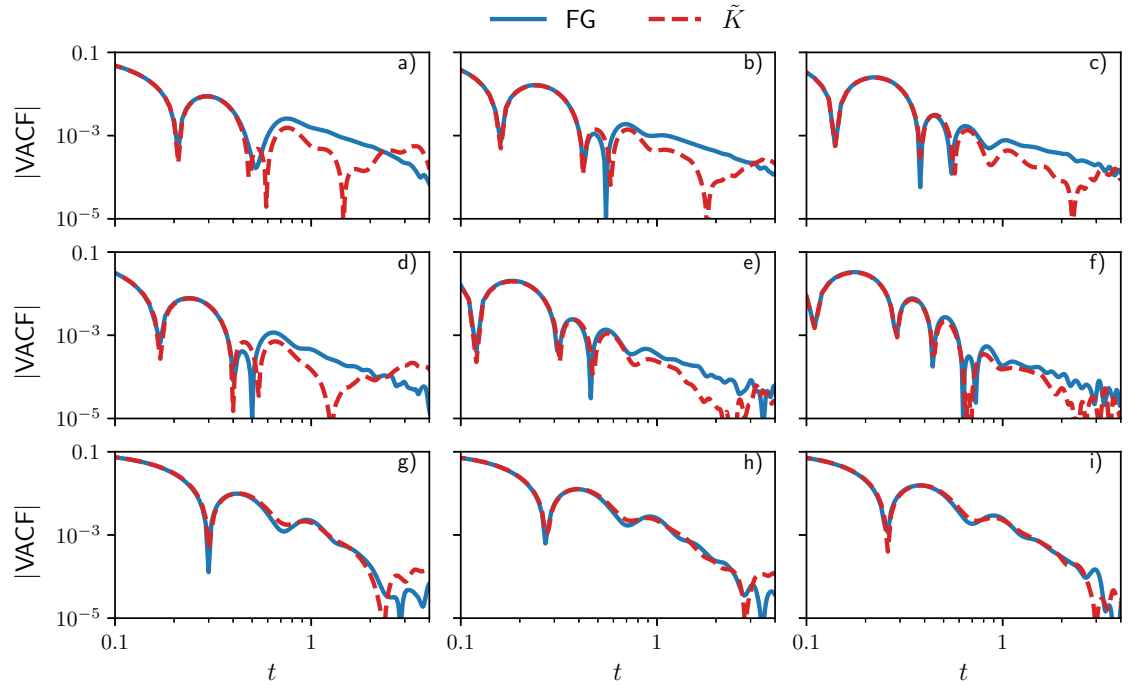

Figure 5.26: Log-log-plot of absolute values of the VACFs for FG and CG AO models. The respective parameters and the assignment to the respective sub-figure are denoted in black in Tab. 5.2.

5.7.3 Iterative Schemes

In the main text we introduced three different update schemes for the iterative optimization of the target model.

$$\tilde{G}_{i+1}(t) = \tilde{G}_i(t) + \left(G^{tgt}(t) - G_i^{CG}(t)\right) \tag{5.47}$$

$$\tilde{G}_{i+1}(t) = \frac{G^{tgt}(t)}{G_i^{CG}(t)}\tilde{G}_i(t) \tag{5.48}$$

$$\tilde{G}_{i+1}(t) = \frac{G^{tgt}(t) - a(t)}{G_i^{CG}(t) - a(t)}\tilde{G}_i(t) \tag{5.49}$$

As target $G^{tgt}(t)$ we used the integrated total memory kernel. To evaluate the optimization process we compared the the integrated memory kernel $G_i^{CG}(t)$, the VACF and the integrated VACF $D(t)$ in any iteration with the target system. We applied the three optimization schemes Eqs. 5.47-5.49 to the two underlined systems in Tab. 5.2 and show all results in Figs. 5.27-5.30. The results for the $q = 0.15$-system are shown in Figs. 5.27-5.28 and the results for the $q = 0.6$-system are shown in Figs. 5.29-5.30. In Fig. 5.27 and Fig. 5.29 we used $\tilde{G}_0(t) \equiv \tilde{G}(t)$ as initial guess while we used the force-correlation function $\tilde{G}_0(t) \equiv \int_0^t dsC_{\delta F \delta F}(s)/(M_I k_B T)$ as initial guess in Fig. 5.28 and Fig. 5.30. In every of these figures we compare the results of all three iterative schemes Eqs. 5.47-5.49, while for the left column we applied Eq. 5.47, for the middle column Eq. 5.48 and for the right column Eq. 5.49.

In Fig. 5.27 we find that all three schemes yield good results within three to five iterations when using $\tilde{G}(t)$ as initial guess, while Eq. 5.47 exhibits some oscillatory behavior, Eq. 5.48 shows the slowest convergence and Eq. 5.49 seems to be both stable and fast. Comparable behavior is found when using the force-correlation function as initial guess.

As indicated in the main text, it can be expected that the performance of three update schemes will differ more strongly if friction due to conservative interactions in the CG simulations is dominant, as it is the case for the $q = 0.6$-model. In Fig. 5.29 we see that that this is indeed the case. Eq. 5.47 and Eq. 5.49 both perform quite well, especially in correcting the minimum of the VACF. The plateau values of $G_i^{CG}(t)$ and $D(t)$ tend to scatter quite strongly for successive iterations for Eq. 5.47, which seems not to be a problem when using Eq. 5.49. Using Eq. 5.48 leads to quite small updates. Interestingly, in Fig. 5.30 we find that Eq. 5.47 and Eq. 5.49 perform comparably well. As the initial guess is further from the ideal solution, the slow convergence of Eq. 5.48 becomes more evident.

In summary, our results show that the update scheme Eq. 5.49 does not show oscillatory behavior while still maintaining very fast convergence. Without a formal mathematical analysis of the stability and convergence properties of the three schemes we can not judge conclusively that any of these schemes is in general superior. But the presented test cases allow to obtain some intuition which might prove to be useful in more complex systems.

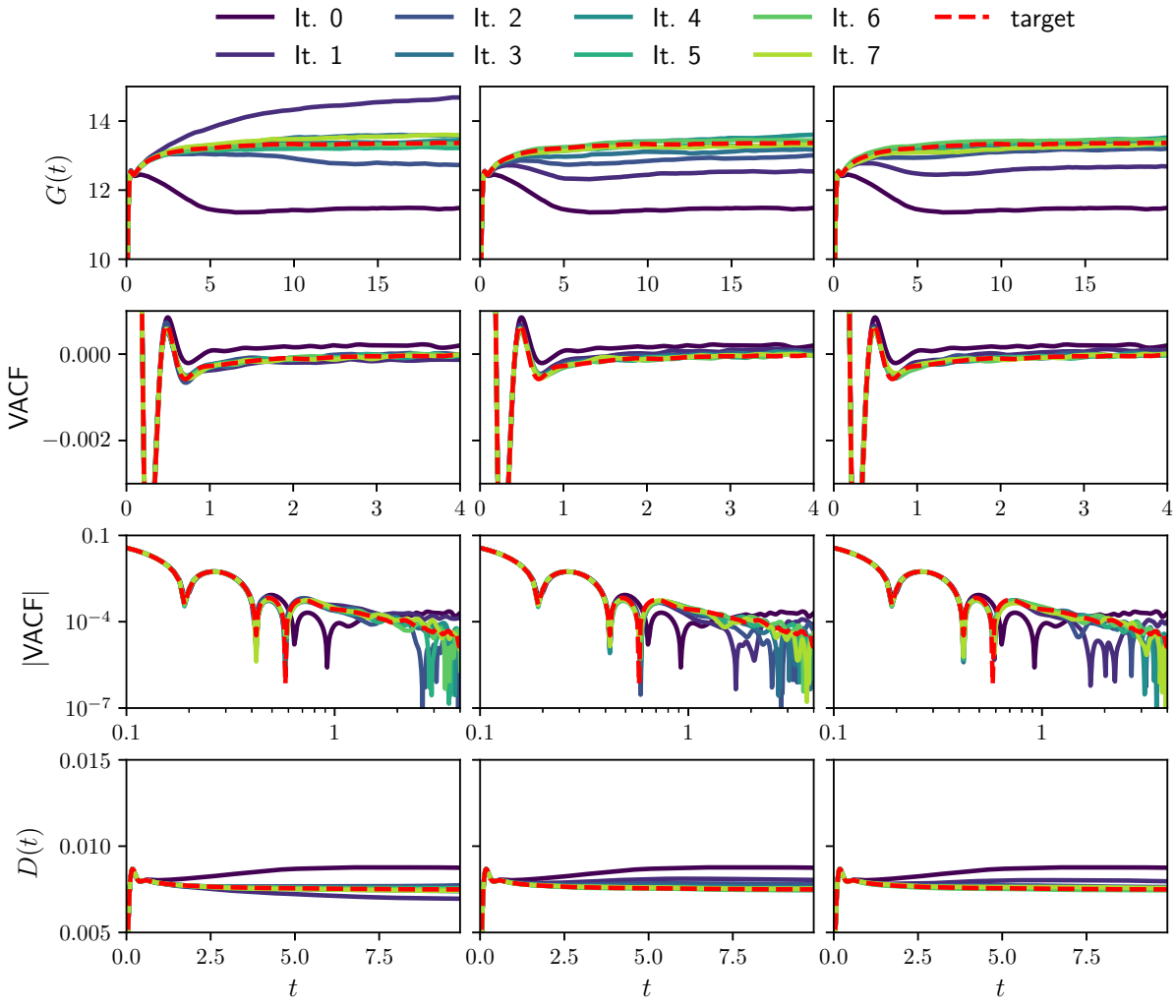

Figure 5.27: Iterative optimization of the CG GLE model for $q = 0.15$, using the update schemes Eqs. 5.47-5.49, with the initial guess $\tilde{G}_0(t) \equiv \tilde{G}(t)$.

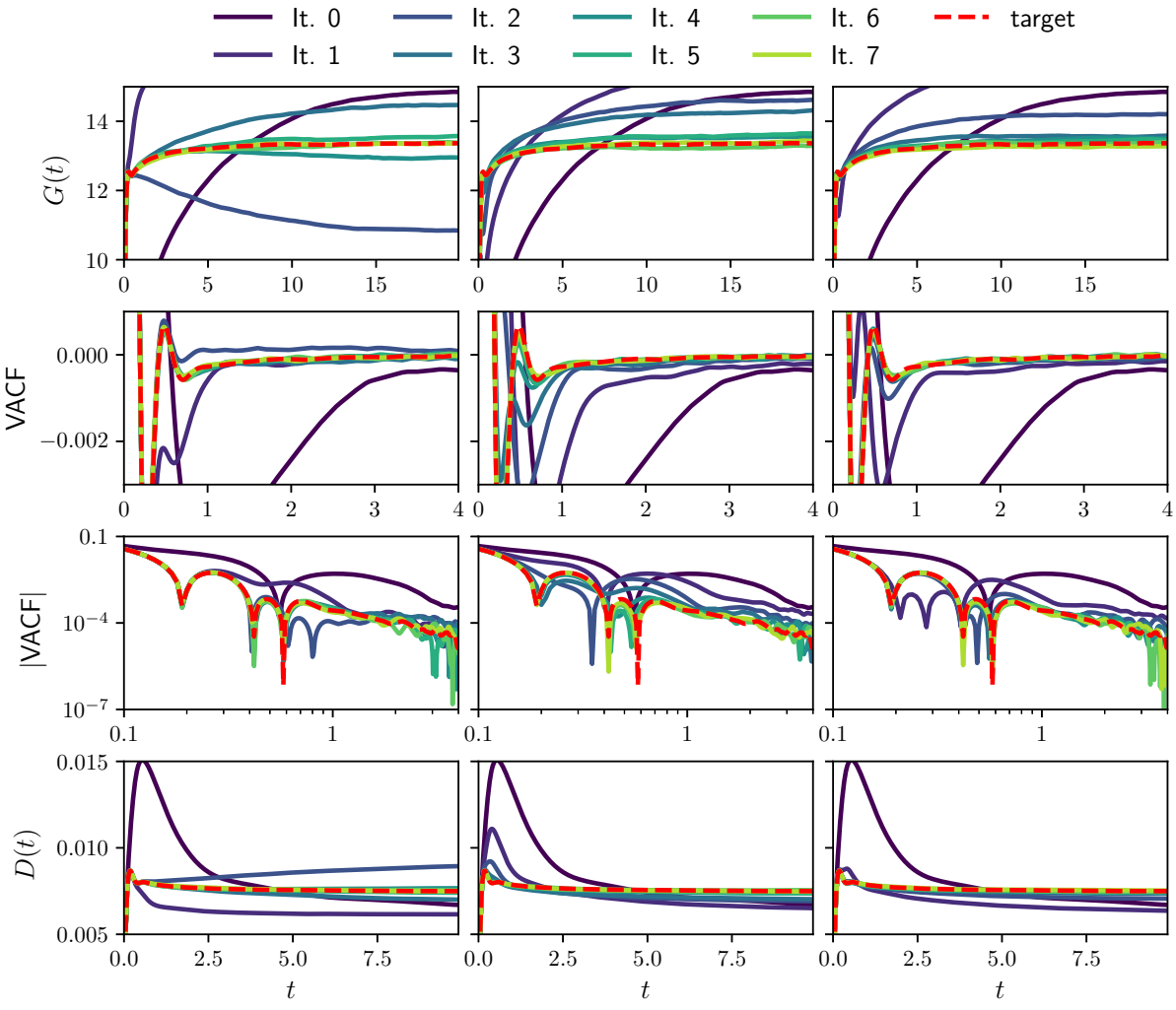

Figure 5.28: Iterative optimization of the CG GLE model for $q = 0.15$, using the update schemes Eqs. 5.47-5.49, with the initial guess $\tilde{G}_0(t) \equiv \int_0^t dsC_{\delta F \delta F}(s)/(M_I k_B T)$.

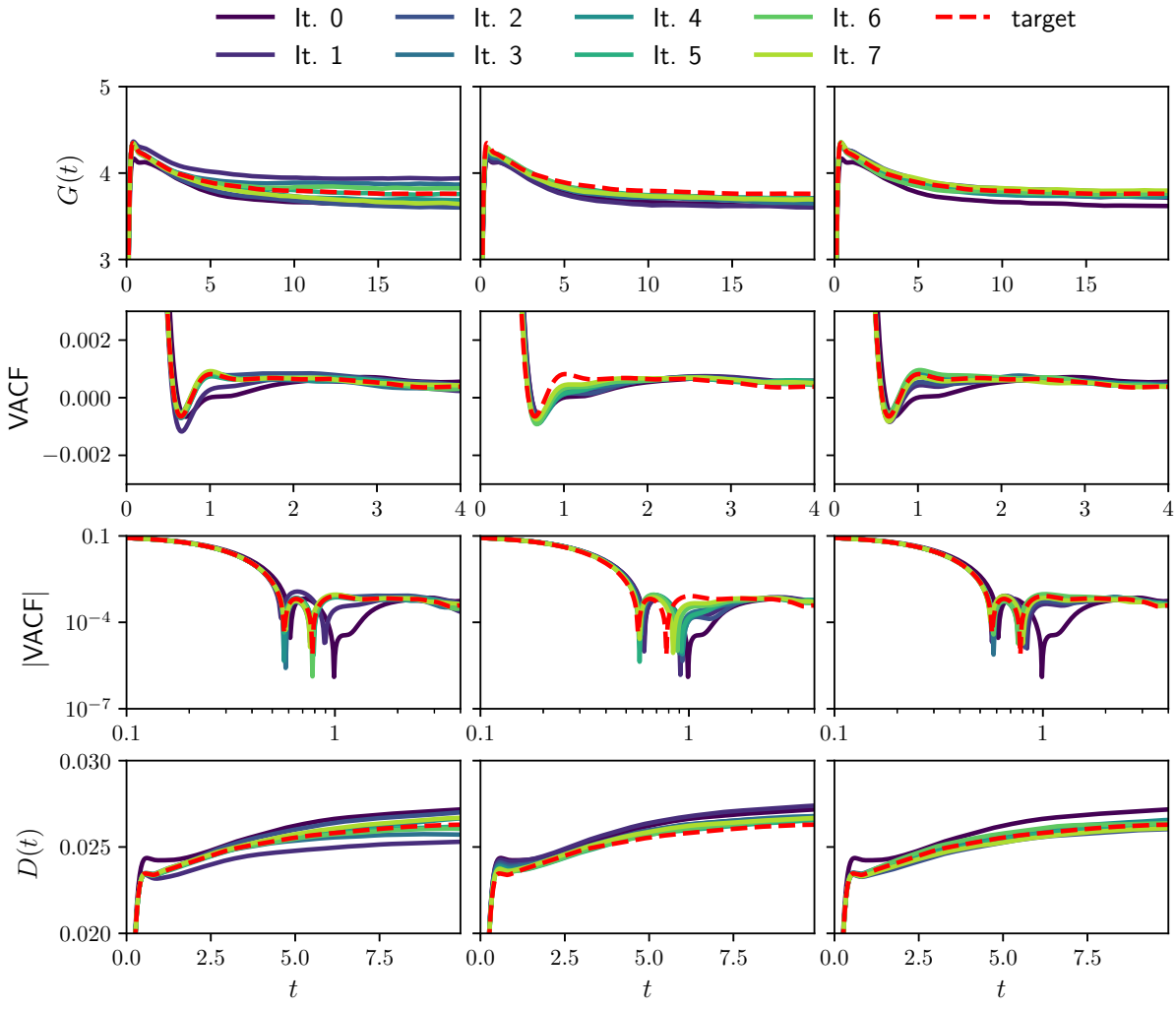

Figure 5.29: Iterative optimization of the CG GLE model for $q = 0.6$, using the update schemes Eqs. 5.47-5.49, with the initial guess $\tilde{G}_0(t) \equiv \tilde{G}(t)$.

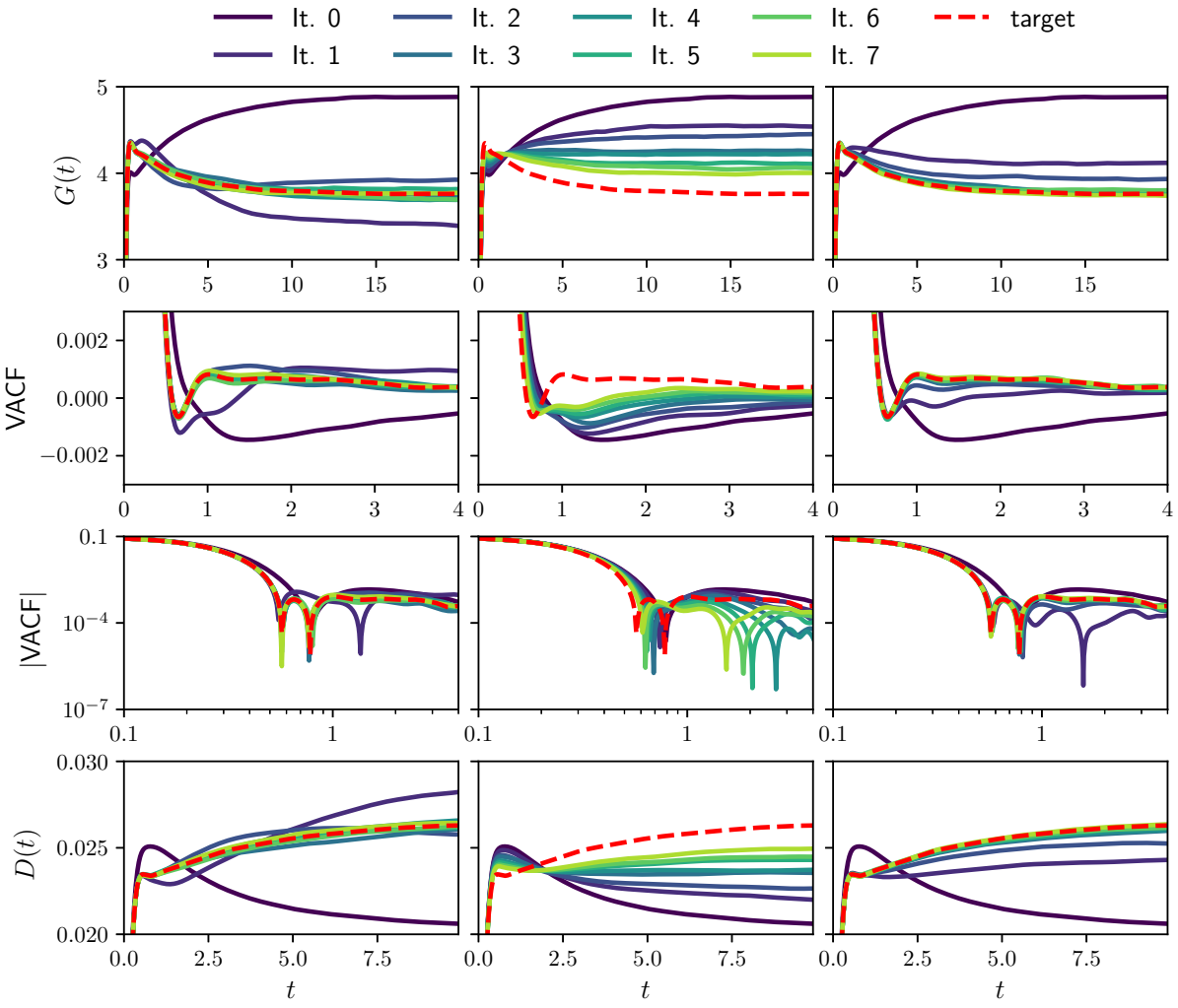

Figure 5.30: Iterative optimization of the CG GLE model for $q = 0.6$, using the update schemes Eqs. 5.47-5.49, with the initial guess $\tilde{G}_0(t) \equiv \int_0^t dsC_{\delta F \delta F}(s)/(M_I k_B T)$.

6 Bottom-Up Informed and Iteratively Optimized Coarse-Grained Non-Markovian Water Models with Accurate Dynamics

Abstract

Molecular dynamics (MD) simulations based on coarse-grained (CG) particle models of molecular liquids generally predict accelerated dynamics and misrepresent the time scales for molecular vibrations and diffusive motions. The parameterization of Generalized Langevin Equation (GLE) thermostats based on the microscopic dynamics of the fine-grained model provides a promising route to address this issue in conjunction with the conservative interactions of the CG model obtained with standard coarse graining methods such as iterative Boltzmann inversion, force matching or relative entropy minimization. We report the application of a recently introduced bottom-up dynamic coarse graining method, based on the Mori-Zwanzig formalism, which provides accurate estimates of isotropic GLE memory kernels for several CG models of liquid water. We demonstrate that with an additional iterative optimization of the memory kernels (IOMK) for the CG water models based on a practical iterative optimization technique, the velocity auto-correlation function of liquid water can be represented very accurately within a few iterations. By considering the distinct Van Hove function, we demonstrate that with the presented methods an accurate representation of structural relaxation can be achieved. We consider several distinct CG potentials to study how the choice of the CG potential affects the performance bottom-up informed and iteratively optimized models.

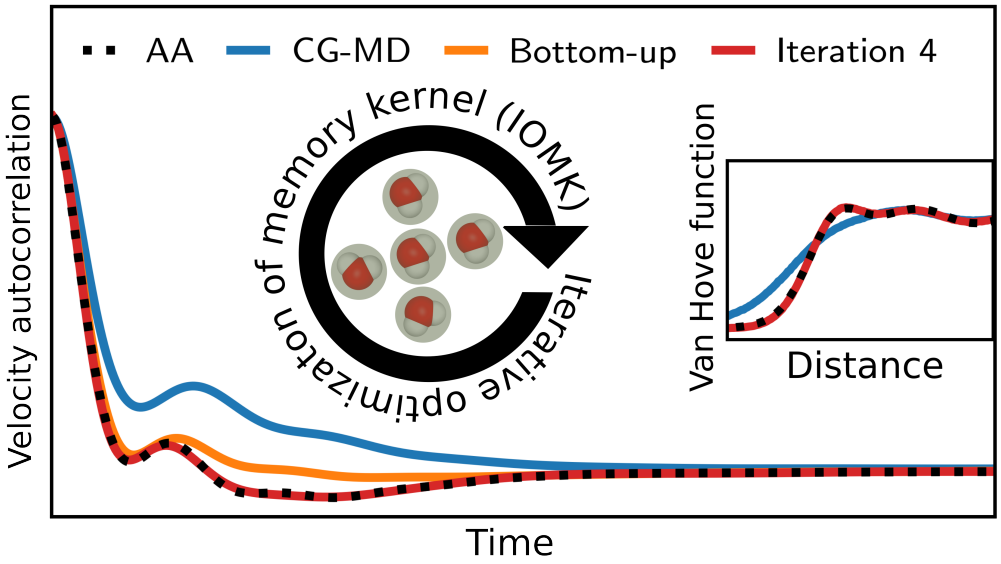

6.1 Introduction

In the field of molecular simulations, methods that involve systematic coarse-graining in space, i.e. structural coarse-graining, are well established.[3–6] The quality of the coarse-grained (CG) models obtained by these methods depends on how well they represent the multibody potential of the mean force (MB-PMF) of the parent fine-grained (FG), often all-atom (AA), model mapped in terms of the CG coordinates/degrees of freedom (DoFs). Over the past two decades, significant progress has been made in the development of representative models for soft matter systems, opening up possibilities for computer simulations at increasingly large length scales and corresponding time scales.

Despite the progress made, molecular dynamics (MD) simulations with CG models generally overestimate the dynamic properties of the systems of interest.[15, 19–21, 201] This occurs because conservative interactions become "softer" upon coarse-graining and (free) energy landscapes become smoother. While this is beneficial for equilibration purposes and studies of stationary structural properties, it often leads to a misrepresentation of the characteristic time scales and the kinetic properties that depend on them.

To overcome this shortcoming, methods for coarse-graining in time have been explored by different groups.[27, 29–34, 36, 57, 60, 64, 65, 158, 196, 231–234] Conceptually, the coarse-graining of a FG model with time reversible dynamics invariably leads to a CG model with time irreversible stochastic dynamics which often includes memory. The corresponding equation of motion (EoM) most commonly takes the form of a non-Markovian generalized Langevin equation (GLE) and is often motivated by the Mori-Zwanzig theory.[23]

While in principle the Mori-Zwanzig theory allows to derive exact CG EoMs for an arbitrary choice of CG DoFs its derivation and exact parameterization in the context of CG MD is often not feasible. Different approximations have to be employed to derive feasible CG models. A common approach is to assume separation of time scales between FG and CG DoFs which allows to render non-Markovian GLEs Markovian. This assumption allows to motivate the parameterization of e.g. Markovian Langevin[36, 196] or dissipative particle dynamics (DPD) thermostats[60, 63–65, 235]. These kind of Markovian dissipative models have been successfully applied to improve the diffusive dynamics in CG models in both generic systems[36, 60, 61] and realistic, chemically specific systems.[63–65, 196, 235] The Markovian approach has the advantage that the CG EoM is comparably inexpensive to evaluate but it cannot represent the dynamics on all time scales if the Markovian approximation is not well justified.

To achieve consistency on all time scales memory effects have to be introduced.[201] In several studies non-Markovian GLEs have been used as target CG EoM. The parameterization strategies used therein were developed and tested on generic models such as star-polymer melts with purely repulsive interactions,[26, 27, 32, 33] or on Lennard-Jones fluids.[29–31]

If the aim is to retain a high degree of detail in the physical description, memory effects can be encoded in configuration dependent memory kernels[26, 27, 29, 30] for example by employing non-Markovian DPD (NM-DPD) models.[26, 27, 29] Both the parameterization and numerical simulation of such models are quite involved and computationally costly. This is particularly unfeasible if the degree of coarse-graining is kept moderate as in the current work.

More feasible, less detailed non-Markovian modeling approaches have been proposed. A noteworthy example, not explicitly based on a GLE, which allows to mimic non-Markovian friction in CG models is the dynamic force matching technique.[158, 234] Herein the friction and memory lost upon coarse-graining is reintroduced in CG models by coupling fictitious Brownian particles to the CG DoFs via a harmonic potential. This strategy has been applied in CG models of liquid methanol and would in principle be applicable to the system studied in the current work. Still, in the original publication a quantitative agreement with the fine-grained reference simulations could not be achieved.[158, 234]

The approach we focus on in the current work is based on parameterizing a non-Markovian, isotropic

and configuration independent *G*LE thermostat in combination with a CG potential obtained with one of the established structural coarse-graining methods.[32–34]

The corresponding EoM reads

$$\boldsymbol{F}_I(t) = \boldsymbol{F}_I^C(t) - \int_0^t ds\tilde{K}(t-s)\boldsymbol{P}_I(s) + \tilde{\boldsymbol{F}}_I^R(t), \tag{6.1}$$

in which $\boldsymbol{F}_I(t)$, $\boldsymbol{F}_I^C(t)$, $\tilde{\boldsymbol{F}}_I^R(t)$ and $\boldsymbol{P}_I(t)$ are the total force, the force due to conservative interactions, the random force and the momentum of a CG particle I. The integral term, involving the memory kernel $\tilde{K}(t)$, represents a non-Markovian, dissipative force. To achieve canonical sampling at a constant temperature the random force and the memory kernel have to fulfill the fluctuation dissipation theorem

$$\left\langle \tilde{\boldsymbol{F}}_I^R(t)\tilde{\boldsymbol{F}}_I^R(0)\right\rangle = 3M_I k_B T\tilde{K}(t), \tag{6.2}$$

in which M_I, k_B and T are the CG bead mass, the Boltzmann constant and the temperature.

This application of Eq. 6.1 allows to introduce memory effects in CG simulations while being computationally cheaper than for example NM-DPD. In several studies, Eq. 6.1 has been used as target CG EoM. The used parameterization strategies were developed and tested on generic models such as star-polymer melts with purely repulsive interactions,[32, 33] or on Lennard-Jones fluids.[31, 34] An exact parameterization of Eq. 6.1 in a purely bottom-up approach is not generally possible and some system dependent deviations from the FG reference have to be expected.[34, 35] We recently demonstrated that these deviations can be kept small with a judicious choice of $\tilde{K}(t)$ (described below) parameterized in combination with a structural CG model which closely represents the FG MB-PMF.[34] In general, but in particular in systems with more complicated directional interactions (e.g. hydrogen bonding), we however expect that this approach leads to larger discrepancies in comparison with the generic models studied so far.

In this paper we, for the first time, apply the dynamic coarse-graining strategies described in Refs. [33] and [34] to a realistic molecular system. As a FG reference we consider the SPC/E water model, using a single-site center-of-mass mapping scheme. The coarse-graining of molecular water is a prominent test case in the development of structural coarse-graining methods.[12, 202, 236–240] Also in dynamic coarse-graining, single-site CG models of water have been considered as test-case for Markovian dissipative models.[232, 235, 241, 242]

The coarse-graining of water is a challenging task as the many-body correlations present in liquid water due to strongly directed hydrogen bonds complicates an accurate description of the MB-PMF based on simple pair potentials,[238] and the implications of the choice of the CG potential on dynamic properties are not a-priori assessable.

We will examine the accuracy of the memory kernel parameterized with the approach described in Ref. [33] and with improvements thereof achieved by iteratively optimizing the memory kernel.[34] Jung *et al.* proposed an iterative optimization scheme for memory kernels with the velocity autocorrelation function (VACF) as target (iterative memory reconstruction from VACF (IMRV)).[30, 39] While in principle applicable to the current task, the IMRV method can suffer from the need for many iterations or instabilities if the step size of the optimization scheme is not well tuned. In Ref. [34], we proposed three novel iterative optimization schemes in which the integrated single-particle memory kernel, $G(t) = \int_0^t dsK(s)$ (see Eq. 6.3 below), was used as a target. In this paper, we apply the most promising of these schemes, which we now refer to as iterative optimization of memory kernels (IOMK). We also compare the performance of this scheme to the IMRV method.

While the VACF is the most prominent measure to assess dynamic consistency in CG models over different time scales, it ultimately is a descriptor for the dynamics of single particles and neglects details on collective behavior. The target model given by Eq. 6.1 introduces independent friction and noise for every

DoF. This approach by construction can only be approximate[34, 35] and thus it is not *a-priori* evident if collective behavior can be correctly modeled.

This is why we also study the distinct Van Hove function (VHF), which is a measure for the relaxation of pair-structure and which is accessible through experiments by e.g. inelastic x-ray scattering experiments.[243–247] Iwashita *et. al.*[243] and Matsumoto *et. al.*[247] concluded that classical MD water models as SPC/E qualitatively reproduce the pair-structure relaxation in space and time quite well. This makes the SPC/E model a good reference target and a CG water model reproducing the VHF of SPC/E water accurately will simultaneously keep a close link to the dynamics of real water.

To further the understanding of the relevance of the choice of the CG potential on the dynamic properties of CG GLE models based on Eq. 6.1, we study four different CG potentials. We consider two two-body potentials derived based on force-matching[193] (FM) and iterative Boltzmann inversion[9] (IBI). We also consider two models which include three-body interactions to more accurately represent the tetrahedral structure of water. These models are based on the Stillinger-Weber (SW) potential.[248] We consider the bottom-up derived SW model based on the relative entropy[197] method (SW-RE)[249] and a bottom-up derived SW model based on the FM method (SW-FM).[238]

6.2 Theoretical Background

6.2.1 Memory Kernels in the Single-Particle Representation

Before we introduce the parameterization schemes for the memory kernel in Eq. 6.1 it is instructive to first consider an (numerically) exactly solvable case. The Mori-Zwanzig theory, by applying a linear projection operator, allows to derive an exact CG EoM for a single freely diffusing particle from Hamiltonian dynamics which takes the form of the following GLE:[23, 25, 201]

$$\boldsymbol{F}_I(t) = -\int_0^t dsK(t-s)\boldsymbol{P}_I(s) + \boldsymbol{F}_I^{\mathcal{Q}}(t) \tag{6.3}$$

In Eq. 6.3, $K(t) = \left\langle \boldsymbol{F}_I^{\mathcal{Q}}(t)\boldsymbol{F}_I^{\mathcal{Q}}(0)\right\rangle / 3M_I k_B T$ denotes the single-particle memory kernel describing the dynamics of a CG DoF from an all-atom (AA) reference. The $\mathcal{Q}$-projected force $\boldsymbol{F}_I^{\mathcal{Q}}(t)$ has an exact relation to the microscopic dynamics. We will not reiterate the derivation and refer the interested reader to the well established literature on that topic.[23–25]

For our purpose, the relevant property of the $\mathcal{Q}$-projected forces is its orthogonality (its statistical independence) to the relevant CG DoF, which is the momentum $\boldsymbol{P}_I(0)$ of a particle I, which can be expressed as

$$\left\langle \boldsymbol{F}_I^{\mathcal{Q}}(t)\boldsymbol{P}_I(0)\right\rangle = 0. \tag{6.4}$$

This allows to derive relations between the memory kernel $K(t)$, which is related to the orthogonal dynamics, and readily accessible time-correlation functions, which can be expressed in a Volterra equation of the form

$$C_{FV}(t) = -\int_0^t dsM_I K(t-s)C_{VV}(s), \tag{6.5}$$

where we defined the VACF $C_{VV}(t) = \langle \boldsymbol{V}_I(t)\boldsymbol{V}_I(0)\rangle /3$ and the force-velocity auto-correlation function $C_{FV}(t) = \langle \boldsymbol{F}_I(t)\boldsymbol{V}_I(0)\rangle /3$.

Eq. 6.5 establishes the connection between the single-particle memory kernel $K(t)$ and all single-particle time-correlation functions. For example, $K(t)$ is related to the long time diffusion coefficient D via

$$D = \frac{k_B T}{M_I \gamma} \tag{6.6}$$

where

$$\gamma = \lim_{t\to\infty} G(t) \tag{6.7}$$

with $G(t) = \int_0^t ds K(s)$. The integrated memory kernel $G(t)$ can also be uniquely related to the VACF, by integration of Eq. 6.5, which yields

$$C_{VV}(t) - C_{VV}(0) = -\int_0^t ds G(t-s) C_{VV}(s). \tag{6.8}$$

Eq. 6.8 can be numerically inverted[95] to determine $G(t)$ directly from a measured VACF.

6.2.2 Memory and Friction due to Conservative Interactions in Many-Body Coarse-Grained Simulations

In the previous section we have discussed how the single-particle memory kernel can be evaluated from Hamiltonian reference simulations. In CG GLE models following Eq. 6.1 the total memory and friction exerted on some tagged particle I consists of the memory explicitly introduced through the GLE-thermostat ($\tilde{K}(t)$) and an additional contribution due to the effective particle-particle interaction as implicitly introduced due to the conservative interactions $\boldsymbol{F}_I^C(t)$. The memory kernel due to conservative interactions ($\Delta K^{CG}(t)$) can be evaluated from CG simulations through a relation analogous to Eq. 6.8, which reads[34]

$$C^{CG}_{F^C V}(t) = -\int_0^t ds M_I \Delta K^{CG}(t-s) C^{CG}_{VV}(s). \tag{6.9}$$

Here we define the conservative force-velocity correlation function $C^{CG}_{F^C V} = \left\langle \boldsymbol{F}_I^C(t) \boldsymbol{V}_I(0) \right\rangle / 3$. We use the superscript CG to denote correlation functions from CG simulations. The explicit evaluation of $\Delta K^{CG}(t)$ from Eq. 6.9 is not needed in the application of the proposed CG schemes, but it allows to numerically test the validity of certain assumptions made in the following sections.

6.2.3 Parameterizing Generalized Langevin Thermostats from $\mathcal{Q}$-Projected Correlation Functions

In our previous work,[33, 34] we used the backward orthogonal dynamics (BOD) method proposed by Carof *et al.*[85] to compute the memory kernel in Eq. 6.1 from $\mathcal{Q}$-projected force-force time correlation functions. As discussed in Ref. [33], this approach should yield the best results when the conservative CG potential (which gives rise to $\boldsymbol{F}_I^C(t)$ in Eq. 6.1) accurately represents the MB-PMF, even though the target EoM Eq. 6.1 by itself comes with limitations.[34, 35] The idea behind the parameterization scheme is the following: in Eq. 6.1 the overall dynamics of particle I is governed by two contributions, the friction and memory induced by the interaction with other particles encoded in $\boldsymbol{F}_I^C(t)$ and the friction and memory explicitly included through $\tilde{K}(t)$. The dynamics of a diffusive DoF in CG simulations can always be mapped onto a simple single-particle GLE of the form

$$\boldsymbol{F}_I(t) = -\int_0^t ds K^{CG}(t-s) \boldsymbol{P}_I(s) + \boldsymbol{F}_I^R(t), \tag{6.10}$$

where with $K^{CG}(t)$ we denote the effective single-particle memory kernel of a particle following the CG EoM Eq. 6.1. In $K^{CG}(t)$, both $\tilde{K}(t)$ and the additional contribution through $\boldsymbol{F}_I^C(t)$ are included, which we denote as $\Delta K^{CG}(t)$, so we can write

$$K^{CG}(t) = \tilde{K}(t) + \Delta K^{CG}(t). \tag{6.11}$$

The relevant conclusion from this discussion is that the many-body EoM given by Eq. 6.1 will yield the same single-particle time correlation functions, as for example the VACF, if, and only if, the effective single-particle memory kernel from the CG simulation ($K^{CG}(t)$) and the single-particle memory kernel from the AA reference ($K(t)$) coincide. To be able to optimally parameterize $\tilde{K}(t)$ in a purely bottom-up way, a good *a-priori* estimate of $\Delta K^{CG}(t)$ is needed. Here we employ a strategy often used in bottom-up dynamic coarse-graining.[26, 28, 29, 31, 33, 34, 36, 61, 63, 65, 196] That is, we first derive CG conservative interactions determining $\boldsymbol{F}_I^C(t)$ and governing the equilibrium structure in CG simulations, and split the total forces $\boldsymbol{F}_I(t)$ in a mapped AA reference simulation into the CG conservative force $\boldsymbol{F}_I^C(t)$ and a residual force $\delta\boldsymbol{F}_I(t)$, such that

$$\boldsymbol{F}_I(t) = \boldsymbol{F}_I^C(t) + \delta\boldsymbol{F}_I(t). \tag{6.12}$$

The BOD method allows to directly evaluate $K(t)$ based on a mapped rerun of a AA-simulation, but also to split the memory kernel into different contributions. Based on the splitting of forces in Eq. 6.12, the memory kernel can then be separated according to

$$K(t) = K_C(t) + K_\delta(t) + 2K_X(t), \tag{6.13}$$

in which the three kernels on the right-hand side are defined as $K_C(t) = \alpha \left\langle \boldsymbol{F}_I^{C,\mathcal{Q}}(t)\boldsymbol{F}_I^{C,\mathcal{Q}}(0)\right\rangle$, $K_\delta(t) = \alpha \left\langle \delta\boldsymbol{F}_I^{\mathcal{Q}}(t)\delta\boldsymbol{F}_I^{\mathcal{Q}}(0)\right\rangle$ and $K_X(t) = \alpha \left\langle \boldsymbol{F}_I^{C,\mathcal{Q}}(t)\delta\boldsymbol{F}_I^{\mathcal{Q}}(0)\right\rangle$ with $\alpha = (3M_I k_B T)^{-1}$.

In the AA reference, $K_C(t)$ is related to the conservative forces, which suggests the approximate relation

$$\Delta K^{CG}(t) \approx K_C(t), \tag{6.14}$$

implying

$$\tilde{K}(t) \equiv K_\delta(t) + 2K_X(t) \tag{6.15}$$

as an optimal *a-priori* choice for the parameterization of Eq. 6.1. As this procedure relies on the analysis of mapped AA trajectories, the implicit assumption of course is that the CG model samples the same configurations as the mapped reference model, as the fluctuations of $\boldsymbol{F}_I^C(t)$ are both related to $K_C(t)$ and $\Delta K^{CG}(t)$. A sampling of different configurations in the CG model and the mapped AA reference will introduce errors. To some extent this is a limitation which applies to all bottom-up derived dynamic CG models.

6.2.4 Iterative Optimization of Memory Kernels (IOMK)

It is generally a non-trivial task to parameterize Eq. 6.1 such that the VACF is reproduced on all timescales. Different iterative optimization schemes to achieve an accurate representation of the VACF have been proposed in literature.[30, 32, 39] We recently proposed three optimization schemes, which use the integrated effective single-particle memory kernel $G^{tgt}(t) = G(t) = \int_0^t dsK(s)$ as target function.[34] $G^{tgt}(t)$ can be easily obtained from the VACF (Eq. 6.8) of the mapped AA reference simulation and accordingly $G_i^{CG}(t)$ for every iteration can be derived from the VACF of the i-th iteration. Considering

that the effective integrated memory kernel for any iteration ($G_i^{CG}(t)$) is composed of the contribution from the GLE thermostat ($\tilde{G}_i(t)$) and some residual friction due to the conservative interactions ($\Delta G_i^{CG}(t)$) suggests to account for any deviations from the target by a corresponding change in $\tilde{G}_i(t)$.[34] While this ansatz is applicable in principle,[34] it assumes that $\Delta G_i^{CG}(t)$ is independent of the parameterization of the GLE thermostat. This in generally not the case, as the thermostat affects the relaxation of CG particle configurations and thus indirectly the relaxation of the conservative interactions, which can lead to oscillatory behavior or slow convergence in naive approaches for optimizing the memory kernel.[34] This is why we proposed a more promising iterative optimization scheme[34] which previously has shown to be both quite stable and fastly converging.[34] For the justification of this scheme (to which we will now refer to as iterative optimization of memory kernels (IOMK)), the dependence of $\Delta G^{CG}(t)$ on the parameterization of the thermostat has to be established. We will demonstrate by a numerical experiment that the linear relation

$$\Delta G_i^{CG}(t) \approx a(t) + b(t)\tilde{G}_i(t) \tag{6.16}$$

is a reasonable ansatz. Note that in Eq. 6.16 the parameters $a(t)$ and $b(t)$ are functions of time. In this approximation, $a(t)$ is given by the integrated memory kernel from standard CG-MD simulation and has to be predetermined. From Eq. 6.16, the following update scheme can be derived:[34]

$$\tilde{G}_{i+1}(t) = \frac{G^{tgt}(t) - a(t)}{G_i^{CG}(t) - a(t)}\tilde{G}_i(t). \tag{6.17}$$

Eq. 6.17 can be understood as a quasi-Newton method using an approximate Jacobian. We provide a derivation and analysis of Eq. 6.17 in terms of a quasi-Newton method in the SI. If Eq. 6.16 were exact, the IOMK method would be an exact Newton method applied to a linear problem and thus converge within a single step, even when a significant fraction of the total friction is due to conservative interactions. The interplay of the thermostat parameterization and the friction due to conservative interactions might in general be more complex in more complicated systems and is also complicated through the application to non-Markovian thermostats. This makes it crucial to evaluate the applicability of the IOMK method to different systems and in particular to compare it to other proposed methods.

This is why we also study an alternative approach, proposed by Jung *et al.*,[39] and called IMRV, which is analogous to the IBI method in structural coarse-graining, and utilizes the VACF directly as target property. The IMRV method was originally proposed for the reconstruction of single-particle memory kernels,[39] instead for the parameterization of multi-particle models. In a later study, Jung *et al.* observed that the original IMRV method tends to be unstable for multi-particle models with conservative pair potentials[30] and proposed an improved version. In the following, we will refer to the original version as IMRV-1 and to the improved version as IMRV-2. Technical details on the IMRV method are described in the section on computational details. From a practical point of view, the main difference between the IOMK method and the IMRV methods is that the IMRV methods rely on hyperparameters to stabilize the optimization procedure and for which the optimal values are not a-priori known. To achieve good results, these parameters have to be manually predetermined. In the IOMK method, $a(t)$ has to be predetermined, but as $a(t)$ has a clear physical interpretation, it can be unambiguously fixed from a single cheap CG simulation by utilizing Eq. 6.8.

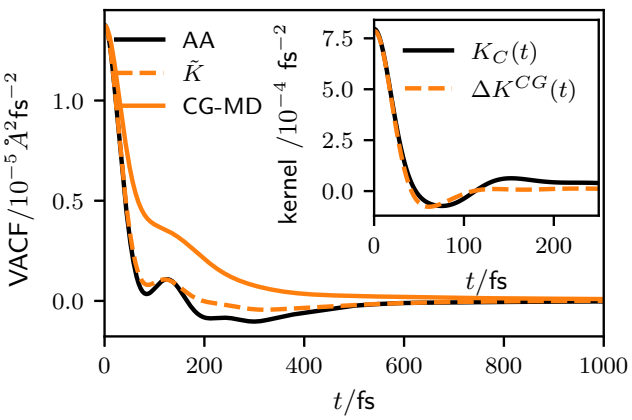

Figure 6.1: VACFs of the IBI water model, parameterized with $\tilde{K}(t)$ (Eq. 6.15) calculated based on the BOD method, compared to the AA reference. For comparison we also show the result of non-dissipative CG-MD simulations. Inset: The memory kernel contribution $K_C(t)$ from the reference simulation compared to the memory due to conservative interactions ($\Delta K^{CG}(t)$) in CG GLE simulations parameterized with $\tilde{K}(t)$.

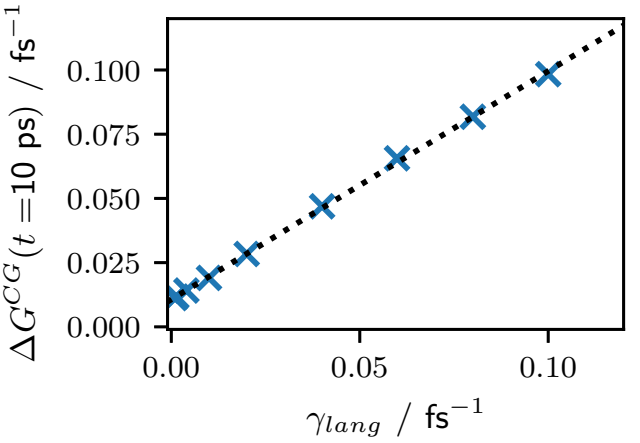

Figure 6.2: Friction introduced by conservative interactions in NVT simulations using a Langevin-thermostat, as a function of the applied friction coefficient. The shown data is based on simulations of the IBI model. A almost perfect linear dependence is found, which is emphasized by the linear fit, shown as black dotted line.

6.3 Results and Discussion

6.3.1 Dynamics of the Bottom-Up Parameterized IBI Model

To test the capability of the bottom-up scheme based on the BOD method, we start by considering the IBI water model. Fig. 6.1 shows the VACF of the CG GLE thermostat simulations, parameterized with $\tilde{K}(t)$ (Eq. 6.15), in comparison to the reference AA and the standard CG-MD simulations. As one would expect, the CG-MD VACF decays much slower than the AA VACF, indicating the expected increased diffusivity. Applying a GLE thermostat with $\tilde{K}(t)$ leads to a considerable improvement in the representation of the VACF. In particular, the initial decay is perfectly matched. Also the first local minimum and maximum is qualitatively well represented. The AA VACF exhibits a broad local well, between $\approx$ 200 fs and 300 fs. This region cannot be fully captured by the GLE model. Overall this leads to a residual overestimation of the diffusivity in the GLE model.

The main assumption of the applied parameterization scheme lies in Eq. 6.14. In the inset of Fig. 6.1 we show that $K_C(t)$ from the reference model and $\Delta K^{CG}(t)$ from the CG GLE simulation indeed coincide very well on short time scales, but $K_C(t)$ exhibits a long positive tail, which is not captured by $\Delta K^{CG}(t)$. This explains the residual deviations in the VACF on longer time scales. If Eq. 6.14 would strictly hold, the target VACF would trivially match exactly. Still, combined with the results of earlier studies,[33, 34] the overall well match between $K_C(t)$ and $\Delta K^{CG}(t)$ underscores the general soundness of the applied approach, at least as an *a-priori* approximation.

The origin of the residual deviations can generally be two-fold: Firstly, at $t = 0$ both $K_C(t)$ and $\Delta K^{CG}(t)$ are proportional to the variance of the CG conservative forces acting upon a CG DoF. This

variance is determined by the CG potential and the sampled configurations. As the same CG potential in determining $K_C(t)$ and $\Delta K^{CG}(t)$ is used, deviations at $t = 0$ can only arise due to deviations in the static structure between AA and CG model. Secondly, on long time scales the EoM given by Eq. 6.1 poses inherent limitations, as the noise and friction on any CG DoF is modeled independently. In *reality*, the CG DoFs exchange momentum via the neglected DoFs, which cannot be captured in terms of Eq. 6.1. This in turn can affect the structural relaxation, which respectively induces deviations in $\Delta K^{CG}(t)$. Any deviation at times $t > 0$ cannot be exactly assigned to one of the two mechanisms, except for well controlled model systems.[34]

Still, despite these limitations, we find that this approach yields good results in conjunction with the IBI potential, without additional optimization of the parameterization.

6.3.2 Dynamics of the Iteratively Optimized IBI Model

Residual deviations of CG models from the AA reference due to the inherent approximations of the pure bottom-up approach can be reduced by iterative optimization of the parameterization of the GLE thermostat. Here we apply the iterative optimization schemes (IOMK, IMRV-1 and IMRV-2) to optimize the parameterization of the memory kernel for the IBI model. But first, to justify the IOMK method given by Eq. 6.17, we will demonstrate the validity of the assumption given by Eq. 6.16. To do so we carried out CG simulations using the IBI potential applying a Markovian Langevin thermostat with varying friction coefficients (γ_{lang}). By evaluating the integrated memory added through conservative interactions ($\Delta G^{CG}(t) = \int_0^t ds \Delta K^{CG}(s)$), Eq. 6.16 can be tested.

In Fig. 6.2 we show the result of this analysis. We find that the friction due to conservative interactions does span over a full order of magnitude for the tested values of γ_{lang}. The relation between $\Delta G^{CG}(t = 10\text{ ps})$ and γ_{lang} is found to be well described by the linear fit

$$\Delta G^{CG}(t = 10\,ps) \approx a + b\gamma_{lang}, \tag{6.18}$$

where a can be interpreted as the single-particle friction coefficient in standard CG-MD simulations in the absence of a Langevin thermostat and b encodes the dependence of the friction due to conservative interactions on the friction coefficient applied through the thermostat. For the IOMK method we extrapolate this finding to Eq. 6.16, assuming the linear relation holds true on all time scales.

In Fig. 6.3, we compare the results of the three iterative schemes, while starting from $\tilde{G}_0(t) = \tilde{G}(t) = \int_0^t ds \tilde{K}(s)$ as initial guess. We first note that the IMRV-1 method does not yield any significant improvement in the representation of the VACF while the IMRV-2 method allows to achieve good results. This is in line with the findings in the original publication.[30] The IOMK method yields satisfying results within 2-3 iterations, while the IMRV-2 method needs around 30-40 iterations to match the target.

This indicates that the IOMK method converges fast compared to the IMRV-2 method. To further test the reliability of the IOMK method, we also applied two different initial guesses: $\tilde{G}_0(t) = \int_0^t ds C_{\delta F \delta F}(s)/k_B T$ and $\tilde{G}_0(t) = 0.1 \int_0^t ds C_{\delta F \delta F}(s)/k_B T$, and present the data in the SI (Figs. S13 and S14). In the former case, the initial guess slightly overestimates optimal friction, yielding too slow dynamics. Herein the IOMK method converges within 3-4 iterations, while the IMRV-2 method requires ten times the number of iterations. In the latter case, the initial guess strongly underestimates the optimal friction, yielding too fast dynamics. Here, the IOMK method also converges within 3-4 steps, while the IMRV-2 method again requires ten times the number of iterations. For the presented system, the IOMK method shows to be very stable and fastly converging, independent of the initial guess for the memory kernel.

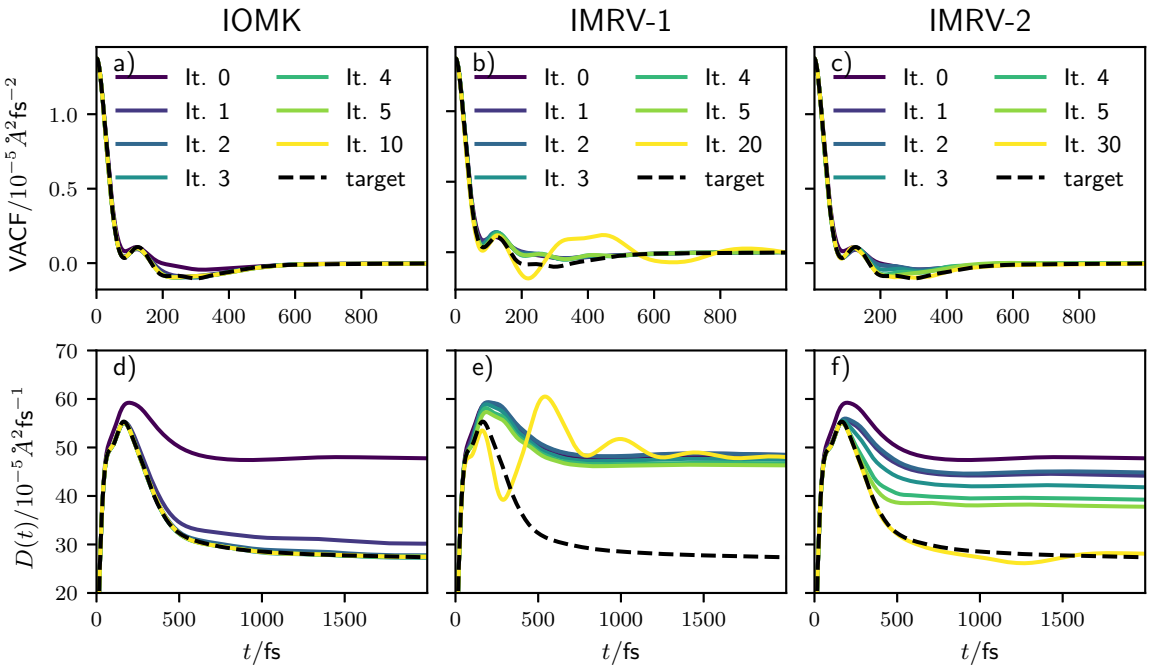

Figure 6.3: Results for iterative optimization of memory kernels for the IBI water model. a), b) and c): Comparison of the VACF for the IOMK, IMRV-1 and IMRV-2 method, respectively. d), e) and f): Comparison of $D(t) = \int_0^t ds C_{VV}(s)$ for the IOMK, IMRV-1 and IMRV-2 method, respectively.

6.3.3 Structural Relaxation: The Distinct Van Hove Function

Both the bottom-up parameterization approach and the IOMK method are motivated by the goal to match dynamic properties of single particles. No information on multi-body correlations are considered in the parameterization of the memory kernels. Thus, it is not *a-priori* clear inhowfar collective dynamic properties involving multiple particles can be captured by applying independent thermostatting to every CG DoF, as e.g. inter-particle correlations can be altered due to the independent thermostatic of every DoF.[34] In this section we want to study the collective dynamics of the CG systems by evaluating the distinct VHF

$$g(R,t) = \frac{1}{4\pi\rho N R^2} \left\langle \sum_I^N \sum_{J\neq I}^N \delta\left(R - |\boldsymbol{R}_I(0) - \boldsymbol{R}_J(t)|\right) \right\rangle . \tag{6.19}$$

In Fig. 6.4 we compare the distinct VHF of the IBI water model with standard CG-MD, the GLE with $\tilde{K}(t)$ and the GLE optimized using the IOMK method. In CG-MD simulations without a GLE thermostat structural correlations relax faster then in the AA reference. Especially in the short distance region, the value of the VHF increases too fast, which is expected as with an increased diffusivity a particle can be more readily displaced and consequently be replaced by its neighbors. Additionally we find that also the pair structure, especially the first peak, relaxes faster than in the AA reference. By introducing friction through the GLE thermostat, the structural relaxation is slowed down and the pair-structure is preserved for longer time scales. The $\tilde{K}(t)$ model overall reproduces the VHF quite accurately at least up to 400 fs. The increased long time diffusivity of the $\tilde{K}$ model compared to the AA reference on short length scales leads to a speed-up in the relaxation beyond 400 fs. The optimization of the memory kernel through the IOMK method does not significantly alter the VHF for the first peak, but by matching the long time diffusivity the relaxation on short length scales is better reproduced.

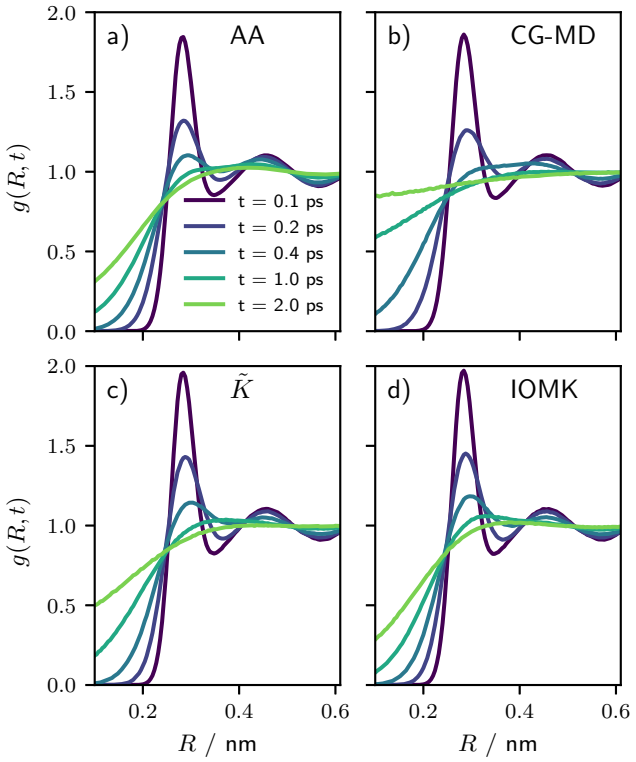

Figure 6.4: Distinct VHF for a) the AA reference, b) the CG-MD IBI model c) the $\tilde{K}$-model, d) the IOMK model.

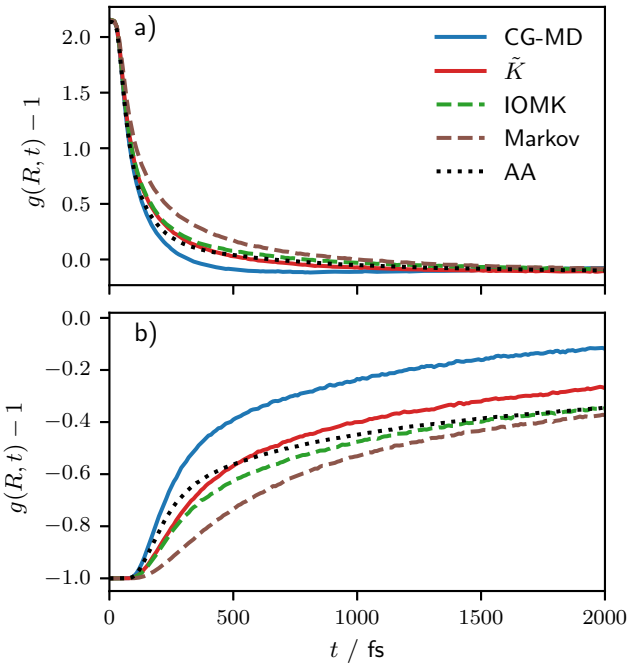

Figure 6.5: Distinct VHF at a) $R = 0.276$ nm and b) $R = 0.2$ nm, for different CG IBI models compared to the AA reference.

In Fig. 6.5 a), we present a slice through the VHFs at $R = 0.276$ nm for a better time resolution of the relaxation of the first peak. Here we see more clearly that the VHF decays too fast for CG-MD, which is improved with the GLE thermostat for both the $\tilde{K}$- and the IOMK model. We additionally present the result of a Markovian Langevin-thermostat model, in which we optimized the friction coefficient such the diffusivity matches the AA reference. Herein we find that in such a Markovian model the relaxation of the pair-structure is too slow.

In Fig. 6.5 b) we present a slice through the VHF at $R = 0.2$ nm, where we again find that the CG-MD model yields too fast relaxation. On short timescales, both the $\tilde{K}$ model and the IOMK model match the reference significantly better, while the Markovian model again relaxes too slowly. On long timescales, the $\tilde{K}$-model relaxes too fast, while the AA, the IOMK model and the Markovian model converge onto each other.

6.3.4 Comparison of the Different CG Water Models

Up to now we only discussed the dynamics of IBI water models. We have shown that the purely bottom-up informed approach allows a semi-quantitative representation of the reference dynamics, while the IOMK method allows to reproduce the VACF quantitatively, while also the representation of collective dynamics in terms of the distinct VHF is significantly improved.

In this section we will compare how the choice of the CG potential influences the dynamic properties of purely bottom-up informed water models. The properties of the memory kernel contributions for the different conservative potentials are shown and discussed in the SI (Fig. 6.13).

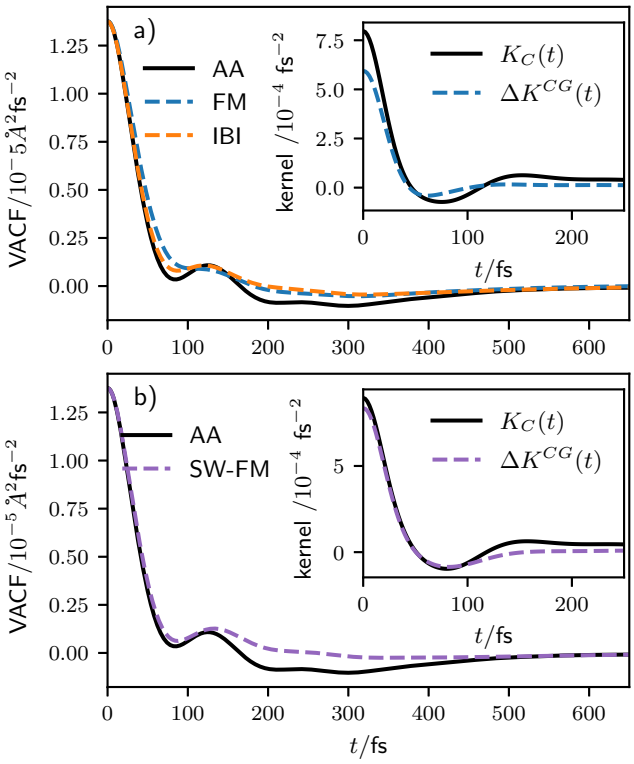

Figure 6.6: VACFs from GLE simulations of CG models with a) two-body potentials b) three-body potentials, parameterized with $\tilde{K}(t)$, compared to the AA reference.

Dynamics of Generalized Langevin Models

In this section, we study the dynamics of the different CG water models applying a GLE thermostat. The VACFs for the two-body and the three-body models are shown in Figs. 6.6 a) and 6.6 b), respectively. In Fig. 6.6 b), only the SW-FM model is considered, as for the SW-RE model the bottom-up approach predicts a nonphysical memory kernel $\tilde{K}(t)$ (see SI Sec. S6 for a discussion on the origin of this behavior). We also studied GLE models parameterized with $K_{\delta,X}(t) = K_\delta(t) + K_X(t)$ and $K_\delta(t)$, to study the relevance of the cross-correlation term $K_X(t)$. Note that $K_{\delta,X}(t)$ is equivalent to a memory kernel which can be evaluated from a Volterra equation derived from Eq. 6.1[33] and has been proposed as a straight forward parameterization for both Markovian Langevin[196] and non-Markovian GLE thermostats.[31] Using $K_\delta(t)$, thus neglecting cross-correlations all together, can be understood as a non-Markovian variant of the approach proposed in Ref. [36]. The data on these models can be found in the SI (Figs. S6 and S7).

In all shown cases in Fig. 6.6, the GLE model yields a significant improvement of the representation of the reference dynamics, when compared to the standard CG-MD simulations (Fig. 6.14). The FM model cannot fully capture the fast initial decay of the VACF. The SW-FM model and the IBI model captures the initial decay quantitatively. The local features around 75-150 fs are qualitatively well matched for the IBI models and the SW-FM models, while the depth of the broad negative valley 200-300 fs is underestimated in all cases, indicating again too fast overall mobility.

A comparison of $K_C(t)$ and $\Delta K^{CG}(t)$ (as shown in the insets of Figs. 6.6 a) and b)) again reveals the origin of the remaining discrepancies. In the FM model, the onset of the memory kernel due to conservative forces in CG simulations is lower than $K_C(t)$ would predict. This is due to mismatch of the pair structure in the FM model, which yields a reduction in the variance of conservative forces. This discrepancy on short

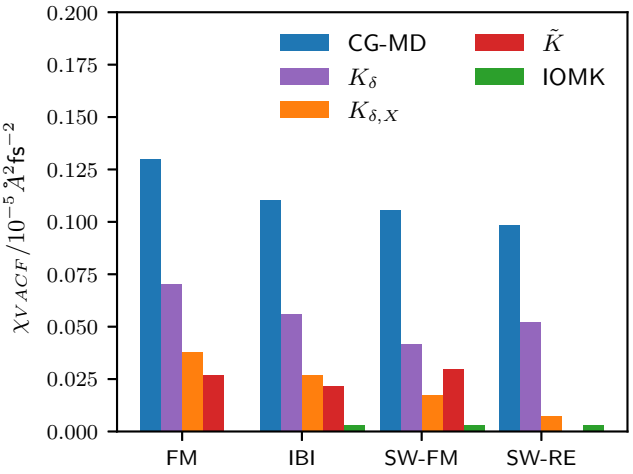

Figure 6.7: Error estimate of the VACF based on Eq. 6.20, for all CG simulations.

time scales leads to the too slow initial decay on small time scales. Also the valley of $K_C(t)$ is not as well reproduced as in the IBI model, leading to larger discrepancies in the VACF on similar time scales. For the SW-FM model, the assumption of Eq. 6.14 is well justified up to 100 fs.

In all cases the overall mobility is overpredicted with $\tilde{K}(t)$. The origin trivially arises from deviation from the assumption of Eq. 6.14.

Additionally to the bottom-up approach, we also applied the IOMK method to optimize the parameterization of the SW-FM and the SW-RE model. We find that the IOMK method can also be successfully applied to optimize the memory kernels in SW-type models. Fig. 6.7 shows an overview over all studied CG models, by defining an error measure as

$$\chi_{VACF} = \sqrt{\frac{1}{N+1}\sum_{n=0}^{N}(C_{VV}^{tgt}(n\Delta t) - C_{VV,i}^{CG}(n\Delta t))^2}, \tag{6.20}$$

with $N = 1000$ and $\Delta t = 2$ fs.

For the pure bottom-up approach, $\tilde{K}(t)$ yields the best results for both CG pair potentials while $K_{\delta,X}(t)$ yields better results for the three-body potentials.

Structural Relaxation

We calculated the distinct VHF for all combinations of CG potentials and GLE thermostat parameterizations. A prerequisite for reproducing the VHF on all time scales is that the static pair structure is reproduced. Because the FM model does not reproduce the static pair structure (see SI Fig. 6.12) we only consider the IBI, the SW-FM and the SW-RE model in this section. Additionally, to single out the influence of the choice of the CG potential, we first consider the simulations optimized through the IOMK method. This allows to study the influence of the CG potential on structural relaxation, given that the static structure and the single-particle dynamics is accurately represented. In Fig. 6.8 a) we show the VHF for the first peak for the described systems, compared to the AA reference. For the relaxation of the first peak, all three models match the AA almost quantitatively. Still, the SW-RE model matches the reference data best, which can be seen by amplifying the plot, as shown in the inset. A more significant deviation between the different models is found for shorter length scales ($R = 0.2$ nm) in Fig. 6.8 b). Here the IBI model deviates

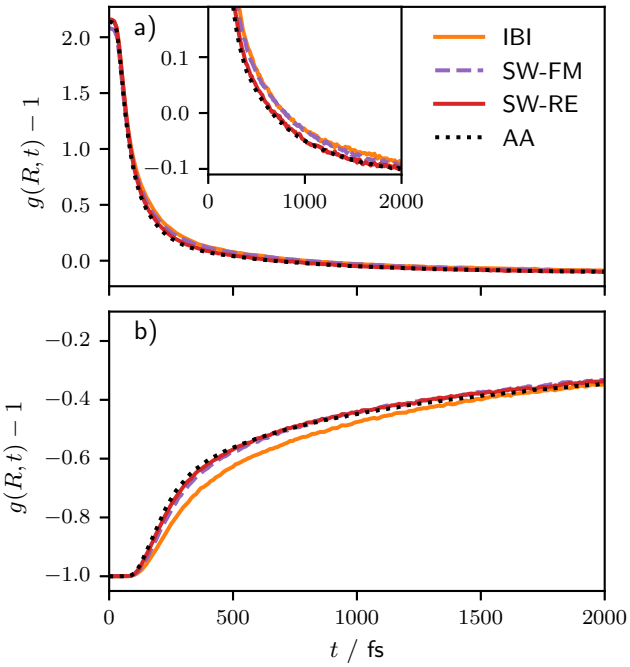

Figure 6.8: The VHF for the IOMK models with the IBI, the SW-FM and the SW-RE model compared to the AA reference for a) $R = 0.276$ nm and b) $R = 0.2$ nm.

significantly from the AA reference, while both SW-type models reproduce the structural relaxation almost quantitatively.

To compare the performance of all different combinations of CG potentials and thermostats we define the error measure

$$\chi_{VH} = \sqrt{\frac{1}{N_i N_j} \sum_i \sum_j \left(g(R_0 + i\delta R, j\delta t) - g^{ref}(R_0 + i\delta R, j\delta t)\right)^2}, \tag{6.21}$$

where N_i and N_j are the considered number of distance bins and time steps, respectively, R_0 is the minimal considered distance, δR is the bin width and δt is the spacing is the resolution in time.

In Fig. 6.9 we summarize the estimated deviations from the reference for the considered CG potentials for all thermostat parameterizations. This allows to draw the following conclusions:

1. In all cases, introducing a dissipative thermostat improves the representation of the VHF.

2. For the IBI potential, the IOMK model performs better than the Markovian model, while having the same diffusivity. One can conclude that matching the diffusivity is not sufficient to correctly model structural relaxation and memory effects have to be taken into account.

3. For all CG potentials, the optimization of the VACF via the IOMK method leads to an improved representation of the VHF.

4. Given that the single-particle dynamics is well matched, as ensured by the IOMK method, and the static structure is well reproduced, the representation of the structural relaxation still depends on the choice of the CG potential. The introduction of an angular potential for coarse-graining SPC/E water, improves, under the stated conditions, the representation of the VHF. Additionally, the SW-RE model performs better than the SW-FM model.

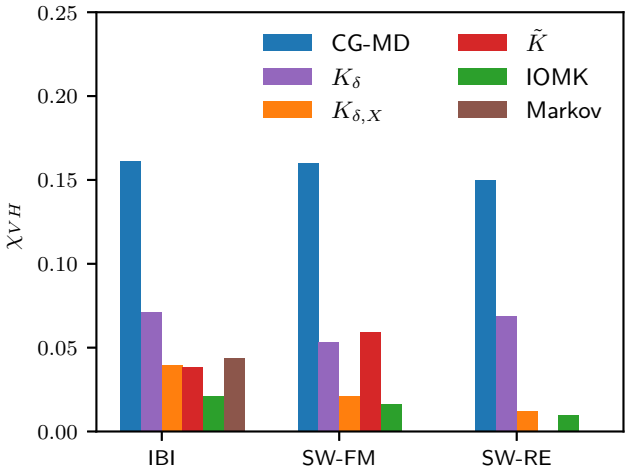

Figure 6.9: Error estimate for the distinct VHF for all studied IBI, SW-FM and SW-RE models.

6.4 Summary and Outlook

We have demonstrated that the previously proposed bottom-up approach for the parameterization of GLE thermostats based on the BOD method is applicable to molecular systems with complex interactions by coarse-graining SPC/E water using effective single-site interactions. In conjunction with pairwise conservative interactions, the proposed parameterization of the GLE thermostat yields good results for most CG potentials. In particular, in accordance with previous studies,[33, 34] taking into account the $\mathcal{Q}$-projected cross-correlations is necessary to correctly reproduce the VACF on short time scales, and its neglection typically yields too slow dynamics. At the same time, we found that for coarse-graining SPC/E water on a single interaction site, considering the cross-correlation term twice (using $\tilde{K}(t)$ for the parameterization of the GLE thermostat) tends to overpredict the diffusivity. This is in line with our findings in Ref. [34] and is due to the independent thermostatting of every CG DoF which leads to a reduction of the correlation of the dynamics between different CG DoFs.

Using the example of the IBI potential, we have demonstrated the applicability of the IOMK method to optimize the VACF for molecular liquids and have demonstrated its stability and good convergence properties compared to previously proposed iterative optimization schemes. Our results indicate that the IOMK method converges fast, even when the initial guess is far from optimal. An additional benefit, compared to other methods, is that the IOMK method does not rely on any parameters which have to be manually predetermined to improve convergence behavior, which significantly increases its applicability as an out of the box tool for dynamic coarse-graining.

By studying the distinct VHF, we have demonstrated that despite of the conceptional limitation of an isotropic and configuration independent thermostat, the application of a GLE thermostat in CG models allows to model structural relaxation quite accurately. This is a non-trivial finding, as nowhere in the parameterization process collective dynamics is considered and indicates that a faithful connection to the underlying AA reference can be established under certain conditions. Of course the prerequisite is that at least the pair structure is well reproduced by the CG potential. By comparing the pairwise IBI potential with two three-body Stillinger-Weber type potentials (SW-FM and SW-RE) we found that an accurate representation of three-body correlations can further improve the accuracy of the distinct VHF, given an accurate representation of single-particle dynamics.

In principle, the choice of the target for the IOMK method is not limited to FG MD models. The single-particle memory kernel is accessible from the mean-squared displacement[81] which by itself can

be calculated from the self-part of the VHF from experiments.[246] This would allow to use the IOMK method in combination with top-down parameterized CG potentials, to improve the representation of dynamic properties in empirical CG models as for example the Molinero-Water model.[250] This would necessitate high quality experimental data with a high resolution in space and time, and methods to accurately extract the center of mass dynamics from experimental measurements. In practice such an approach has to to evaluated carefully, as it is unclear if current experimental data is sufficiently reliable to be used as quantitative reference. For example, the reported VHF in Ref. [247] does not quantitatively agree with earlier results in Refs. [243, 244].

In summary, we have shown that it is possible to derive good estimates of memory kernels in a purely bottom-up approach, which allow to maintain a direct link between the parameterization of the GLE thermostat and the underlying AA reference. For the considered system the bottom-up approach performs more reliably for CG pair potentials than for three-body potentials. Arguably this is due to the increased complexity of the CG energy landscape as in such a case even small discrepancies in the sampling of configuration space between AA and CG models can lead to significant errors in the prediction of memory due to conservative forces. The IOMK method allows to efficiently circumvent these issues by allowing to derive CG models which exactly reproduce the single-particle dynamics. Our results indicate that also collective dynamics can be accurately described by applying optimized memory kernels as long as the CG potential accurately reproduces the pair-structure.

6.5 Methods

6.5.1 All-Atom Water Simulations

As a FG reference we consider atomistic water at ambient conditions, applying the SPC/E model.[251] The atomistic simulations were carried out using the GROMACS[212, 214] package, using a time step of 2 fs integrated via the velocity Verlet method. We use a cutoff of 1.2 nm for short-range van der Waals and electrostatic interactions and long-range dispersion corrections for energy and pressure. Long-range electrostatic interactions are treated with the particle mesh Ewald method with a grid spacing of 0.12 nm. The reference system was set up by preparing a cubic simulation box with 3000 water molecules. The box was equilibrated under NPT conditions at 1 bar and 298 K using the velocity-rescale thermostat with a time constant of 1 ps and the Berendsen barostat with a time constant 2 ps and compressibility parameter of experimental water of 4.5x10^{-5} bar^{-1} . The average box-length of a NPT simulation was chosen to fix the box length to 4.47934 nm for further simulations.

For the evaluation of structural properties (the radial distribution function) a NVT-run was carried out for 200 ps. Snapshots were stored every 20 fs. To efficiently obtain sufficiently uncorrelated snapshots, a the stochastic dynamics integrator was applied with a time constant of 1 ps.

For the evaluation of dynamic properties (VACF, memory kernels, distinct VHF), 10 independent NVE-simulations were carried out from different initial conditions drawn from a sample of NVT-snapshots. Here, every run was carried out for 50 ps using the velocity-Verlet integrator. Frames were stored every timestep.

6.5.2 CG Simulations

We derived all tabular CG pair potentials using the VOTCA-CSG[202] package. We applied a center of mass mapping scheme for the CG representation.

For the IBI model, we set cutoff distance for the CG pair potential to 1 nm. For every IBI iteration, simulations were carried out for 120 ps under NVT conditions using the stochastic integrator with a time

constant of 0.5 ps. Snapshots for the evaluation of the RDF were taken every 20 fs. We stopped the optimization process after 300 iterations. For the derivation of the FM potential we set the range of the potential to 0.24 nm to 0.9 nm, with a spacing of 0.012 nm. The three-body SW-type potentials were obtained from literature. See Ref. [238] for details on the SW-FM potential and Ref. [249] for details on the SW-RE potential.

CG simulations were carried out using the LAMMPS[227] package. All CG simulations were carried out under NVT conditions, with 3000 CG beads, at 298 K, a box length of 4.47934 nm and a time step of 2 fs.

For every CG system, we generated ten 20 ps trajectories. Dynamic properties were evaluated for every distinct trajectory, and averaged to reduce statistical uncertainty.

For standard CG-MD simulations the the Nosé-Hoover thermostat was applied with a time constant of 2000 fs. For GLE simulations the GLE thermostat due to Ceriotti[151] was applied. This thermostat is based on an auxiliary variable approach, which allows to simulate non-Markovian dynamics by applying a Markovian EoM in extended phase space. For its application in the context of CG, the coupling between the CG momenta and the auxiliary momenta has to be defined in terms of a coupling matrix. This matrix can be determined from a given memory kernel, by fitting with exponentially dampened oscillators. For all CG GLE models we chose to fit six exponentially dampened oscillators, yielding 12 auxiliary momenta for the Markovian embedding. In practice we fitted the integrals of the memory kernels. For all BOD method based parameterizations the memory kernels were fitted up to $t = 800$ fs. For the IOMK method we fitted the memory kernels up to $t = 2000$ fs, to better capture the hydrodynamic tail of the VACF. Further details on the Markovian embedding of GLEs can be found in our earlier publications[34, 201] or for example in Refs. [27, 32, 92, 221].

6.5.3 Bottom-Up Derivation of Memory Kernels from Backward-Orthogonal Dynamics

Details on the BOD method can be found in Refs.[33, 34, 39, 85], so we will only shortly summarize the overall workflow. The first step is always to carry out FG (AA) simulations, where frames are stored sufficiently frequently (every time step in the current work) to reduce numerical errors in the BOD method. Both velocities and total forces for every DoF have to be stored. Next we apply the center of mass mapping on the AA trajectory (using the VOTCA-CSG software[202]) to obtain a mapped reference trajectory. Based on this mapped trajectory, a rerun is carried out using the required CG potential to obtain a trajectory for the conservative interactions $\boldsymbol{F}_I^C(t)$, which through $\delta\boldsymbol{F}_I(t) = \boldsymbol{F}_I(t) - \boldsymbol{F}_I^C(t)$ also yield a time series for the residual forces. From the time series of $\boldsymbol{F}_I(t)$, $\boldsymbol{F}_I^C(t)$, $\delta\boldsymbol{F}_I(t)$ and $\boldsymbol{V}_I(t)$ the respective $\mathcal{Q}$-projected force-correlation functions can be obtained applying the BOD method. As a numerical scheme we utilize the second-order scheme proposed by Jung *et al.*.[33, 34, 39]

6.5.4 The IMRV Method

The update scheme for the IMRV-1 method and the IMRV-2 method is given by

$$\tilde{K}_{i+1}(t) = \tilde{K}_i(t) + h_i(t)\Delta\phi_i(t). \tag{6.22}$$

The update function $\Delta\phi_i(t)$ is given by

$$\Delta\phi_i(t) = \phi^{tgt}(t) - \phi_i(t), \tag{6.23}$$

where the superscript tgt denotes the target function and the subscript i denotes the current iteration. For IMRV-1 the function $\phi_i(t)$ is defined by the respective VACF $C_{VV,i}(t)$ as

$$\phi_i(t) = -M_I \frac{C_{VV,i}(t+\Delta t) - 2C_{VV,i}(t) + C_{VV,i}(t-\Delta t)}{k_B T \Delta t^2}, \tag{6.24}$$

and analogously for $\phi^{tgt}(t)$. The function $h_i(t)$ defines the step size for the iterations and can be tuned to improve the stability of the scheme. Jung *et al.*[39] proposed

$$h_i(t) = \begin{cases} 1, & \text{if } t/t_{corr} \leq \frac{i}{2} \\ 1 - t/t_{corr} + i/2, & \text{if } i/2 < t/t_{corr} < i/2+1 \\ 0, & \text{if } t/t_{corr} \geq i/2+1. \end{cases} \tag{6.25}$$

The IMRV-2 method defines a different function $\phi_i(t)$ (and accordingly $\phi^{tgt}(t)$), which reads[30]

$$\phi_i(t) = -M_I \alpha \frac{C_{VV,i}(t+\Delta t) - C_{VV,i}(t)}{k_B T \Delta t}. \tag{6.26}$$

Note that for the IMRV2 method, an additional constant α has to be set. After manual optimization we applied $t_{corr} = 80$ fs and $\alpha = 0.05$ fs^{-1}.

Data Availability

The data that supports the findings of this study are available within the article and its supplementary material. At https://doi.org/10.48328/tudatalib-937 we provide all results (memory kernels, VACFs etc.) as text files. We also provide input data for the AA model and the CG models discussed in this work including tabular potentials and the coupling matrices for the application of the auxiliary variable GLE thermostat.

At https://github.com/vklip/IOMK we provide a minimal working example for the application of the IOMK method to derive optimized GLE thermostat models, based on the IBI potential. An implementation of the IOMK method within the VOTCA software will be developed at https://github.com/vklip/votca-iomk.

Funding

Funded by the Deutsche Forschungsgemeinschaft (DFG, German Research Foundation) - Project number 233630050 - TRR 146.

Supporting Information

In the supporting information we discuss the relation of the IOMK and the IMRV-2 to the Newton method. Additionally, we present most of the data shown in the main text alongside the results for two additional CG potentials which is an IBI potential where we applied a pressure ramp (IBI-p) and the well known SW-type model due to Molinero *et al.*[250] (MW).

In Fig. 6.11 we show the CG pair potentials derived for this study and in Fig. 6.12 we compare the structure (in terms of the RDF and the angular distribution function) of all CG water models with SPC/E water. In Fig. 6.13 we show all memory kernels derived from the BOD-method and, where applicable, the optimized IOMK memory kernels. In Fig. 6.14 we show the VACFs from CG-MD simulations for all CG potentials. In Figs. 6.15-6.17 we show the VACFs from CG GLE thermostat simulations, including parameterizations of the GLE thermostat with $K_\delta(t)$ and $K_{\delta,X}(t) = K_\delta(t) + K_X(t)$. In Fig. 6.18 we compare the memory due to conservative interactions in the SW-RE and the MW model to the predictions ($K_C(t)$)

due to the BOD-method, to demonstrate why for these models a meaningful parameterization of the GLE thermostat, using $\tilde{K}(t)$ is not possible. In Fig. 6.19 we again show all VACFs and the corresponding integrals ($D(t) = \int_0^t dsC_{VV}(s)$) to compare long time diffusion coefficients. In Fig. 6.20 we summarize the modeling errors of all CG models, including the IBI-p and the MW models.

In Fig. 6.21 we visualize the convergence of the IOMK, IMRV-1 and IMRV-2 method. In Figs. 6.22 and 6.23 we show the results for the IOMK and IMRV-2 method with alternative initial guesses. In Figs. 6.24-6.26 we show the results for the IOMK method for the SW type potentials.

In Figs. 6.27-6.38 we show all VHFs and in Fig. 6.39 we summarize the modeling errors of the VHFs for all models, including the results for the IBI-p and MW models.

6.6 Supporting Information

6.6.1 Overview of Supporting Information

In the following supporting information we present additional data, not presented in the main text to allow to focus on the key results. Most of the data shown in the main text, is duplicated in this supporting information, to allow for a direct comparison to the additional data.

In the main text, we discussed CG models using four different CG potentials (FM, IBI, SW-FM, SW-RE). We additionally studied an IBI model, for which we applied a pressure correction (IBI-p) and the prominent top-down parameterized Stillinger-Weber type Molinero water (MW) model.[250] We applied the same techniques described in the main text to study these models.

Additionally, in Sec. 6.6.2 we discuss the relation of the IOMK method and the IMRV-2 method to the Newton method.

6.6.2 The IOMK and IMRV Method as Quasi-Newton Iterations

Some general remarks and notations

The Newton method is a numerical algorithm to find the root of a function, or in its multi dimensional generalization to find a solution for a system of equations. In its generalized form, Newton's method in vector notation is given by

$$\boldsymbol{x}_{i+1} = \boldsymbol{x}_i - (\boldsymbol{J}(\boldsymbol{x}_i))^{-1}\boldsymbol{y}(\boldsymbol{x}_i) = \boldsymbol{x}_i - \boldsymbol{J}_i^{-1}\boldsymbol{y}_i \tag{6.27}$$

where $\boldsymbol{y}$ is the vector of functions for which the roots have to be found, $\boldsymbol{x}$ a vector of parameters to optimize and $\boldsymbol{J}$ is the Jacobian and the subscript i denotes the current iteration. The Jacobian, a NxN matrix, for the i-th iteration is given by

$$\boldsymbol{J}_i = \boldsymbol{J}(\boldsymbol{x}_i) = \begin{bmatrix} \frac{\partial y_{i,1}}{\partial x_{i,1}} & \cdots & \frac{\partial y_{i,1}}{\partial x_{i,N}} \\ \vdots & \ddots & \vdots \\ \frac{\partial y_N}{\partial x_{i,1}} & \cdots & \frac{\partial y_{i,N}}{\partial x_{i,N}} \end{bmatrix}. \tag{6.28}$$

We denote distinct entries in the Jacobian as

$$J_{i,nm} = \frac{\partial y_{i,n}}{\partial x_{i,m}} \tag{6.29}$$

where $y_{i,n}$ and $x_{i,m}$ are the n-th and m-th element of the vectors $\boldsymbol{x}_i$ and $\boldsymbol{y}_i$ respectively. We use a analogue notation for all other vectors and matrices in the following sections.

The IOMK method as quasi-Newton iteration

In the IOMK method we want to minimize the residual between $G^{tgt}(t)$ and $G^{CG}(t)$ with respect to the thermostat memory kernel $\tilde{G}(t)$. These time-dependent functions are discretized in the numerical implementation, so we can represent them as vectors in which the n-th element of the vector corresponds to time $t = (n-1)\Delta t$ with $n = 1, ..., N$.

$$\boldsymbol{y}_i = \boldsymbol{G}_i^{CG} - \boldsymbol{G}^{tgt} \tag{6.30}$$

$$\boldsymbol{x}_i = \tilde{\boldsymbol{G}}_i \tag{6.31}$$

For this inverse problem, the exact Jacobian is not known, so it has to be approximated.

To do so, we start from the ansatz

$$G_i^{CG}(t) \approx a(t) + (1 + b(t))\tilde{G}_i(t) \tag{6.32}$$

or written in vector notation

$$\boldsymbol{G}_i^{CG} \approx \boldsymbol{a} + (\boldsymbol{I} + \hat{\boldsymbol{b}})\tilde{\boldsymbol{G}}_i. \tag{6.33}$$

Here $\boldsymbol{I}$ is the identity matrix and

$$\hat{\boldsymbol{b}} = \begin{bmatrix} b_1 & 0 & \cdots & 0 \\ 0 & b_2 & \ddots & 0 \\ \vdots & \ddots & \ddots & \vdots \\ 0 & 0 & \cdots & b_N \end{bmatrix}. \tag{6.34}$$

As $\boldsymbol{I} + \hat{\boldsymbol{b}}$ is a diagonal matrix, the approximate Jacobian is given by $J_{i,nm} = 1 + b_n$ for $n = m$ and $J_{i,nm} = 0$ for $n \neq m$. Eq. 6.33 implies that the update of every entry $\tilde{G}_{i,n}$ is independent of all other entries $\tilde{G}_{i,m}$ and we can write

$$\tilde{G}_{i+1,n} = \tilde{G}_{i,n} - (1 + b_n)^{-1}(G_{i,n}^{CG} - G_n^{tgt}). \tag{6.35}$$

Finally, we replace $(1 + b_n)$ by $\frac{G_{i,n}^{CG} - a_n}{\tilde{G}_{i,n}}$ to get the quasi-Newton update

$$\tilde{G}_{i+1,n} = \tilde{G}_{i,n} - \frac{\tilde{G}_{i,n}}{G_{i,n}^{CG} - a_n}(G_{i,n}^{CG} - G_n^{tgt}) \tag{6.36}$$

which can be reformulated as

$$\begin{aligned} \tilde{G}_{i+1,n} &= \tilde{G}_{i,n} - \frac{G_{i,n}^{CG} - G_n^{tgt}}{G_{i,n}^{CG} - a_n}\tilde{G}_{i,n} \\ &= \left(1 - \frac{G_{i,n}^{CG} - G_n^{tgt}}{G_{i,n}^{CG} - a_n}\right)\tilde{G}_{i,n} \\ &= \frac{G_n^{tgt} - a_n}{G_{i,n}^{CG} - a_n}\tilde{G}_{i,n}. \end{aligned} \tag{6.37}$$

This recovers the original formulation of the IOMK method

$$\tilde{G}_{i+1}(t) = \frac{G^{tgt}(t) - a(t)}{G_i^{CG}(t) - a(t)} \tilde{G}_i(t). \tag{6.38}$$

Note that from Eq. 6.35 to Eq. 6.36 we reintroduced a dependence of the Jacobian on the current iteration. Thus the IOMK method is a quasi-Newton scheme, where an approximate Jacobian is used based on Eq. 6.32. From numerical experiments for Markovian CG water models we found that Eq. 6.32 is very well justified for the tested case, in the Markovian limit. If Eq. 6.32 were exact, the IOMK method would be an exact Newton scheme, applied to a linear problem and always yield to convergence within a single iteration. The number of required iterations will naturally grow if the relation between $G^{CG}(t)$ and $\tilde{G}(t)$ becomes non-linear or if the cross-terms of the (unknown) exact Jacobian become significantly large.

Note that the IOMK method can also be understood as a variation of a secant method. The secant method for the given problem reads

$$\tilde{G}_{i+1,n} = \tilde{G}_{i,n} - \frac{\tilde{G}_{i,n} - \tilde{G}_{i-1,n}}{G_{i,n}^{CG} - G_{i-1,n}^{CG}} (G_{i,n}^{CG} - G^{tgt}). \tag{6.39}$$

By fixing one point of the secant, by replacing $\tilde{G}_{i-1,n}$ by 0 and accordingly $G_{i-1,n}^{CG}$ by a_n, again the IOMK method can be directly recovered.

In general, both exact and approximate Newton methods can become unstable under certain conditions, especially if the initial guess is far from optimal and the optimization problem is highly non-linear. For now it is unclear if under relevant conditions the IOMK method might become unstable.

In the following, by considering *hypothetical* non-linear relations between $\Delta G^{CG}(t)$ and $\tilde{G}(t)$ we will visualize the IOMK process to better understand the IOMK method in non-ideal applications.

In the most general case, we can write

$$G_n^{CG} = a_n + \tilde{G}_n + f_n(\tilde{\boldsymbol{G}}), \tag{6.40}$$

where $a_n + \tilde{G}_n$ represents the effective integrated single particle memory kernel for the idealized case where $\Delta G^{CG}(t) = a(t)$ and is therefore independent of $\tilde{G}(t)$. The function $f_n(\tilde{\boldsymbol{G}})$ captures all non-idealities, including linear and non-linear contributions from $\tilde{G}_n$ and potential codependencies between G_n^{CG} and $\tilde{G}_m$ for $m \neq n$.

Let us consider the following cases:

$$\text{a) } G_n^{CG} = a_n + \tilde{G}_n + 4\sqrt{\tilde{G}_n} \tag{6.41}$$

$$\text{b) } G_n^{CG} = a_n + \tilde{G}_n + 2\sin\left(\tilde{G}_n\right) \tag{6.42}$$

$$\text{c) } G_n^{CG} = a_n + \tilde{G}_n + 0.1\tilde{G}_n^2 \tag{6.43}$$

$$\text{d) } G_n^{CG} = a_n + \tilde{G}_n + 0.5\tilde{G}_n^3 \tag{6.44}$$

The IOMK iterations for these cases are visualized in Figs. 6.10 a)-d), whereby we set $a_n = 1$, $\tilde{G}_{0,n} = 20$, $G_n^{tgt} = 10$.

From Fig. 6.10 it is evident that for non-linear problems the update of the IOMK method is determined by the x-intercept of the secant determined by the points (0,$a_n - G_n^{tgt}$) and ($\tilde{G}_{i,n}, G_{i,n}^{CG} - G_n^{tgt}$). We find, that for Eqs. 6.41-6.43 (Fig. 6.10 a)-c)) the IOMK update finds the root within a few steps. Herein case b) is of particular interest, as the presence of many local extrema would cause problems in an exact Newton

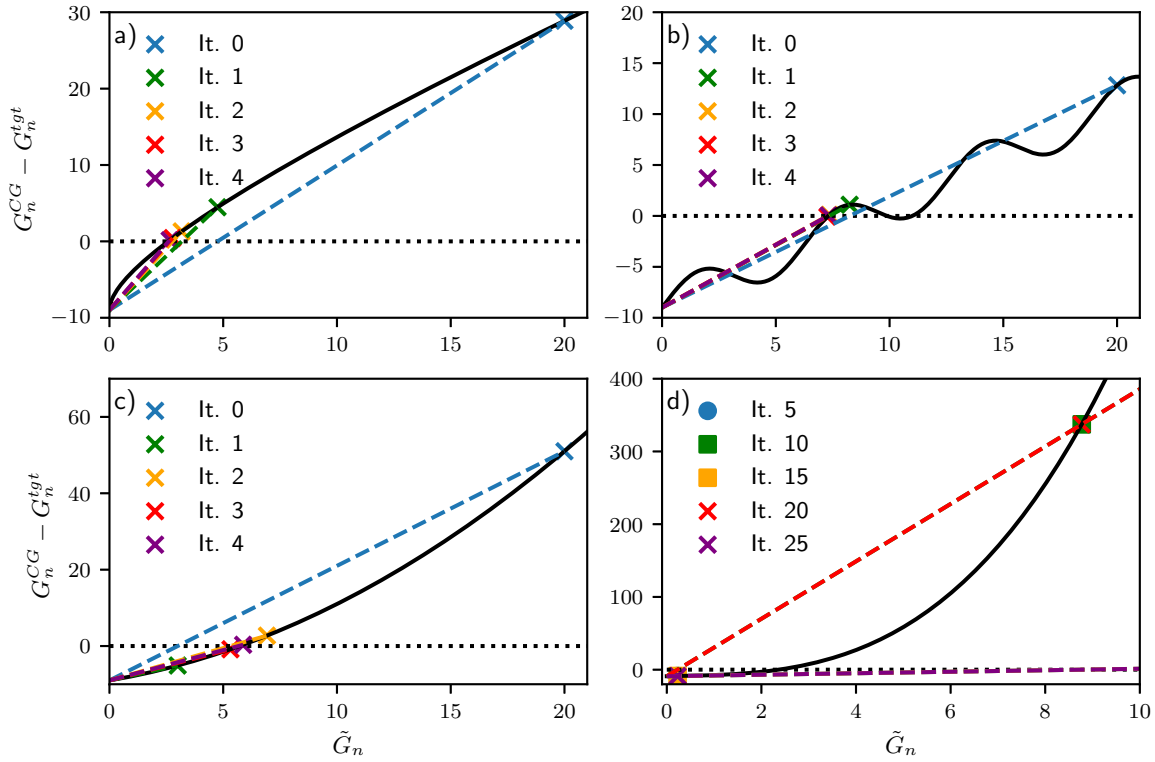

Figure 6.10: Results for the IOMK method, applied to the functions given by Eqs. 6.41-6.44. The black line is the function for which the root has to be found, the colored markers show the points of respective iterations and the colored dashed lines show the secant which determines the update step.

method if the initial guess is far from the optimum, as the step size would become infinitely large at the extrema. For very strong non-linearities on the other hand, as in Eq. 6.44, the IOMK update can lead to stable oscillations, which prevent the process from finding the root.

In summary, for linear problems the IOMK method is an exact Newton update, whereas for non-linear problems it can be understood as a modified secant method. In practical problems, the performance of the IOMK will depend on the magnitude and type of non-linearities and can be either more or less stable than an exact Newton method. The relevance of this insights for practical applications in coarse-graining can not be easily predicted and more testing has to be done in future research.

The IMRV-2 method as quasi-Newton iteration

In the IMRV-2 method, effectively the first derivative of the VACF is used as target. In this section, we thus redefine $\phi(t)$ as

$$\phi(t) = \frac{C_{VV}(t + \Delta t) - C_{VV}(t)}{\Delta t}. \tag{6.45}$$

Accordingly, in discretized vector notation, $\boldsymbol{y}$ reads

$$\boldsymbol{y} = \boldsymbol{\phi} - \boldsymbol{\phi}^{tgt}. \tag{6.46}$$

The input vector $\boldsymbol{x}$ is given by

$$\boldsymbol{x} = \tilde{\boldsymbol{K}}. \tag{6.47}$$

The vector notation of the IMRV-2 update reads

$$\boldsymbol{x}_{i+1} = \boldsymbol{x}_i + \alpha \frac{M}{k_B T} \hat{\boldsymbol{h}}_i \boldsymbol{y}_i, \tag{6.48}$$

whereby

$$\hat{\boldsymbol{h}}_i = \begin{bmatrix} h_{i,1} & 0 & \cdots & 0 \\ 0 & h_{i,2} & \ddots & 0 \\ \vdots & \ddots & \ddots & \vdots \\ 0 & 0 & \cdots & h_{i,N} \end{bmatrix}. \tag{6.49}$$

Thus, with the window function

$$h_i(t) = \begin{cases} 1, & \text{if } t/t_{corr} \leq \frac{i}{2} \\ 1 - t/t_{corr} + i/2, & \text{if } i/2 < t/t_{corr} < i/2 + 1 \\ 0, & \text{if } t/t_{corr} \geq i/2 + 1, \end{cases} \tag{6.50}$$

the Jacobian is approximated by

$$\boldsymbol{J}_i \approx -\frac{k_B T}{\alpha M} \hat{\boldsymbol{h}}_i^{-1}. \tag{6.51}$$

Similar to the IOMK method, the assumed approximate Jacobian in the IMRV-2 method is diagonal. Also the Jacobian does not depend on the input vector $\boldsymbol{x}$, and the slope for every time at any given iteration is predetermined by the parameters t_{corr} and α. While a proper tuning of t_{corr} and α allows to iteratively improve $\tilde{\boldsymbol{K}}$ in successive iterations, without a good understanding of the relation between $\tilde{\boldsymbol{K}}$ and $\boldsymbol{\phi}$, rapid convergence cannot be guaranteed. In our numerical experiments, we tuned α and t_{corr} such that the initial iterations yields rapid changes without introducing instabilities. Still, in subsequent iterations the rate of change strongly decreases.

Deriving an exact Newton scheme for IMRV-2

Let us now consider how an exact newton scheme for the IMRV-2 method could be in principle derived. The strategy we use here is to first establish a relation between $\boldsymbol{\phi}$ and $\boldsymbol{G}^{CG} = \tilde{\boldsymbol{G}} + \Delta \boldsymbol{G}^{CG}$.

To do so, we use the Volterra equation

$$C_{VV}(t) = C_{VV}(0) - \int_0^t ds G^{CG}(t-s) C_{VV}(s) \tag{6.52}$$

which can be discretized using the trapezoid rule as

$$C_{VV,n} = C_{VV,1} - \Delta t \sum_{m=1}^{n} \alpha_m G^{CG}_{1+n-m} C_{VV,m}, \tag{6.53}$$

wherein $t = (n+1)\Delta t$, $\alpha_1 = \alpha_n = 0.5$, $\alpha_m = 1$ for $m \neq n$ and $m \neq 1$. To conform with the definition of $\boldsymbol{y}$, we multiply Eq. 6.53 by -1, add $C_{VV,n+1}$ and divide by Δt.

$$\begin{aligned}\phi_n &= \frac{C_{VV,n+1} - C_{VV,n}}{\Delta t} \\ &= -C_{VV,1}/\Delta t + C_{VV,n+1}/\Delta t + \sum_{m=1}^{n} \alpha_m G^{CG}_{1+n-m} C_{VV,m}\end{aligned} \tag{6.54}$$

In vector/matrix notation we thus have

$$\boldsymbol{\phi} = -\frac{1}{\Delta t}\boldsymbol{C}^0_{VV} + \frac{1}{\Delta t}\boldsymbol{M}\boldsymbol{C}_{VV} + \frac{1}{\Delta t}\hat{\boldsymbol{G}}\boldsymbol{C}_{VV}. \tag{6.55}$$

where $C^0_{VV,n} = C_{VV}(t=0) = C_{VV,1}$ for all n, and

$$\hat{\boldsymbol{G}} = \begin{bmatrix} 0.5\Delta t G^{CG}_1 & 0 & \dots & 0 \\ 0.5\Delta t G^{CG}_2 & \ddots & \ddots & \vdots \\ \vdots & \ddots & \ddots & \vdots \\ 0.5\Delta t G_N & \Delta t G^{CG}_{N-1} & \dots & 0.5\Delta t G_1 \end{bmatrix} \tag{6.56}$$

and

$$\boldsymbol{M} = \begin{bmatrix} 0 & \dots & \dots & 0 \\ 1 & \ddots & \ddots & \vdots \\ \vdots & \ddots & \ddots & \vdots \\ 0 & \dots & 1 & 0 \end{bmatrix}. \tag{6.57}$$

With this definition of the matrix M, we assume that $C_{VV,n} = 0$ for $n = N$, with N being the total number of entries in $\boldsymbol{C}_{VV}$.

We can also rewrite Eq. 6.53 as a vector/matrix relation as

$$\boldsymbol{C}_{VV} = \boldsymbol{C}^0_{VV} - \hat{\boldsymbol{G}}\boldsymbol{C}_{VV} \tag{6.58}$$

and thus

$$\boldsymbol{C}_{VV} = (\boldsymbol{I} + \hat{\boldsymbol{G}})^{-1}\boldsymbol{C}^0_{VV} \tag{6.59}$$

By combining Eq. 6.59 and Eq. 6.55, we get

$$\begin{aligned}\boldsymbol{\phi} &= -\frac{1}{\Delta t}\boldsymbol{C}^0_{VV} + \frac{1}{\Delta t}\boldsymbol{M}(\boldsymbol{I} + \hat{\boldsymbol{G}})^{-1}\boldsymbol{C}^0_{VV} + \frac{1}{\Delta t}\hat{\boldsymbol{G}}(\boldsymbol{I} + \hat{\boldsymbol{G}})^{-1}\boldsymbol{C}^0_{VV} \\ &= \frac{1}{\Delta t}(-\boldsymbol{C}^0_{VV} + (\boldsymbol{M} + \hat{\boldsymbol{G}})(\boldsymbol{I} + \hat{\boldsymbol{G}})^{-1}\boldsymbol{C}^0_{VV})\end{aligned} \tag{6.60}$$

The inverse matrix $(\boldsymbol{I} + \hat{\boldsymbol{G}})^{-1}$ can be evaluated from the characteristic polynomial of $(\boldsymbol{I} + \hat{\boldsymbol{G}})$ and thus

$$\boldsymbol{\phi} = \frac{1}{\Delta t}\left(-\boldsymbol{C}^0_{VV} + (\boldsymbol{M} + \hat{\boldsymbol{G}})\left(-\frac{1}{\det\left(\boldsymbol{I} + \hat{\boldsymbol{G}}\right)}\sum_{n=1}^{N} c_n(\boldsymbol{I} + \hat{\boldsymbol{G}})^{n-1}\right)\boldsymbol{C}^0_{VV}\right). \tag{6.61}$$

From $G_1^{CG} = 0$ it follows that $\det\left(\boldsymbol{I} + \hat{\boldsymbol{G}}\right) = 1$. Similarly the the coefficients c_n of the characteristic polynomial of $(\boldsymbol{I} + \hat{\boldsymbol{G}})$ can be easily computed because $(\boldsymbol{I} + \hat{\boldsymbol{G}})$ is a triangular matrix where the diagonal elements are 1. The coefficients are given by

$$c_n = (-1)^{N-n} \begin{pmatrix} N \\ n \end{pmatrix}, \tag{6.62}$$

where $\begin{pmatrix} N \\ n \end{pmatrix}$ is a binomial coefficient. Thus Eq. 6.61 can finally be transformed into

$$\boldsymbol{\phi} = \frac{1}{\Delta t}\left(-\boldsymbol{I} + (\boldsymbol{M} + \hat{\boldsymbol{G}})\left(\sum_{n=1}^{N}(-1)^{N-n-1}\begin{pmatrix} N \\ n \end{pmatrix}(\boldsymbol{I} + \hat{\boldsymbol{G}})^{n-1}\right)\right)\boldsymbol{C}_{VV}^{0} \tag{6.63}$$

Any further formal derivation of an exact Newton scheme for the IMRV-2 method becomes notationally cumbersome, so we will only sketch the remaining steps and make some general remarks.

Up to now we only have derived a relation between $\boldsymbol{\phi}$ and $\boldsymbol{G}^{CG}$. To derive a relation with respect to $\tilde{\boldsymbol{K}}$, by using the trapezoid rule, we can set $G_1^{CG} = 0$ and replace every entry G_n^{CG} with $n \neq 1$ in $\hat{\boldsymbol{G}}$ by $G_n^{CG} = \sum_{m=1}^{n} \alpha_m K_m^{CG} = \sum_{m=1}^{n} \alpha_m (\tilde{K}_m + \Delta K_m^{CG})$. Finally one would have to derive the Jacobian, so one would have to compute every partial derivative

$$J_{nm}(\boldsymbol{x}) = \frac{\partial y_n}{\partial x_m} = \frac{\partial \phi_n - \phi_n^{tgt}}{\partial \tilde{K}_m} = \frac{\partial \phi_n}{\partial \tilde{K}_m}. \tag{6.64}$$

As in general, as can be seen from Eq. 6.63, ϕ_n depends on higher powers of the entries in $\tilde{\boldsymbol{K}}$, also the Jacobian will non-linearly depend on the entries of $\tilde{\boldsymbol{K}}$. Furthermore, the Jacobian will clearly involve non-trivial non-diagonal terms. Due to these complications, it is not a-priori clear if, and how efficiently, an exact Newton method for the chosen problem would converge. Additionally, one would have to evaluate partial derivatives of the form

$$\frac{\partial \Delta K_n^{CG}}{\partial \tilde{K}_m}. \tag{6.65}$$

As there is no known exact relation between $\Delta K^{CG}(t)$ and $\tilde{K}(t)$, some approximation has to be invoked for multi-particle systems. One could make use of the same approximation used in the IOMK method, which would in principle allow for a closed form for a quasi-Newton scheme with a well defined Jacobian. If this approximation holds true exactly, both the IOMK method and the reformulation of the IMRV-2 approach would constitute exact Newton methods. Because the relation between the target function and the optimized function in the IOMK method is so simple, the formulation of the IOMK method in such a case guarantees convergence within a single step while for the Newton variant of the IMRV-2 method the Jacobian would still be non-linear in the input function and will have non-trivial non-diagonal elements and thus convergence is not guaranteed even in an ideal case.

Summary

The preceding discussion hints to the origin of the favorable properties of the IOMK method, compared to IMRV-2. By directly optimizing one integrated memory kernel $G^{CG}(t)$ through another integrated memory kernel ($\tilde{G}(t)$) we greatly simplify the relation between the input and the output function and thus a simple path to the optimal input can be found more easily. Even when using exactly the same approximations and

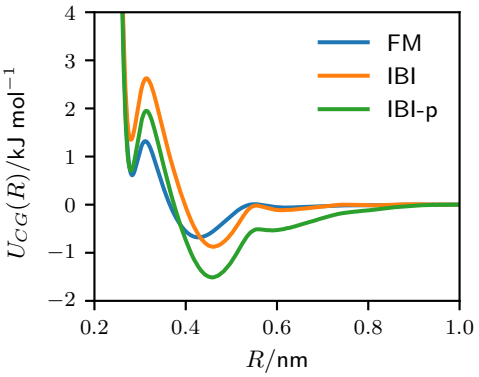

Figure 6.11: Coarse-grained pair potentials.

assumptions, the relation between input and output in the IMRV-2 method are much more complex and the optimization of the input automatically becomes less efficient, even if one would take the considerations of the preceding sections into account. The IMRV-2 method as described in Ref. [30], invokes a Jacobian which is independent on $\tilde{\boldsymbol{K}}_i$, neglecting the the complex relation between $\boldsymbol{\phi}_i$ and $\tilde{\boldsymbol{K}}_i$ and thus its performance is fully determined by tuning parameters.

6.6.3 Pair Potentials and Structure

In Fig. 6.11 we present the CG pair potentials derived using the VOTCA-CSG software.[202] IBI potentials tend to yield too high pressures. Applying a pressure ramp in the derivation of the IBI-p potential reduces the pressure by making the potentials more attractive, without significantly affecting the structure under NVT conditions.

Now we want to evaluate the accuracy of the six CG models in reproducing the structure. In Fig. 6.12 we compare the radial distribution function (RDF) and the angular distribution function (ADF) of the CG models and the AA reference. The ADF is given by

$$P(\Theta) = \left\langle \frac{1}{N_i n_\Theta} \sum_i^{N_i} \sum_j^{n_c} \sum_{k>j}^{n_c} \delta(\Theta - \Theta_{ijk}) \right\rangle , \tag{6.66}$$

where N_i is the number of molecules, n_c is the number of neighbor around an atom i within the cutoff radius of 0.32 nm, Θ_{ijk} is the angle formed by the connecting vector of molecules i and j to the connecting vector between molecules i and k. n_Θ is given by the total number of angles evaluated in the respective frame.

The IBI and the IBI-p model both reproduce the pair structure exactly, as expected. FM yields a CG potential which shows a significantly lower first peak in the RDF and overall yields less structuring. This is inline with findings in literature.[238] Adding three-body contributions allows to achieve a more accurate pair-structure using the FM-method,[238] as is demonstrated with the SW-FM model. This indicates, that the MB-PMF is overall better captured in this model. Also the SW-RE model captures the main features of the pair structure quite well. In particular the first peak is matched. The MW model does not reproduce the structure of SPC/E water, as it was parameterized top-down to recover properties of real water and not to reproduce SPC/E water. The MW model is thus a very good water model but a bad CG SPC/E water model.[249]

In SPC/E water, the maximum of the ADF is found at 104°, which is close to the tetrahedral angle of 109.5°. A minor secondary peak is found at 56 °. For all two-body CG potentials we find that the ADF is

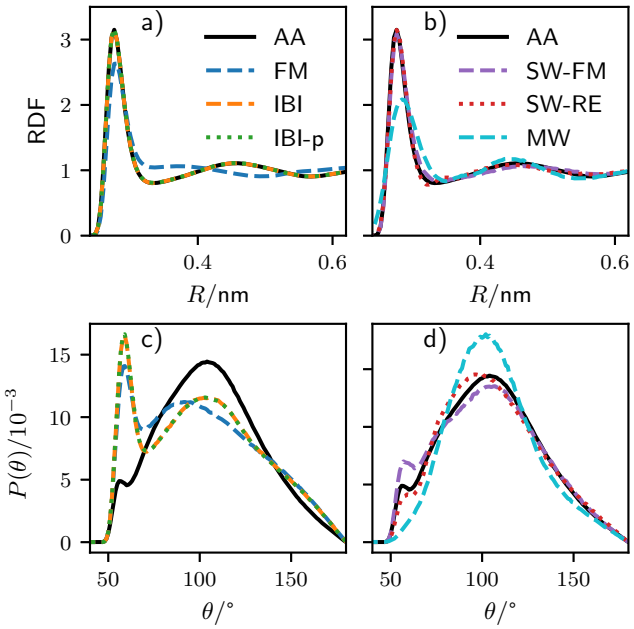

Figure 6.12: RDFs and ADFs of the CG models compared to SPC/E water (AA). In a) and c) we compare the RDFs and ADFs for the pair potentials. In b) and d) we compare the RDFs and ADFs for the SW-type potentials.

not well captured. For the IBI model, we find that the location of the two peaks are well captured, but the relative intensity is interchanged. The lower angle configurations are thus less penalized in the IBI model. The ADF of the FM model is comparable to the IBI model, but shows a slightly shifted and broader second peak. The three-body potentials yield a stronger penalization of small angles, effectively yielding a more pronounced peak at $\theta > 100$. Qualitatively the SW-FM and the SW-RE model capture the ADF very well, inline with the literature.[238, 249] The MW model shows a significant overstructering in the ADF compared to the AA model.

Overall, the structural properties in our simulations are well inline with previous findings in literature, validating the correct implementation of the models.

6.6.4 Memory Kernels

In Fig. 6.13 in the left column we present the memory kernels and its contributions as derived based on the BOD method for all six CG potentials. We also show $\tilde{K}(t) = K_\delta(t) + 2K_X(t)$ and, where applicable, the optimized memory kernel from the IOMK method. (Here we respectively show the memory kernel of the fourth iteration.) In the right column we show the integrals, of the memory kernels, to discern the relative contribution to the total friction.

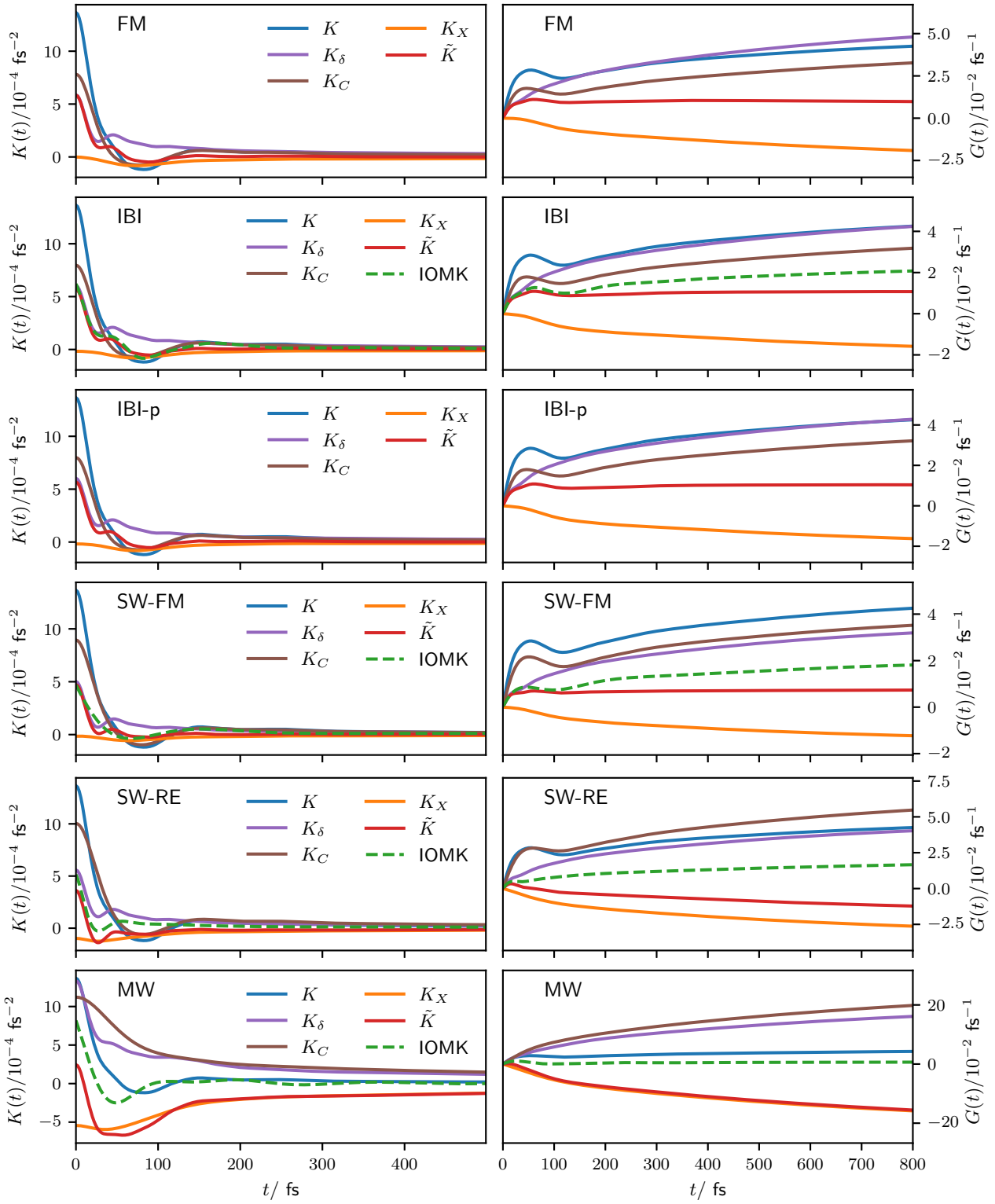

Figure 6.13: Left column: all memory kernels due to the BOD method for all potentials. We also show $\tilde{K}(t)$ and, where applicable, the optimized memory kernel due to the IOMK method. Right column: respective integrals of the memory kernels.

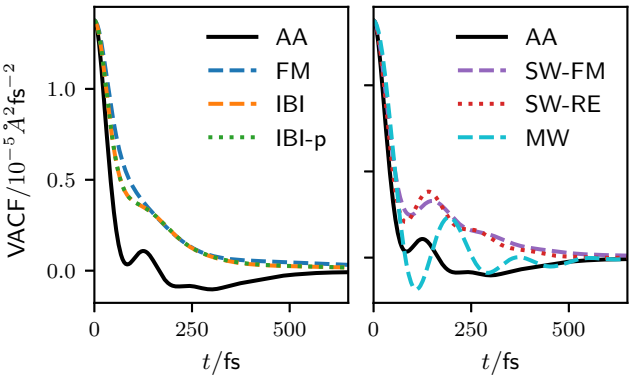

Figure 6.14: VACFs for all CG-MD simulations (applying a Nosé-Hoover thermostat) for all CG pair potentials (left column) and all SW-type potentials (right column) compared to the AA reference.

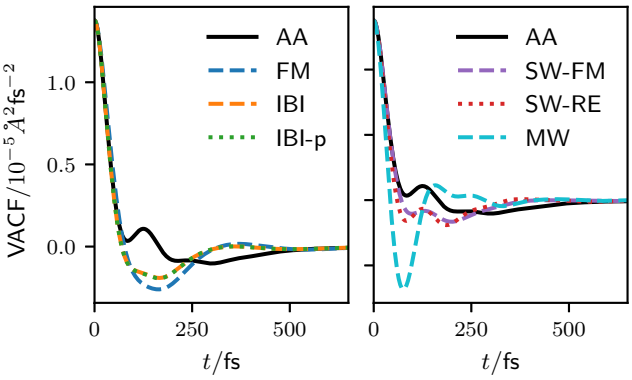

Figure 6.15: VACFs for all K_δ-simulations simulations for all CG pair potentials (left column) and all SW-type potentials (right column) compared to the AA reference.

6.6.5 Dynamics of Non-Dissipative Models

In this section, we study the dynamics of the different CG models using standard molecular dynamics simulations, without taking dissipation into account. This allows to get an basic intuition of the influence the different conservative potentials have on the dynamics of the final GLE models. In Fig. 6.14 the VACFs for the two-body and three-body respectively are compared with the AA reference.

For the IBI model, between 75 fs and 150 fs the VACF exhibits a pronounced *kink*. This feature is present on a comparable time scale, as the first local minimum and local maximum of the AA VACF. For the FM model, no comparable feature is found. This can be explained by the fact that the FM model is less structured than the IBI model, exhibiting a lower first peak in the RDF. The dynamics at 75-150 fs is thus probably linked to the collisions of the water molecules within cage of neighboring water molecules. The three-body potentials all yield significantly more pronounced features on this time scale which is related to the increased tetrahedral structuring. In particular the VACF of the SW-FM and the SW-RE model qualitatively reproduce the position of the first local minimum and the local maximum of the VACF of in the AA model. On times smaller than 100 fs the VACF of the FM model decays significantly slower than for the IBI model.

The VACFs of the SW-type models shown in Fig. 6.14 exhibit additional distinguished features. In particular the VACFs here show a local minimum around 100 fs. This feature is also found in the AA model. This indicates that this feature in the AA reference can, at least partially, be attributed to features in the MB-PMF and is not purely due to the internal DoFs. Still, as shown in the main text, $\tilde{K}(t)$ encodes these features and allows to correct the VACF on these time scales.

6.6.6 Dynamics of Dissipative Models

In Figs. 6.15-6.17 we present the VACFs for all bottom-up parameterizations based on the BOD method (K_δ, $K_{\delta,X} = K_\delta + K_X$ and $\tilde{K} = K_\delta + 2K_X$) for all CG potentials (including IBI-p and MW). This allows to discern the effect of including or excluding the cross-correlation term $K_X(t)$ in the parameterization of the GLE thermostat. In the left column Fig. 6.19 we show the VACFs of all studied models, including the IOMK models (for IBI, SW-FM, SW-RE and MW), while we respectively show the the fourth iteration. For

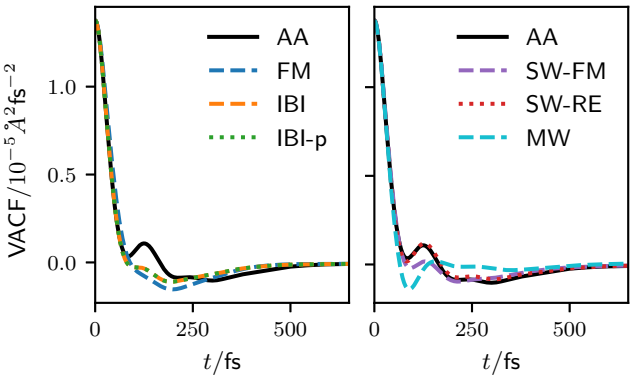

Figure 6.16: VACFs for all $K_{\delta,X}$-simulations simulations for all CG pair potentials (left column) and all SW-type potentials (right column) compared to the AA reference.

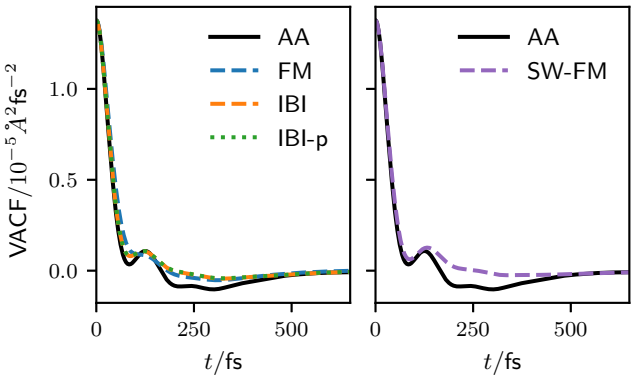

Figure 6.17: VACFs for all $\tilde{K}$-simulations simulations for all CG pair potentials (left column) and SW-FM potential (right column) compared to the AA reference.

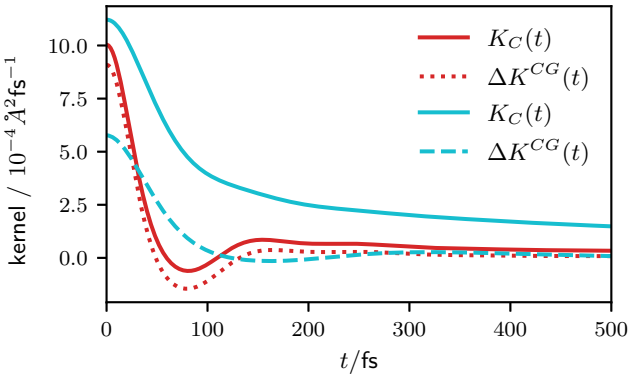

Figure 6.18: Memory due to conservative interactions ($\Delta K^{CG}(t)$) the the SW-RE and the MW model, in GLE thermostat simulations parameterized with $K_{\delta,X}(t)$, compared to the prediction due to the BOD method ($K_C(t)$).

the IBI potential we also present the VACF of the Markovian model mentioned in the main text. In in the right column of Fig. 6.19 we present the integrals $D(t)$ of the respective VACFs. The plateau values of $D(t)$ represent the diffusion coefficient.

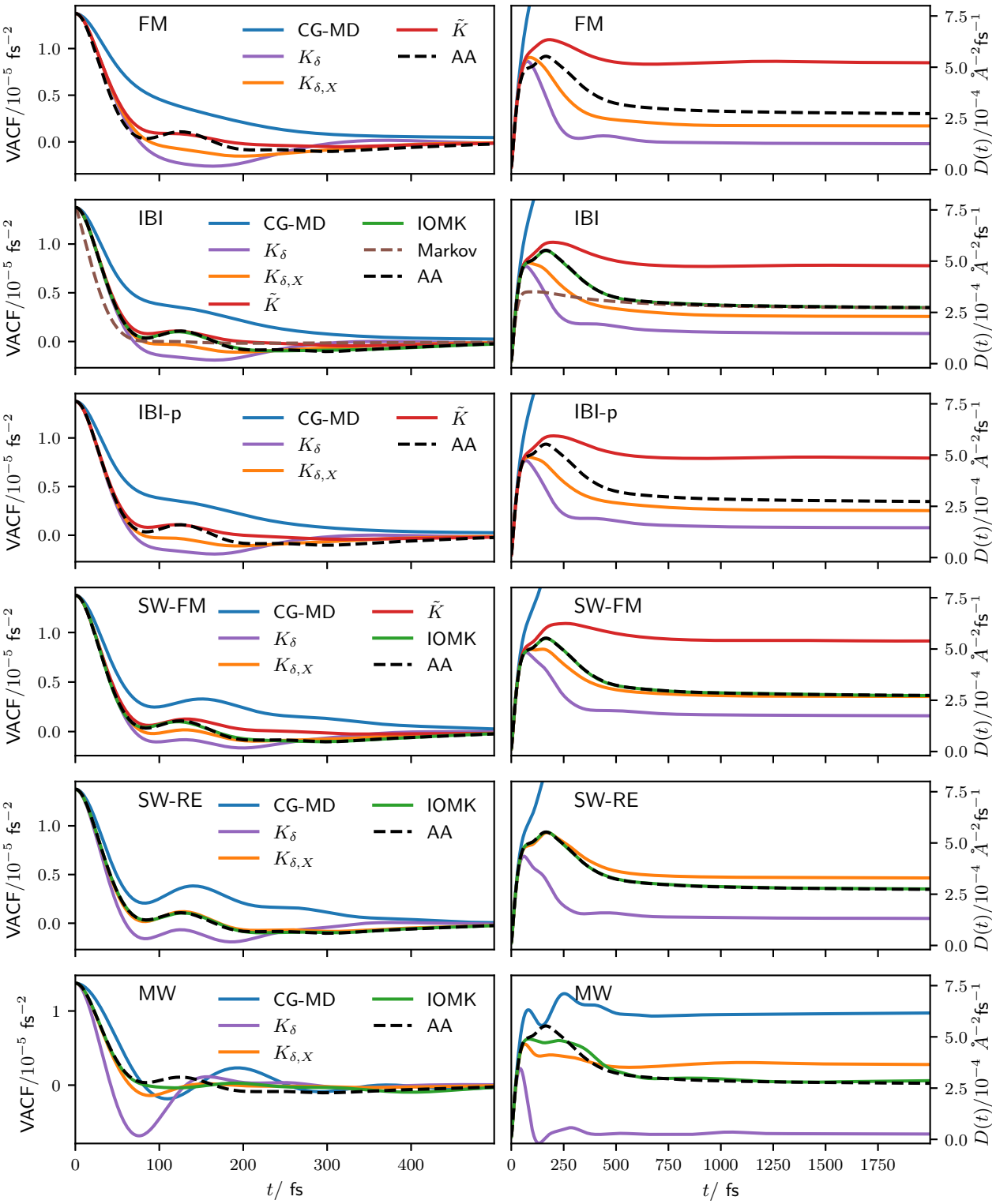

Figure 6.19: All VACFs (left column) and respective integrals $D(t)$ (right column) for all CG potentials and GLE thermostat parameterizations, including the optimized Markovian IBI model, compared to the AA reference.

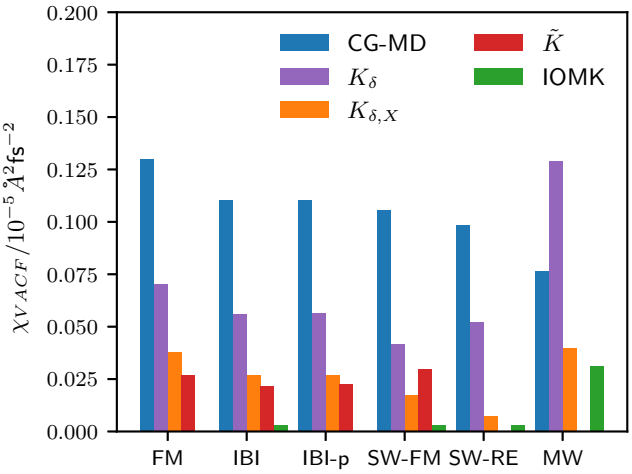

Figure 6.20: Error estimate of the VACF, for all CG simulations.

For all pair potentials, and for the SW-FM model, the $\tilde{K}$-model yields the most accurate representation on short and intermediate time scales, which is inline with earlier findings.[33, 34] In particular the shape of the VACF at ≈70-150 fs is modulated by introducing $K_X(t)$, such that the match with the AA reference is significantly improved. For $t > 250$ fs the $K_{\delta,X}$ models tend to perform better. For the SW-RE model and the MW model, a meaningful parameterization with $\tilde{K}(t)$ is not possible. This is directly evident by comparing $G_C(t)$ and $G(t)$ in Fig. 6.13. For these two models the BOD method predicts that $G_C(t) > G(t)$, which is incompatible with the fluctuation-dissipation theorem and incompatible with the idea that the reduction of DoFs should decrease friction. This indicates that the BOD method clearly overestimates the friction induced due to conservative interactions, which we can validate by comparing $K_C(t)$ with $\Delta K^{CG}(t)$ for the SW-RE and the MW models (in $K_{\delta,X}$-simulations) as shown in Fig. 6.18.

Interestingly, by considering $K_{\delta,X}(t)$ for the SW-RE potential, very good results can be achieved. Arguably this is, to some extent, due to error cancellation. The complete neglection of $K_X(t)$, by parameterizing the GLE thermostat using $K_\delta(t)$, always yields significant discrepancies.

As discussed in the main text and as can be seen from the plateau values of $D(t)$ in Fig. 6.19, the diffusion coefficient is typically overpredicted with $\tilde{K}(t)$. Using $K_{\delta,X}(t)$ instead generally, at least for the pair potentials, tends to underpredict the diffusion coefficient. Still, for practical purposes, $K_{\delta,X}(t)$ might be a reasonable estimate for the parameterization of CG GLE models as it can be readily derived from alternative approaches.[33]

A summary of the error estimates for all studied models is shown in Fig. 6.20.

6.6.7 Further Results from the IOMK Method

Convergence

In Fig. 6.21 we present the error χ_{VACF} for the the three iterative methods (IOMK, IMRV-1, IMRV-2), over successive iterations. In this representation, one can see clearly that the IOMK method converges much faster that the IMRV-2 method, while the IMRV-1 diverges.

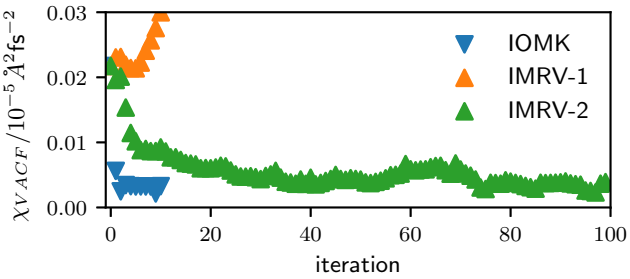

Figure 6.21: Here we illustrate the convergence properties of the three applied iterative methods by plotting the estimated error against the iteration.

Alternative initial guesses

In the main text we discussed, that the IOMK method can also be applied with alternative initial guesses for the memory kernel. A prominent estimate for such a memory kernel can be readily computed from the force-correlation function of fluctuating forces δF[36, 39] and is given by $\tilde{G}_0(t) = \int_0^t ds C_{\delta F \delta F}(s)/(M_I k_B T)$. To further test the dependence of the convergence of the IOMK method on the initial guess, we also considered $\tilde{G}_0(t) = \int_0^t ds 0.1 \cdot C_{\delta F \delta F}(s)/(M_I k_B T)$ as initial guess. The results for both the IOMK and the IMRV-2 method are given in Figs. 6.22 and 6.23, respectively. We find that the number of needed iterations does not strongly depend on the initial guess, for either of the two methods. The IOMK-method again converges within the first few steps, while the IMRV-2 method needs roughly ten times as many iterations to yield comparable results.

IOMK for SW-type potentials

In the main text we discussed the IOMK models for the SW-FM and the SW-RE potentials. In Figs. 6.24 and 6.25 we present the VACFs and the integrals $D(t)$ for all iterations. We find that also for the SW-type potentials the IOMK-method yields satisfactory results within few iterations.

We also applied the IOMK method to the top-down MW model. By trying to match the dynamic properties of SPC/E water in combination with an empirical CG model one has to consider the caveat, that it is not guaranteed that a parameterization of the GLE thermostat can be found to match the SPC/E water dynamics exactly. Still, as the SPC/E model reproduces some dynamic properties of real water quite accurately,[243, 249] matching the dynamics of SPC/E water with MW would simultaneously allow to derive a model more closely representing experiments.

In Fig. 6.26 we show the results from applying the IOMK-method to the MW model. The MW water model, on certain time scales, exerts friction due to conservative interactions exceeding the total friction in the SPC/E model. The IOMK-method in such a case yields memory kernels, which are not easy to fit with dampened oscillators. Thus we could not derive a GLE thermostat parameterization which yields an exact match of the target VACF. Still, the IOMK-method allows a closer representation of the reference and in particular allows to match the plateau of the integral of the VACF and thus the diffusion coefficient.

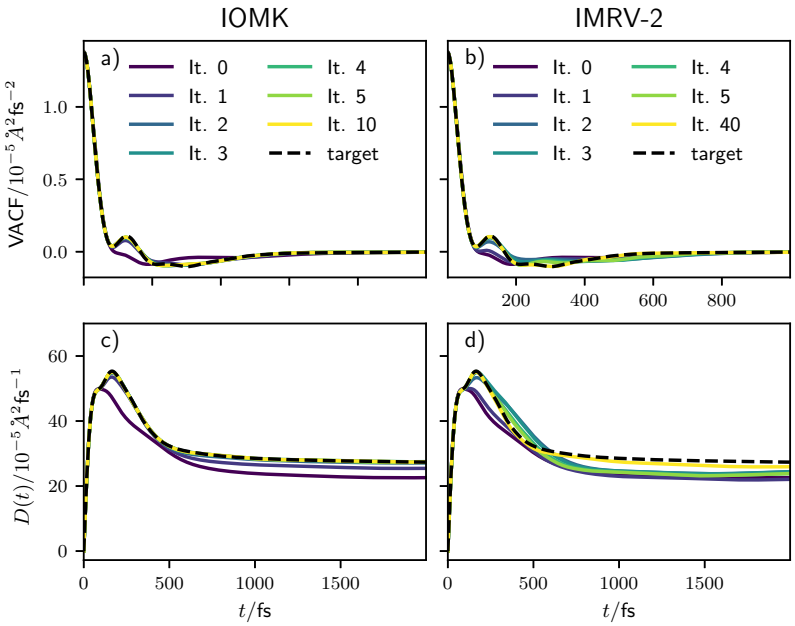

Figure 6.22: Results for iterative optimization of memory kernels for the IBI model. a) and b): Comparison of the VACF for the IOMK and IMRV-2 method, respectively. c) and d): Comparison of $D(t)$ for the IOMK and IMRV-2 method, respectively. Here $\tilde{G}_0(t) = \int_0^t ds C_{\delta F \delta F}(s)/(M_I k_B T)$ was applied as initial guess.

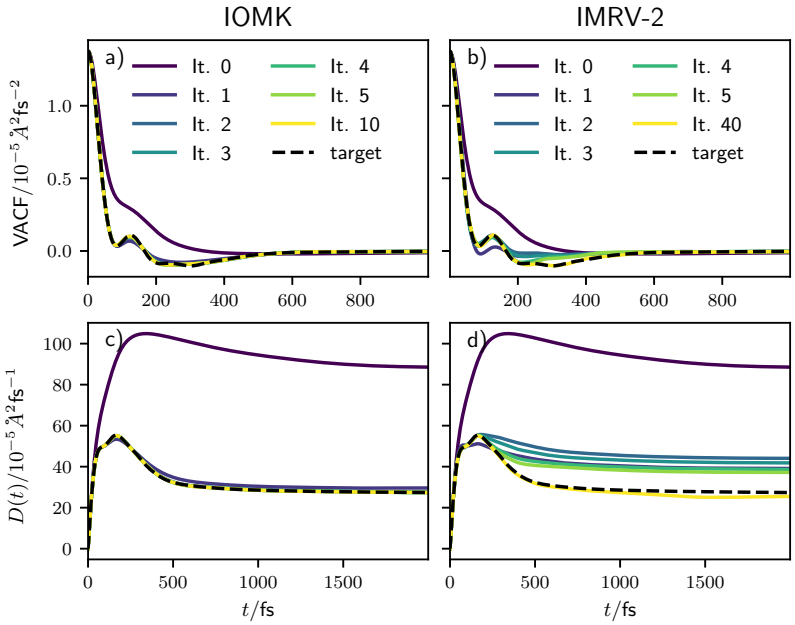

Figure 6.23: Results for iterative optimization of memory kernels for the IBI model. a) and b): Comparison of the VACF for the IOMK and IMRV-2 method, respectively. c) and d): Comparison of $D(t)$ for the IOMK and IMRV-2 method, respectively. Here $\tilde{G}_0(t) = \int_0^t ds 0.1 \cdot C_{\delta F \delta F}(s)/(M_I k_B T)$ was applied as initial guess.

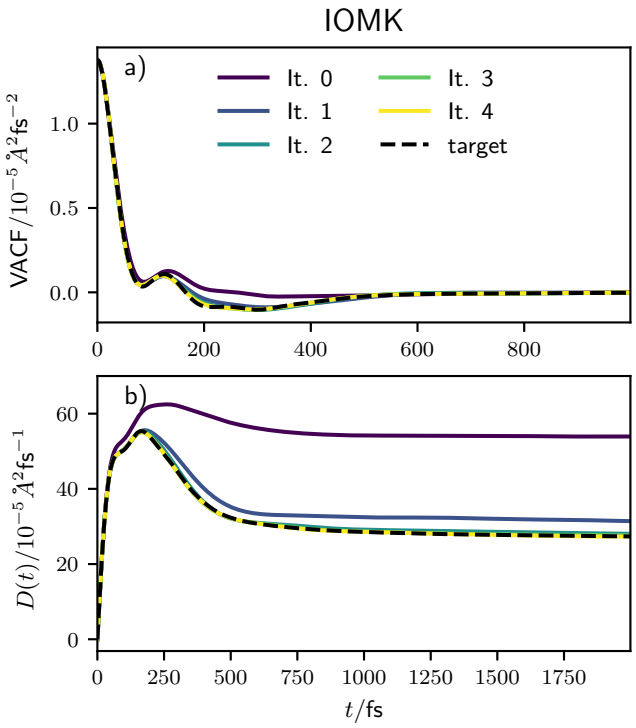

Figure 6.24: Results for iterative optimization of memory kernels by means of the IOMK-method for the SW-FM model. a): VACFs of successive iterations. b): $D(t)$ of successive iterations. Here $\tilde{G}_0(t) = \int_0^t ds\tilde{K}(s)$ was applied as initial guess.

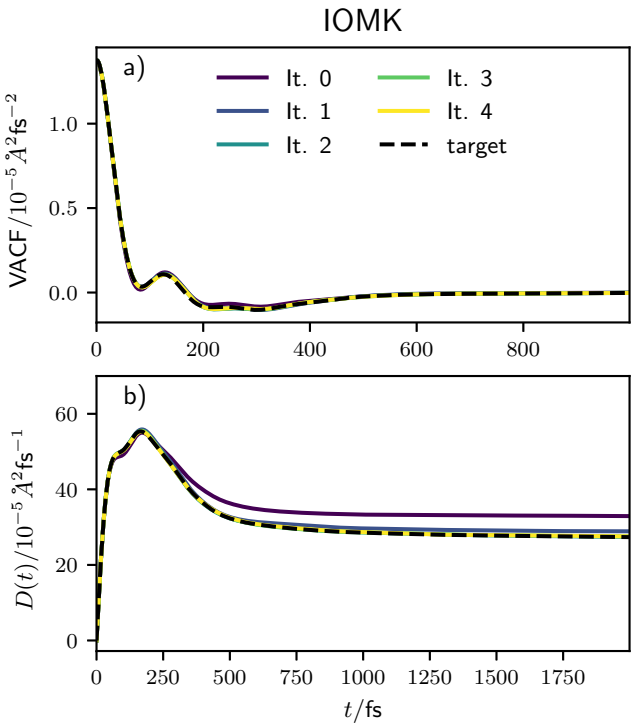

Figure 6.25: Results for iterative optimization of memory kernels by means of the IOMK-method for the SW-RE model. a): VACFs of successive iterations. b): $D(t)$ of successive iterations. Here $\tilde{G}_0(t) = \int_0^t ds K_{\delta,X}(s)$ was applied as initial guess.

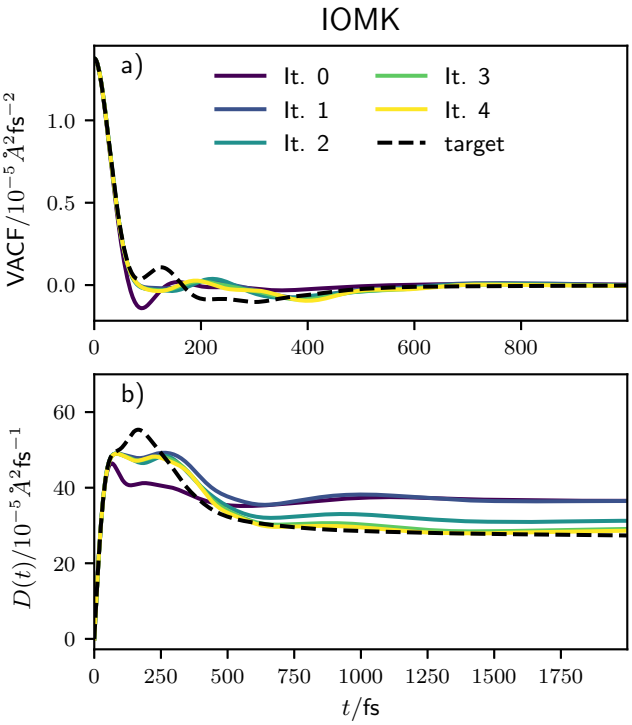

Figure 6.26: Results for iterative optimization of memory kernels by means of the IOMK-method for the MW model. a): VACFs of successive iterations. b): $D(t)$ of successive iterations. Here $\tilde{G}_0(t) = \int_0^t ds K_{\delta,X}(s)$ was applied as initial guess.

6.6.8 Van Hove Function

In the main text we have presented the distinct Van Hove function (VHF) for a limited set of studied systems. Here we show the VHF for all CG models, compared to the AA reference, including the FM and the MW model, which do not correctly represent the pair-structure of the AA reference and thus naturally cannot fully capture the structural relaxation (at least on short time scales). For completeness we also show the VHF for the IBI-p models, while the IBI and the IBI-p model do not show any significant deviation on any measure studied in this work. In Figs. 6.27, 6.29, 6.31, 6.33, 6.35 and 6.37 we show all VHFs for the FM, IBI, IBI-p, SW-FM, SW-RE, and MW models in the same representation as in the main text, and in Figs. 6.28, 6.30, 6.32, 6.34, 6.36 and 6.38 the respective slices at $R = 0.278$ nm and $R = 0.2$ nm. Finally, in Fig. 6.39 we summarize the errors χ_{VH} as defined in the main text, including the FM-, IBI-p- and MW-modles.

The results for the IBI-p models do not differ significantly from the results for the IBI models.

For the FM and the MW model we find, that due to the difference of the pair structure compared to the AA reference, the VHF cannot be matched on short time scales. Still, the application of the GLE thermostat, parameterized with $\tilde{K}(t)$ (FM) or $K_{\delta,X}(t)$ (MW) significantly improves the match of the structural relaxation with the AA reference. In particular, the relaxation of the first peak, beyond a certain time scale, is well matched in both cases.

The optimization of the MW model with the IOMK method further improves the match with the AA reference for the MW potential, especially for shorter length scales.

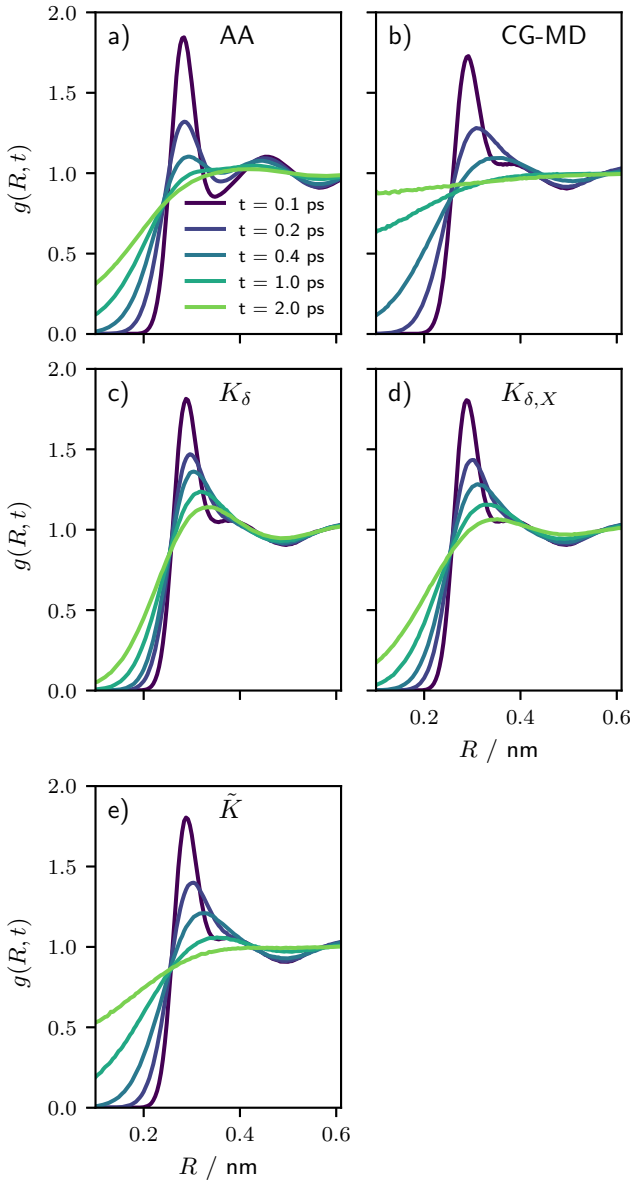

Figure 6.27: Distinct VHF for all FM models, compared to the AA reference.

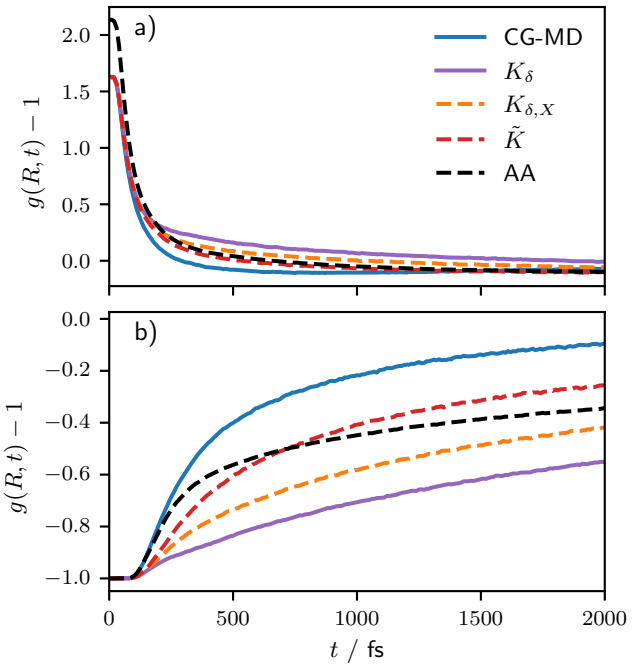

Figure 6.28: Distinct VHF at a) $R = 0.276$ nm and b) $R = 0.2$ nm, all FM models compared to the AA reference.

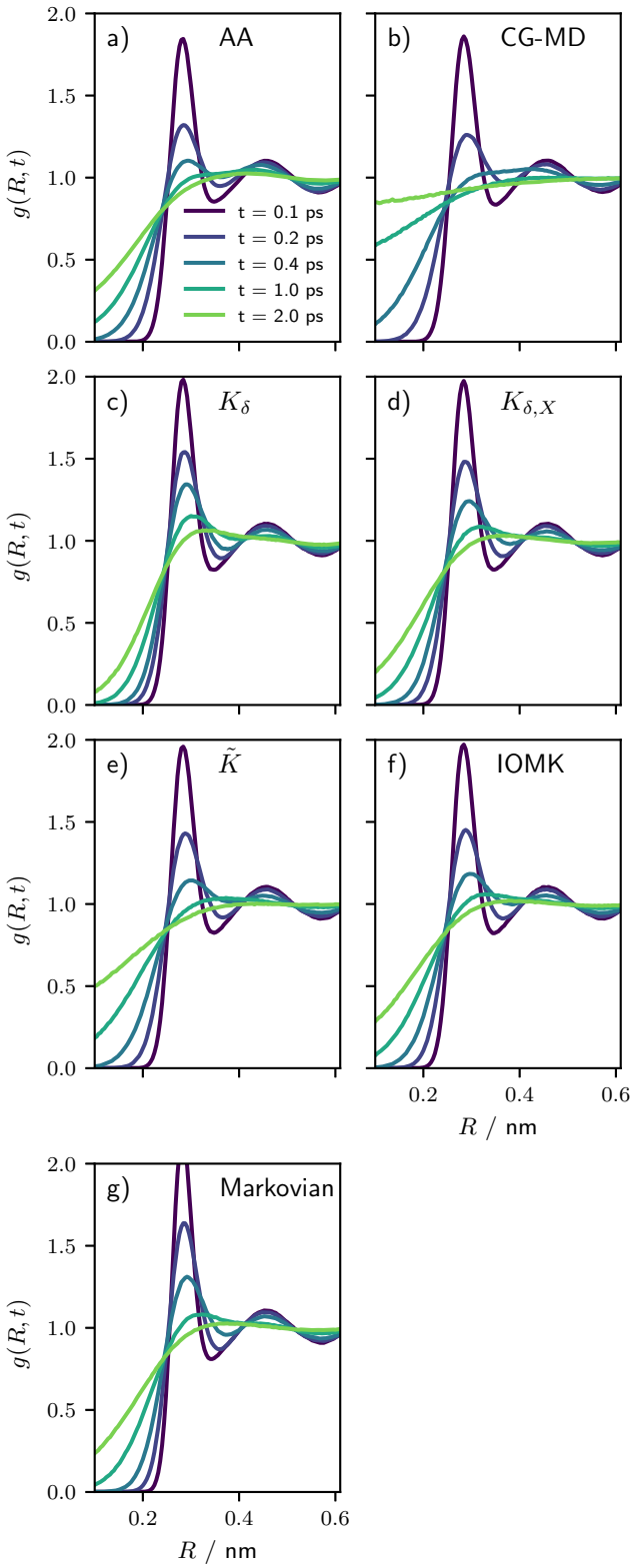

Figure 6.29: Distinct VHF for all IBI models, compared to the AA reference.

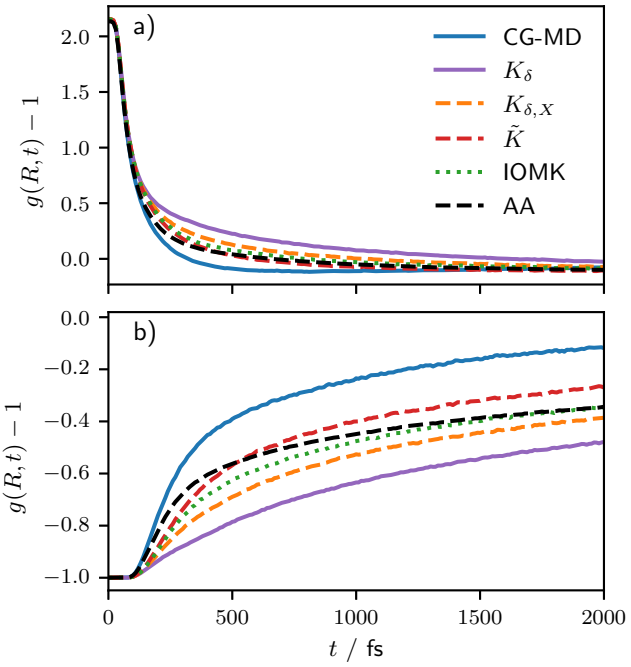

Figure 6.30: Distinct VHF at a) $R = 0.276$ nm and b) $R = 0.2$ nm, all IBI models compared to the AA reference.

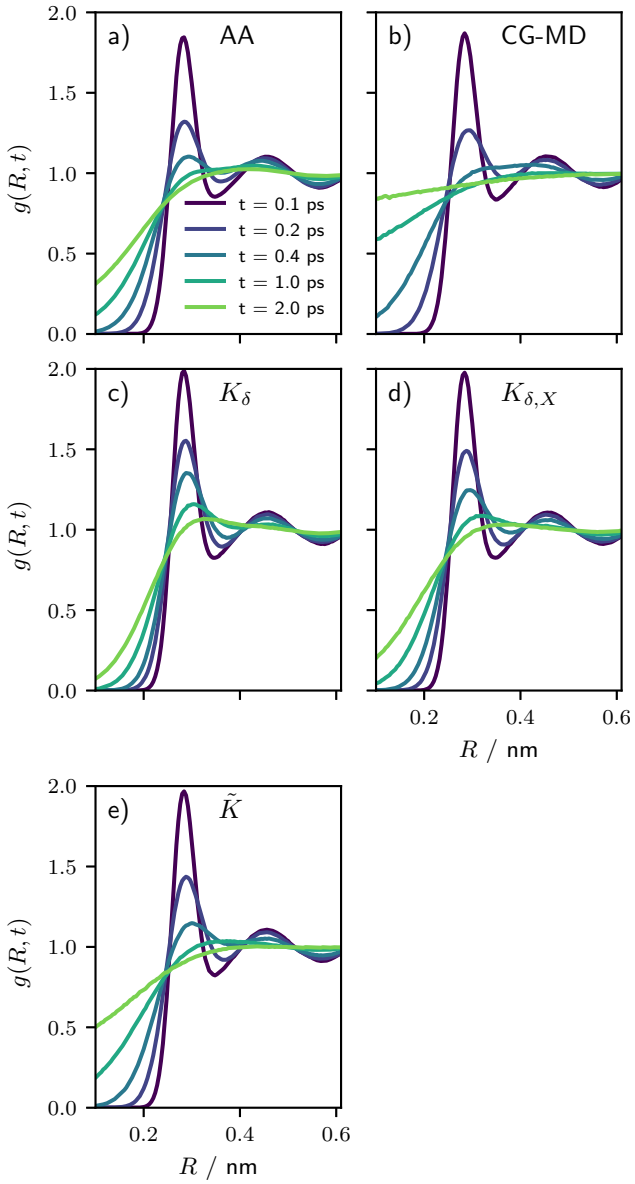

Figure 6.31: Distinct VHF for all IBI-p models, compared to the AA reference.

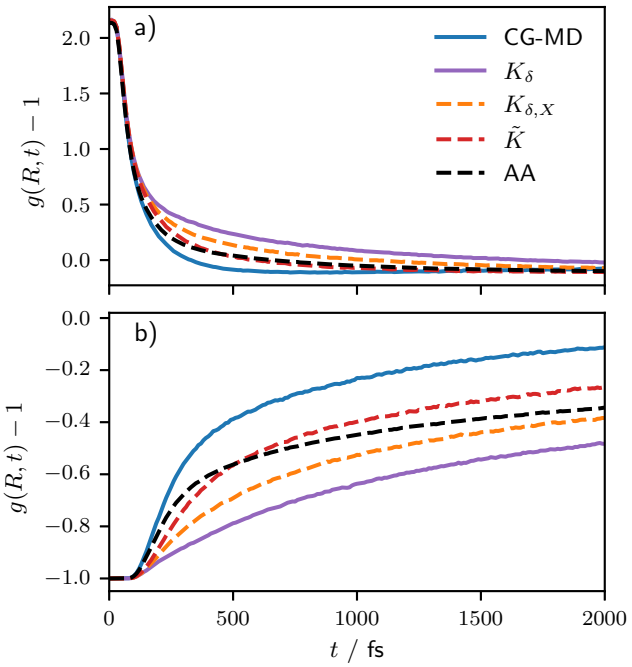

Figure 6.32: Distinct VHF at a) $R = 0.276$ nm and b) $R = 0.2$ nm, all IBI-p models compared to the AA reference.

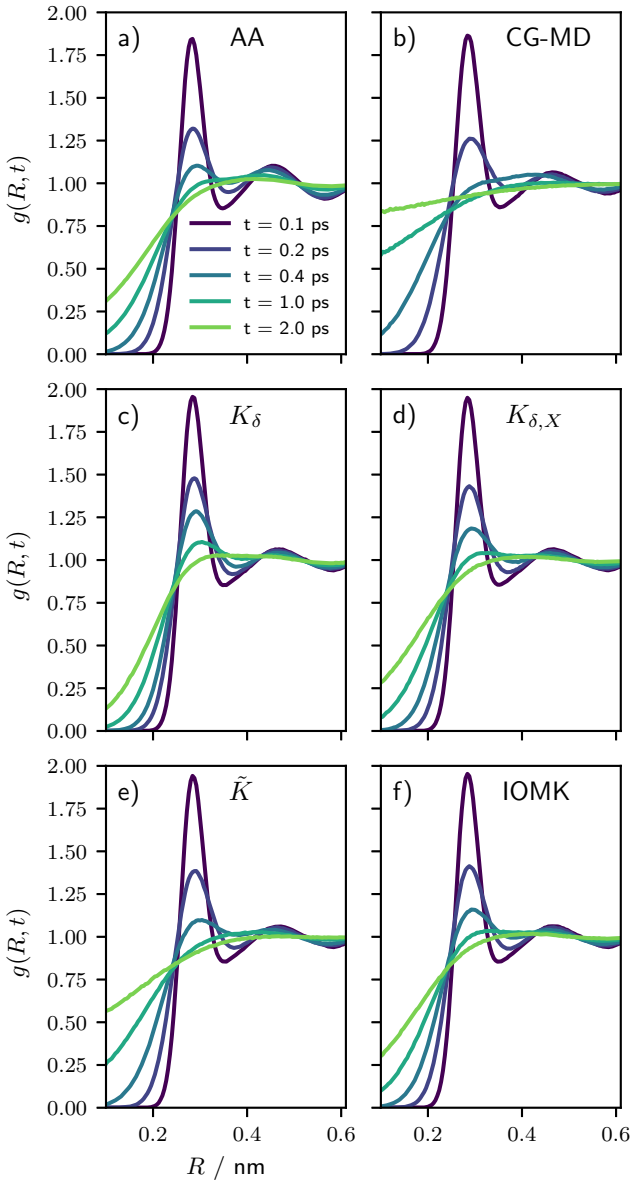

Figure 6.33: Distinct VHF for all SW-FM models, compared to the AA reference.

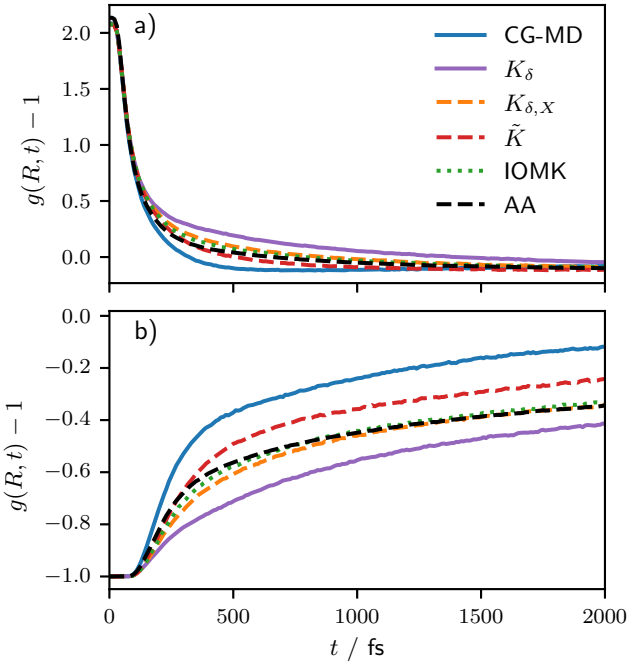

Figure 6.34: Distinct VHF at a) $R = 0.276$ nm and b) $R = 0.2$ nm, all SW-FM models compared to the AA reference.

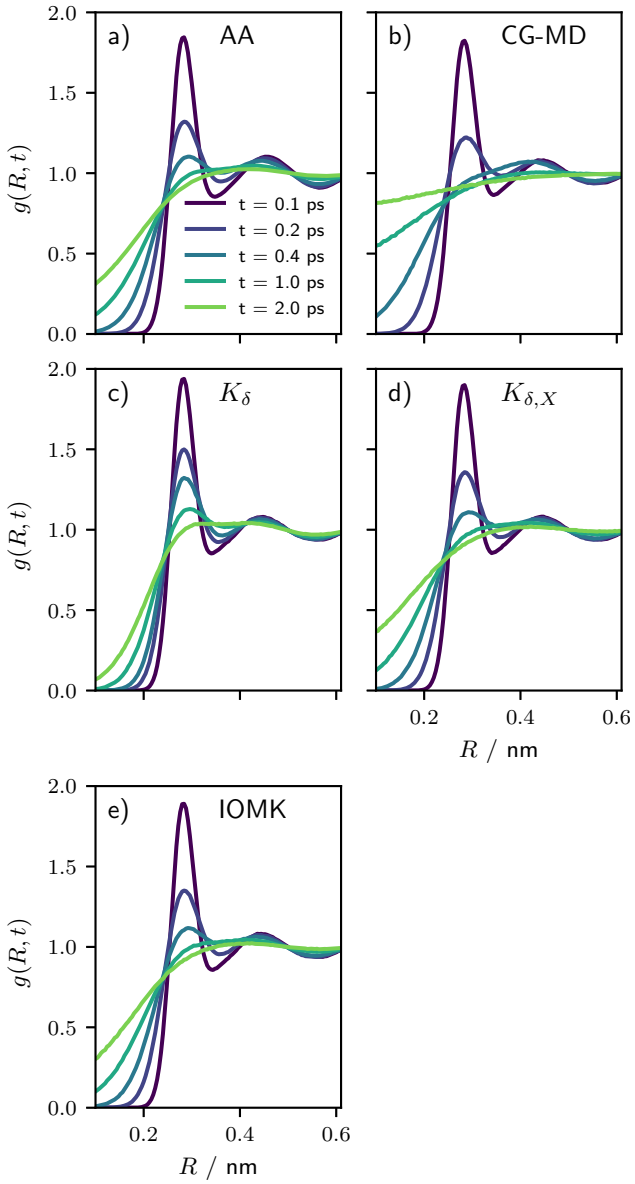

Figure 6.35: Distinct VHF for all SW-RE models, compared to the AA reference.

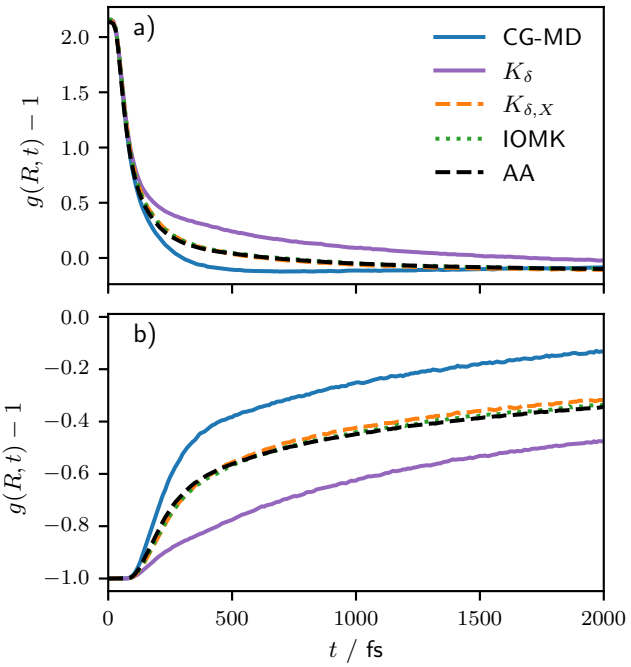

Figure 6.36: Distinct VHF at a) $R = 0.276$ nm and b) $R = 0.2$ nm, all SW-RE models compared to the AA reference.

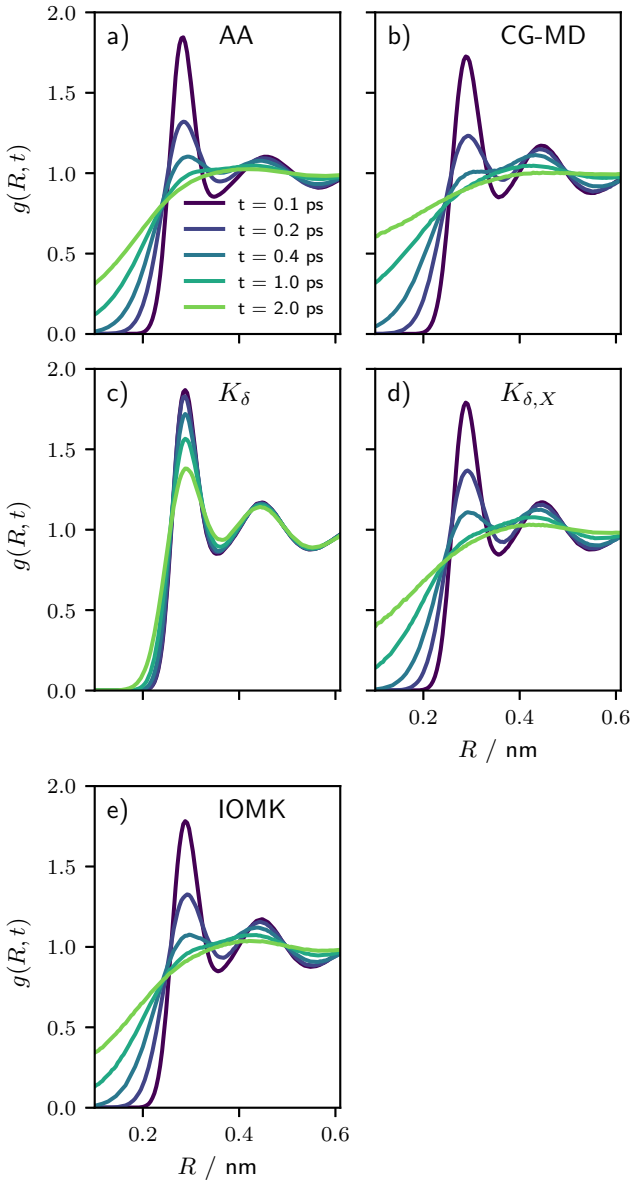

Figure 6.37: Distinct VHF for all MW models, compared to the AA reference.

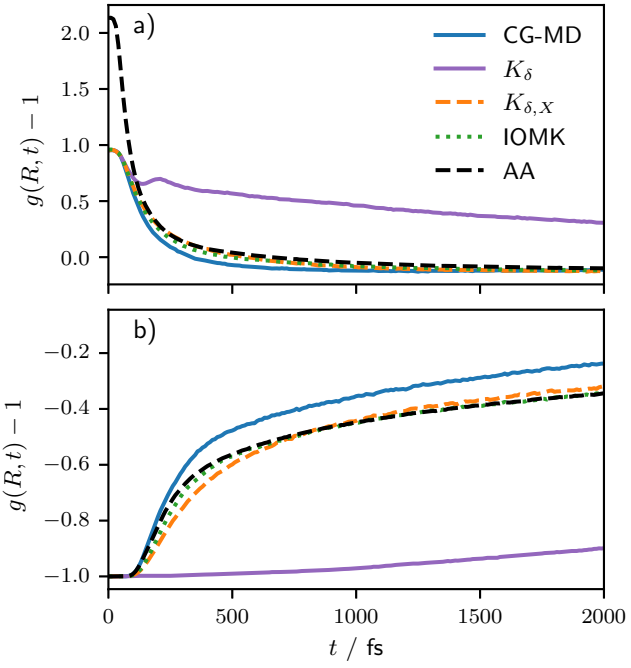

Figure 6.38: Distinct VHF at a) $R = 0.276$ nm and b) $R = 0.2$ nm, all MW models compared to the AA reference.

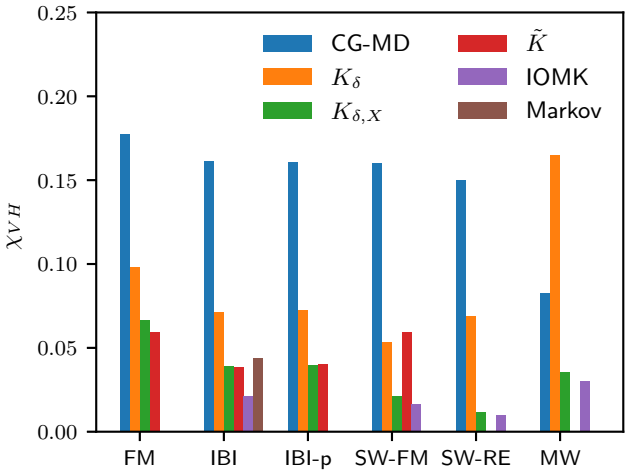

Figure 6.39: Error estimate for the distinct VHF for all studied models.

7 Preliminary Results and Conceptualization of Ideas for Future Research

In this chapter, preliminary results and ideas for not yet fully solved problems are discussed. In Sec. 7.1, the potential hurdles in applying the IOMK method to systems with bonds on the CG scale are discussed and potential solutions proposed. In Sec. 7.2, a reformulations of the IOMK-method in terms of a Gauss-Newton method is proposed, which would allow for a direct optimization of parameters in an auxiliary variable GLE-thermostat rather than optimizing the memory kernel in a non-Markovian GLE.

7.1 Extending the IOMK-Method for Mapping Schemes Involving Bonds

In the previous chapters, only mapping schemes were considered in which no bonded interactions are present on the CG scale. In coarse-graining soft matter systems, e.g. polymers, depending on the properties of interest, it may be desirable to retain a certain degree of detail in the CG model, such that the molecular nature of the studied system is preserved. In such cases, it was shown that additional complications in dynamic coarse-graining can occur.[65] The specific complications may depend on the chosen EoM and on the strategy in its parametrization. This is why in this section one of the systems described in Ref. [65] is revisited.

Deichmann in Ref. [65] applied a bottom-up strategy for the parameterization of different CG Markovian DPD models for neopentane and N-mers of neopentane repeat units. While this work was very successful in the development of CG models which faithfully represent diffusion coefficients in the systems with low viscosity (monomeric and dimeric liquids and a low concentration polymer solution), this could not be achieved in systems with high viscosity (the polymer melt, high concentration polymer solution and penetrant diffusion in polymer networks). Interestingly, even in the case of the dimeric liquid, the correct representation of the diffusion coefficient does not seem to translate to a correct representation of

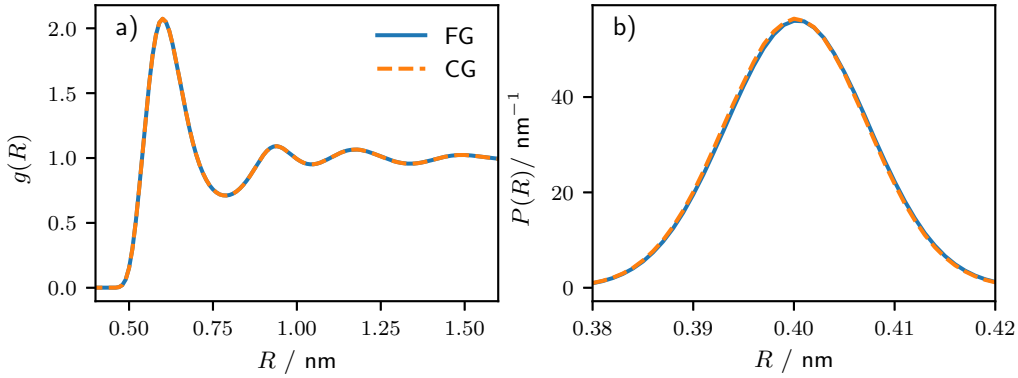

Figure 7.1: a) Comparison of the radial distribution function between the COM of NEP units and b) bond distribution for FG and CG simulations of DNEP.

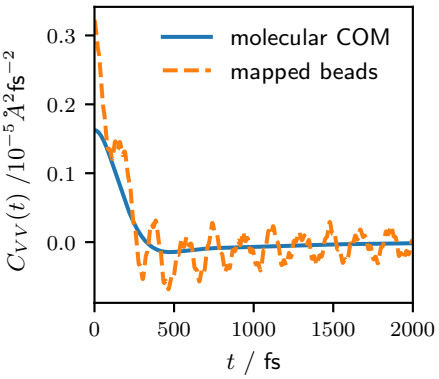

Figure 7.2: VACF for the FG DNEP system, based on the COM and the two-bead mapping scheme.

rotational dynamics of the molecules.

To better understand the origin of this shortcoming, the IOMK method is extended in this section for systems with bonds on the CG level, by revisiting the dimer system (dineopentane (DNEP)) of Ref. [65]. The FG reference system is modeled by using the TraPPE-UA[252] force field with flexible bonds.

As the previous chapters indicate, an exact match of structural properties usually also improves dynamic properties. Thus the CG interactions are derived using the IMC method,[10] as implemented in the VOTCA[202] software package. In Fig. 7.1, the structural properties in terms of the RDF ($g(R)$) and the bond length probability distribution ($P(R)$) are compared between the FG and the CG model and it is found that structural properties are successfully reproduced.

7.1.1 High Frequency Modes in Bonded Mapping Schemes

In Fig. 7.2 the VACFs from FG simulations are shown, both for the center-of-mass (COM) motion of the whole molecule, and for the CG beads based on the mapping scheme of Ref. [65].

While the VACF for the COM-mapping is very smooth, as is the case for all systems studied in the previous chapters, for the two-bead mapping the VACF shows high-frequency modes induced by intramolecular interactions between the mapped beads. With a naive application of the IOMK method, the target effective memory kernel would be given by the inversion of the VACF (see Eq. 3.33) of the two-bead mapping. The respective integrated memory kernel $G(t)$ is shown in Fig. 7.3 a) (FG two-bead), alongside the integrated memory kernel for the COM mapping and a CG-MD simulation.

As expected, the memory kernel for the COM mapping is very smooth, and would make an easy target for the IOMK method. The memory kernel for the two-bead mapping scheme on the other hand, appears to be noisy. The direct comparison of the two memory kernels implies that the origin of the high-frequency modes lies in the intramolecular interactions. Due to Newton's third law, intramolecular interactions do not have any direct effect on the center of mass motions of the molecule, as all intramolecular forces are symmetrically counteracted by an equal counterforce. The motion of the individual bead however contains high-frequency components due to its intramolecular bond defined by the two-bead mapping. Now the intramolecular forces on the first bead due to interactions with the second bead, do affect the dynamics of the former. These intramolecular forces are dominated by high frequency bonded interactions. The single-particle memory kernel (Eq. 3.26) from a FG trajectory with a two-bead mapping captures all high-frequency intramolecular interactions alongside the interactions with the medium. This results in an apparently noisy memory kernel as seen in Fig. 7.3 a). Using this memory function as a target in the IOMK method introduces a set of potential problems. Two technical problems arise from the complexity of the

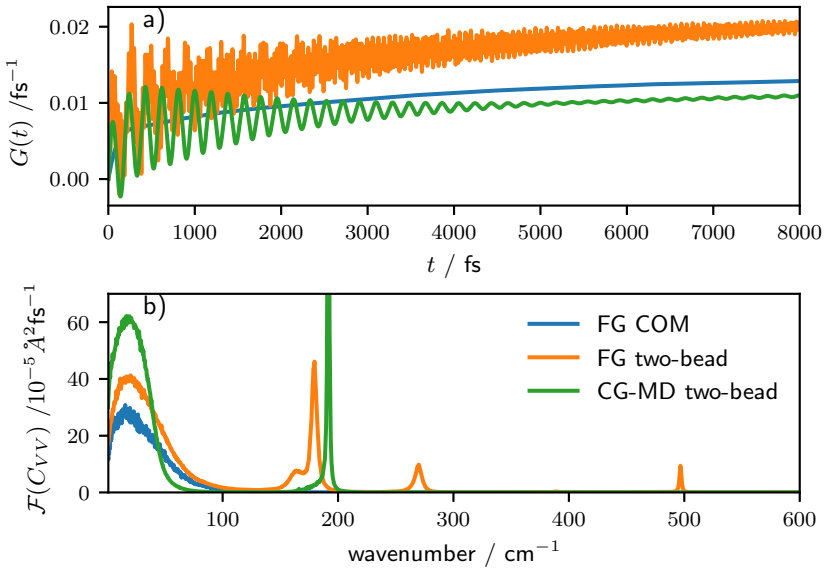

Figure 7.3: a) The integrated memory kernel $G(t)$ as derived from the VACF for the COM and the two-bead mapping scheme based on FG trajectories. For comparison, also the integrated memory kernel from CG-MD simulations are shown. As the CG model involves a bonded interaction, the fluctuations induced by the bond are also represented in $G(t)$, leading to strong fluctuations. b) Fourier-transform of the VACF for the COM and two-bead mapping scheme based on FG trajectories. For comparison, also results from CG-MD simulations are shown. The CG-MD results indicate increased diffusivity and a blue shift in the bond frequency at $\approx$ 200 cm^{-1}.

target memory kernel itself. Firstly, the IOMK method is based on the assumption given by Eq. 3.66, which was demonstrated to hold very well at long time scales. Still, it is not clear if this relation holds to the same extent for memory kernels of such a complex form as in the current case. Secondly, a problem arises due to the fitting of memory kernels needed for the parameterization of the auxiliary variable GLE thermostat. It is unclear if it is meaningful to attempt to match the high frequency modes to a high degree of accuracy. The reason for that is that they originate from intramolecular interactions. The simple isotropic GLE thermostat applied in the current work, cannot capture this fact, as it applies friction and noise independently to every bead. So even if one were able to capture the correct VACF on the single bead level (in the two-bead representation) through matching the respective integrated single particle memory kernel, the effect of the GLE-thermostat would not capture the momentum conserving nature of the interactions from which the high frequency modes arise. This would predictably lead to spurious features in the COM dynamics.

A more promising strategy might be to neglect the high-frequency interactions due to intramolecular interactions in the first place. As the goal is to have a CG model it is not necessarily desirable to preserve all features from the FG scale if they do not affect any relevant features on the CG scale. So the question is, how can the IOMK method be extended to CG models with bonds, while only targeting the low frequency modes of the dynamics. Some kind of "smoothing" has to be applied to the memory kernel, and clearly there are different approaches which could be explored. In the following, a single straight-forward approach is described.

Firstly, the reference VACF is Fourier transformed ($\mathcal{C}_{\mathcal{VV}}$ in Fig. 7.3 b)). In this representation, the features which shall be neglected in the CG process are easy to distinguish. From the Fourier transform of the CG-MD simulation the bond-stretching mode can be easily identified. This bond-stretching mode is the lowest frequency mode, which shall be neglected. Thus the Fourier transform is set to zero, for all

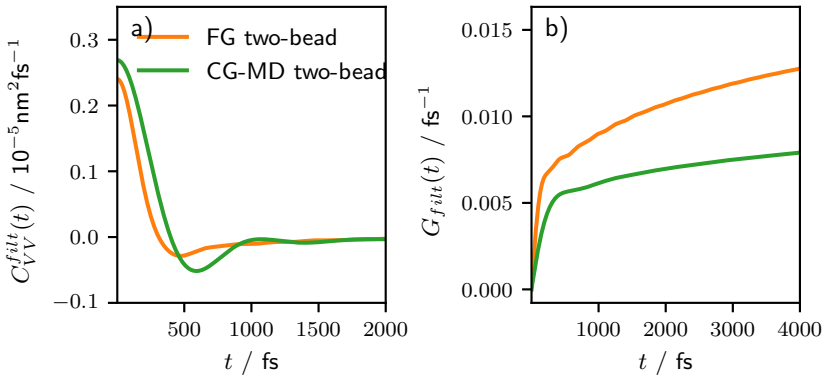

Figure 7.4: Demonstration of the effect of the filtering process on the VACF (a)) and the integrated memory kernel (b)) from FG mapped trajectories and CG-MD trajectories.

wavenumbers larger than 133 cm^{-1}. Inverting this altered Fourier-transform back to the time domain, results in a filtered VACF $C_{VV}^{filt}(t)$ as shown in Fig. 7.4 a), from which smooth integrated memory kernels $G_{filt}(t)$ can be obtained as shown in Fig. 7.4 b).

When using the smoothed integrated memory memory kernels in the IOMK method, the target property to match is now not the full VACF but only the low frequency modes while high frequency modes are either introduced through bonded interactions or fully neglected as being "irrelevant".

It has to be noted, that this approach is an ad-hoc attempt to treat bonded systems. The complete neglect of high-frequency modes in the VACF reduces the temperature that the VACF represents. At the same time, as the evaluation of $G(t)$ from a VACF effectively relies on a normalized VACF (see. Eq. 3.33), this might not constitute a serious drawback and is worth testing.

The bonded IOMK update scheme can now be summarized as

$$\tilde{G}_{i+1}(t) = \frac{G_{filt}^{tgt}(t) - a_{filt}(t)}{G_{i,filt}^{CG}(t) - a_{filt}(t)} \tilde{G}_i(t), \tag{7.1}$$

where the subscript $filt$ indicates that the respective integrated memory kernel is derived from a filtered VACF. By consistently using the same filtering procedure to all integrated memory kernels used as input, inconsistencies due to the filtering process are mitigated.

7.1.2 Results

The described procedure was applied to optimize a memory kernel for the CG DNEP model with two-bead mapping.

The resulting (unfiltered) VACFs, after three optimization steps are shown in Fig. 7.5 a), while the improvement is better visualized as integral (Fig. 7.5 b)) or in Fourier space (Fig. 7.6 a)) .

It is found that indeed by using the filtering technique on the VACFs, the IOMK method can be applied to at least very well reproduce the low frequency modes on the chosen resolution. The lowest frequency of the high-frequency modes is introduced by the bonded potential, and is found to be slightly too high and too sharp.

The question now is if the dynamics of the COM motion of the DNEP molecules is correctly modeled. In Figs. 7.7 a) and 7.7 b) the COM VACFs and their respective integrals are compared. See Fig. 7.6 b) for the Fourier transform of the COM VACFs. It is found that the COM dynamics in terms of the VACF can be

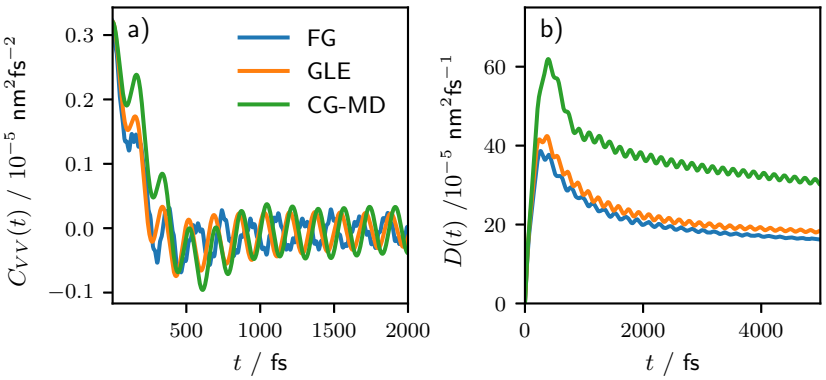

Figure 7.5: a) Two-bead VACFs of GLE and CG-MD simulations compared to the FG reference. b) The respective integral $D(t)$.

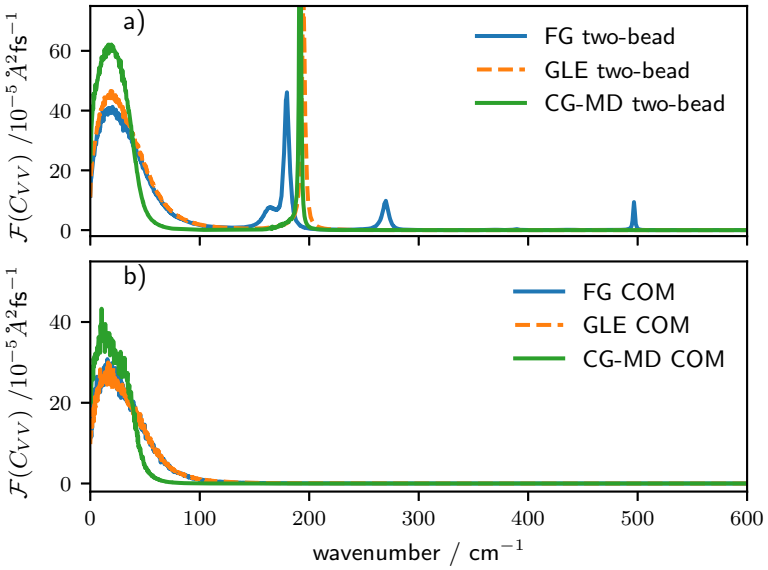

Figure 7.6: Fourier transforms of FG, GLE and CG-MD simulations of VACFs from a) two-bead and b) COM representation.

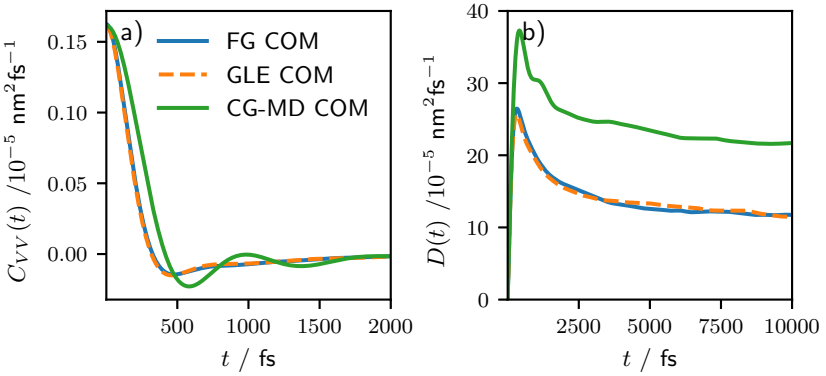

Figure 7.7: a) COM VACFs of GLE and CG-MD simulations compared to the FG reference. b) The respective integral $D(t)$.

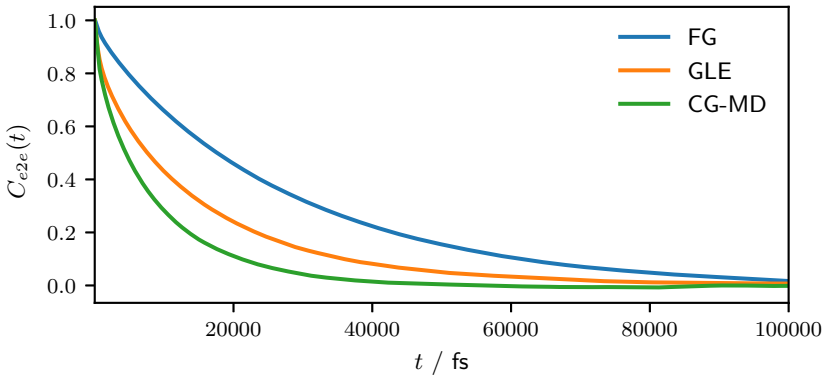

Figure 7.8: Normalized end-to-end vector autocorrelation function $C_{e2e}(t) = \langle \boldsymbol{e}_{e2e}(0) \cdot \boldsymbol{e}_{e2e}(t) \rangle$, where $\boldsymbol{e}_{e2e}$ is the unit vector parallel to the connection vector between the two CG sites, from FG, GLE and CG-MD simulations.

reproduced quantitatively by using the filtered IOMK method. In comparison, this accuracy cannot be reached with Markovian DPD models even when the diffusion coefficient is well matched.[65]

Finally, the main purpose of this section is the improve our understanding of the significant problem is rotational dynamics which was found in the original work of Deichmann.[65] In Fig. 7.8, the normalized end-to-end autocorrelation function is shown for the mapped AA trajectories and for the GLE and the standard CG-MD simulations. While the GLE-thermostat leads to an increase of the correlation time scale of the rotational dynamics compared to the standard CG-MD model, these correlation times are still significantly too low compared to the FG reference. This shortcoming thus shows persistence between very different approaches (DPD-thermostat[65] and isotropic GLE-thermostat). The current data allows for a better understanding of this phenomenon. In the next section, two hypothesis on the origin of the misrepresented rotational dynamics will be discussed from which a path forward for future research can be drawn.

7.1.3 Origin of the Speed-Up of Rotational Dynamics in Dissipative Coarse-Grained Models

The role of accurate conservative forces

As stressed many times throughout this thesis, to preserve accurate dynamics in CG models, it is important to keep in mind that the accuracy of the CG potential plays a significant role for dynamic properties beyond the diffusion coefficient, even when a dissipative thermostat is carefully optimized. A (in principle) quantifiable way to asses the quality of a CG potential is how well it reproduces the MB-PMF of the FG reference system, mapped onto the CG scale. In general, systematic coarse-graining procedures tend to show reduced potential energy barriers compared to the "real" MB-PMF[15] which can lead to a dynamic speed-up which cannot be attributed to a lack of friction.

A very nice illustration of one potential mechanism of this reduced energy barriers can be found in the work of Bereau and Rudzinski.[204] Consider a scenario in which a complex dynamic system gives rise to a probability distribution $P(x, y)$ of two observables of interest x and y, with corresponding probability distributions $P(x)$ and $P(y)$. In general, x and y can be correlated, such that

$$P(x|y = y_1) \neq P(x|y = y_2) \tag{7.2}$$

for two distinct values of y. In such a case, only the individual probability distributions $P(x)$ and $P(y)$ can be reconstructed by using an additive potential of the form

$$U(x,y) \approx U(x) + U(y). \tag{7.3}$$

whereby $U(x) \propto -ln(P(x))$ and $U(y) \propto -ln(P(y))$. With this approximation of the MB-PMF, the joint probability distribution is approximated by a product as

$$P(x,y) \approx P(x)P(y). \tag{7.4}$$

While this approach guarantees a correct representation of the individual probability distributions, the neglect of cross-correlations can lead to spurious potential energy minima on the two-dimensional energy landscape.[204] These can introduce transition paths with lowered energy barriers and thus alter the relative transition times for the hopping between energy basins in dynamic simulations.[204] Based on the study of mean-first-passage times of the dihedral dynamics of tetraalanine the authors demonstrated that it is necessary to consider cross-correlations between intramolecular distances and dihedral angles to correctly model the relative transition time scales between "extended" and "helical" states.[204]

Similarly, in Chapter 6 of the current work, it was demonstrated that the introduction of many-body interactions in CG water models allows for a more accurate modeling of dynamic properties.

Based on these considerations, it cannot be ruled out that one contribution to the enhanced rotational dynamics is due to the choice of too simple pair-wise interactions in the conservative potential used for CG modeling of DNEP. At the same time, the TraPPE-UA force field does not include any electrostatic interactions and the NEP repeat unit is close to being spherical. Thus, the relevance of many-body interactions are expected to be small and errors in dynamic properties cannot be assumed to dominantly stem from the choice of the CG potential.

Rotational libration and intramolecular memory

In order to better understand the origin of the discrepancies in rotational dynamics between FG and CG models with type of dumbbell two-bead mapping scheme, it is insightful to consider what mechanisms are involved in the rotational motion in the mapped representation of FG reference simulations. Bernhardt *et al.*[253] carried out such an analysis for a set of molecular liquids, from which relevant insights can be drawn for the problem of this section.

In Ref. [253] the authors studied the density of state (DoS) of different molecular liquids, while separating the total DoS into translational, rotational and vibrational contributions. What was found is that the rotational DoS for the molecular liquids are mainly diffusive showing only low frequency contributions. By running the same analysis on mapped trajectories, also using a two-body dumbbell mapping scheme as is the case for the DNEP system of this work, the authors found that the rotational DoS exhibits high frequency peaks which are not present in the FG representation of the same trajectory. These high frequency peaks in the mapped rotational DoF occur because vibrational motion on the FG scale can occur as librations of rotational motion on the mapped scale.

This means that in a mapped FG trajectory, a change of the orientation of a molecule can be governed by (crudely) two very distinct mechanisms. Firstly, an actual rotation of the whole molecule takes place giving rise to low frequency and diffusive motion. This mechanism is mainly determined through intermolecular interactions. Secondly, an intramolecular reorganization, governed mainly by intramolecular bonded and non-bonded interactions.

While the first mechanism can be in principle represented in standard CG models, the second cannot be represented with standard CG potentials. This means that the total kinetic energy stored in rotation motion in the mapped FG system is distributed between diffusive and libration modes. As the libration modes are quasi-harmonic, they only contribute to fluctuations around some transient mean orientation

but do not contribute to an irreversible change in orientation. In CG-MD simulations on the other hand, the total kinetic energy of rotation is stored in diffusive modes and thus a strong increase in orientational diffusion is observed. In the context of this work, the question is if one can construct a (generalized) Langevin type thermostat such that these high-frequency libration modes can be mimicked.

A naive straight forward approach would be to just increase the friction in a LE-, GLE-, or DPD-thermostat, until at least the rough timescale of rotational dynamics is corrected. This approach would simultaneously dampen translational motion and thus yield errors in diffusivity.

A more promising approach is to distinctly enforce the excitation of modes at the frequency range of observed librations.

This can in principle be achieved with a GLE. Ceriotti *et al.* demonstrated, how to deliberately excite arbitrary modes in molecular simulations using the same GLE-thermostat used in the current work.[153] This is achieved by constructing a memory kernel which has a δ-like shape in Fourier-space, centered around the desired frequency.[153] So, with a careful construction of the coupling matrix in the auxiliary variable GLE-thermostat, one can induce fluctuations at the frequency range of the librations in mapped trajectories. But as the GLE-thermostat is coupled to every DoF independently, high-frequency modes would be induced in the overall motion of any DoF, and not specifically in librations.

To target this problem, adjustments to the GLE-thermostat have to be made. In the following, a possible solution is proposed. The isotropic GLE-thermostat approach is mainly suitable to mimic dissipation and memory effects due to intermolecular interactions. To directly control rotational and vibrational modes in CG simulations, intramolecular dissipation and memory effects have to be treated explicitly. In principle, this can be achieved by adding non-Markovian dissipative interactions between bonded DoFs in a similar way as in NM-DPD.

$$\boldsymbol{F}_{IJ}^{b-NM}(t) = -\int_0^t dsM_J \boldsymbol{K}_{IJ}^{b}(t-s)\boldsymbol{V}_{IJ}^{b}(s) + \boldsymbol{F}_{IJ}^{R}(t) \tag{7.5}$$

The total bonded non-Markovian ($b-NM$) force can be split up into a parallel and a perpendicular part by decomposing the memory matrix accordingly.[27, 28] Then parallel and perpendicular contributions can be treated independently as

$$\boldsymbol{F}_{IJ}^{b-NM,||/\perp}(t) = -\int_0^t dsM_J K_{IJ}^{b,||/\perp}(t-s)\boldsymbol{V}_{IJ}^{b,||/\perp}(s) + \boldsymbol{F}_{IJ}^{R,||/\perp}(t). \tag{7.6}$$

By adding these kind of interactions, it should be possible to utilize Ceriotti's δ-like kernels[153] to correctly model vibration and libration modes. As the rotational DoS typically has also diffusive modes, the filtering strategy discussed above can be applied complementary, via explicitly neglecting low frequency modes, to distinctly model librations via Eq. 7.6. If the frequencies of librations are well separated from translational modes, the parameterization of $K_{IJ}^{b,\perp}(t)$ can be carried out independently of the GLE-thermostat parameterization, and the modified filtered IOMK strategy can be applied subsequently. Similarly, the blue shift of the bond stretching mode seen in Fig. 7.6 can be accounted for, by introducing appropriate memory effects.

7.1.4 Summary

In this section, the problems arising from a naive application of the IOMK method for bonded CG models were discussed. High frequency modes are present in single-bead based memory kernels in multiple-bead mapping schemes. A modification based on a filtering of VACFs in Fourier space was proposed, which allows for a straightforward parameterization of an isotropic GLE-thermostat, with which dynamics on low frequency scales can be reproduced accurately. In particular, while the GLE-thermostat acts on every CG DoF independently, it was found that this approach allows for an accurate representation of the center

of mass dynamics, for which it was not explicitly parameterized. In this respect, the IOMK approach outperforms the bottom-up DPD approach.[65] At the same time, the timescale of rotational dynamics could not be fully fixed and the current approach performs comparably to the bottom-up DPD approach in this respect.[65] To fix this short-coming, libration modes have to be deliberately introduced in the CG model, as these would take out parts of the rotational energies from diffusive modes and thus restrict rotational motion in a way which is consistent with the reference system.

Inspired by Ceriotti's[153] work and non-Markovian DPD,[27, 28] a potential solution was proposed, which entails the introduction of high-frequency with non-Markovian bonded interactions. This approach should be compatible with the application of the isotropic GLE-thermostat parameterized with the modified IOMK method. Working out the details and the implementation of non-Markovian bonded interactions is out of the scope of this thesis and for now remains a task for future research.

As a final note, one could ask why one should combine an isotropic GLE-thermostat with interactions similar to NM-DPD, if one could just use a complete NM-DPD description. There are at least three potential downsides to a full NM-DPD description.

- Up to now, the NM-DPD approach has been only tested on systems without bonds on the CG scale. It is unclear, how well strategies for extraction of memory kernels in more complex cases perform.

- The NM-DPD EoM involves configuration-dependent memory kernels. The use of NM-DPD assumes a time-scale separation between configurational changes on the CG scale and typical timescales of the memory kernels, both in typical parameterization strategies[27, 28] and in CG simulations.[30] The validity of this assumption has to be tested in chemically specific coarse-graining.

- NM-DPD is in general much more computationally expensive than an isotropic GLE-thermostat, even if the auxiliary variable approach is utilized. By restricting the use of pairwise memory to bonded interactions, the computational overhead can be minimized.

7.2 An Iterative Gauss-Newton Method for Optimizing Memory Kernels in Extended Phase Space

While the IOMK method has been established to be a very efficient procedure, one remaining downside is that if applied in combination with the auxiliary variable approach the coupling matrix has to be determined independently in every iteration by fitting $\tilde{G}_i$ by a sum of several dampened oscillators. While this fitting is typically computationally cheap compared to simulations, it is a potential source of errors. It would be convenient, if one could use an optimization scheme which gives a prescription on how to optimize the auxiliary variable coupling matrix directly. In fact, an approach that does exactly that was proposed by Wang *et al.*[32] but compared to the IOMK method, which typically needs less than 5 iterations to achieve satisfactory results, the method proposed in Ref. [32] relies on up to thousands CG GLE simulations to find the optimal parameters. Ideally, one should find a way to utilize the efficiency of the IOMK method in a method which would allow a direct optimization of parameters. In this section, a Gauss-Newton (GN) method is derived, which in principle would allow to directly optimize the GLE-parameters instead of the memory kernel, while applying the same assumptions as the IOMK method.

In Sec. 6.6.2, a description of the IOMK method as a approximate Newton method has been established. A Newton step for minimizing $|\boldsymbol{y}|^2$ for some vector $\boldsymbol{y}$ with respect to an input vector $\boldsymbol{x}$ can be written as

$$\boldsymbol{x}_{i+1} = \boldsymbol{x}_i - \boldsymbol{J}_i^{-1}\boldsymbol{y}_i, \tag{7.7}$$

where i indicates the ith iteration step. Such an update can only be used when the Jacobian $\boldsymbol{J}$ is a NxN matrix, where N is the dimensionality of vectors $\boldsymbol{x}_i$ and $\boldsymbol{y}_i$. When the dimensionalities of the vectors $\boldsymbol{x}_i$ and $\boldsymbol{y}_i$ are not equal, Eq. 7.7 is not applicable.

One can formally derive a Gauss-Newton (GN) method, which allows solve non-linear least-squares problems where the dimensionality of $\boldsymbol{x}_i$ is smaller than the dimensionality of $\boldsymbol{y}_i$, to directly optimize the parameters of a sum of N_{osc} (integrated) dampened oscillators

$$\begin{aligned}\tilde{G}(t) \approx \sum_{i=1}^{N_{osc}} \Bigg(& 2\frac{a_i b_i + 2c_i d_i}{a_i^2 + 4d_i^2} \\ & - \frac{2e^{-\frac{a_i t}{2}} \left((a_i b_i + 2c_i d_i)\cos(d_i t) + (a_i c_i - 2b_i d_i)\sin(d_i t) \right)}{a_i^2 + 4d_i^2} \Bigg).\end{aligned} \tag{7.8}$$

(Note that in Eq. 7.8 i refers to the ith dampened oscillator, not to be confused with the enumeration of iterations in e.g. Eq. 7.7) For simplicity, one can start with the case of simple curve fitting of a single-particle integrated memory kernel $G^{tgt}(t)$ (or $\boldsymbol{G}^{tgt}$ in vector notation). The least-squares problem which needs to be solved is then given by

$$\min_{\boldsymbol{x}}\{\frac{1}{2}|\tilde{\boldsymbol{G}} - \boldsymbol{G}^{tgt}|^2\} = \min_{\boldsymbol{x}}\{\frac{1}{2}|\boldsymbol{y}|^2\}, \tag{7.9}$$

where $\boldsymbol{x} = (a_1, b_1, c_1, d_1, ..., a_{N_{osc}}, b_{N_{osc}}, c_{N_{osc}}, d_{N_{osc}})^T$ The GN update reads as follows:

$$\boldsymbol{x}_{i+1} = \boldsymbol{x}_i - (\boldsymbol{J}_i^T \boldsymbol{J}_i)^{-1} \boldsymbol{J}_i^T \boldsymbol{y}_i, \tag{7.10}$$

where $(\boldsymbol{J}_i^T \boldsymbol{J}_i)^{-1} \boldsymbol{J}_i^T$ is the pseudo-inverse of $\boldsymbol{J}_i$. For numerical stability, Eq. 7.10 is typically not explicitly solved, but rather rewritten in the form of a system of linear equations as

$$\boldsymbol{J}_i^T \boldsymbol{J}_i (\boldsymbol{x}_{i+1} - \boldsymbol{x}_i) = -\boldsymbol{J}_i^T \boldsymbol{y}_i. \tag{7.11}$$

Eq. 7.11 can be solved for $(\boldsymbol{x}_{i+1} - \boldsymbol{x}_i)$ by standard methods for systems of linear equations. For the minimization problem given by Eq 7.9 the Jacobian $\boldsymbol{J}_i$ is defined via

$$J_{i,mn} = \frac{\partial \tilde{G}_{i,n}}{\partial x_{i,m}}. \tag{7.12}$$

The partial derivatives can be either evaluated analytically or numerically via finite differences.

As can be seen, at least for the purpose of plain fitting, a GN method can be derived straight-forwardly for the case of optimizing memory kernel. In practice, additional considerations have to be made:

1. The space of $\boldsymbol{x}$ is restricted for physically meaningful models. So appropriate bounds have to be incorporated into the GN method.

2. A GN method can become numerically unstable, in particular when $\boldsymbol{J}_i^T \boldsymbol{J}_i$ has very small singular values. In such cases the problem should be regularized.

3. For a simple fitting problem, the Jacobian can be easily evaluated (analytically or numerically via numerical finite differences) from Eq. 7.8. In order to derive a GN scheme for optimizing memory kernels for many-body molecular simulations a suitable approximation for the Jacobian has to be found.

Concerning 1., the relevant bounds are given by $a_i > 0$, $\frac{b}{2} - \frac{c_i d_i}{a_i} >= 0$ and $\frac{b}{2} + \frac{c_i d_i}{a_i} >= 0$.[92] (For numerical stability, it might also be useful to include upper bounds for all variables, in particular for the frequency d_i.) In Eq. 7.8,the parameters b_i and c_i, can be substituted with $e_i = \frac{b}{2} - \frac{c_i d_i}{a_i}$ and $f_i = \frac{b}{2} + \frac{c_i d_i}{a_i}$. By redefining $\boldsymbol{x}$ accordingly as $\boldsymbol{x} = (a_1, e_1, f_1, d_1, ..., a_{N_o}, e_{N_o}, f_{N_o}, d_{N_o})^T$, the GN method can be simply reformulated. By using this transformed set of variables, strategies to enforce the bounds can be explored.

Concerning 2., different regularization strategies might be explored. A straight-forward way to regularize Eq. 7.11 is by using a Tikhonov regularization[254] such that the update step reads

$$(\boldsymbol{J}_i^T \boldsymbol{J}_i + \alpha \boldsymbol{I})(\boldsymbol{x}_{i+1} - \boldsymbol{x}_i) = -\boldsymbol{J}_i^T \boldsymbol{y}_i, \tag{7.13}$$

where α is a small positive constant and $\boldsymbol{I}$ is the identity matrix. By adding a positive constant to the diagonal elements of $\boldsymbol{J}_i^T \boldsymbol{J}_i$, in the case where $\boldsymbol{J}_i^T \boldsymbol{J}_i$ is (close to) singular, the update scheme is stabilized and unreasonably large update steps can be prevented. A potential downside of regularization is that the efficiency of convergence may be slowed down. Thus, it is important to choose the regularization parameter α sufficiently small to not deteriorate performance, but sufficiently large to ensure stability.

Finally, concerning 3., in order to approximate the Jacobian $\boldsymbol{J}_i$ for using the GN scheme for the optimization of a auxiliary variable GLE-thermostat for many-body CG simulations, an approximation for the partial derivatives

$$J_{i,mn} = \frac{\partial G_{i,n}^{CG}}{\partial x_{i,m}}. \tag{7.14}$$

has to be found. For that, one can use the assumption, as introduced in the IOMK method:

$$G_i(t) \approx a(t) + (1 + b(t))\tilde{G}_i(t, \boldsymbol{x}_i) \approx a(t) + \frac{G_i(t) - a(t)}{\tilde{G}_i(t)} \tilde{G}_i(t, \boldsymbol{x}_i). \tag{7.15}$$

Herein, the trick is to ignore the dependency of $\tilde{G}_i(t)$ in the prefactor and use it as a scalar function for scaling the Jacobian, which can be calculated from $\tilde{G}_i(t, \boldsymbol{x}_i)$ the same way, as in simple fitting. Thus, as an approximation the partial derivatives can be expressed as

$$\frac{\partial G_{i,n}^{CG}}{\partial x_{i,m}} = \frac{G_{i,n}^{CG} - a_n}{\tilde{G}_{i,n}} \frac{\partial \tilde{G}_{i,n}}{\partial x_{i,m}}. \tag{7.16}$$

In summary, in this section a GN variant of the IOMK method (IOMK-GN) is proposed. Implementation and analysis of convergence is a task for future research. But as the IOMK-GN method relies on the same approximations as the IOMK method, it seems reasonable to assume that such a GN might prove useful in dynamically consistent CG molecular simulation.

8 Conclusions and Outlook

In this work, novel strategies for the parameterization of simple isotropic, non-Markovian generalized Langevin (GLE) thermostats for coarse-grained (CG) models have been developed with the aim of accurately representing the dynamics of the underlying reference system. The GLE models parameterized with these new methods were tested on a set of different problems. The backward-orthogonal dynamics method due to Carof *et al.* was exploited to separate the memory and friction on a single bead level into different contributions stemming from conservative forces on the CG scale, fluctuating forces on the fine-grained (FG) scale, and their cross-correlations. This splitting of contributions to the total memory kernel was used to estimate the optimal parametrization of isotropic GLE-thermostats for CG simulations purely based on the analysis of reference FG simulations. In chapter 4, it was demonstrated that it is the neglection of the cross-correlation of interactions on the CG and FG scale, which in previously published approaches led to an underestimation of diffusivities[36] and thus the inclusion of the cross-correlations can be considered a correction term. While a rigorous interpretation of the physical meaning of the cross-correlation term is not straight-forward, in the case of implicit-solvent models the cross correlation term can be interpreted as effectively (implicitly) incorporating the effects of hydrodynamic interactions between CG degrees of freedom (DoFs). (See chapter 5) As discussed in chapter 4, a non-zero cross-correlation term in the memory kernels hints to the fact that time scales are not separated and significant memory effects can be expected.

Throughout chapters 4-6, the assumptions, approximations and potential shortcomings of the bottom-up approach are discussed, and their relevance for different systems explored. In chapter 5, it is established, that the bottom-up approach yields particularly accurate CG models when conservative CG interactions are used which capture the many-body potential of mean force accurately. In particular, the short time dynamics in such cases can be quantitatively captured. This was demonstrated based on the development of implicit solvent Asakura-Oosawa (AO) models. Simultaneously, the study of AO models revealed some conceptional limitations of using a thermostat which couples to all DoFs independently. In such models, the exchange of momentum through DoFs which are coarse-grained away is only considered in an averaged manner. Thus, in the CG model, the dynamics of a set of DoFs is less correlated than in the corresponding FG reference. This gives rise to subtle, but persistent deviations of e.g. the velocity auto-correlation function (VACF) on long time scales.

To account for these residual deviations from the target dynamics, three novel iterative optimization schemes are presented. The conceptual novelty of all three schemes, compared to previously reported approaches, is the utilization of the (integrated) effective single particle memory kernel as direct target function. This greatly simplifies the relation of input and target property and thus allows for a very efficient optimization of the GLE-thermostat parametrization. The one-to-one correspondence between the effective single-particle memory kernel and the VACF ensures that the correct representation of the former corresponds to a correct representation of the latter.

The three presented optimization schemes differ in the formulation of the update step. The most promising of these, the IOMK method, explicitly takes into account that the usage of a dissipative thermostat in CG simulations alters the structural relaxation and thus the effective friction exerted through conservative interactions. The IOMK method has been shown to be very simple in its implementation, as it does not rely on any arbitrary tuning parameters to stabilize the optimization procedure and in all tested cases

yields satisfactory results within a single digits number of iterations. The advantages of the IOMK method, compared to the previously proposed IMRV method,[30] were demonstrated based on the coarse-graining of liquid water. The results in chapter 6 indicate that the IOMK method needs an order of magnitude less iterations to yield satisfactory results. The origin of these favorable results can be ascribed to its relation to the Newton method. The IOMK method constitutes an approximate Newton method, with a well-informed approximation for the Jacobian, while in the IMRV-method, when understood as an approximate Newton method, the Jacobian has to be manually tuned to stabilize the procedure.

Whenever a CG model is developed reproduce a particular target property, one legitimate question is, to what extent the correct representation of this specific property translates to an accurate representation of observables for which the model is not explicitly optimized for. Throughout this thesis the target property for all models was, explicitly or implicitly, the single particle VACF. As the single-particle memory kernel optimized for that purpose does not include any information about the systems configuration, it is not *a-priori* clear if an optimization of the VACF automatically allows a correct representation of e.g. collective dynamics. In chapter 6 the newly developed methods have been applied to a realistic molecular system. By studying the distinct van Hove function, which is a measure for the relaxation of the pair structure, it was demonstrated that parameterizing the GLE thermostat such that the VACF is reproduced also greatly improves the structural relaxation. This finding is crucial, as it indicates a more general representability of the type of studied GLE models, beyond single-particle dynamics. Furthermore, the data in chapter 6 reinforce the importance of a careful choice of the conservative potential for the correct representation of dynamic properties . While on the level of single particle dynamics an appropriate tuning of the memory kernel allows to compensate for errors in the CG potential to a large extent, the structural relaxation in many-body systems strongly depends on the chosen conservative interactions. As a rule of thumb the current results seem to indicate, that when one is concerned with dynamic properties, structural coarse-graining yields favorable results compared to force-based approaches as, for example, force matching. It has also been demonstrated, that the structural relaxation is strongly affected by memory effects. The application of a Markovian Langevin thermostat has shown to yield significantly too slow structural relaxation, even if tuned to exactly match the long time diffusive behavior.

In summary, due to the work presented in this thesis the toolbox for dynamic coarse-graining has gained additional methods which are comparably simple in their implementation and quite efficient. Still, a lot of work has to be done to allow the systematic development of CG models of predictive power. The remainder of this chapter shall be dedicated to discuss open questions for future research.

So far, to a large extent, including the work presented in this thesis, the methodological development of systematic procedures in non-Markovian dynamic coarse-graining was carried out on quite simple test cases. In particular, all methods involving generalized Langevin thermostats, both with and without configuration dependence of the memory kernels, so far were only applied to systems without bonded interactions on the CG scale. A natural progression of the field would involve to extend the available methods to bonded systems. This would allow to illuminate the origin of the insufficient accuracy of Markovian approaches, which have been tested for bonded CG models. For example, Ref. [65] reports bottom-up informed CG DPD models for monomers, dimers, polymers, polymer solutions and penetrants in a polymer matrix. It was found, that the long time dynamics in terms of the diffusion coefficients could be well reproduced with the proposed procedure for low viscosity systems, namely the monomer-, dimer- and a low concentration polymer solution. But even if the diffusion coefficient is correctly matched in bonded systems, rotational dynamics could not be quantitatively captured. Also, the proposed approach did not perform well for reproducing the diffusion coefficients of the penetrant in the polymer matrix. It is still an open question if the inaccuracies of previous approaches can be ascribed to the neglection of memory effects, errors in the modeling of CG conservative potentials or in other unknown errors sources. In

chapter 4 it was demonstrated, that inclusion of memory effects can alter the long-time diffusive behavior compared to otherwise equivalent Markovian models. Depending on the form of the memory kernel, this can lead to a memory induced increase or decrease in diffusivity. For a more complex energy landscape on the CG level, it can be anticipated that memory effects become more complex, as different dynamic modes dictated by the conservative interactions couple to different degrees to a non-Markovian thermostat and thus are distinctly affected. Thus in more complicated setups, namely where bonded interactions and energy barriers larger than k_BT are present in the CG representations, it can be anticipated that memory effects might become more complex. In particular, studying how a simultaneous representation of diffusion, structural relaxation, conformational dynamics of intramolecular DoFs, collective dynamics of different species, etc. can be achieved in an efficient way, poses the opportunity for novel methodological developments and physical insights into the effects of memory in relevant applications. With sec. 7.1, a small step into the direction of modeling complex CG non-Markovian systems is taken. The results therein seem to indicate that dissipative interactions between bonded interactions need to be modeled explicitly. The high-frequency nature of dynamic modes on a CG scale can in principle only be captured by a non-Markovian approach, but an independent thermostatting of distinct DoFs does not suffice. It can be anticipated that the explicit introduction of memory effects in bonded interactions might yield better results. Alternatively, the discussion in sec. 7.1 hints to an alternative approach: the 2PT-method[253] would allow to investigate different mapping schemes, before an explicit development of CG models. Based on short test runs, different mapping schemes can be screened. This would allow to identify mapping schemes, which minimize the "leakage" of energy into librations while maintaining sufficiently highly resolved molecular structure. For optimal mapping schemes, the application of an isotropic generalized Langevin thermostat might suffice for an accurate representation of different dynamic properties beyond the center of mass motion.

Also, a thorough comparison of the isotropic GLE-thermostat, as applied in the current work, to momentum conserving formulations as non-Markovian DPD has to be carried out. Non-Markovian DPD simulations in principle allow to correctly preserve the cross-correlations of frictional and random forces of pairs of beads and additionally, through configuration-dependent memory kernels, allow for a more detailed description. Thus it would be of significant interest to study in depth what aspects of dynamics are explicitly lost due to the simplified formulation of an isotropic thermostat.

Finally, a major problem in dynamic coarse-graining is transferability. Memory kernels, friction and noise in any system are strongly state point dependent. Thus, it is not sufficient to parameterize a models memory kernels at e.g. a single temperature to find a parametrization which is accurate for a broad temperature range. For interpolation and extrapolation between different thermodynamic state points, machine learning approaches might proof to be useful in future applications.[255] At the same time, these kind of data driven approaches typically rely on a quite substantial set of training data. An improved understanding of the state point dependence of memory kernels is needed, to develop general and tractable interpolation and extrapolation strategies for transferable CG models with dynamic consistency. Transferability along the dimension of chemical composition, might be improved by incorporation of some level of configuration dependence in the memory kernels,[30] while the trade off between complexity of the CG model and accuracy has to be kept in mind.

Bibliography

[1] H. J. C. Berendsen, *Simulating the Physical World: Hierarchical Modeling from Quantum Mechanics to Fluid Dynamics*, Cambridge University Press, Cambridge, **2007**.

[2] W. G. Noid, "Perspective: Coarse-grained Models for Biomolecular Systems", *The Journal of Chemical Physics* **2013**, *139*, 090901.

[3] W. G. Noid in *Biomolecular Simulations: Methods and Protocols*, (Eds.: L. Monticelli, E. Salonen), Methods in Molecular Biology, Humana Press, Totowa, NJ, **2013**, pp. 487–531.

[4] E. Brini, E. A. Algaer, P. Ganguly, C. Li, F. Rodríguez-Ropero, N. F. A. van der Vegt, "Systematic Coarse-Graining Methods for Soft Matter Simulations-a Review", *Soft Matter* **2013**, *9*, 2108–2119.

[5] F. Müller-Plathe, "Coarse-Graining in Polymer Simulation: From the Atomistic to the Mesoscopic Scale and Back", *Chemphyschem : a European journal of chemical physics and physical chemistry* **2002**, *3*, 754–769.

[6] S. Dhamankar, M. A. Webb, "Chemically Specific Coarse-Graining of Polymers: Methods and Prospects", *Journal of Polymer Science* **2021**, *59*, 2613–2643.

[7] J. Jin, A. J. Pak, A. E. P. Durumeric, T. D. Loose, G. A. Voth, "Bottom-up Coarse-Graining: Principles and Perspectives", *Journal of Chemical Theory and Computation* **2022**, *18*, 5759–5791.

[8] P. C. T. Souza, R. Alessandri, J. Barnoud, S. Thallmair, I. Faustino, F. Grünewald, I. Patmanidis, H. Abdizadeh, B. M. H. Bruininks, T. A. Wassenaar, P. C. Kroon, J. Melcr, V. Nieto, V. Corradi, H. M. Khan, J. Domański, M. Javanainen, H. Martinez-Seara, N. Reuter, R. B. Best, I. Vattulainen, L. Monticelli, X. Periole, D. P. Tieleman, A. H. de Vries, S. J. Marrink, "Martini 3: A General Purpose Force Field for Coarse-Grained Molecular Dynamics", *Nature Methods* **2021**, *18*, 382–388.

[9] D. Reith, M. Pütz, F. Müller-Plathe, "Deriving Effective Mesoscale Potentials from Atomistic Simulations", *Journal of Computational Chemistry* **2003**, *24*, 1624–1636.

[10] A. P. Lyubartsev, A. Laaksonen, "Calculation of Effective Interaction Potentials from Radial Distribution Functions: A Reverse Monte Carlo Approach", *Physical Review E* **1995**, *52*, 3730–3737.

[11] F. Delbary, M. Hanke, D. Ivanizki, "A Generalized Newton Iteration for Computing the Solution of the Inverse Henderson Problem", *Inverse Problems in Science and Engineering* **2020**, *28*, 1166–1190.

[12] M. P. Bernhardt, M. Hanke, N. F. A. van der Vegt, "Iterative Integral Equation Methods for Structural Coarse-Graining", *The Journal of Chemical Physics* **2021**, *154*, 084118.

[13] W. Tschöp, K. Kremer, J. Batoulis, T. Bürger, O. Hahn, "Simulation of Polymer Melts. I. Coarse-graining Procedure for Polycarbonates", *Acta Polymerica* **1998**, *49*, 61–74.

[14] W. Tschöp, K. Kremer, O. Hahn, J. Batoulis, T. Bürger, "Simulation of Polymer Melts. II. From Coarse-Grained Models Back to Atomistic Description", *Acta Polymerica* **1998**, *49*, 75–79.

[15] J. F. Rudzinski, "Recent Progress towards Chemically-Specific Coarse-Grained Simulation Models with Consistent Dynamical Properties", *Computation* **2019**, *7*, 42.

[16] S. León, N. van der Vegt, L. Delle Site, K. Kremer, "Bisphenol A Polycarbonate: Entanglement Analysis from Coarse-Grained MD Simulations", *Macromolecules* **2005**, *38*, 8078–8092.

[17] I. Y. Lyubimov, J. McCarty, A. Clark, M. G. Guenza, "Analytical Rescaling of Polymer Dynamics from Mesoscale Simulations", *The Journal of Chemical Physics* **2010**, *132*, 224903.

[18] I. Lyubimov, M. G. Guenza, "First-Principle Approach to Rescale the Dynamics of Simulated Coarse-Grained Macromolecular Liquids", *Physical Review E: Statistical Physics Plasmas Fluids and Related Interdisciplinary Topics* **2011**, *84*, 031801.

[19] D. Fritz, K. Koschke, V. A. Harmandaris, N. F. A. van der Vegt, K. Kremer, "Multiscale Modeling of Soft Matter: Scaling of Dynamics", *Physical Chemistry Chemical Physics* **2011**, *13*, 10412–10420.

[20] M. K. Meinel, F. Müller-Plathe, "Loss of Molecular Roughness upon Coarse-Graining Predicts the Artificially Accelerated Mobility of Coarse-Grained Molecular Simulation Models", *Journal of Chemical Theory and Computation* **2020**, *16*, 1411–1419.

[21] M. K. Meinel, F. Müller-Plathe, "Roughness Volumes: An Improved RoughMob Concept for Predicting the Increase of Molecular Mobility upon Coarse-Graining", *The Journal of Physical Chemistry B* **2022**, *126*, 3737–3747.

[22] H. Mori, "Transport, Collective Motion, and Brownian Motion*)", *Progress of Theoretical Physics* **1965**, *33*, 423.

[23] R. Zwanzig, *Nonequilibrium Statistical Mechanics*, Oxford University Press, **2001**.

[24] M. te Vrugt, R. Wittkowski, "Projection Operators in Statistical Mechanics: A Pedagogical Approach", *European Journal of Physics* **2020**, *41*, 045101.

[25] T. Schilling, "Coarse-Grained Modelling out of Equilibrium", *Physics Reports* **2022**, *972*, 1–45.

[26] Z. Li, X. Bian, X. Li, G. E. Karniadakis, "Incorporation of Memory Effects in Coarse-Grained Modeling via the Mori-Zwanzig Formalism", *The Journal of Chemical Physics* **2015**, *143*, 243128.

[27] Z. Li, H. S. Lee, E. Darve, G. E. Karniadakis, "Computing the Non-Markovian Coarse-Grained Interactions Derived from the Mori–Zwanzig Formalism in Molecular Systems: Application to Polymer Melts", *The Journal of Chemical Physics* **2017**, *146*, 014104.

[28] Y. Yoshimoto, Z. Li, I. Kinefuchi, G. E. Karniadakis, "Construction of Non-Markovian Coarse-Grained Models Employing the Mori-Zwanzig Formalism and Iterative Boltzmann Inversion", *Journal of Chemical Physics* **2017**, *147*, 244110.

[29] Y. Han, J. Jin, G. A. Voth, "Constructing Many-Body Dissipative Particle Dynamics Models of Fluids from Bottom-up Coarse-Graining", *The Journal of Chemical Physics* **2021**, *154*, 084122.

[30] G. Jung, M. Hanke, F. Schmid, "Generalized Langevin Dynamics: Construction and Numerical Integration of Non-Markovian Particle-Based Models", *Soft Matter* **2018**, *14*, 9368–9382.

[31] Y. Han, J. F. Dama, G. A. Voth, "Mesoscopic Coarse-Grained Representations of Fluids Rigorously Derived from Atomistic Models", *The Journal of Chemical Physics* **2018**, *149*, 044104.

[32] S. Wang, Z. Ma, W. Pan, "Data-Driven Coarse-Grained Modeling of Polymers in Solution with Structural and Dynamic Properties Conserved", *Soft Matter* **2020**, *16*, 8330–8344.

[33] V. Klippenstein, N. F. A. van der Vegt, "Cross-Correlation Corrected Friction in (Generalized) Langevin Models", *The Journal of Chemical Physics* **2021**, *154*, 191102.

[34] V. Klippenstein, N. F. A. van der Vegt, "Cross-Correlation Corrected Friction in Generalized Langevin Models: Application to the Continuous Asakura–Oosawa Model", *The Journal of Chemical Physics* **2022**, *157*, 044103.

[35] F. Glatzel, T. Schilling, “The Interplay between Memory and Potentials of Mean Force: A Discussion on the Structure of Equations of Motion for Coarse-Grained Observables”, *Europhysics Letters* **2022**, *136*, 36001.

[36] H. Lei, B. Caswell, G. E. Karniadakis, “Direct Construction of Mesoscopic Models from Microscopic Simulations”, *Physical Review E* **2010**, *81*, 026704.

[37] S. Asakura, F. Oosawa, “On Interaction between Two Bodies Immersed in a Solution of Macromolecules”, *The Journal of Chemical Physics* **1954**, *22*, 1255–1256.

[38] S. Asakura, F. Oosawa, “Interaction between Particles Suspended in Solutions of Macromolecules”, *Journal of Polymer Science* **1958**, *33*, 183–192.

[39] G. Jung, M. Hanke, F. Schmid, “Iterative Reconstruction of Memory Kernels”, *Journal of Chemical Theory and Computation* **2017**, *13*, 2481–2488.

[40] C. Peter, K. Kremer, “Multiscale Simulation of Soft Matter Systems”, *Faraday Discussions* **2010**, *144*, 9–24.

[41] W. G. Noid, “Perspective: Coarse-grained Models for Biomolecular Systems”, *The Journal of Chemical Physics* **2013**, *139*, 090901.

[42] Schütte, Ch. and Sarich, M., “A Critical Appraisal of Markov State Models”, *Eur. Phys. J. – Special Topics* **2015**, *224*, 2445–2462.

[43] B. Hess, S. León, N. van der Vegt, K. Kremer, “Long Time Atomistic Polymer Trajectories from Coarse Grained Simulations: Bisphenol-A Polycarbonate”, *Soft Matter* **2006**, *2*, 409–414.

[44] V. A. Harmandaris, N. P. Adhikari, N. F. A. van der Vegt, K. Kremer, “Hierarchical Modeling of Polystyrene: From Atomistic to Coarse-Grained Simulations”, *Macromolecules* **2006**, *39*, 6708–6719.

[45] V. A. Harmandaris, D. Reith, N. F. A. van der Vegt, K. Kremer, “Comparison between Coarse-Graining Models for Polymer Systems: Two Mapping Schemes for Polystyrene”, *Macromolecular Chemistry and Physics* **2007**, *208*, 2109–2120.

[46] V. A. Harmandaris, K. Kremer, “Dynamics of Polystyrene Melts through Hierarchical Multiscale Simulations”, *Macromolecules* **2009**, *42*, 791–802.

[47] V. A. Harmandaris, N. P. Adhikari, N. F. A. van der Vegt, K. Kremer, B. A. Mann, R. Voelkel, H. Weiss, C. Liew, “Ethylbenzene Diffusion in Polystyrene: United Atom Atomistic/Coarse Grained Simulations and Experiments”, *Macromolecules* **2007**, *40*, 7026–7035.

[48] D. Fritz, C. R. Herbers, K. Kremer, N. F. A. van der Vegt, “Hierarchical Modeling of Polymer Permeation”, *Soft Matter* **2009**, *5*, 4556.

[49] P. K. Depa, J. K. Maranas, “Speed up of Dynamic Observables in Coarse-Grained Molecular-Dynamics Simulations of Unentangled Polymers”, *The Journal of Chemical Physics* **2005**, *123*, 094901.

[50] M. S. Shell, “Systematic Coarse-Graining of Potential Energy Landscapes and Dynamics in Liquids”, *The Journal of Chemical Physics* **2012**, *137*, 084503.

[51] R. Zwanzig, “Ensemble Method in the Theory of Irreversibility”, *The Journal of Chemical Physics* **1960**, *33*, 1338–1341.

[52] R. Zwanzig, “Memory Effects in Irreversible Thermodynamics”, *Physical Review* **1961**, *124*, 983–992.

[53] D. S. Lemons, A. Gythiel, “Paul Langevin’s 1908 Paper “On the Theory of Brownian Motion” [“Sur La Théorie Du Mouvement Brownien,” C. R. Acad. Sci. (Paris) 146, 530–533 (1908)]”, *American Journal of Physics* **1997**, *65*, 1079–1081.

[54] H. Meyer, T. Voigtmann, T. Schilling, “On the Non-Stationary Generalized Langevin Equation”, *The Journal of Chemical Physics* **2017**, *147*, 214110.

[55] P. Español in *Novel Methods in Soft Matter Simulations*, (Eds.: M. Karttunen, A. Lukkarinen, I. Vattulainen), Springer Berlin Heidelberg, Berlin, Heidelberg, **2004**, pp. 69–115.

[56] H. C. Oettinger, *Beyond Equilibrium Thermodynamics*, Wiley, Hoboken, New Jersey, **2005**.

[57] R. L. Akkermans, W. J. Briels, “Coarse-Grained Dynamics of One Chain in a Polymer Melt”, *Journal of Chemical Physics* **2000**, *113*, 6409–6422.

[58] T. Kinjo, S. Hyodo, “Equation of Motion for Coarse-Grained Simulation Based on Microscopic Description”, *Physical Review E: Statistical Physics Plasmas Fluids and Related Interdisciplinary Topics* **2007**, *75*, 051109.

[59] R. D. Groot, P. B. Warren, “Dissipative Particle Dynamics: Bridging the Gap between Atomistic and Mesoscopic Simulation”, *The Journal of Chemical Physics* **1997**, *107*, 4423–4435.

[60] C. Hijón, P. Español, E. Vanden-Eijnden, R. Delgado-Buscalioni, “Mori–Zwanzig Formalism as a Practical Computational Tool”, *Faraday Discussions* **2010**, *144*, 301–322.

[61] Z. Li, X. Bian, B. Caswell, G. E. Karniadakis, “Construction of Dissipative Particle Dynamics Models for Complex Fluids via the Mori-Zwanzig Formulation”, *Soft Matter* **2014**, *10*, 8659–8672.

[62] S. Trèment, B. Schnell, L. Petitjean, M. Couty, B. Rousseau, “Conservative and Dissipative Force Field for Simulation of Coarse-Grained Alkane Molecules: A Bottom-up Approach”, *The Journal of Chemical Physics* **2014**, *140*, 134113.

[63] G. Deichmann, V. Marcon, N. F. A. van der Vegt, “Bottom-up Derivation of Conservative and Dissipative Interactions for Coarse-Grained Molecular Liquids with the Conditional Reversible Work Method”, *The Journal of Chemical Physics* **2014**, *141*, 224109.

[64] C. A. Lemarchand, M. Couty, B. Rousseau, “Coarse-Grained Simulations of Cis- and Trans-Polybutadiene: A Bottom-up Approach”, *The Journal of Chemical Physics* **2017**, *146*, 074904.

[65] G. Deichmann, N. F. A. van der Vegt, “Bottom-up Approach to Represent Dynamic Properties in Coarse-Grained Molecular Simulations”, *Journal of Chemical Physics* **2018**, *149*, 244114.

[66] J. G. Kirkwood, “The Statistical Mechanical Theory of Transport Processes I. General Theory”, *The Journal of Chemical Physics* **1946**, *14*, 180–201.

[67] J. T. Padding, W. J. Briels, “Time and Length Scales of Polymer Melts Studied by Coarse-Grained Molecular Dynamics Simulations”, *The Journal of Chemical Physics* **2002**, *117*, 925–943.

[68] S. Izvekov, “Microscopic Derivation of Particle-Based Coarse-Grained Dynamics: Exact Expression for Memory Function”, *The Journal of Chemical Physics* **2017**, *146*, 124109.

[69] R. Kubo, “The Fluctuation-Dissipation Theorem”, *Reports on Progress in Physics* **1966**, *29*, 255–284.

[70] T. Sanghi, R. Bhadauria, N. R. Aluru, “Memory Effects in Nanoparticle Dynamics and Transport”, *The Journal of Chemical Physics* **2016**, *145*, 134108.

[71] D. Kauzlarić, J. T. Meier, P. Español, S. Succi, A. Greiner, J. G. Korvink, “Bottom-up Coarse-Graining of a Simple Graphene Model: The Blob Picture”, *The Journal of Chemical Physics* **2011**, *134*, 064106.

[72] C. Junghans, M. Praprotnik, K. Kremer, “Transport Properties Controlled by a Thermostat: An Extended Dissipative Particle Dynamics Thermostat”, *Soft Matter* **2008**, *4*, 156–161.

[73] E. Brini, V. Marcon, N. F. A. van der Vegt, "Conditional Reversible Work Method for Molecular Coarse Graining Applications", *Physical Chemistry Chemical Physics* **2011**, *13*, 10468–10474.

[74] E. Brini, N. F. A. van der Vegt, "Chemically Transferable Coarse-Grained Potentials from Conditional Reversible Work Calculations", *The Journal of Chemical Physics* **2012**, *137*, 154113.

[75] J. Kappler, J. O. Daldrop, F. N. Brünig, M. D. Boehle, R. R. Netz, "Memory-Induced Acceleration and Slowdown of Barrier Crossing", *The Journal of Chemical Physics* **2018**, *148*, 014903.

[76] Y. Wang, W. G. Noid, P. Liu, G. A. Voth, "Effective Force Coarse-Graining", *Physical Chemistry Chemical Physics* **2009**, *11*, 2002–2015.

[77] A. A. Gusev, U. W. Suter, "Dynamics of Small Molecules in Dense Polymers Subject to Thermal Motion", *The Journal of Chemical Physics* **1993**, *99*, 2228–2234.

[78] F. Müller-Plathe, "Permeation of Polymers — a Computational Approach", *Acta Polymerica* **1994**, *45*, 259–293.

[79] P. Español, J. A. de la Torre, D. Duque-Zumajo, "Solution to the Plateau Problem in the Green-Kubo Formula", *Physical Review E: Statistical Physics Plasmas Fluids and Related Interdisciplinary Topics* **2019**, *99*, 022126.

[80] H. K. Shin, C. Kim, P. Talkner, E. K. Lee, "Brownian Motion from Molecular Dynamics", *Chemical Physics* **2010**, *375*, 316–326.

[81] B. Kowalik, J. O. Daldrop, J. Kappler, J. C. F. Schulz, A. Schlaich, R. R. Netz, "Memory-Kernel Extraction for Different Molecular Solutes in Solvents of Varying Viscosity in Confinement", *Physical Review E* **2019**, *100*, 012126.

[82] H. Meyer, P. Pelagejcev, T. Schilling, "Non-Markovian out-of-Equilibrium Dynamics: A General Numerical Procedure to Construct Time-Dependent Memory Kernels for Coarse-Grained Observables", *Epl* **2019**, *128*, 40001.

[83] H. Meyer, S. Wolf, G. Stock, T. Schilling, "A Numerical Procedure to Evaluate Memory Effects in Non-Equilibrium Coarse-Grained Models", *Advanced Theory and Simulations* **2021**, *4*, 2000197.

[84] I. Goychuk, "Viscoelastic Subdiffusion: Generalized Langevin Equation Approach", *Advances in Chemical Physics* **2012**, *150*, 187.

[85] A. Carof, R. Vuilleumier, B. Rotenberg, "Two Algorithms to Compute Projected Correlation Functions in Molecular Dynamics Simulations", *Journal of Chemical Physics* **2014**, *140*, 124103.

[86] D. Lesnicki, R. Vuilleumier, A. Carof, B. Rotenberg, "Molecular Hydrodynamics from Memory Kernels", *Physical Review Letters* **2016**, *116*, 147804.

[87] H. Lei, N. A. Baker, X. Li, "Data-Driven Parameterization of the Generalized Langevin Equation", *Proceedings of the National Academy of Sciences* **2016**, *113*, 14183–14188.

[88] B. Schnurr, F. Gittes, F. C. MacKintosh, C. F. Schmidt, "Determining Microscopic Viscoelasticity in Flexible and Semiflexible Polymer Networks from Thermal Fluctuations", *Macromolecules* **1997**, *30*, 7781–7792.

[89] J. Fricks, L. Yao, T. C. Elston, M. G. Forest, "Time-Domain Methods for Diffusive Transport in Soft Matter", *SIAM Journal on Applied Mathematics* **2009**, *69*, 1277–1308.

[90] J. E. Straub, M. Borkovec, B. J. Berne, "Calculation of Dynamic Friction on Intramolecular Degrees of Freedom", *Journal of Physical Chemistry* **1987**, *91*, 4995–4998.

[91] B. J. Berne, G. D. Harp in *Advances in Chemical Physics*, John Wiley & Sons, Ltd, **1970**, pp. 63–227.

[92] S. Wang, Z. Li, W. Pan, "Implicit-Solvent Coarse-Grained Modeling for Polymer Solutions via Mori-Zwanzig Formalism", *Soft matter* **2019**, *15*, 7567–7582.

[93] A. Córdoba, T. Indei, J. D. Schieber, "Elimination of Inertia from a Generalized Langevin Equation: Applications to Microbead Rheology Modeling and Data Analysis", *Journal of Rheology* **2012**, *56*, 185–212.

[94] A. Córdoba, J. D. Schieber, T. Indei, "The Effects of Hydrodynamic Interaction and Inertia in Determining the High-Frequency Dynamic Modulus of a Viscoelastic Fluid with Two-Point Passive Microrheology", *Physics of Fluids* **2012**, *24*, 073103.

[95] A. V. Straube, B. G. Kowalik, R. R. Netz, F. Höfling, "Rapid Onset of Molecular Friction in Liquids Bridging between the Atomistic and Hydrodynamic Pictures", *Communications Physics* **2020**, *3*, 126.

[96] J. O. Daldrop, B. G. Kowalik, R. R. Netz, "External Potential Modifies Friction of Molecular Solutes in Water", *Physical Review X* **2017**, *7*, 041065.

[97] M. Baity-Jesi, D. R. Reichman, "On Mean-Field Theories of Dynamics in Supercooled Liquids", *The Journal of Chemical Physics* **2019**, *151*, 084503.

[98] N. Bockius, J. Shea, G. Jung, F. Schmid, M. Hanke, "Model Reduction Techniques for the Computation of Extended Markov Parameterizations for Generalized Langevin Equations", *J. Phys.: Cond. Matter* **2021**, to appear (preprint: arxiv.org/abs/2101.02657).

[99] K. C. Neuman, A. Nagy, "Single-Molecule Force Spectroscopy: Optical Tweezers, Magnetic Tweezers and Atomic Force Microscopy", *Nature Methods* **2008**, *5*, 491–505.

[100] M. Tassieri, G. M. Gibson, R. M. L. Evans, A. M. Yao, R. Warren, M. J. Padgett, J. M. Cooper, "Measuring Storage and Loss Moduli Using Optical Tweezers: Broadband Microrheology", *Physical Review E: Statistical Physics Plasmas Fluids and Related Interdisciplinary Topics* **2010**, *81*, 026308.

[101] J. O. Daldrop, R. R. Netz, "Mass-Dependent Solvent Friction of a Hydrophobic Molecule", *Journal of Physical Chemistry B* **2019**, *123*, 8123–8130.

[102] D. Forster, *Hydrodynamic Fluctuations, Broken Symmetry, and Correlation Functions*, Westview Press, **1975**.

[103] J. P. Boon, S. Yip, *Molecular Hydrodynamics*, McGraw-Hill New York ; London, **1980**.

[104] R. Tsekov, B. Radoev, "Velocity Autocorrelation Function in Fluctuating Hydrodynamics: Frequency Dependence of the Kinematic Viscosity", *J. Phys.: Cond. Matter* **1992**, *4*, L303–L305.

[105] T. Franosch, M. Fuchs, A. Latz, "Light-Scattering Spectra of Supercooled Molecular Liquids", *Physical Review E: Statistical Physics Plasmas Fluids and Related Interdisciplinary Topics* **2001**, *63*, 061209.

[106] B. J. Alder, T. E. Wainwright, "Decay of the Velocity Autocorrelation Function", *Physical Review A: Atomic Molecular and Optical Physics* **1970**, *1*, 18–21.

[107] L. P. Kadanoff, J. Swift, "Transport Coefficients near the Liquid-Gas Critical Point", *Physical Review* **1968**, *166*, 89–101.

[108] W. Götze, *Complex Dynamics of Glass-Forming Liquids - A Mode-Coupling Theory*, Oxford University Press, Oxford, **2009**.

[109] F. Höfling, T. Franosch, "Anomalous Transport in the Crowded World of Biological Cells", *Reports on progress in physics. Physical Society (Great Britain)* **2013**, *76*, 046602.

[110] L. M. C. Janssen, "Mode-Coupling Theory of the Glass Transition: A Primer", *Frontiers in Physics* **2018**, *6*, 97.

[111] A. Zaccone, "Relaxation and Vibrational Properties in Metal Alloys and Other Disordered Systems", *Journal of Physics: Condensed Matter* **2020**, *32*, 203001.

[112] G. Amati, H. Meyer, T. Schilling, "Memory Effects in the Fermi–Pasta–Ulam Model", *Journal of Statistical Physics* **2019**, *174*, 219–257.

[113] G. Amati, T. Schilling, "Structural Localization in the Classical and Quantum Fermi–Pasta–Ulam Model", *Chaos: An Interdisciplinary Journal of Nonlinear Science* **2020**, *30*, 033116.

[114] M. Chen, X. Li, C. Liu, "Computation of the Memory Functions in the Generalized Langevin Models for Collective Dynamics of Macromolecules", *The Journal of Chemical Physics* **2014**, *141*, 064112.

[115] L. Ma, X. Li, C. Liu, "The Derivation and Approximation of Coarse-Grained Dynamics from Langevin Simulations", *The Journal of Chemical Physics* **2016**, *145*, 204117.

[116] H. S. Lee, S.-H. Ahn, E. F. Darve, "The Multi-Dimensional Generalized Langevin Equation for Conformational Motion of Proteins", *The Journal of Chemical Physics* **2019**, *150*, 174113.

[117] A. Kuhnhold, H. Meyer, G. Amati, P. Pelagejcev, T. Schilling, "Derivation of an Exact, Nonequilibrium Framework for Nucleation: Nucleation Is a Priori Neither Diffusive nor Markovian", *Physical Review E: Statistical Physics Plasmas Fluids and Related Interdisciplinary Topics* **2019**, *100*, 052140.

[118] D. E. Smith, C. B. Harris, "Generalized Brownian Dynamics. I. Numerical Integration of the Generalized Langevin Equation through Autoregressive Modeling of the Memory Function", *The Journal of chemical physics* **1990**, *92*, 1304–1311.

[119] D. E. Smith, C. B. Harris, "Generalized Brownian Dynamics. II. Vibrational Relaxation of Diatomic Molecules in Solution", *The Journal of Chemical Physics* **1990**, *92*, 1312–1319.

[120] M. E. Tuckerman, B. J. Berne, "Stochastic Molecular Dynamics in Systems with Multiple Time Scales and Memory Friction", *The Journal of Chemical Physics* **1991**, *95*, 4389–4396.

[121] Z. Li, X. Bian, X. Yang, G. E. Karniadakis, "A Comparative Study of Coarse-Graining Methods for Polymeric Fluids: Mori-Zwanzig vs. Iterative Boltzmann Inversion vs. Stochastic Parametric Optimization", *The Journal of Chemical Physics* **2016**, *145*, 044102.

[122] C. Hohenegger, S. A. McKinley, "Fluid–Particle Dynamics for Passive Tracers Advected by a Thermally Fluctuating Viscoelastic Medium", *Journal of Computational Physics* **2017**, *340*, 688–711.

[123] C. Hohenegger, R. Durr, D. Senter, "Mean First Passage Time in a Thermally Fluctuating Viscoelastic Fluid", *Journal of Non-Newtonian Fluid Mechanics* **2017**, *242*, 48–56.

[124] D. L. Ermak, H. Buckholz, "Numerical Integration of the Langevin Equation: Monte Carlo Simulation", *Journal of Computational Physics* **1980**, *35*, 169–182.

[125] G. Ciccotti, J.-P. Ryckaert, "Computer Simulation of the Generalized Brownian Motion", *Molecular Physics* **1980**, *40*, 141–159.

[126] M. Tuckerman, B. J. Berne, "Vibrational Relaxation in Simple Fluids: Comparison of Theory and Simulation", *The Journal of Chemical Physics* **1993**, *98*, 7301–7318.

[127] J. Snoek, H. Larochelle, R. P. Adams in Advances in Neural Information Processing Systems, **2012**, pp. 2951–2959.

[128] A. Dequidt, J. G. Solano Canchaya, "Bayesian Parametrization of Coarse-Grain Dissipative Dynamics Models", *The Journal of Chemical Physics* **2015**, *143*, 084122.

[129] J. E. Straub, B. J. Berne, B. Roux, "Spatial Dependence of Time-dependent Friction for Pair Diffusion in a Simple Fluid", *The Journal of Chemical Physics* **1990**, *93*, 6804–6812.

[130] A. van den Noort, W. K. den Otter, W. J. Briels, "Coarse Graining of Slow Variables in Dynamic Simulations of Soft Matter", *Europhysics Letters (EPL)* **2007**, *80*, 28003.

[131] L. Liu, W. K. den Otter, W. J. Briels, "Coarse Grain Forces in Star Polymer Melts", *Soft matter* **2014**, *10*, 7874–7886.

[132] V. R. Ahuja, J. van der Gucht, W. J. Briels, "Hydrodynamically Coupled Brownian Dynamics: A Coarse-Grain Particle-Based Brownian Dynamics Technique with Hydrodynamic Interactions for Modeling Self-Developing Flow of Polymer Solutions", *The Journal of Chemical Physics* **2018**, *148*, 034902.

[133] G. Jung, F. Schmid, "Frequency-Dependent Hydrodynamic Interaction between Two Solid Spheres", *Physics of Fluids* **2017**, *29*, 126101.

[134] A. Russo, M. A. Duran-Olivencia, P. Yatsyshin, S. Kalliadasis, "Memory Effects in Fluctuating Dynamic Density Functional Theory: Theory and Simulations", *Journal of Physics A: Mathematical and Theoretical* **2020**, *53*, 445007.

[135] A. Semenov, "Relaxation of Long-Wavelength Density Fluctuations in a Concentrated Polymer Solution", *JETP* **1986**, *63*, 717–720.

[136] M. Guenza, "Many Chain Correlated Dynamics in Polymer Fluids", *The Journal of Chemical Physics* **1999**, *110*, 7574–7588.

[137] D. Panja, "Anomalous Polymer Dynamics Is Non-Markovian: Memory Effects and the Generalized Langevin Equation Formulation", *Journal of Statistical Mechanics: Theory and Experiment* **2010**, *2010*, P06011.

[138] G. Wang, Y. Ren, M. Müller, "Collective Short-Time Dynamics in Multicomponent Polymer Melts", *Macromolecules* **2019**, *52*, 7704–7720.

[139] J. Rottler, M. Müller, "Efficient Pathways of Block Copolymer Directed Self-Assembly: Insights from Efficient Continuum Modeling", *ACS Nano* **2020**, *14*, 13986–13994.

[140] A. Vázquez-Quesada, M. Ellero, P. Espanõl, "A SPH-based Particle Model for Computational Microrheology", *Microfluidics and Nanofluidics* **2012**, *13*, 249–260.

[141] M. Hütter, M. A. Hulsen, P. D. Anderson, "Fluctuating Viscoelasticity", *Journal of Non-Newtonian Fluid Mechanics* **2018**, *256*, 42–56.

[142] M. Hütter, M. A. Carrozza, M. A. Hulsen, P. D. Anderson, "Behavior of Viscoelastic Models with Thermal Fluctuations", *The European Physical Journal E* **2020**, *43*, 24.

[143] J.-L. Barrat, D. Rodney, "Portable Implementation of a Quantum Thermal Bath for Molecular Dynamics Simulations", *Journal of Statistical Physics* **2011**, *1*, 679–689.

[144] M. Ferrario, P. Grigolini, "A Generalization of the Kubo—Freed Relaxation Theory", *Chemical Physics Letters* **1979**, *62*, 100–106.

[145] G. Ciccotti, J. .-. Ryckaert, "On the Derivation of the Generalized Langevin Equation for Interacting Brownian Particles", *Journal of Statistical Physics* **1981**, *26*, 73–82.

[146] H. Mori, "A Continued-Fraction Representation of the Time-Correlation Functions", *Progress of Theoretical Physics* **1965**, *34*, 399–416.

[147] F. Marchesoni, P. Grigolini, "On the Extension of the Kramers Theory of Chemical Relaxation to the Case of Nonwhite Noise", *The Journal of Chemical Physics* **1983**, *78*, 6287–6298.

[148] N. J. Higham, *Functions of Matrices*, Society for Industrial and Applied Mathematics, **2008**.

[149] N. Grønbech-Jensen, Oded Farago, "A Simple and Effective Verlet-type Algorithm for Simulating Langevin Dynamics", *Molecular Physics* **2013**, *111*, 983–991.

[150] M. Ceriotti, G. Bussi, M. Parrinello, "Langevin Equation with Colored Noise for Constant-Temperature Molecular Dynamics Simulations", *Physical Review Letters* **2009**, *102*, 020601.

[151] M. Ceriotti, G. Bussi, M. Parrinello, "Colored-Noise Thermostats à La Carte", *Journal of Chemical Theory and Computation* **2010**, *6*, 1170–1180.

[152] M. Ceriotti, G. Bussi, M. Parrinello, "Nuclear Quantum Effects in Solids Using a Colored-Noise Thermostat", *Physical Review Letters* **2009**, *103*, 030603.

[153] M. Ceriotti, M. Parrinello, "The δ-Thermostat: Selective Normal-Modes Excitation by Colored-Noise Langevin Dynamics", *Procedia Computer Science* **2010**, *1*, 1607–1614.

[154] M. Ceriotti, M. Parrinello, T. E. Markland, D. E. Manolopoulos, "Efficient Stochastic Thermostatting of Path Integral Molecular Dynamics", *The Journal of Chemical Physics* **2010**, *133*, 124104.

[155] M. Ceriotti, Doctoral Thesis, ETH Zurich, **2010**.

[156] A. D. Baczewski, S. D. Bond, "Numerical Integration of the Extended Variable Generalized Langevin Equation with a Positive Prony Representable Memory Kernel", *The Journal of Chemical Physics* **2013**, *139*, 044107.

[157] L. Stella, C. D. Lorenz, L. Kantorovich, "Generalized Langevin Equation: An Efficient Approach to Nonequilibrium Molecular Dynamics of Open Systems", **2014**, *89*, 134303.

[158] A. Davtyan, J. F. Dama, G. A. Voth, H. C. Andersen, "Dynamic Force Matching: A Method for Constructing Dynamical Coarse-Grained Models with Realistic Time Dependence", *The Journal of Chemical Physics* **2015**, *142*, 154104.

[159] L. Ma, X. Li, C. Liu, "From Generalized Langevin Equations to Brownian Dynamics and Embedded Brownian Dynamics", *The Journal of Chemical Physics* **2016**, *145*, 114102.

[160] J. Kappler, V. B. Hinrichsen, R. R. Netz, "Non-Markovian Barrier Crossing with Two-Time-Scale Memory Is Dominated by the Faster Memory Component", *The European Physical Journal E* **2019**, *42*, 119.

[161] L. Berthier, G. Biroli, "Theoretical Perspective on the Glass Transition and Amorphous Materials", **2011**, *83*, 587–645.

[162] M. D. Ediger, P. Harrowell, "Perspective: Supercooled Liquids and Glasses", **2012**, *137*, 080901.

[163] S. Napolitano, E. Glynos, N. B. Tito, "Glass Transition of Polymers in Bulk, Confined Geometries, and near Interfaces", **2017**, *80*, 036602.

[164] B. Cui, J. Yang, J. Qiao, M. Jiang, L. Dai, Y.-J. Wang, A. Zaccone, "Atomic Theory of Viscoelastic Response and Memory Effects in Metallic Glasses", *Physical Review B* **2017**, *96*, 094203.

[165] B. Cui, J. F. Gebbia, M. Romanini, S. Rudić, R. Fernandez-Perea, F. J. Bermejo, J.-L. Tamarit, A. Zaccone, "Secondary Relaxation in the Terahertz Range in 2-Adamantanone from Theory and Experiments", *Physical Review B* **2020**, *101*, 104202.

[166] R. Metzler, J. Klafter, "The Random Walk's Guide to Anomalous Diffusion: A Fractional Dynamics Approach", **2000**, *339*, 1–77.

[167] R. Mankin, K. Laas, N. Lumi, "Memory Effects for a Trapped Brownian Particle in Viscoelastic Shear Flows", *Physical Review E: Statistical Physics Plasmas Fluids and Related Interdisciplinary Topics* **2013**, *88*, 042142.

[168] A. Sauga, K. Laas, R. Mankin, "Memory-Induced Sign Reversals of the Spatial Cross-Correlation for Particles in Viscoelastic Shear Flows", *Chaos Solitons and Fractals* **2015**, *81*, 443–450.

[169] J. Boussinesq, *Théorie Analytique de La Chaleur Mise En Harmonic Avec La Thermodynamique et Avec La Théorie Mécanique de La Lumière: Tome I-[II]... Vol. 2*, Gauthier-Villars, **1903**.

[170] T. S. Chow, J. J. Hermans, "Effect of Inertia on the Brownian Motion of Rigid Particles in a Viscous Fluid", *The Journal of Chemical Physics* **1972**, *56*, 3150–3154.

[171] S. L. Seyler, S. Presse, "Long-Time Persistence of Hydrodynamic Memory Boosts Microparticle Transport", **2019**, *1*, 032003R.

[172] S. L. Seyler, S. Presse, "Surmounting Potential Barriers: Hydrodynamic Memory Hedges against Thermal Fluctuations in Particle Transport", **2020**, *153*, 041102.

[173] I. Goychuk, "Fractional Hydrodynamic Memory and Superdiffusion in Tilted Washboard Potentials", **2019**, *123*, 180603.

[174] I. Goychuk, T. Poeschel, "Hydrodynamic Memory Can Boost Enormously Driven Nonlinear Diffusion and Transport", **2020**, *102*, 012139.

[175] P. Reimann, C. Van den Broeck, H. Linke, P. Hanggi, J. M. Rubi, A. Perez-Madrid, "Giant Acceleration of Free Diffusion by Use of Tilted Periodic Potentials", **2001**, *87*, 010602.

[176] L. Lavacchi, J. Kappler, R. R. Netz, "Barrier Crossing in the Presence of Multi-Exponential Memory Functions with Unequal Friction Amplitudes and Memory Times", *EPL (Europhysics Letters)* **2020**, *131*, 40004.

[177] K. Nagai, Y. Sumino, R. Montang, I. Aranson, H. Chaté, "Collective Motion of Self-Propelled Particles with Memory", **2015**, *114*, 168001.

[178] N. Narinder, C. Bechinger, J. R. Gomez-Solano, "Memory-Induced Transition from a Persistent Random Walk to Circular Motion for Achiral Microswimmers", **2018**, *121*, 078003.

[179] V. R. Ardham, G. Deichmann, N. F. A. van der Vegt, F. Leroy, "Solid-Liquid Work of Adhesion of Coarse-Grained Models of n-Hexane on Graphene Layers Derived from the Conditional Reversible Work Method", *The Journal of Chemical Physics* **2015**, *143*, 243135.

[180] D. Fritz, V. A. Harmandaris, K. Kremer, N. F. A. van der Vegt, "Coarse-Grained Polymer Melts Based on Isolated Atomistic Chains: Simulation of Polystyrene of Different Tacticities", *Macromolecules* **2009**, *42*, 7579–7588.

[181] C. Liu, K. Kremer, T. Bereau, "Polymorphism of Syndiotactic Polystyrene Crystals from Multiscale Simulations", *Advanced Theory and Simulations* **2018**, *1*, 1800024.

[182] V. Marcon, D. Fritz, N. F. A. van der Vegt, "Hierarchical Modelling of Polystyrene Surfaces", *Soft Matter* **2012**, *8*, 5585–5594.

[183] V. A. Harmandaris, G. Floudas, K. Kremer, "Temperature and Pressure Dependence of Polystyrene Dynamics through Molecular Dynamics Simulations and Experiments", *Macromolecules* **2011**, *44*, 393–402.

[184] M. Langeloth, Y. Masubuchi, M. C. Böhm, F. Müller-Plathe, "Recovering the Reptation Dynamics of Polymer Melts in Dissipative Particle Dynamics Simulations via Slip-Springs", *The Journal of Chemical Physics* **2013**, *138*, 104907.

[185] G. Falasco, M. V. Gnann, K. Kroy, "Effective Temperatures of Hot Brownian Motion", *Physical Review E* **2014**, *90*, 032131.

[186] M. Srivastava, D. Chakraborty, “The Effective Temperature for the Thermal Fluctuations in Hot Brownian Motion”, *The Journal of Chemical Physics* **2018**, *148*, 204902.

[187] S. A. Loos, S. H. Klapp, “Force-Linearization Closure for Non-Markovian Langevin Systems with Time Delay”, *Physical Review E* **2017**, *96*, 012106.

[188] S. A. Loos, S. H. Klapp, “Heat Flow Due to Time-Delayed Feedback”, *Scientific reports* **2019**, *9*, 1–11.

[189] B. Cui, A. Zaccone, “Generalized Langevin Equation and Fluctuation-Dissipation Theorem for Particle-Bath Systems in External Oscillating Fields”, *Physical Review E: Statistical Physics Plasmas Fluids and Related Interdisciplinary Topics* **2018**, *97*, 060102.

[190] B. G. Mitterwallner, C. Schreiber, J. O. Daldrop, J. O. Rädler, R. R. Netz, “Non-Markovian Data-Driven Modeling of Single-Cell Motility”, *Physical Review E: Statistical Physics Plasmas Fluids and Related Interdisciplinary Topics* **2020**, *101*, 032408.

[191] M. P. Allen, D. J. Tildesley, *Computer Simulation of Liquids*, Oxford University Press, **2017**.

[192] M. Tuckerman, *Statistical Mechanics: Theory and Molecular Simulation*, OUP Oxford, **2010**.

[193] W. G. Noid, J.-W. Chu, G. S. Ayton, V. Krishna, S. Izvekov, G. A. Voth, A. Das, H. C. Andersen, “The Multiscale Coarse-Graining Method. I. A Rigorous Bridge between Atomistic and Coarse-Grained Models”, *The Journal of Chemical Physics* **2008**, *128*, 244114.

[194] V. Klippenstein, N. F. A. van der Vegt, “Bottom-Up Informed and Iteratively Optimized Coarse-Grained Non-Markovian Water Models with Accurate Dynamics”, *Journal of Chemical Theory and Computation* **2023**, *19*, 1099–1110.

[195] H. Vroylandt, P. Monmarché, “Position-Dependent Memory Kernel in Generalized Langevin Equations: Theory and Numerical Estimation”, *The Journal of Chemical Physics* **2022**, *156*, 244105.

[196] S. Izvekov, G. A. Voth, “Modeling Real Dynamics in the Coarse-Grained Representation of Condensed Phase Systems”, *The Journal of Chemical Physics* **2006**, *125*, 151101.

[197] M. S. Shell, “The Relative Entropy Is Fundamental to Multiscale and Inverse Thermodynamic Problems”, *The Journal of Chemical Physics* **2008**, *129*, 144108.

[198] H. Vroylandt, “On the Derivation of the Generalized Langevin Equation and the Fluctuation-Dissipation Theorem”, *Europhysics Letters* **2022**, *140*, 62003.

[199] M. Murat, K. Kremer, “From Many Monomers to Many Polymers: Soft Ellipsoid Model for Polymer Melts and Mixtures”, *Journal of Chemical Physics* **1998**, *108*, 4340–4348.

[200] P. Español, P. B. Warren, “Perspective: Dissipative Particle Dynamics”, *The Journal of Chemical Physics* **2017**, *146*, 150901.

[201] V. Klippenstein, M. Tripathy, G. Jung, F. Schmid, N. F. A. van der Vegt, “Introducing Memory in Coarse-Grained Molecular Simulations”, *The Journal of Physical Chemistry B* **2021**, *125*, 4931–4954.

[202] V. Rühle, C. Junghans, A. Lukyanov, K. Kremer, D. Andrienko, “Versatile Object-Oriented Toolkit for Coarse-Graining Applications”, *Journal of Chemical Theory and Computation* **2009**, *5*, 3211–3223.

[203] M. Rossi, V. Kapil, M. Ceriotti, “Fine Tuning Classical and Quantum Molecular Dynamics Using a Generalized Langevin Equation”, *The Journal of chemical physics* **2018**, *148*, 102301.

[204] T. Bereau, J. F. Rudzinski, “Accurate Structure-Based Coarse Graining Leads to Consistent Barrier-Crossing Dynamics”, *Physical Review Letters* **2018**, *121*, 256002.

[205] M. E. Johnson, T. Head-Gordon, A. A. Louis, “Representability Problems for Coarse-Grained Water Potentials”, *The Journal of Chemical Physics* **2007**, *126*, 144509.

[206] J. W. Wagner, J. F. Dama, A. E. P. Durumeric, G. A. Voth, "On the Representability Problem and the Physical Meaning of Coarse-Grained Models", *The Journal of Chemical Physics* **2016**, *145*, 044108.

[207] N. J. H. Dunn, T. T. Foley, W. G. Noid, "Van Der Waals Perspective on Coarse-Graining: Progress toward Solving Representability and Transferability Problems", *Accounts of Chemical Research* **2016**, *49*, 2832–2840.

[208] P. Ganguly, N. F. A. van der Vegt, "Representability and Transferability of Kirkwood–Buff Iterative Boltzmann Inversion Models for Multicomponent Aqueous Systems", *Journal of Chemical Theory and Computation* **2013**, *9*, 5247–5256.

[209] D. Rosenberger, M. Hanke, N. F. A. van der Vegt, "Comparison of Iterative Inverse Coarse-Graining Methods", *The European Physical Journal Special Topics* **2016**, *225*, 1323–1345.

[210] H. C. Andersen, J. D. Weeks, D. Chandler, "Relationship between the Hard-Sphere Fluid and Fluids with Realistic Repulsive Forces", *Physical Review A: Atomic Molecular and Optical Physics* **1971**, *4*, 1597–1607.

[211] K. Kremer, G. S. Grest, "Dynamics of Entangled Linear Polymer Melts:Â€‰ A Molecularâ€dynamics Simulation", *The Journal of Chemical Physics* **1990**, *92*, 5057–5086.

[212] H. Berendsen, D. van der Spoel, R. van Drunen, "GROMACS: A Message-Passing Parallel Molecular Dynamics Implementation", *Computer Physics Communications* **1995**, *91*, 43–56.

[213] B. Hess, C. Kutzner, D. van der Spoel, E. Lindahl, "GROMACS 4: Algorithms for Highly Efficient, Load-Balanced, and Scalable Molecular Simulation", *Journal of Chemical Theory and Computation* **2008**, *4*, 435–447.

[214] M. J. Abraham, T. Murtola, R. Schulz, S. Páll, J. C. Smith, B. Hess, E. Lindahl, "GROMACS: High Performance Molecular Simulations through Multi-Level Parallelism from Laptops to Supercomputers", *SoftwareX* **2015**, *1–2*, 19–25.

[215] V. Rühle, C. Junghans, "Hybrid Approaches to Coarse-Graining Using the VOTCA Package: Liquid Hexane", *Macromolecular Theory and Simulations* **2011**, *20*, 472–477.

[216] S. Y. Mashayak, M. N. Jochum, K. Koschke, N. R. Aluru, V. Rühle, C. Junghans, "Relative Entropy and Optimization-Driven Coarse-Graining Methods in VOTCA", *PLOS ONE* **2015**, *10*, e0131754.

[217] S. Plimpton, "Fast Parallel Algorithms for Short-Range Molecular Dynamics", *Journal of computational physics* **1995**, *117*, 1–19.

[218] *Coarse-Graining of Condensed Phase and Biomolecular Systems*, (Ed.: G. A. Voth), CRC Press, **2009**.

[219] H. Meyer, P. Pelagejcev, T. Schilling, "Non-Markovian out-of-Equilibrium Dynamics: A General Numerical Procedure to Construct Time-Dependent Memory Kernels for Coarse-Grained Observables", *EPL (Europhysics Letters)* **2020**, *128*, 40001.

[220] M. Hanke, "Mathematical Analysis of Some Iterative Methods for the Reconstruction of Memory Kernels", *Electronic Transactions on Numerical Analysis* **2021**, *54*, 483–498.

[221] M. Ceriotti, G. Bussi, M. Parrinello, "Langevin Equation with Colored Noise for Constant-Temperature Molecular Dynamics Simulations", *Physical Review Letters* **2009**, *102*, 20601.

[222] C. Ayaz, L. Scalfi, B. A. Dalton, R. R. Netz, "Generalized Langevin Equation with a Nonlinear Potential of Mean Force and Nonlinear Memory Friction from a Hybrid Projection Scheme", *Physical Review E* **2022**, *105*, 054138.

[223] K. Binder, P. Virnau, A. Statt, "Perspective: The Asakura Oosawa Model: A Colloid Prototype for Bulk and Interfacial Phase Behavior", *The Journal of Chemical Physics* **2014**, *141*, 140901.

[224] J. Zausch, P. Virnau, K. Binder, J. Horbach, R. L. Vink, "Statics and Dynamics of Colloid-Polymer Mixtures near Their Critical Point of Phase Separation: A Computer Simulation Study of a Continuous Asakura–Oosawa Model", *The Journal of Chemical Physics* **2009**, *130*, 064906.

[225] A. P. Gast, C. K. Hall, W. B. Russel, "Polymer-Induced Phase Separations in Nonaqueous Colloidal Suspensions", *Journal of Colloid and Interface Science* **1983**, *96*, 251–267.

[226] D. Chandler, J. D. Weeks, H. C. Andersen, "Van Der Waals Picture of Liquids, Solids, and Phase Transformations", *Science (New York N.Y.)* **1983**, *220*, 787–794.

[227] A. P. Thompson, H. M. Aktulga, R. Berger, D. S. Bolintineanu, W. M. Brown, P. S. Crozier, P. J. in 't Veld, A. Kohlmeyer, S. G. Moore, T. D. Nguyen, R. Shan, M. J. Stevens, J. Tranchida, C. Trott, S. J. Plimpton, "LAMMPS - a Flexible Simulation Tool for Particle-Based Materials Modeling at the Atomic, Meso, and Continuum Scales", *Computer Physics Communications* **2022**, *271*, 108171.

[228] B. Dünweg, K. Kremer, "Molecular Dynamics Simulation of a Polymer Chain in Solution", *The Journal of Chemical Physics* **1993**, *99*, 6983–6997.

[229] P. Virtanen, R. Gommers, T. E. Oliphant, M. Haberland, T. Reddy, D. Cournapeau, E. Burovski, P. Peterson, W. Weckesser, J. Bright, S. J. van der Walt, M. Brett, J. Wilson, K. J. Millman, N. Mayorov, A. R. J. Nelson, E. Jones, R. Kern, E. Larson, C. J. Carey, İ. Polat, Y. Feng, E. W. Moore, J. VanderPlas, D. Laxalde, J. Perktold, R. Cimrman, I. Henriksen, E. A. Quintero, C. R. Harris, A. M. Archibald, A. H. Ribeiro, F. Pedregosa, P. van Mulbregt, "SciPy 1.0: Fundamental Algorithms for Scientific Computing in Python", *Nature Methods* **2020**, *17*, 261–272.

[230] M. A. Branch, T. F. Coleman, Y. Li, "A Subspace, Interior, and Conjugate Gradient Method for Large-Scale Bound-Constrained Minimization Problems", *SIAM Journal on Scientific Computing* **1999**, *21*, 1–23.

[231] S. Izvekov, "Mori-Zwanzig Theory for Dissipative Forces in Coarse-Grained Dynamics in the Markov Limit", *Physical Review E* **2017**, *95*, 013303.

[232] S. Markutsya, M. H. Lamm, "A Coarse-Graining Approach for Molecular Simulation That Retains the Dynamics of the All-Atom Reference System by Implementing Hydrodynamic Interactions", *The Journal of Chemical Physics* **2014**, *141*, 174107.

[233] T. D. Stoffel, J. B. Haskins, J. W. Lawson, S. Markutsya, "Coarse-Grained Dynamically Accurate Simulations of Ionic Liquids: [Pyr14][TFSI] and [EMIM][BF4]", *The Journal of Physical Chemistry B* **2022**, *126*, 1819–1829.

[234] A. Davtyan, G. A. Voth, H. C. Andersen, "Dynamic Force Matching: Construction of Dynamic Coarse-Grained Models with Realistic Short Time Dynamics and Accurate Long Time Dynamics", *The Journal of Chemical Physics* **2016**, *145*, 224107.

[235] L. Gao, W. Fang, "Semi-Bottom-up Coarse Graining of Water Based on Microscopic Simulations", *The Journal of Chemical Physics* **2011**, *135*, 184101.

[236] S. Izvekov, G. A. Voth, "Multiscale Coarse Graining of Liquid-State Systems", *The Journal of Chemical Physics* **2005**, *123*, 134105.

[237] A. Lyubartsev, A. Mirzoev, L. Chen, A. Laaksonen, "Systematic Coarse-Graining of Molecular Models by the Newton Inversion Method", *Faraday Discussions* **2010**, *144*, 43–56.

[238] C. Scherer, D. Andrienko, "Understanding Three-Body Contributions to Coarse-Grained Force Fields", *Physical Chemistry Chemical Physics* **2018**, *20*, 22387–22394.

[239] C. Scherer, R. Scheid, D. Andrienko, T. Bereau, "Kernel-Based Machine Learning for Efficient Simulations of Molecular Liquids", *Journal of Chemical Theory and Computation* **2020**, *16*, 3194–3204.

[240] A. Moradzadeh, N. R. Aluru, "Many-Body Neural Network-Based Force Field for Structure-Based Coarse-Graining of Water", *The Journal of Physical Chemistry A* **2022**, *126*, 2031–2041.

[241] A. Eriksson, M. N. Jacobi, J. Nyström, K. Tunstrøm, "Effective Thermostat Induced by Coarse Graining of Simple Point Charge Water", *The Journal of Chemical Physics* **2008**, *129*, 024106.

[242] A. Eriksson, M. N. Jacobi, J. Nyström, K. Tunstrøm, "Bottom-up Derivation of an Effective Thermostat for United Atoms Simulations of Water", *The Journal of Chemical Physics* **2009**, *130*, 164509.

[243] T. Iwashita, B. Wu, W.-R. Chen, S. Tsutsui, A. Q. R. Baron, T. Egami, "Seeing Real-Space Dynamics of Liquid Water through Inelastic x-Ray Scattering", *Science Advances* **2017**, *3*.

[244] Y. Shinohara, W. Dmowski, T. Iwashita, B. Wu, D. Ishikawa, A. Q. R. Baron, T. Egami, "Viscosity and Real-Space Molecular Motion of Water: Observation with Inelastic x-Ray Scattering", *Physical Review E* **2018**, *98*, 022604.

[245] Y. Shinohara, W. Dmowski, T. Iwashita, D. Ishikawa, A. Q. R. Baron, T. Egami, "Local Correlated Motions in Aqueous Solution of Sodium Chloride", *Physical Review Materials* **2019**, *3*, 065604.

[246] Y. Shinohara, W. Dmowski, T. Iwashita, D. Ishikawa, A. Q. R. Baron, T. Egami, "Local Self-Motion of Water through the Van Hove Function", *Physical Review E* **2020**, *102*, 032604.

[247] R. A. Matsumoto, M. W. Thompson, V. Q. Vuong, W. Zhang, Y. Shinohara, A. C. T. van Duin, P. R. C. Kent, S. Irle, T. Egami, P. T. Cummings, "Investigating the Accuracy of Water Models through the Van Hove Correlation Function", *Journal of Chemical Theory and Computation* **2021**, *17*, 5992–6005.

[248] F. H. Stillinger, T. A. Weber, "Computer Simulation of Local Order in Condensed Phases of Silicon", *Physical Review B* **1985**, *31*, 5262–5271.

[249] J. Lu, Y. Qiu, R. Baron, V. Molinero, "Coarse-Graining of TIP4P/2005, TIP4P-Ew, SPC/E, and TIP3P to Monatomic Anisotropic Water Models Using Relative Entropy Minimization", *Journal of Chemical Theory and Computation* **2014**, *10*, 4104–4120.

[250] V. Molinero, E. B. Moore, "Water Modeled As an Intermediate Element between Carbon and Silicon", *The Journal of Physical Chemistry B* **2009**, *113*, 4008–4016.

[251] H. J. C. Berendsen, J. R. Grigera, T. P. Straatsma, "The Missing Term in Effective Pair Potentials", *The Journal of Physical Chemistry* **1987**, *91*, 6269–6271.

[252] S. J. Keasler, S. M. Charan, C. D. Wick, I. G. Economou, J. I. Siepmann, "Transferable Potentials for Phase Equilibria–United Atom Description of Five- and Six-Membered Cyclic Alkanes and Ethers", *The Journal of Physical Chemistry B* **2012**, *116*, 11234–11246.

[253] M. P. Bernhardt, M. Dallavalle, N. F. A. Van der Vegt, "Application of the 2PT Model to Understanding Entropy Change in Molecular Coarse-Graining", *Soft Materials* **2020**, *18*, 274–289.

[254] H. W. Engl, M. Hanke, A. Neubauer, *Regularization of Inverse Problems*, Springer Science & Business Media, **2000**.

[255] Z. Ma, S. Wang, M. Kim, K. Liu, C.-L. Chen, W. Pan, "Transfer Learning of Memory Kernels for Transferable Coarse-Graining of Polymer Dynamics", *Soft Matter* **2021**, *17*, 5864–5877.